



HAL
open science

Natural Killer (NK) and Innate Lymphoid Cell responses to autologous and allogeneic tumors

Anna Louisa Thaller

► **To cite this version:**

Anna Louisa Thaller. Natural Killer (NK) and Innate Lymphoid Cell responses to autologous and allogeneic tumors. Immunology. Université Paris Cité, 2023. English. NNT: 2023UNIP5025 . tel-04748810

HAL Id: tel-04748810

<https://theses.hal.science/tel-04748810v1>

Submitted on 22 Oct 2024

HAL is a multi-disciplinary open access archive for the deposit and dissemination of scientific research documents, whether they are published or not. The documents may come from teaching and research institutions in France or abroad, or from public or private research centers.

L'archive ouverte pluridisciplinaire **HAL**, est destinée au dépôt et à la diffusion de documents scientifiques de niveau recherche, publiés ou non, émanant des établissements d'enseignement et de recherche français ou étrangers, des laboratoires publics ou privés.

Université Paris Cité
École Doctorale Bio Sorbonne Paris Cité (ED 562)
Institut PASTEUR

Unité d'Immunité Innée (INSERM U1223)

Natural Killer (NK) and Innate Lymphoid Cell responses to autologous and allogeneic tumors

Par Anna Louisa THALLER

Thèse de doctorat d'Immunologie

Dirigée par Dr. Hélène STRICK-MARCHAND
Présentée et soutenue publiquement le 30 Mars 2023

Devant un jury composé de :

Aura MUNTASELL CASTELLVÍ Associate Professor, IMIM, Universitat Autònoma de Barcelona	Rapportrice
Ofer MANDELBOIM Full Professor, The Hebrew University of Jerusalem	Rapporteur
Jan SPANHOLTZ Principal Investigator, Glycostem	Examineur
Eliane PIAGGIO DR, Institut Curie, Université Paris Sciences & Lettres	Examinatrice
Sylvain LATOUR DR, Institut Imagine, Université Paris Cité	Examineur
Friederike JÖNSSON DR, Institut Pasteur, Sorbonne Université	Invitée
James DI SANTO DR, Institut Pasteur, Université Paris Cité	Invité
Hélène STRICK-MARCHAND CR, Institut Pasteur, Université Paris Cité	Directrice de thèse

Table of contents

TABLE OF CONTENTS	2
ACKNOWLEDGEMENTS	5
ABSTRACT	9
RESUME	11
LIST OF FIGURES	13
LIST OF ABBREVIATIONS	15
<u>CHAPTER I</u>	<u>19</u>
GENERAL INTRODUCTION	19
1.1 THE HUMAN IMMUNE SYSTEM.....	19
1.2 HUMAN IMMUNE SYSTEM MOUSE MODELS	46
1.3 ANTI-TUMOR IMMUNE RESPONSES.....	53
1.4 STATE OF THE ART	63
1.5 SPECIFIC AIMS OF THE THESIS.....	65
<u>CHAPTER II</u>	<u>67</u>
DELINEATING MECHANISMS UNDERLYING ANTIBODY-MEDIATED EFFECTS VIA FcRs IN HUMAN IMMUNE SYSTEM (HIS) MICE 67	
2.1 ABSTRACT	68
2.2 INTRODUCTION	69
2.3 RESULTS	71
2.4 DISCUSSION.....	80
2.5 MATERIAL AND METHODS	81
2.6 SUPPLEMENTARY FIGURES.....	85
2.7 REFERENCES	91
2.8 ACKNOWLEDGEMENTS	94
<u>CHAPTER III</u>	<u>95</u>
A NOVEL LYMPHOMA MODEL TO STUDY HUMAN ANTI-TUMOR IMMUNE RESPONSES IN HIS MICE	95
3.1 INTRODUCTION	95
3.2 RESULTS	96
3.3 CONCLUSION	121
3.4 MATERIAL AND METHODS	123
<u>CHAPTER IV</u>	<u>127</u>
DISCUSSION	127
REFERENCES	139
RESUME SUBSTANTIEL EN FRANÇAIS	160
ANNEXES	165
LISTE DES ELEMENTS SOUS DROITS	250

Acknowledgements

I want to thank all the people that contributed to my thesis and were there for me in the last 4 years during which I was working on my PhD project.

Jim, thank you for always taking the time whenever I asked for a meeting despite your busy schedule, for the discussions about my experiments and my data and for guiding me through my project. Throughout my PhD I always felt supported by you and I am proud that I could be a part of your lab.

Hélène, thank you for being my supervisor and helping me to work with humanized mice and everything connected to this. And for your support, I really appreciate that in the last weeks you put a lot of effort into reading through my thesis, helping me with the jury composition for my defense and reassuring me that everything will be fine.

Carys, having you in the lab was invaluable for me. Not only did you show me all the techniques, taught me how to use the machines, shared your knowledge on ILCs with me, patiently told me over and over again where to find reagents and never complained that I was 10x slower than you in about everything. You also made sure that people switched to English so I could be part of conversations, you took me along to social events and you introduced me to a lot of people. Thank you for taking care of me and all your help and advice, for sure I would have had a much harder time without you. I learned a lot from you and I always enjoyed working together with you.

To Priyanka and Evgeny, I really enjoyed working with you and my project definitely profited from all your help with the HIS mice as well as from discussing and exchanging about our work. I had a lot of fun during our lunches and goûters together with Carys, these breaks (even if they were sometimes short or interrupted by cleaning the FACS at the same time) managed to make up for failed experiments and all the other frustrations in the life of a PhD student. I am very grateful that I have found friends like you and for all the activities we did together in- and outside of the lab. Carys, the space next to me feels empty since you are not there anymore. Priyanka, working late is not the same since you have left, I miss our late-in-the-evening dinners to have enough energy for finish our experiments and cycle home together. Evgeny, thank you so much for your support in the last weeks and helping me to find the motivation to keep going.

Laura, for me, you were someone to look up to from the very beginning, I always liked your seemingly endless energy, your enthusiasm and spontaneity. It was a pleasure to work with you and I want to thank you a lot for always encouraging me, pushing me when it was needed and for letting me know that you believe in me. All of this really helped me to move forward and gave me more self-confidence.

Oriane, I am very thankful that you patiently introduced me to all the mouse work and took the time to properly train me. Even though the animal facility is not the nicest place to be I always looked forward to go there together with you. Learning from you, working together with you and sharing stories about our life made going to the animal facility even enjoyable. I miss our time together in the animal facility and getting regular updates since you changed to the platform.

Solenne, thank you for all your help in my project and for always taking the time to listen to me and give some advice no matter whether this was concerning technical, administrative or interpersonal issues.

Jean-Marc, all the training, help and advice I got from you was crucial for my project and I really learned a lot about flow cytometry from you. Thank you for all of this and also everything you taught me about French culture. In addition to all the invaluable advices on flow cytometry I also appreciate a lot your advice that I got in the first week when I arrived, that it's always worth to pay the extra 10 cent to get a "tradition" instead of a regular baguette – an advice I always followed ;)

To Toshiki, Nico, Angélique, Christian, Giulia, Lucy, Eva, Gosia, Dylan, Magali, Guillemette, Remy, Danièle, Angèle, Pedro and all the other past and present members of the lab. Thank you so much for the discussions, advices, techniques you taught me, help and support I received from you throughout the time of my PhD.

To everyone from the ITN program, the people involved in the coordination, the supervisors, and all the students. The few meetings we had together were really great and I am very glad that I am part of this network.

A big thanks to all the collaborators, members of the department of Immunology and all the services at Pasteur, particularly the CB UTechS and the animal facility.

To all the Bunkœurians, Mig, Eleonore, Seb, Nico, Mike, Eva, Léa, ML, Mika, Sean, Anna, Romain, Claire, Maud and Eddy, I want to thank you a lot! The Bunkœur was not only a shared house for me, but a place where I always felt well, it is my home here in Paris. I am extremely grateful for all your encouragement and support, inspiring discussions, projects and holidays we had together, for all the food you kept aside

when I came home after long experiments or intense days of writing. And thank you for so many more things you did for me and experiences we shared during these last 4 years. I learned a lot from each of you!

A tous les jeunes migrants qui ont vécu avec nous, en particulier Moussa et Mamadou, votre présence a toujours égayé mes journées et vous m'avez beaucoup aidé à améliorer mon français. Je suis très heureuse d'avoir pu vous connaître.

I want to thank the association TIMMY and all its volunteers, especially Chloé for supporting us with the hosting project, for always being there, especially in difficult situations and for being so responsive.

Vanessa, it was a pleasure to have you as a lab neighbor and I could have not wished for a better companion throughout all this time. I am extremely glad that we got to know each other and together with Hanno I think we really were a dream team. Thank you both for your friendship and all the good times we had together.

To Lena and Lisa, I am very happy that I met you in Paris and I enjoyed the hiking trips and other activities we did together a lot.

Thanks to all my friends outside of Paris, especially Betty, Vroni, Beadi, Kathi, Laura, Andrea, Sven, Natie, Flitzi, Dali, Athina, Moni and Helene for always being there for me, for checking up on me, visiting me in Paris and supporting me whenever you could. You are extremely important to me and I would not be the same person without you!

ML, thank you a lot for all your support in the last years and going through this second half of my PhD with me. Thanks for the efforts you made in trying to understand my project, for helping me to find methods in structuring my tasks better and become more efficient. For your encouragement, for being there for me and respecting that I often needed a lot of time for my PhD.

To all my family, especially my parents and my sisters, Lisa, Sophia and Vroni. You have supported me in so many ways throughout all my life and also in the last years, despite the geographical distance between us. I am very happy that you visited me here several times and could get an idea of my life in Paris. Knowing that you are always there for me and that I can count on you gave me a lot of strength and confidence.

Abstract

Natural Killer (NK) and Innate Lymphoid Cell responses to autologous and allogeneic tumors

In the last years innate lymphoid cells (ILCs), especially natural killer (NK) cells have moved into the focus for novel immunotherapeutic approaches in different diseases and particularly for the treatment of cancer. To understand the impact of ILCs and NK cells in anti-tumor responses, advanced experimental setups, including *in vivo* models, are essential. Mice reconstituted with a Humanized Immune System (HIS) have been shown to harbor human NK cells and ILCs, allowing to investigate the function of these subsets *in vivo*.

The aim of my thesis project is to define the roles for human NK cells and human ILC subsets in the anti-tumor immune response *in vivo* using HIS mice.

Monoclonal antibodies have made a tremendous impact as therapeutic agents for the treatment of a variety of cancers. Antibodies exert their effects via Fc Receptors (FcRs) expressed on several immune cells including neutrophils, macrophages and NK cells. Still, the precise effector cells and mechanisms underlying effective anti-tumor responses in humans remain unclear. Studying human antibody-mediated anti-tumor responses in HIS mice is complicated by the presence of residual mouse FcR+ cells that can elicit immune effects. To better define cellular mechanisms involved in antibody-mediated tumor clearance, I characterized a novel FcR-deficient HIS mouse model that was developed in the laboratory. We demonstrated deletion in the *Fcgr1g* gene at DNA and RNA levels by PCR and sequencing. We further validated the absence of functional activating mouse FcRs by flow cytometry and with a passive systemic anaphylaxis assay in mice. I tested how target cell depletion by different antibodies, and antibody variants, are affected in this new FcR-deficient HIS model, and observed that mouse FcR bearing cells, mouse complement, and human FcR bearing cells could all contribute to antibody-mediated cell depletion. Furthermore, by using a complement inactive antibody variant in the FcR-deficient HIS mice I was able

to show the importance of human FcR+ NK cells in antibody-mediated cell depletion *in vivo*.

In order to generate an autologous HIS-tumor mouse model, we created syngeneic lymphoblastoid cell lines (LCLs) by transforming human B cells that had differentiated in HIS mice, using Epstein Barr virus (EBV). We then tested the tumor potential of these EBV B cell lines (B-LCLs) *in vivo*. Intraperitoneally injected B-LCLs showed efficient grafting and expansion in non-humanized, immunodeficient hosts. At early time points the B-LCLs were mostly confined to the peritoneal cavity but with time tumor cells disseminated in the blood and formed tumors in the spleen, liver and peritoneal cavity. Interestingly, when injected into reconstituted partially HLA-matched HIS mice, anti-tumor immune responses were observed and the data suggest an expansion of human CD8+ cytotoxic T cells and NK cells with a reduction in the number of tumor cells.

Taken together, we have generated a novel FcR deficient HIS mouse model which will allow to study antibody-mediated responses by the human immune system against autologous tumors.

Keywords:

Natural Killer cells, Innate Lymphoid cells, Human immune system mice, autologous tumor models, Fc Receptors, complement, B-LCL, therapeutic antibodies, innate immunity

Résumé

Réponses des cellules Natural Killer (NK) et des cellules lymphoïdes innées aux tumeurs autologues et allogéniques

Ces dernières années, les cellules lymphoïdes innées (ILC), en particulier les cellules Natural Killer (NK), sont au centre des recherches pour des nouvelles approches immunothérapeutiques, notamment pour le traitement du cancer. Pour mieux comprendre l'impact des cellules ILC et NK dans les réponses antitumorales, il est essentiel de disposer de modèles expérimentaux avancés, notamment *in vivo*. Des souris humanisées pour le système immunitaire (HIS) constituent un tel modèle chez lesquels la présence de cellules NK et ILC humaines a été démontrée.

Le but de mon projet de thèse est de définir les rôles des cellules NK humaines et des sous-ensembles d'ILC humains dans la réponse immunitaire anti-tumorale *in vivo* dans le modèle souris HIS.

Les anticorps monoclonaux ont un impact considérable en tant qu'immunothérapeutiques pour le traitement de nombreux cancers. Les anticorps exercent leurs effets via les récepteurs Fc (FcR) exprimés sur plusieurs cellules immunitaires, notamment les neutrophiles, les macrophages et les cellules NK. Cependant, les cellules effectrices et les mécanismes qui régulent ces réponses antitumorales efficaces chez l'homme ne sont toujours pas clairement définis. L'étude des réponses anti-tumorales, médiées par les anticorps humains chez les souris HIS est compliquée par la présence des cellules FcR⁺ résiduelles de souris qui peuvent participer à l'immunité. Afin de mieux définir les mécanismes cellulaires impliqués dans l'élimination des tumeurs médiée par les anticorps, j'ai caractérisé un nouveau modèle de souris HIS inactivé pour le FcR qui a été développé dans le laboratoire. Nous avons démontré la délétion du gène *Fcer1g* au niveau ADN et ARN par PCR et séquençage. L'absence de FcRs fonctionnels activateurs a été validé par cytométrie de flux et par un test d'anaphylaxie systémique passive chez la souris. J'ai caractérisé la déplétion des cellules cibles par différents anticorps, et variantes d'anticorps, dans ce nouveau modèle HIS inactivé pour FcR, et déterminé que les cellules exprimant le

FcR de souris, le complément murin, et les cellules porteuses de FcR humains peuvent tous contribuer à la déplétion cellulaire médiée par les anticorps. De plus, en utilisant une variante d'anticorps déficiente pour le complément chez les souris HIS inactivé pour FcR, j'ai pu démontrer l'importance des cellules NK humaines FcR+ dans la déplétion cellulaire médiée par les anticorps *in vivo*.

Afin de générer un modèle autologue de souris HIS portant des tumeurs, nous avons créé des lignées cellulaires lymphoblastoïdes syngéniques (LCLs), en transformant des cellules B humaines, provenant des souris HIS, avec le virus d'Epstein Barr (EBV). J'ai ensuite testé le potentiel tumoral de ces lignées cellulaires B EBV transformées (B-LCLs) *in vivo*. Les B-LCL injectées par voie intrapéritonéale ont greffé et ont proliféré chez des hôtes non humanisés et immunodéficients. Initialement, les B-LCL étaient principalement confinés à la cavité péritonéale, mais progressivement, les cellules tumorales se sont disséminées dans le sang et ont formé des tumeurs dans la rate, le foie, et la cavité péritonéale. De manière intéressante, lorsque les B-LCL ont été injectées à des souris HIS reconstituées et partiellement appariées HLA, une réponse immunitaire antitumorale comprenant une expansion et une activation des cellules T cytotoxiques CD8+ et des cellules NK humaines a été observé, ainsi qu'une réduction du nombre de tumeurs.

En résumé, nous avons généré un nouveau modèle de souris HIS déficient en FcR qui permettra d'étudier les réponses médiées par les anticorps du système immunitaire humain contre les tumeurs autologues.

Mots-clés :

Cellules tueuses naturelles, cellules lymphoïdes innées, système immunitaire humain, souris, modèles de tumeurs autologues, récepteurs Fc, complément, B-LCL, anticorps thérapeutiques, immunité innée

List of Figures

- Figure 1** The Hematopoietic lineage tree – from HSCs to mature immune cells
- Figure 2** An overview of innate lymphoid cells
- Figure 3** NK cell CD56^{bright} and CD56^{dim} subsets
- Figure 4** Cell surface receptors expressed by human and mouse ILCs
- Figure 5** Schematic representation of physiological NK cell functions
- Figure 6** Schematic representation of human FcγRs
- Figure 7** Differences in the immune cell composition in the blood of humans and mice
- Figure 8** Immune cell compositions in different HIS mouse models compared to human in bone marrow and blood
- Figure 9** Mechanism of SIRPα-CD47 interaction
- Figure 10** The cancer-natural killer cell immunity cycle
- Figure 11** EBV oncogenic mechanisms

List of Abbreviations

ADCC	Antibody dependent cellular cytotoxicity
ADCP	Antibody dependent cellular phagocytosis
B-ALL	B cell acute lymphoblastic leukemia
BCR	B cell receptor
B-LCL	B lymphoblastoid cell line
BLT	Bone marrow, liver, thymus
BM	Bone marrow
BRG	BALB/c <i>Rag2^{tm1Flv}Il2rg^{tm1Flv}</i>
BRGS	BALB/c <i>Rag2^{tm1Flv}Il2rg^{tm1Flv} SIRPα^{NOD}</i>
BRGSA2DR2	BALB/c <i>Rag2^{-/-} Il2rg^{-/-} Sirpa^{NOD} Tg(HLA-A/H2-D/B2M)^{1Bpe}, Tg(HLA-DRB1*1501)^{#Lfug}</i>
BRGSF	BALB/c <i>Rag2^{tm1Fwa} Il2rg^{tm1Cgn} Sirpa^{NOD} Flt3^{tm1lr}</i>
BRGST	BALB/c <i>Rag2^{tm1Flv}Il2rg^{tm1Flv} SIRPα^{NOD} TSLP^{tg}</i>
CAR	Chimeric antigen receptor
cDC	Conventional dendritic cell
CDC	Complement dependent cytotoxicity
CDP	Complement dependent phagocytosis
CDR	Complementarity determining region
CHILP	Common helper ILC progenitor
CILP	Common innate lymphoid progenitor
CM	Central memory
CMV	Cytomegalovirus
CSR	Class switch recombination
CTLA-4	Cytotoxic T-lymphocyte antigen-4
DAMP	Damage associated molecular pattern
DC	Dendritic cell
EBER	Epstein Barr virus encoded RNA
EBNA	Epstein Barr nuclear antigen
EBV	Epstein-Barr virus
EILP	Early innate lymphoid progenitors
EM	Effector memory

EMP	Early myeloid progenitor
EOMES	Eomesodermin
Fc	Fragment crystallizable
FcR	Fc receptor
FcR γ	Fc receptor gamma chain
FCS	Fetal calf serum
Fc γ R	Fc gamma receptor
Flt3	Fms-like tyrosine kinase 3
GATA-3	GATA-binding protein-3
GM-CSF	Granulocyte-macrophage colony stimulating factor
gp	Glycoprotein
GvHD	Graft versus host disease
HDI	Human development index
HIS	Human immune system
HLA	Human leukocyte antigen
HSC	Hematopoietic stem cell
IELs	Intraepithelial T lymphocytes
IFN- γ	Interferon gamma
Ig	Immunoglobulin
ILC	Innate lymphoid cell
ILCp	Innate lymphoid cell precursor
ILCP	Innate lymphoid cell progenitor
iNKT	Invariant NKT
i.p.	Intraperitoneal
iPSC	Induced pluripotent stem cell
ITAM	Immunoreceptor tyrosine-based activation motif
ITIM	Immunoreceptor tyrosine-based inhibitory motif
JAK	Janus-associated kinases
KIR	Killer-cell immunoglobulin-like receptor
LTi	Lymphoid tissue inducer cells
LMP	Latent membrane protein
LP	Leader protein
mAb	Monoclonal antibody
MAIT	Mucosal associated invariant T cell

M-CSF	Macrophage colony stimulation factor
MHC	Major Histocompatibility complex
MDSC	Myeloid derived suppressor cells
NCR	Natural cytotoxicity receptor
NET	Neutrophil extracellular traps
NK	Natural killer
NKG2	Natural killer group 2
NKT	Natural killer T
NOG	NOD.Cg- <i>Prkdc^{scid}Il2rg^{tm1Sug}</i>
NSG	NOD.Cg- <i>Prkdc^{scid}Il2rg^{tm1Wjl}</i>
NSCLC	Non-small cell lung cancer
PAMP	Pathogen associated molecular pattern
PBMC	Peripheral blood mononuclear cell
PBS	Phosphate buffered saline
pDC	Plasmacytoid dendritic cell
PD-L1	Programmed death ligand 1
PDX	Patient derived xenograft
PD-1	Programmed cell death protein 1
Prkdc	Protein kinase DNA-activated catalytic polypeptide
PSA	Passive systemic anaphylaxis
PRR	Pattern recognition receptor
RAG	Recombination activating gene
RAR	Retinoic acid receptor
ROR α	RAR-related orphan receptor alpha
ROR γ t	RAR-related orphan receptor gamma t
ROS	Reactive oxygen species
RT	Room temperature
RTX	Rituximab (IgG1)
SCID	Severe combined immunodeficiency
SHM	Somatic hyper mutation
SIRP α	Signal regulatory protein alpha
sp	Spleen
STAT	Signal transducer and activator of transcription
TAA	Tumor associated antigens

TAM	Tumor associated macrophage
TCR	T cell receptor
TEMRA	CD45 ⁺ effector memory
TF	Transcription factor
Tfh	T follicular helper
TGFβ	Transforming growth factor beta
Th	Helper T cell
TIL	Tumor infiltrating lymphocyte
TLR	Toll-like receptor
TLS	Tertiary lymphoid structure
TME	Tumor microenvironment
TNF	Tumor necrosis factor
TNP	Trinitrophenyl
TRAIL	TNF-related apoptosis-inducing ligand
TSA	Tumor specific antigens
TSLP	Thymic-stromal-cell-derived lymphopoietin
Treg	Regulatory T cell
Tx mAbs	Therapeutic monoclonal antibodies
UMAP	Uniform manifold approximation and projection

Chapter I

General Introduction

1.1 The Human Immune System

Roles of the immune system

The human body has several lines of defense consisting of physical and chemical barriers like the skin, mucous membranes and stomach acids as well as the innate and the adaptive parts of the immune system. Classically the immune system is thought of as a defense mechanism, protecting from pathogenic viruses, bacteria, fungi and parasites¹. Yet, the immune system has a multiplicity of functions beyond pathogen defense. It is further involved in elimination of malignant cells, tissue repair, wound healing, vascularization, processes of development and reproduction. Hence, the role of the immune system is currently thought of as the maintenance of tissue homeostasis and system integrity².

Immune system development

The human immune system is composed of cellular and humoral factors. In the mammalian embryo three waves of hematopoietic progenitor generation have been identified, of which all are derived from the mesoderm³. Primitive erythrocytes, megakaryocytes, macrophages and early erythroid-myeloid progenitors (EMP) of the first wave and late EMP and lymphoid-myeloid progenitors of the second wave are emerging from the blood islands and the vascular plexus of the extraembryonic yolk sac respectively, whereas hematopoietic stem cells (HSCs) are of intra-embryonic origin⁴⁻⁸. In the last years multiple publications have shown that immune cells, like for example specific tissue resident macrophage subsets are derived from yolk sac precursors⁹⁻¹¹. Yet, the majority of immune cells present in adult individuals differentiate from HSCs^{12,13}. HSCs are defined as self-renewing and multipotent, meaning that they have the capability to either retain multipotency or differentiate and

give rise to all blood lineages through a process termed hematopoiesis¹⁴. HSCs arise during embryonic development in big vessels, in the aorta-gonad-mesonephros region, from where they migrate to the fetal liver, in which they amplify and mature during the periods of mid and late gestation¹⁵. Before birth the HSCs migrate to the bone marrow where they can persist throughout life¹⁶. In the bone marrow HSCs reside in distinct microenvironments, termed niches, in which the surrounding cells such as stromal and endothelial cells exert a regulatory influence on the HSCs. For example, HSCs remain in a quiescent state in the arteriolar niche while the perivascular niche has been identified to promote HSC maintenance^{17,18}. Based on surface marker phenotyping and *in vivo* transplantation experiments of human immune cell populations into immunodeficient mouse recipients, the Lin⁻ CD34⁺ CD38⁻ CD90⁺ CD45RA⁻ cell population has been identified to contain HSCs^{19,20}. Classically, hematopoiesis is thought of as a hierarchical tree in which HSCs give rise to multipotent progenitors which in turn give rise to lineage committed common lymphoid progenitors and common myeloid progenitors (Figure 1). These differentiate into mature immune cells through further lineage restrictive steps. The common myeloid progenitor has the potential to give rise to platelets and erythrocytes as well as all granulocytes, e.g., neutrophils, eosinophils, basophils and also to monocytes, macrophages and myeloid derived dendritic cells (DCs)²¹. The common lymphoid progenitor can give rise to B cells, T cells, innate lymphoid cells (ILC), including cytotoxic ILC1 called Natural killer (NK) cells, non-cytotoxic ILC1, ILC2, ILC3 and lymphoid derived DCs. It should be noted that this classical model of lineage commitment has been challenged with the availability of new techniques, such as single cell RNA sequencing but the most recent results from fate mapping studies by barcoding largely support the classical model. Still, further investigations are required to precisely understand all the precursor-product relationships^{22,23}. In hematopoiesis, decisions regarding lineage commitment and stem cell self-renewal are mostly dictated by transcription factors networks and regulatory chemokines and cytokines²⁴. The following section will cover the major populations of innate as well as adaptive immune cells and detail their characteristics and functions.

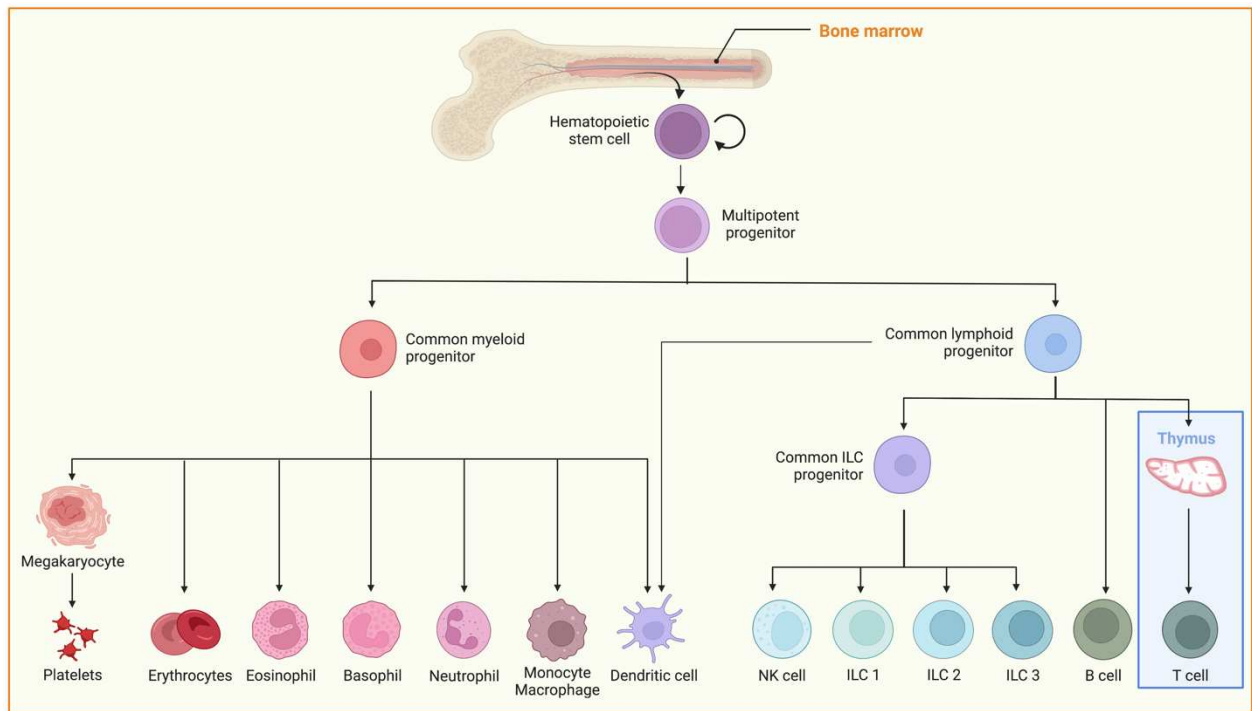


Figure 1. The Hematopoietic lineage tree – from HSCs to mature immune cells

Innate Immunity

The Immune system can conceptually be divided into innate and adaptive immune responses. The innate immune response is the first one to be induced and is characterized by its instant and invariant response. In contrast to adaptive immune responses, no prior encounter with the stimulus is required to evoke an innate immune response. One mechanism by which innate immune cells can sense abnormalities is the missing-self recognition^{25,26}. Moreover, innate immune responses involve the recognition of pathogen associated molecular patterns (PAMPs) by sentinel cells, like DCs, macrophages and mast cells which are strategically located in tissues and at barriers to detect the invasion of pathogens. The sensing of PAMPs, which are common structural or functional components of microorganisms such as lipopolysaccharides, mannoses or teichoic acids, is realized by genetically encoded pattern recognition receptors (PRRs)^{27,28}. Further, damage associated molecular patterns (DAMPs) which are released by necrotic cells or cells that undergo high stress are recognized by PRRs²⁹. A prominent example of PRRs is the toll-like receptor (TLR) family, where cell surface TLRs recognize microbial molecular structures while TLRs located in the endosome membrane are able to detect double stranded viral RNA, viral and bacterial DNA³⁰. These receptor interactions activate sentinel cells, which then

based on the sensed pathogen or abnormality, release inflammatory cytokines and chemokines, thus initiating the recruitment of other cell types such as monocytes, neutrophils and effector lymphocytes from the circulation^{28,31}. Depending on the cell type, different effector mechanisms like phagocytosis and degranulation of cytotoxic enzymes are executed for clearing of pathogens or abnormal cells. Innate immune cells are also crucial in the initiation of adaptive immune responses, particularly through antigen presentation by DCs and non-cellular based mechanisms like the complement system³².

Dendritic cells

At steady state, DCs patrol tissues to detect foreign molecules, for example by binding of ligands to their TLRs. Subsequently, they produce various polarizing cytokines such as type I interferon (IFN), interleukin (IL)-12, IL-23 or tumor necrosis factor (TNF) α , and thereby determine the type of immune response that is induced. Furthermore, DCs are specialized in taking up and processing antigens which they present either to surrounding T-cells or to naïve T cells in the lymph nodes³³. There are two major types of DCs, conventional DC (cDC) that are derived from the myeloid lineage, and plasmacytoid DC (pDC) that are derived from the lymphoid lineages, both are dependent on the cytokine receptor Flt3³⁴. The cDCs have a role in priming and polarizing naïve T cells³³. Human pDCs are identified by their expression of CD123 and cDCs are CD11c⁺ and can be distinguished by CD141 (cDC1) and CD1c (cDC2) expression³⁵.

Within the cDCs, cDC1 are mainly associated with viral and intracellular bacterial infections. They mainly secrete the Th1 polarizing cytokine IL-12 and have the capability of cross-presenting antigens on major histocompatibility complex (MHC) I molecules to CD8⁺ cytotoxic T cells. Further, in mice cDC1 were identified as the predominant source of CXCL9 and CXCL10 in the tumor microenvironment (TME) and were required for CD8⁺ effector T cell recruitment³⁶. Since CD8⁺ T cells are often the main effectors in anti-tumor responses, the initiation of the immune response by cDC1 may be crucial for tumor control. Indeed, the lack of the CD8 α ⁺ DC subset in a mouse tumor model showed reduced CD8⁺ T cell infiltration, failure to produce tumor specific cytotoxic T cells and as a result the tumor was not rejected^{37,38}.

cDC2 get activated in response to helminth or fungal infections, causing them to induce Th2 responses by secretion of pro-inflammatory cytokines IL-4, IL-5 and IL-13 or Th17 responses by IL-23 secretion, respectively. Correspondingly, cDC2 present antigens to CD4⁺ T cells via MHCII to induce either Th2 or Th17 responses³³.

In pDCs TLR7 and TLR9 that are localized on the endosomal membrane, allow a rapid response to viruses, bacteria and self-nucleic acids and cause the release of type I interferon^{39,40}.

Neutrophils

Neutrophils are polymorphonuclear granulocytes and the most abundant leukocytes in the peripheral blood. Typical marker for human neutrophils are CD66b, CD15 and CD16⁴¹. In the beginning of the acute phase of inflammation they are among the first cells that migrate to tissues by following chemokine gradients and other chemotactic agents like complement components⁴². They are activated through ligand binding of PRRs on their membrane surface and exert multiple effector functions. Through phagocytosis they take up microorganisms into intracellular vesicles which then fuse with granules, resulting in the killing of the ingested microorganisms by antimicrobial proteins and reactive oxygen species (ROS) in a structure called the phagosome⁴³. Alternatively, the content of the granules can be released by degranulation to kill microorganisms extracellularly⁴⁴. Neutrophils also secrete immunomodulatory molecules which may lead to the recruitment of further immune cells at the site of inflammation⁴⁵. NETosis is another mechanism of Neutrophils in which they release partially decondensed chromatin forming neutrophil extracellular traps (NETs). The NET chromatin is decorated with histones and granule proteins, enabling to trap and limit the spread of infections by killing bacteria⁴⁶. Even though neutrophils usually contribute to the resolution of inflammation, emerging evidence suggests that dysregulation of neutrophils can cause chronic inflammatory diseases and autoimmune disorders^{47,48}. With respect to cancer, a high neutrophil-to-lymphocyte concentration in the circulation, and high levels of intra-tumoral neutrophils, are associated with unfavorable outcomes^{49,50}. However, there is evidence that neutrophils contribute to antibody-mediated tumor cell destruction *in vivo*, and recently it has been shown *in vitro* that human neutrophils can kill antibody opsonized tumor cells by trogoptosis^{51,52}. It is important to note that in humans neutrophils express

overlapping surface markers with granulocytic myeloid-derived suppressor cells (MDSCs) which complicates their distinction and it is also not clear how closely these cell populations are related⁵³.

Eosinophils, Basophils and Mast cells

Eosinophils, Basophils and Mast cells are part of the myeloid lineage and together with neutrophils they represent the granulocytes and all contain cytoplasmic granules⁵⁴.

Eosinophils circulate within the bloodstream where they make up 1-3% of the overall cells and migrate to inflamed tissues upon activation. They are implicated in the host defense against parasites like helminths, fight viral and bacterial infections, are involved in allergic reactions and asthma. These effects are elicited by the cationic granular proteins within secondary granules⁵⁵. Mast cells are tissue resident cells residing near blood vessels, within the airways, the gastrointestinal and the genitourinary tract where they mature *in situ*. The activation of mast cells is highly associated with the binding of IgE through its high affinity receptor FcεRI, yet many other stimuli have been shown to activate mast cells, like complement components, TLR agonists, reptile and insect venoms⁵⁶. Basophils are the rarest granulocyte population making up less than 1% of peripheral blood leukocytes. As they possess phenotypic similarities with mast cells, like the expression of FcεRI, they have erroneously been considered circulating mast cells⁵⁷. Basophils circulate under homeostatic conditions and migrate to inflamed tissues where they get activated by IgE-dependent or IgE-independent pathways causing the release of mediators leading to immune reactions. For example, release of IL-4 has an immunomodulatory impact by recruiting eosinophils, polarizing macrophages, and influencing T cell differentiation. Moreover, basophils are involved in allergic disorders like food allergies, asthma and anaphylaxis⁵⁷.

Macrophages

The eponymous feature of Macrophages that fostered their discovery by Ilya Metchnikov in 1884 is their ability to carry out phagocytosis, which is defined as the cellular uptake of particles within a plasma-membrane envelope⁵⁸. Macrophages are found throughout many tissues and organs, like the liver, spleen, gut, lung and brain.

Depending on their location they have morphological and phenotypical specificities and have been given different names, e.g. Kupffer cells in the liver and microglia in the brain⁵⁹. For a long time, tissue-resident macrophages have been thought to differentiate exclusively from HSC derived monocytes in the circulation that migrate to tissues and become macrophages⁶⁰, but in recent years, several distinct tissue-resident macrophage populations have been shown to have an embryonic origin^{10,61}. Macrophages are involved in many processes including tissue homeostasis, tissue remodeling, immunosurveillance, host defense, antigen presentation and pathologies⁶². The ability to phagocytose allows the removal of apoptotic cells, dead cells and cellular debris to maintain tissue homeostasis, as well as the uptake and killing of bacteria and fungi which clears infections^{63,64}. In mouse models and *in vitro* it has been shown that macrophages can eliminate tumor cells by antibody dependent cellular phagocytosis (ADCP)^{65,66}. Macrophages are highly plastic with phenotypical and functional alterations due to environmental stimuli and signals. Hence, they have been classified into two discrete polarization states (M1/M2)⁶⁷. Macrophages can be identified by their expression of CD11b and CD68 (intracellular) and whereas CD64, CD80 and CD86 are markers associated with M1, CD206 is highly expressed on M2⁶⁸. M1 are described to encourage inflammation upon interferon gamma (IFN- γ) mediated activation, while M2 in turn decrease inflammation, encourage tissue repair and wound healing due to activation through IL-4 and IL-13. However, with increasing evidence of different activation modes, it is recognized that macrophage states go beyond the M1/M2 dichotomy, as many other macrophage polarization states have been described, the appropriateness of this classification has been questioned^{60,69}. Furthermore, tumor associated macrophages (TAMs) are abundant in solid tumors and involved in the immunosuppression of the TME, for example by producing immunosuppressive cytokines IL-10 and transforming growth factor β (TGF- β) and by releasing CCL20 which recruits Treg cells⁷⁰⁻⁷². Consequently, high frequency of TAMs in the TME correlates with poor prognosis in most human tumors⁷³. A mechanism for tumor cells to evade phagocytic elimination is the upregulation of CD47, a “do not eat me” signal which inhibits phagocytosis by binding to Signal regulatory protein alpha (SIRP α) expressed on macrophages⁷⁴. In a recent clinical phase 1b study in cancer patients, a CD47-blocking antibody in combination with Rituximab (anti-CD20) showed promising results, whereas anti-CD47 antibody monotherapy was mostly ineffective^{75,76}.

Innate Lymphoid cells

The family of innate lymphoid cells (ILCs) with its three distinct groups 1, 2 and 3 had been proposed only 10 years ago⁷⁷. The characteristics that unify different cell populations as innate lymphoid cells are (1) the lack of specific antigen receptors, (2) morphological characteristics of lymphoid cells and (3) a lack of myeloid and dendritic cell phenotypical markers^{77,78}. All ILCs share an ontogenetic origin and are derived from the common lymphoid progenitor. The discovery of progressively more restricted progenitor stages of ILCs has been facilitated by techniques such as single cell sorting, clonal expansion, single cell RNA sequencing, adoptive transfer, knock out and reporter mouse models. Early innate lymphoid progenitors (EILP) can give rise to the full range of ILCs, while the common helper ILC progenitor (CHILP), which expresses high levels of the transcription factor Id2, can differentiate to all ILCs except for cytotoxic natural killer (NK) cells^{79,80}. The ILC precursor (ILCp) expresses the transcription factor Plzf and only gives rise to ILC1, ILC2, ILC3 excluding NK and lymphoid tissue inducer cells (LTi)⁸¹. In humans a CD34⁺ common innate lymphoid progenitor (CILP) in secondary lymphoid organs, restricted to ILC potential, including NK cells, has been discovered^{82,83}. Further, a human CD34⁻ population of ILC progenitors (ILCPs) with the potential to generate all ILCs has been identified in tonsils, blood, lung, cord blood and fetal liver⁸⁴. Whereas cytotoxic NK cells require IL-15 for their development, all other ILC subsets are characterized by expression of IL-7R α (CD127) and IL-7R α signaling is indispensable for their efficient development^{85,86}. ILC groups 1, 2 and 3 have been classified based on the TFs they express and their cytokine production profiles (Figure 2). This classification was strongly inspired by the already existing classification of T cells, as ILCs were found to have remarkable functional parallels with T cells⁸⁷. Moreover, ILCs have been found to be plastic, a feature that describes the ability of differentiated cells to change their functions and phenotype based on changes in their microenvironment, which has already been revealed for T cells^{88,89}. For example, it has been shown in the intestine of mice and human immune system mice, that ILC3s can convert into ILC1s which is driven by IL-23^{90,91}.

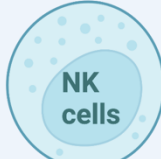




	Group 1 ILCs	Group 2 ILCs	Group 3 ILCs		
	cytotoxic	non-cytotoxic			
					
Transcription Factors	T-bet EOMES	T-bet	GATA-3	RORγT	RORγT
Activating cytokines	IL-12 IL-15 IL-18	IL-12 IL-15 IL-18	IL-25 IL-33 TSLP	IL-1β IL-23	IL-1β IL-23
Effector molecules	IFNγ TNF-α Granzyme Perforin	IFNγ TNF-α	IL-5 IL-9 IL-13 Amphiregulin	IL-17A IL-22	IL-17A IL-22 TNF LTα/β
Processes	Tumors Virus Intracellular bacteria	Intracellular pathogens Chronic inflammation	Helminths Allergy Tissue Repair	Extracellular bacteria Intestinal homeostasis	Lymphoid tissue organogenesis

Figure 2. An overview of innate lymphoid cells

NK cells

Natural killer (NK) cells belong to the group 1 ILC as they are able to produce large quantities of interferon-γ (IFN-γ) and express the TF T-bet. Furthermore, NK cells also express TF Eomesodermin (EOMES) and are cytotoxic, both distinguishing them from non-cytotoxic ILC1s^{77,92}.

When NK cells were discovered, they were found to naturally lyse certain tumor cells and antibody opsonized cells without delay or previous sensitization⁹³. Hence, NK cells are best known for their function of killing infected or transformed cells, as well as their role in immune regulation by cytokine secretion⁹⁴. Several studies revealed that reduced NK cell activities in humans are associated with increased rates of malignancies, attributing them a crucial role in tumor immunosurveillance^{95–97}.

NK cells can kill target cells either by directed release of lytic granules or induction of apoptosis via expression of Fas ligand or TNF-related apoptosis-inducing ligand

(TRAIL) that bind death receptors on target cells⁹⁸. The target cell lysis by lytic granules containing perforin and granzyme starts with the integrin-mediated adhesion of NK cells to target cells, leading to the formation of an immunological synapse. This results in the fusion of granules with the plasma membrane and release of lytic molecules like perforin monomers which form aggregates and subsequently pores in the membrane of the target cell. Granzymes can enter the target cell through these pores and cause cell death by inducing apoptotic pathways^{98,99}.

Further, NK cells are able to produce high amounts of pro-inflammatory cytokines IFN- γ and TNF- α following either, interaction of NK cell activating receptors with their ligands or activation by IL-12, IL-15 or IL-18, which are cytokines produced by other immune cells, like DCs and monocytes in inflammatory environments^{100–104}. By secreting cytokines NK cells can have immunoregulatory roles, most prominently IFN- γ which can regulate CD8⁺ T cell effector function¹⁰⁵.

In contrast, TGF- β has immunosuppressive implications on NK cells, as it modulates the expression of effector molecules, activating and chemokine receptors leading to reduced cytotoxicity and impaired anti-tumor responses¹⁰⁶. TGF- β was found to be upregulated in some cancer patients, notably in the plasma of lung and colorectal cancer patients compared to healthy donors^{107,108}. TGF- β downregulates expression of the activating receptor NKG2D on human NK cells, thus limiting their response¹⁰⁹. It has also been shown that TGF- β interferes with the mTOR pathway, blocking IL-15 induced activation of mTOR¹¹⁰.

Regulation of NK cell effector functions is dictated by the integration of inhibitory and activating signals received through a multitude of germ-line-encoded receptors expressed on NK cells (Figure 4), which can be grouped according to their ligand type¹¹¹.

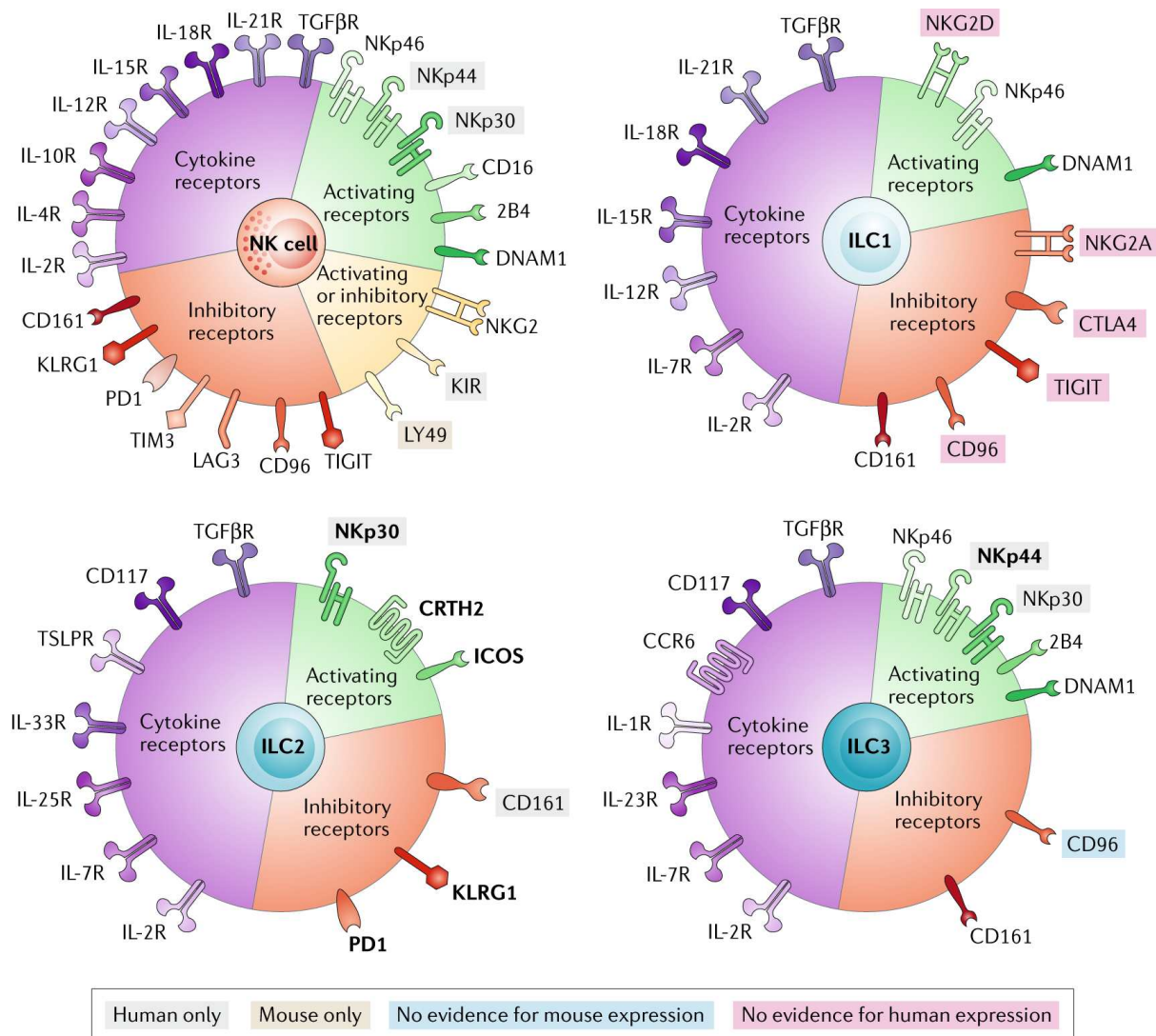


Figure 4. Cell surface receptors expressed by human and mouse ILCs (from Chiossone *et al.*¹¹²)

Killer-cell immunoglobulin-like receptors (KIRs) are stochastically expressed receptors that bind to self-MHC class I molecules which are ubiquitously expressed on all cells. Since most KIRs are inhibitory, binding to self-MHC class I facilitates self-tolerance (Figure 5). In virally infected or transformed cells MHC class I molecules are often downregulated leading to reduced inhibitory signals which changes the NK cell balance to a more activated state, and induces lysis of target cells. This mechanism of recognition based on MHC class I downregulation is termed the “missing self” concept¹¹³.

Natural killer group 2 (NKG2) proteins belonging to the c-type lectin family are complexed with CD94 and form heterodimeric receptors which bind non-classical MHC-molecules. NKG2A binding to HLA-E leads to a more inhibited state of NK cells

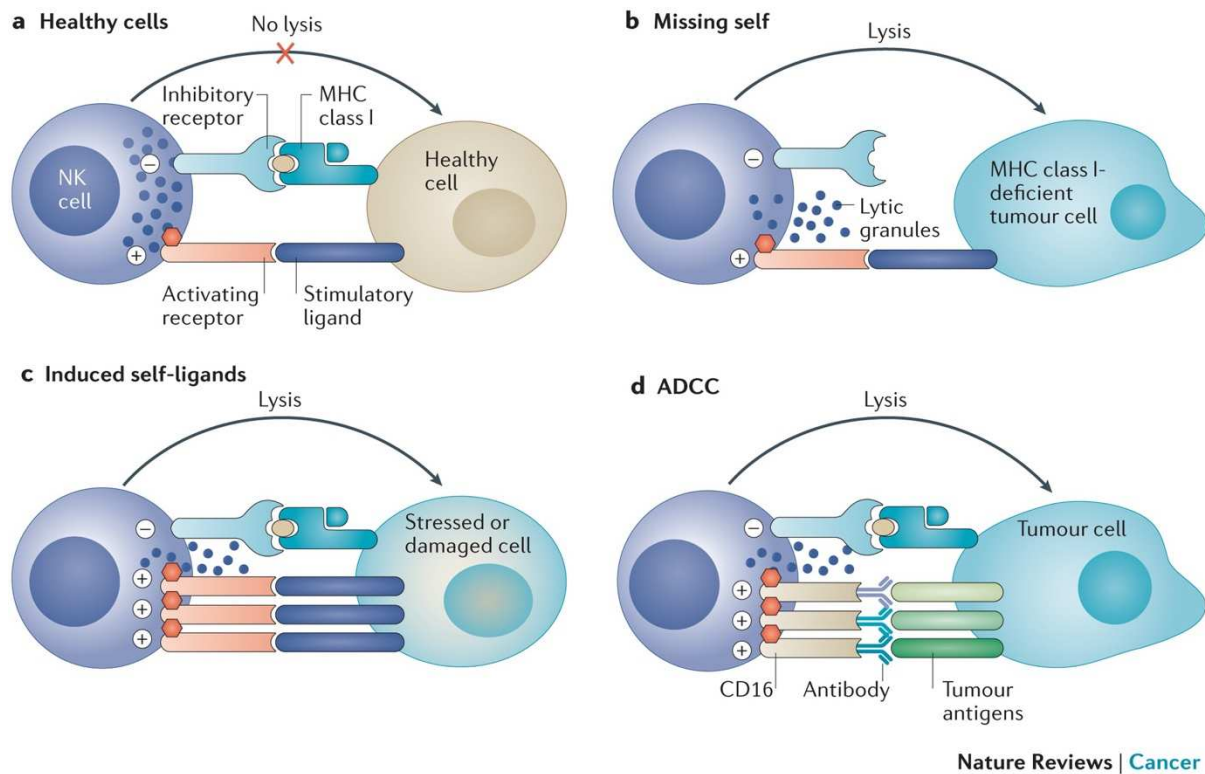
as it contains a cytoplasmic ITIM motif¹¹⁴. In contrast, NKG2C, -E, -H are activating receptors and associate with the immunoreceptor tyrosine-based activation motif (ITAM) containing adaptor protein DAP-12¹¹⁵. NKG2D is also an activating receptor that binds to MICA, MICB and ULBP family in humans, which are upregulated on tumor cells, and induces activation signals through association with DAP-10, independently of CD94¹¹⁵⁻¹¹⁷.

Further, a large variety of receptors are expressed on the surface of NK cells, e.g. natural cytotoxicity receptors (NCRs), CD16, DNAM-1, KLRG1 and PD-1 which bind MHC-independent ligands.

NCRs include NKp30, NKp44, NKp46 which are potent activators of and mediators of NK cell cytotoxicity. NCRs have been shown to bind heparan sulfates on cancer cells and for NKp30 binding to B7-H6 on the surface of tumor cells has been described^{118,119}. Accumulating evidence suggests that further cellular and pathogen-associated ligands are recognized by NCRs but many have not yet been identified^{120,121}.

CD16, the Fcγ receptor IIIA (FcγRIIIA) is predominantly expressed on CD56^{dim} NK cells and allows them to bind to the Fc region of IgG antibodies bound to their specific antigen. Through its association with subunits containing an ITAM, CD16 triggers NK cell activation and induces killing of the antibody-coated target cell, a process known as antibody dependent cellular cytotoxicity (ADCC)¹²².

The combination of signals received through all these receptors fine-tune the functional state of NK cells. Different signals on tumor cells can alter the balance and induce killing, for example when NK cells recognize the missing of self-MHC class I, the upregulation of stress associated ligands, or antibodies bound to tumor antigens (Figure 5).



Nature Reviews | Cancer

Figure 5. Schematic representation of physiological NK cell functions (from Morvan & Lanier¹²³)

In order for NK cells to become functionally competent they have to go through a process referred to as “NK cell education”. Therefore, inhibitory receptors, such as KIRs on human NK cells (Ly49 in mice) and NKG2A need to interact with MHC class I molecules during their development and NK cells that do not interact with MHC I molecules through their inhibitory receptors are found to be hyporesponsive. Different modalities have been proposed, comprising the arming/disarming, cis/trans interaction and rheostat/on-off models to explain how NK cells reach an educated state, allowing them to be balanced in terms of sensitivity to activation and inhibition, and able to eliminate cells expressing reduced levels of MHC class I while maintaining self-tolerance^{124–128}.

In humans, NK cells can be identified by their surface expression of CD56 and NKp46¹²⁹. In the peripheral blood (PB) of humans, NK cells make up about 10% of total lymphocytes and two subpopulations are distinguished based on functional and phenotypic differences (Figure 3). CD56^{bright}CD16^{+/-} (CD56^{bright}) are efficient cytokine producers whereas CD56^{dim}CD16⁺ (CD56^{dim}) show stronger cytolytic capacities, they respectively make up 10% and 90% of total NK cells in PB¹³⁰. However, for tissue

resident NK cells which express CD69 this ratio is altered; for example, in the lymph nodes, colorectum, stomach and liver CD56^{bright} are more abundant than CD56^{dim} NK cells. Further, in lung and breast tumor tissues significantly higher abundance of CD56^{bright} NK cells was shown than in the respective healthy organs¹³¹. A particular subset of NK cells are present in the decidua, which have a CD56^{bright}CD16⁻KIR⁺CD9⁺CD49a⁺ phenotype and are involved in angiogenesis, tissue remodeling and placentation during pregnancy¹³². In mice four populations of NK cells with distinct effector potency are subdivided based on their expression of CD11b and CD27 which mark different developmental stages¹³³.

Élément sous droit, diffusion non autorisée

Figure 3. NK cell CD56^{bright} and CD56^{dim} subsets (A) Flow cytometric analysis (B) schematic representation of phenotype and effector functions (adapted from Cooper *et al.*¹²²). NK receptors (NKR), Lymphokine-activated killer activity (LAK).

At the moment, the developmental relationship of NK cells and NK cell precursors in humans is not fully understood. A NK lineage-restricted CD34⁺CD38⁺CD123⁻CD45RA⁺CD7⁺CD10⁺CD127⁻ precursor has been identified in human bone marrow, tonsil, umbilical cord blood and fetal tissues which can give rise to fully mature and functional NK cells *in vitro* and *in vivo*¹³⁴. And more recently,

CD45⁺CD34⁻CD7⁺CD127⁺CD117⁺CD45RA⁺ ILCPs were described by our lab, which among helper ILC subsets also give rise to NK cells⁸⁴ but it is not clear how these are developmentally related to the CD34⁺ NKP. Further, a long-standing question is whether CD56^{bright} NK cells give rise to CD56^{dim} NK cells¹³⁵. Convincing evidence, like the higher frequency of CD56^{bright} NK cells in the first month after HSC transplantation, longer telomere repeats in CD56^{bright} NK cells and experiments in which sorted CD56^{bright} develop a CD56^{dim} phenotype *in vitro* and in immunodeficient mice, support this precursor-product relationship between CD56^{bright} and CD56^{dim} NK cells^{136,137}. Nevertheless, barcoding experiments in rhesus macaques shows clonally distinct patterns between CD56^{bright} and CD56^{dim} NK cells^{138,139}.

In mice and humans, populations of memory NK cells, which respectively express Ly49H and NKG2C, expand following species-specific cytomegalovirus (CMV) infection, with a clonal-like expansion resulting in a long-lived pool of memory NK cells. These memory NK cells are more potent and show a more efficient response against CMV during re-infection^{140–142}. In addition to CMV, other stimuli, e.g. influenza virus, HIV, haptens and cytokines have been associated with the induction of memory and memory-like NK cells¹⁴². The discovery of memory NK cells with several adaptive immunity characteristic features has blurred the line between innate and adaptive immunity¹⁴³.

ILC 1

Helper-type ILC1s express the TF T-bet and secrete “type I” cytokines like IFN- γ and TNF- α .

In mice the existence of ILC1s which are distinct from NK cells is commonly accepted and murine ILC1s are identified by their Lin⁻NKp46⁺NK1.1⁺CD49a⁺CD49⁻ surface marker expression. The EOMES^{-/-} mouse model in which no NK cells are found in the intestine, but ILC1 levels are not significantly altered provides a proof of concept that two separate lineages of NK cells and ILC1 exist and ILC1s can develop independently of the TF EOMES⁸⁰.

In contrast, the discrimination between ILC1 and NK cells in humans is not as straightforward since TF and surface marker expressions largely overlap between these two populations and currently no ILC1 definitive marker exists. Hence, ILCs are mostly distinguished as Lin⁻ CD127⁺ (IL-7R α ⁺) CRTH2⁻ CD117⁻ “non-ILC2-non-ILC3”

ILCs which bears the risk of contamination with other cell types such as T cells, NK cells and ILC3¹⁴⁴. A single cell transcriptome study of tonsil ILCs demonstrated that most ILC1s sorted based on this combination of markers clustered apart from NK cells, ILC2 and ILC3 in an unsupervised t-SNE analysis. But indeed, the NK, ILC2 and ILC3 clusters were each contaminated with some cells from the ILC1 sorting gate¹⁴⁵. Further, in humans EOMES expression is not entirely discriminatory between ILC1 and NK cells, as some ILC1 like intraepithelial ILC1 (ieILC1), which are different from NK cells in phenotype and function, have been shown to express EOMES¹⁴⁶. Recently, the distribution of ILCs in tissues of healthy donors has been systematically studied and ILC1s (Lin⁻ CD127⁺ CRTH2⁻ CD117⁻ NKp44^{+/-}) were found in every tissue analyzed, including fat, colon, small intestine, lymph nodes, lung and spleen¹⁴⁷. In some human tumors, such as non-squamous cell lung carcinoma and breast cancers, ILC1s have been detected and in gastrointestinal tumor tissue they were found to be more abundant than in para-lesional tissue, but to date their role remains largely unknown^{148,149}. In mice, a study showed that TGF- β can drive conversion of NK cells to ILC1-like, which may be a mechanism of tumor evasion as the ILC1-like cells were unable to control tumor growth and metastasis¹⁵⁰.

ILC 2

Group 2 ILCs have been demonstrated to depend on IL-25 and IL-33. They can secrete large amounts of type 2 cytokines IL-5 and IL-13, thereby contributing to protective immunity against parasites like helminths¹⁵¹. Elimination of helminths relies on the recruitment of eosinophils through type 2 cytokines released by ILC2s in the gastrointestinal tract¹⁵². Different ILC populations express the TF GATA-binding protein-3 (GATA-3), however ILC2s specifically are characterized by high expression of GATA-3. GATA-3 expression is essential for ILC2s and induces CRTh2 expression as well as IL-4, IL-5 and IL-13 production¹⁵³. Moreover, the development of ILC2s is also dependent on the TF retinoic acid receptor (RAR)-related orphan receptor alpha (ROR α)¹⁵⁴. ILC2s reside in peripheral tissues, such as the gut, lung, skin and fat associated lymphoid clusters^{155–158}. ILC2s are involved in different allergic responses including atopic dermatitis and asthma and can also regulate metabolic homeostasis and tissue repair for e.g., in the lung after influenza virus infection^{159–162}. The restoration of airway epithelial integrity after influenza infection has been shown to be

mediated through Amphiregulin, a member of the epidermal growth factor family, that can be produced by ILC2s¹⁶². The presence of ILC2s has been reported in several different tumor types, such as breast, gastrointestinal and prostate cancer^{149,163}. In non-muscle bladder cancer patients, the ILC2s frequency was associated with high levels of IL-13 and correlated with monocytic MDSC, which in turn were associated with shorter recurrence free survival¹⁶⁴. This suggests ILC2s are involved in promoting immunosuppression. However, another study in pancreatic ductal adenocarcinoma patients showed that intra-tumoral ILC2 levels and ILC2-activating cytokine IL-33 were associated with longer survival¹⁶⁵. ILC2s are also involved in the recruitment of eosinophils and studies in mice have shown that specific ILC2 mediated eosinophil infiltration was associated with better tumor control^{166,167}. Consequently, ILC2s may have both tumor suppressive and tumor promoting activities, which is in line with data generated in mouse tumor models, suggesting strong modulations of ILC2 activity by the TME¹⁶⁸.

ILC 3

Group 3 ILCs include two members, lymphoid tissue inducer cells (LTi) and postnatally developing ILC3s, both of which are defined by the production of IL-17 and IL-22 cytokines and whose development and function depends on expression of TF RAR-related orphan receptor γ t (ROR γ t)⁷⁷. LTi arise in the fetus and are indispensable for lymph node and Peyer's patch formation¹⁶⁹. During the initial process of lymph node organogenesis, LTi migrate to the lymph node anlagen where they interact with stromal lymphoid tissue organizer cells. These upregulate adhesion molecules, IL-7, and chemokines leading to the survival, proliferation and differentiation of LTi and recruitment of further LTi as well as B cells, T cells and DCs to populate the nascent lymph node¹⁷⁰.

ILC3s reside in the tonsils, intestinal lamina propria, spleen, decidua, skin, lung and liver of humans^{171–176}. They are involved in the development of cryptopatches and isolated lymphoid follicles, in the maintenance of epithelial barrier functions and protection against bacterial infections¹⁷⁰. A major player in ILC3 function is IL-22, a cytokine which mainly impacts non-hematopoietic epithelial cells¹⁷⁷. The secretion of IL-22 in ILC3 is triggered by IL-23¹⁷¹. IL-22 can induce elevated levels of antimicrobial proteins and mucus associated molecules in epithelial cells subsequently providing

protection against extracellular pathogens, like *Citrobacter rodentium*, a mouse pathogen used as a model for *Escherichia coli* infection of humans^{178,179}. Furthermore, ILC3s are also implicated in plaque formation in psoriasis and inflammatory bowels disease^{180,181}. Human ILC3s show several antitumor properties, for example they have recently been shown to release IFN γ and mediate cytotoxicity upon tumor cell encounter¹⁸². Furthermore, ILC3s at the border of colorectal cancer tissue co-localized with T cells and displayed elevated levels of HLA-DR suggesting their potential in antigen presentation¹⁸³. Along this line, the presence of ILC3s in non-small cell lung cancer has been associated with intra-tumoral tertiary lymphoid structure (TLS) density, a predictor of favorable clinical outcome¹⁴⁸. However, in a study on lymph node metastasis of breast cancers, presence of ILC3 in the tumor correlated with increased metastasis¹⁸⁴. Hence, the impact of ILC3s in tumors may be context dependent.

Unconventional T cells

Unlike MHC-restricted T cells with highly diverse T cell receptors (TCRs) that recognize classical peptide antigens, unconventional T cells recognize lipids, small-molecule metabolites and specially modified peptides, which are not donor restricted and have a more limited receptor diversity¹⁸⁵. Unconventional T cells include natural killer T (NKT) cells, mucosal associated invariant T cells (MAITs), $\gamma\delta$ T cells, CD1-/H2-M3-/Qa-1-/HLA-E-/restricted T cells and TCR $\alpha\beta$ CD8 $\alpha\alpha$ intraepithelial T lymphocytes (IELs)¹⁸⁶.

NKT cells, defined as CD1d-restricted and TCR- $\alpha\beta$ positive T cells in humans are present in blood, spleen, BM, thymus and liver. Invariant NKT (iNKT) cells have a specific TCR- α rearrangement (V α 24-J α 18) while non-classical NKT cells have more diverse TCR- α chains. They can recognize lipids and glycolipids presented on CD1d, a MHC-like molecule expressed on professional antigen presenting cells (APCs) which activates them and induces the production of type I and type II cytokines, that in turn activate other immune cells¹⁸⁷. One prominent ligand of iNKT is the glycolipid α -galactosylceramide which has been shown to mount potent anti-tumor reactivity^{188,189}. MAIT cells are restricted to the MHC-1-related molecule and like NKT cells, express a semi-invariant TCR with V α 7.2-J α 33 for the TCR- α chain and a limited set of V β segments¹⁸⁷. It has been demonstrated that MAIT cells can get activated by vitamin B

metabolites, compounds which are produced by most bacteria and yeast, and thus help to fight off microbial infections^{190,191}.

$\gamma\delta$ T cells possess elements of innate and adaptive immunity. They have similarities to NK cells as most $\gamma\delta$ T cells express NKG2D and some subsets CD16. It has been shown that the latter can induce antibody-mediated IFN- γ production^{192,193}. While their $\gamma\delta$ TCRs are highly variable, the recognition of target antigens is independent of MHC haplotype. As ligand recognition by $\gamma\delta$ TCRs often requires costimulatory signals, this provides a mechanism to prevent harmful self-reactivity¹⁹³. $\gamma\delta$ T cells make up 1-5% of the total T cells in circulation, and show much higher percentages in the epithelial tissues of the skin or the gastrointestinal tract¹⁹⁴. They are involved in the immunosurveillance against many types of tumors and rapidly expand and react in response to invading pathogens by secreting proinflammatory cytokines IFN- γ and TNF- α following activation^{195,196}.

Adaptive Immunity

While the germline encoded PRRs enable rapid sensing and subsequent elimination of pathogens, the range of pathogenic molecular patterns that can be recognized by the innate immune system is limited and hence, not sufficient to safeguard against newly encountered pathogens or mutated PAMPs. Therefore, adaptive immunity offers a very flexible way to achieve a more diverse repertoire of recognition receptors which are highly specific. Characterizing features of adaptive immunity are the capability to produce combinatorially rearranged, antigen specific receptors as well as the establishment of immunologic memory, meaning that a faster and more effective immune response can be mounted upon re-encounter of the same antigen¹⁹⁷. These diverse, antigen specific receptors are the TCRs in T cells and immunoglobulins in B cells and they are generated through a somatic rearrangement mechanism called V(D)J recombination. This process is initiated by the recombination activating gene (RAG) recombinase, a protein complex encoded by RAG1 and RAG2, which introduces DNA-double strand breaks at the flanks of V, D and J gene segments. Thereafter, enzymes of the non-homologous end joining pathway lead to DNA end processing, repair and ligation of the V, (D; only present in some receptor chains) and J gene sets¹⁹⁸. The resulting DNA sequence determines the amino acid sequence of the rearranged receptor and consequently the binding specificity¹⁹⁹. The combinatorial

diversity caused by the different gene sets together with the junctional diversity introduced during the DNA repair and ligation process gives rise to a plethora of antigen receptors with different specificities²⁰⁰. Since this is a randomized mechanism to some degree, also a multitude of self-reactive receptors arises, therefore, the adaptive immune system bears a high risk of autoimmunity. In order to ensure self-tolerance and reduce the risk of autoimmune disorders, the cells go through selection processes before they are fully mature and reactive²⁰¹. In addition, B cells go through affinity maturation, a step that tailors and increases the B cell receptor (BCR) antigen specificity. During an adaptive immune response, there is a strong clonal amplification of antigen-reactive cells which participate in the immune response. After the immune response, this pool of cells contracts and only subsets of antigen-specific cells remain that get maintained as memory cells. Overall, the adaptive immune response is slower than the innate immune system during the primary response but due to the antigen specificity and memory generation it is highly efficient upon re-encounter of the same antigen. Primary and secondary lymphoid organs including the thymus, spleen and lymph nodes are required for adequate development and functioning of the adaptive immune system, and are the structures where both processes are controlled by innate immune cells, particularly DCs^{28,202,203}.

T cells

The effectors of the adaptive immune system are T cells, also called thymocytes, which owe their name to the development in the thymus, where the progenitors that originate from the bone marrow give rise to naïve T cells. CD4⁻ CD8⁻ double negative progenitors undergo TCR rearrangement and become co-receptor CD4⁺ CD8⁺ double positive cells. Through negative selection on thymic DCs, strongly self-reactive clones are removed while positive selection on thymic epithelial cells expressing self-MHC class II and class I generates single positive CD4⁺ or CD8⁺ naïve T cells, respectively^{204,205}. Naïve T cells are released into the periphery and when they encounter their cognate antigen i.e. a peptide presented on the respective MHC molecule, they proliferate and differentiate into effector T cells²⁰⁶. CD8⁺ T cells are cytotoxic and CD4⁺ are so called helper T cells (Th). As ILCs are considered the innate counterpart of T cells, likewise T cells are distinguished by the cytokines they produce. Briefly, Th-1 produce the signature cytokines IFN- γ and TNF- α , Th-2 secrete IL-4, IL-

5 and IL-13, while Th-17 and Th-22 express IL-17 and IL-22^{207,208}. T cells have numerous roles such as elimination of virally infected or abnormal cells (CD8⁺ T cells), and boosting in the immune response against virally infected or abnormal cells (Th-1), parasitic infections (Th-2) and extracellular pathogens like bacteria (Th-17 and Th-22). Once the infection is cleared, the pool of antigen specific T cells contracts and only a fraction of cells remain as memory T cells. These can be maintained over long periods of time, expand very fast and provide more efficient protection upon reinfection²⁰⁹. Especially CD8⁺ T cells are extremely powerful effectors in anticancer immune responses and high abundance of CD8⁺ T cells is associated with favorable outcomes in many cancers²¹⁰⁻²¹². Similar to NK cells, CD8⁺ T cells can exert killing of tumor cells either by degranulation or initiation of apoptosis by binding to death receptors²¹³. However, as a consequence of the immunosuppressive TME most T cells become exhausted, express high levels of inhibitory receptors and are unable to eliminate cancer cells²¹⁴. Blocking immune checkpoint inhibitors with antibodies allows T cells to overcome this exhausted state and enhances anti-tumor reactivity²¹⁵.

Regulatory T cells (Tregs), which are a subset of CD4⁺ T cells make up a separate population. In the thymus these cells undergo a different selection process as they have higher self-reactivity than other T-cell subsets²¹⁶. Tregs are essential to maintain immune homeostasis and prevent autoimmunity by regulating immune cell responses against self-antigens, allergens and commensal microbiota through their suppressor activity²¹⁷. Conversely, in the context of cancers, Treg infiltrated tumors are strongly associated with poor survival rates and further implicated in the resistance to immunotherapies^{218,219}.

Another distinct subset of CD4⁺ T cells are the T follicular helper (Tfh) cells, which differentiate from naïve T cells upon interaction with APCs. The Tfh cells stay in the lymph nodes or spleen, where they provide help to B-cells in the process of antibody affinity maturation²²⁰.

B cells

The main functions of B cells are antibody production as well as T cell activation via antigen presentation and secretion of cytokines. B cells undergo VDJ recombination in a multi-step process giving rise to IgM⁺ immature B cells independent of antigens that exit the bone marrow. While T-cell independent maturation of B cells is possible,

the majority of B cells mature in follicles of secondary lymphoid organs in an antigen-dependent process during which they receive help from Tfh cells^{197,221}. B cells get activated by engagement of the BCR with a cognate antigen and subsequently migrate to the T-B follicle border. If they find a cognate CD4⁺ T cell they receive proliferation signals and divide rapidly²²². The germinal center is divided into two separate areas, one is the dark zone in which the B cells proliferate and go through somatic hypermutation (SHM) that diversifies the BCR by specifically increasing the mutation rate in the targeted regions of *Ig* genes²²³. In the light zone of the germinal center Tfh and follicular DCs aid in the selection of B cells based on the affinity of the BCR. The cycling between these two germinal center zones results in B cell affinity maturation^{222,224}.

Another diversification process of the BCR is the class switch recombination (CSR) in which the constant region of the BCR gets exchanged with another isotype while the specificity of the variable region is kept. Recently, it has been confirmed that in fact CSR mainly occurs already prior to germinal center entry and SHM²²⁵.

In the end, B cells with two different fates emerge from the germinal centers, plasma cells and memory B cells. Plasma cells are long lived antibody (secreted BCR) producing cells that differentiate from high-affinity germinal center B cells allowing a highly efficient antibody response whereas memory B cells preferentially arise from low affinity compartments and provide a pool of cells with broad antigen specificity for recall responses²²⁶.

In many human cancers high intra-tumoral density of B cells is associated with good prognosis. Specifically in TLSs of tumors many B cells were found and these were shown to differentiate into plasma cells and produce antibodies against tumor-associated antigens²²⁷.

The interplay among immune cells and between Innate and Adaptive Immunity

Numerous links exist between the innate and adaptive immune system and this direct or indirect interaction of immune cells with each other is indispensable for certain processes in development, maturation, mounting and regulation of immune

responses. In the following section, some of these bridging elements of the immune system are detailed.

Cytokines and Chemokines

Cytokines are important signaling molecules for the communication between cells with a wide range of actions. Due to the diversity in cytokines, they are broadly described as polypeptide factors typically of the immune system and are thought to act locally. But potentially they can also act at a distance and some are produced by or act on non-immune cells. Cytokines can act in a paracrine (on other cells) or autocrine (on same cell) fashion. Multiple families of cytokines exist that have been grouped on the basis of the structure of cytokines and cytokine receptor and the signaling mechanism²²⁸.

Here, I will take IL-15, which is crucial in the development of NK cells as an example and describe this cytokine in more detail⁸⁵. IL-15 belongs to the “four α -helix bundle” cytokine family and is involved in the development, survival, proliferation and activation of multiple lymphocyte lineages. Secreted IL-15 binds with high affinity to either soluble or membrane bound IL-15R α and this complex binds to the heterodimer receptor composed of the IL-2R β and IL-2R common γ chain²²⁹. In fact, signaling of many interleukins (IL-2, IL-4, IL-7, IL-9, IL-15, IL-21) depends on the IL2R common gamma chain²³⁰. The binding of IL15-IL15R α to the IL-2R $\beta\gamma$ complex induces the Janus-associated kinases (JAK) and signal transducer and activator of transcription (STAT) signaling pathways which leads to cellular activation²²⁹.

Due to their strong immunomodulatory capacity, cytokines have high potential as therapeutic agents while their dysregulation can lead to severe diseases such as cytokine release syndrome^{231,232}.

The family of chemokines, also referred to as chemotactic cytokines, is characterized by signaling through cell surface G protein-coupled heptahelical chemokine receptors. Their central biological role is the mediation and regulation of cell movement, most notably the migration of immune cells, which is essential for functioning of the immune system²³³. In addition, chemokines are also involved in other functions, like cell survival, proliferation, differentiation, activation, polarization and degranulation²³⁴. Chemokines are essential for the recruitment immune cells to the TME, for example cytotoxic T cells and NK cells both express chemokine receptors CXCR3 and CXCR4

which bind to CXCL9/10/11 and CXCL12, respectively²³⁵. In colorectal cancer patients increased CXCL9 and CXCL10 was associated with higher CD8⁺ T cell infiltration of tumors and longer disease-free survival²³⁶.

Antibodies

Antibodies or Immunoglobulins (Ig) are glycoproteins produced by plasma cells that possess antigen specific binding domains²³⁷. As humoral components of adaptive immunity, they get secreted into blood or tissue fluids where they elicit various effector functions of the innate immune system¹⁹⁷. Epitopes are the precise binding sites on antigens that are recognized by the complementarity determining region (CDR) of the immunoglobulin with high specificity and high affinity²³⁸.

Human antibodies are composed of two identical light chains and two identical heavy chains, connected by disulfide bonds which form Y-shaped proteins. Both the light and heavy chains contain a constant region and a variable region. The light chain can belong to either the κ or λ class and the possible heavy chain isotypes are IgA, IgD, IgE, IgG and IgM. Most antibodies exist as monomers, IgA and IgM antibodies can form dimers and pentamers, respectively. While the variable region (fragment variable, Fv) of the antibody that contains the CDR allows the specific binding of a target antigen, the fragment crystallizable (Fc) gets bound by Fc receptors or other immune system components that determine effector functions²³⁹.

Antibodies can contribute to the killing and depletion of microbes or cells that they target in many ways. The opsonization of cells, e.g. tumor cells or pathogens, with antibodies can trigger the classical complement pathway and lead to complement dependent cellular cytotoxicity²⁴⁰. Alternatively, the binding of activating Fc γ receptors (Fc γ R) (CD16A, CD32A, CD64), which are expressed on various innate immune cells, like neutrophils, macrophages and NK cells, to immune complexes (antibodies bound to their antigen) can induce ADCC or ADCP against the target cell. Another mechanism by which antibodies can have an impact without additional effectors is neutralization, for example when antibodies bind to viruses and block cell entry²⁴¹.

Since antibodies can modulate immune responses very efficiently they are excellent therapeutic agents and many are clinically available²⁴², such as IgG isotype monoclonal antibodies. As the affinity to Fc receptors and complement varies between IgG subclasses (IgG1, IgG2, IgG3, IgG4) these are chosen according to the desired

effects of the antibody^{239,243}. Antibodies made for target cell depletion are often IgG1 antibodies whereas those for immune checkpoint inhibitors are mostly of the IgG4 subclass and are made to block the interaction between an inhibitory receptor on immune cells and its ligand²⁴⁴. Furthermore, many different aspects of therapeutic antibodies have been optimized for clinical applications by antibody engineering. To reduce the immunogenicity of antibodies which are largely produced in other animals, humanized antibodies in which only the regions crucial for the binding of the antigen are kept while the rest of the antibody is substituted by domains of a human antibody are now the standard for therapeutic use. Other engineering improvements affect for example, the stability, affinity, solubility and post translational modifications of antibodies²³⁹. Currently, the potential of next generation immunotherapies are being explored, like bi- and tri-specific antibodies designed to bring target and effector cells together²⁴⁵.

Fc Receptors

Fc Receptors (FcRs) have no antigen specificity; however, they can adopt antigen specificity by binding to the Fc portion of antigen specific antibodies. The binding of immune complexes (antigens bound to antibodies) by FcRs can trigger different effector functions, notably ADCC and ADCP, depending on the type of FcR and the cell on which the FcR is expressed^{246,247}. These effects are exploited in antibody therapies that aim at eliminating for example cancer cells, like with anti-CD20 and anti-HER2 monoclonal antibodies^{248,249}. FcRs are grouped according to the antibody isotype they bind and in humans Fc μ R (IgM), Fc α R (IgA), Fc ϵ R (IgE) and Fc γ R (IgG) exist. Based on whether they are associated with an intracellular immunoreceptor ITAM or intracellular immunoreceptor tyrosine-based inhibitory motif (ITIM) some FcR can be subdivided into activating or inhibitory FcRs, respectively. However, exceptions to this categorization exist as some ITAMs have generated inhibitory signals when binding to monomeric Ig. Additionally, some FcR, like FcRn, TRIM21, FcRLs do not fall into the categories of ITAM or ITIM expression and are instead involved in recycling, intracellular trafficking for degradation or antigen presentation and cell differentiation, or induce activation/inhibition through other mechanisms²⁵⁰. The effector response which is induced by FcRs is dependent on the cells types on which

the FcRs are expressed on and the antibody isotypes/subclasses, as these have different binding affinities (Figure 6)²⁴⁶.

Élément sous droit, diffusion non autorisée

Figure 6. Schematic representation of human FcγRs (adapted from Bruhns and Jönsson²⁵⁰) Alleles are identified by the amino acid variant in the protein (e.g. H₁₃₁), or by the name of the allelic variant (NA1, NA2 or SH). *Upper part:* Binding affinities are indicated as K_A (M^{-1}); high-affinity interactions with monomeric Ig are indicated in bold; -, no binding; ND, not determined. *Lower part:* Expression patterns of FcRs are summarized as follows: +, expression; +/-, expression on a subpopulation; [+], inducible expression; ¹, detectable and functional expression in non-conventional *Fcgr2c*-Stop individuals and on a rare subpopulation of CD56^{dim}/FcγRII^{bright} NK cells

The binding affinity of FcRs to antibodies and subsequently the efficiency of the response is further complicated by multiple factors, like polymorphisms in both, FcRs and the Fc of the immunoglobulin^{251,252}. For example, for NK cells, which express the activating receptor FcγRIIIa (CD16a) it has been demonstrated *in vitro* that different IgG1 and IgG3 allotypes efficiently trigger ADCC to various extents but not IgG2 and IgG4 allotypes²⁵¹. Of note, human and mouse FcRs cross-react with immunoglobulins of other species²⁵³. It is further important to take into account that there are striking

differences in the expression pattern of FcRs between mice and humans and the functional ortholog of hFcγRIIA is mFcγRIII and that of hFcγRIIIA is mFcγRI²⁵⁰.

Complement system

The complement system is part of the innate immune system but has links to the adaptive immune system. It is named after its enhancing/ “complementing” effects in clearing microbes by antibodies or phagocytes, promoting inflammation and lysis of pathogens. Furthermore, complement contributes to tissue homeostasis and organ development by mediating clearance of cellular debris, apoptotic cells and immune complexes²⁵⁴. Over 50 different proteins are part of the complement system and while the main source of circulating complement proteins are hepatocytes, some complement components can also be locally secreted by various cells types or expressed in an intracellular or membrane bound form. These proteins mostly exist in precursor states which can rapidly be activated by different molecular patterns, inducing three distinct proteolytic, cascade-like pathways²⁵⁵. The classic complement pathway, the alternative complement pathway and the lectin pathway all converge at the cleavage of the complement component C3^{254,256}. In complement dependent cytotoxicity (CDC), binding of C1q to immune complexes of IgM or hexameric IgG bound to an antigen induces the classic complement pathway. Which eventually leads to the generation of the membrane attack complex (C5b-9) which induces cytolysis by permeabilizing the cell membrane, causing the influx of water, ions and also Ca²⁺ which poisons the cell^{256,257}. As complement can efficiently fix human IgG1 and IgG3 and many therapeutic antibodies are IgG1 based complement may contribute to the anti-tumor responses of antibody therapies. This is supported by a study that associated different complement gene polymorphisms in rituximab treated lymphoma patients with event free survival²⁵⁸.

1.2 Human Immune System mouse models

Tremendous knowledge in immunology has been and is still gained through studying the mouse immune system. However, 65 to 75 million years of evolution separate humans and mice from their last common ancestor and a multitude of differences exist between the human and the mouse immune systems. For example, for NK cells there are different subsets, mice have no KIR receptors, and FcRs have different binding properties^{259,260}. Also, the frequency of different immune cell populations is strongly altered between humans and mice (see Figure 7).

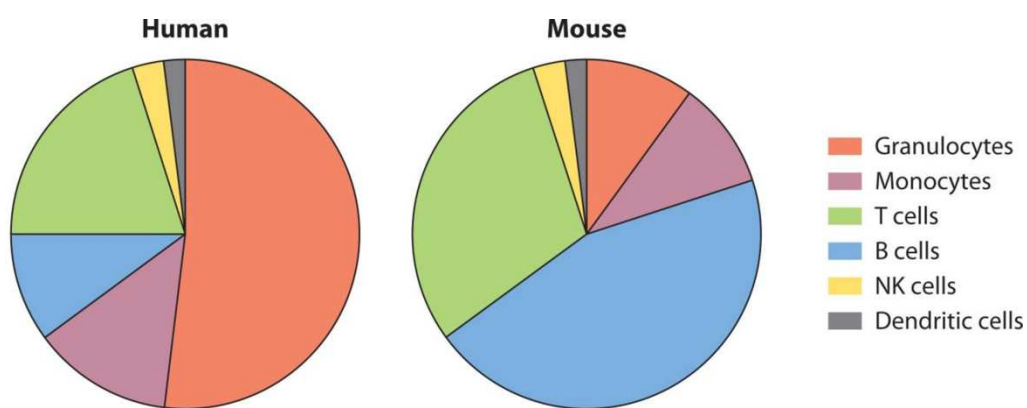


Figure 7. Differences in the immune cell composition in the blood of humans and mice. (from Rongvaux et al.²⁶¹)

So, to better understand the human immune system and improve therapeutic approaches there is a need for ways to study human immune cells in an *in vivo* or *in vivo*-like setting. Human immune system (HIS) mice offer a solution for this.

Basic principles of Human immune system mice

Human immune system (HIS) mice are generated in immunodeficient mice which allow the grafting with human cells or tissues that comprise either hematopoietic stem cells, precursors or mature immune cells. These HIS mouse models serve as valuable preclinical models to test novel therapeutic agents, combinations of drugs and study the elicited immune responses *in vivo*. Moreover, they are useful in studying viral infections with human immune cell tropism (EBV, HIV) and human immune cell development since they offer a way to perform *in vivo* experiments with human cells. Over the last decades, many different variations of HIS mice have been created which

mainly differ with respect to the mouse strain from which they originate, the mutations introduced to cause immunodeficiency and improve grafting and finally in the source and type of human cells that are grafted. All these features entail certain benefits and drawbacks²⁶².

Mouse immunodeficiency is achieved by the severe combined immunodeficiency (SCID) mutation on the protein kinase DNA-activated catalytic polypeptide (Prkdc) gene or the knockout of recombination activating gene (RAG) 1 or RAG2. This results in the lack of V(D)J-recombination and disables the generation of mature B and T cells^{263,264}. In addition, the knockout of the cytokine receptor common gamma chain (IL-2R γ), inhibits the development of innate lymphoid cells, including NK cells^{265,266}. The immunodeficient mouse strains which are currently widely used to generate HIS mice are: NOD.Cg-Prkdc^{scid}Il2rg^{tm1Wjl} (NSG), NOD.Cg-Prkdc^{scid}Il2rg^{tm1Sug} (NOG), and BALB/c Rag2^{tm1Flv}Il2rg^{tm1Flv} (BRG) mice²⁶⁷. In NOD mice better hematopoietic engraftment has been associated with a polymorphism within the SIRP α gene, which is inherent to the NOD strain. This is due to the enhanced binding of SIRP α on macrophages of NOD mice to human CD47, which is a “self-marker” that inhibits phagocytosis by macrophages²⁶⁸. Therefore, SIRP α ^{NOD} was introduced into the BRG mice (called BRGS) and led to similar grafting efficiency as in NSG mice, since the SIRP α ^{NOD}-hCD47 binding inhibits the phagocytosis of the engrafted human cells (Figure 8)²⁶⁹.

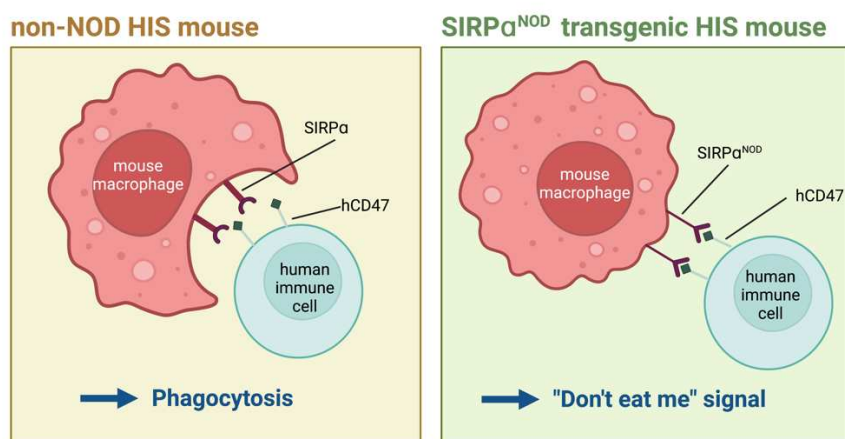


Figure 8. Mechanism of SIRP α -CD47 interaction

Three major approaches exist for the engraftment of mice with a human immune system. (1) They can be injected with peripheral blood mononuclear cells (PBMCs)

which expand *in vivo*, leading to a graft of predominantly mature T cells. However, these T cells are xeno-reactive and induce lethal graft-versus-host disease (GvHD). (2) Human CD34⁺ HSC can be used to establish a human immune system²⁷⁰. These can be obtained from different sources, including umbilical cord blood, fetal liver, bone marrow, and mobilized blood of which the first two result in the highest engraftment efficiency²⁷¹. (3) Bone marrow, liver, thymus (BLT) HIS mice are generated by transplantation of fragments from the human fetal liver and thymus and injection of fetal liver derived CD34⁺ HSCs. These HSCs engraft the mouse bone marrow and give rise to human cells of the lymphoid and myeloid lineage whereas the human thymus implant allows for active T cell education²⁷². If HSCs are grafted the recipient mice usually need to be preconditioned by sublethal irradiation or radiomimetic drugs to free the HSC-niche for the human HSCs^{262,271}.

Even though many different HIS mouse models have been generated, many constraints and limitations exist. These are the restricted availability of fetal tissues, the lack of human specific growth factors and cytokines, low levels of innate immune cells, the suboptimal T cell education in models without a human thymus graft, the poor development of lymphoid architecture, and, the impaired class switching and affinity maturation of B cells²⁶². Nevertheless, these humanized models are constantly being refined to overcome these limitations. For example, in MISTRG mice several human cytokines are expressed leading to enhanced differentiation of innate immune cells (detailed below)²⁷³. In Flk3 knockout BRGS mice (BRGSF) increased numbers of DCs, macrophages and innate lymphoid cells including NK cells were found²⁷⁴. In TSLP expressing BRGS mice (BRGST) an improved development of thymus and lymph nodes could be achieved²⁷⁵. Finally, BRGS mice with transgenic HLAs (BRGSA2DR2) engrafted with HLA-matched HSCs were demonstrated to have a more efficient T cell development²⁷⁶.

Additionally, more complex models have been generated in which the human immune system in the mice is complemented with other human derived grafts, like human hepatocytes or even the human microbiome^{277,278}. Multiple disease models have been set up in HIS mice, including viral infections with HIV, EBV or HBV and tumor grafts^{279–282}.

Studying innate immunity in HIS mouse models

As mentioned above, innate immune cells develop very poorly in most HIS mouse models, they are found only at low frequencies (see Figure 9) and subsets of innate lymphoid cells are not fully functional²⁶¹.

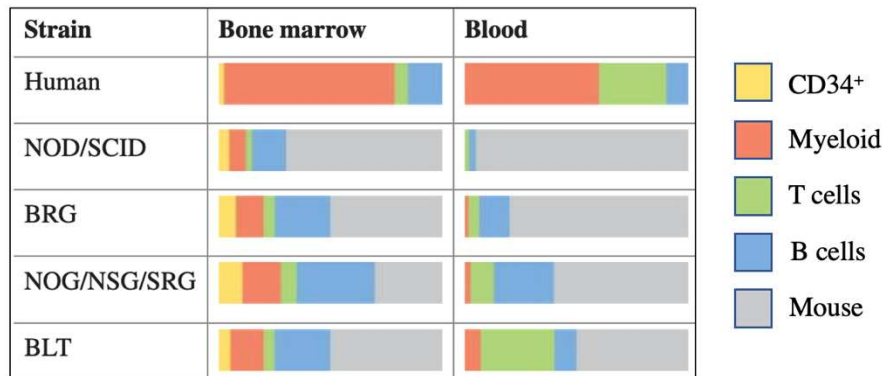


Figure 9. Immune cell compositions in different HIS mouse models compared to human in bone marrow and blood (adapted from Rongvaux et al.²⁶¹)

The reason for this is thought to be the limited ability of mouse cytokines to sufficiently cross-react with the grafted human cells²⁸³. This is supported by the fact that administration or expression of various human cytokines in HIS mice lead to improved development and functions of certain cell populations. For example, higher numbers of more differentiated NK cells were found in HIS mice injected with IL-15-IL-15Ra recombinant protein complex²⁸⁴. In mice that have been hydrodynamically injected with DNA plasmids encoding for macrophage colony stimulation factor (M-CSF) numbers of monocytes/macrophages were increased²⁸⁵. A more targeted way of expression is to knock-in the gene of a human cytokine into the genomic position of the respective mouse gene. This approach has several advantages as it leads to long-term cytokine expression at physiological levels in locations where they are usually expressed. In addition, this gene swap indirectly impairs the mouse cell differentiation and leads to a competitive advantage for the human cells²⁸⁶. Based on these findings, several HIS mouse models have been created in which innate immune cell populations, including NK cells, develop more robustly.

Importantly, when studying innate immune effector functions that depend on Fc interactions in HIS mice, as when testing antibodies, it has to be considered that in most HIS mouse models functional mouse innate immune system components are

present which can bind to Fc regions. Mainly, Fc receptor bearing myeloid cells including macrophages and neutrophils as well as the complement system are retained in many models. However, FcγR deficient HIS mice on NOG and NSG strains have been created^{287,288}.

hIL-15 transgenic HIS mice

Up to date, several human IL-15 transgenic HIS mouse models have been generated including NOG-IL15, SRG-15 and NSG-Tg(Hu-IL15) mice^{289–291}.

The NOG-IL-15 model is based on the NOG strain whereby the human IL-15 transgene has been introduced into the genome under the control of a CMV promoter, resulting in abundant hIL-15 levels in plasma. In these mice, NK cells purified from peripheral blood can expand in the first month, transiently reaching cell numbers in the order of magnitude of 10^6 NK cells/ml of blood. The grafted NK cells maintain cytotoxic capacities, although at lower levels compared to blood NK cells they can delay tumor growth *in vivo*²⁸⁹. The NOG-hIL-15 Tg model has also been combined with a model deficient in *Fcer1g* and *Fcgr2b* genes which eliminates activating (FcγRI, III, and IV) and inhibitory (FcγRIIB) mouse FcγRs. In the NOG-FcγR^{-/-}-hIL-15 Tg mice engrafted with human NK cells ADCC mediated by human NK cells can be segregated from mouse cell mediated ADCC in an *in vivo* assay of tumor transplantation combined with tumor cell depleting antibody treatment²⁸⁸. Caveats of this model are the restricted timeframe, as NK cells start to decrease after 5 weeks and are rare after 8 weeks. In addition, only pure, peripheral blood derived NK cells have been shown to graft, so this setting does not allow study NK cell responses in the context of other human immune cells.

SRG-15 are BALB/c x 129 Rag2^{-/-} Il2rg^{-/-} mice with a human SIRPα and a human IL15 knock-in in were grafted with human CD34⁺ cells and developed human myeloid, T, B and NK cells. Compared to NSG mice, NK cell numbers in blood and spleen were significantly increased as well as the numbers of ILC1s and ILC2s in spleen and liver. Phenotypically, CD56^{dim}CD16⁺ NK cells from SRG-15 mice have very similar NK cells marker expression to human CD56^{dim}CD16⁺ NK cells. Furthermore, in SRG-15 mice more K562 cells were eliminated compared to NSG mice and tumor volumes were lower in an ADCC *in vivo* assay with Raji cells and Rituximab²⁹⁰.

Most recently, the NSG-Tg(Hu-IL15) model was created by introducing a BAC with the entire human IL15 gene. This model has lower serum IL-15 levels than the SRG-15 model, which is closer to the serum levels in humans. In the NSG-Tg(Hu-IL15) mice CD34⁺ cells graft efficiently with significantly higher NK cell numbers, especially the CD16⁺ NK subsets. The NK cells of NSG-Tg(Hu-IL15) mice were shown to have similar ex vivo killing ability as human peripheral blood NK cells. Upon engraftment with a patient derived xenograft (PDX) melanoma, the tumor volume increased significantly slower in the NSG-Tg(Hu-IL15) mice compared to NSG mice and depletion with an anti-NKp46 antibody demonstrated that NK cells contributed to the observed delay in the PDX melanoma growth kinetics²⁹¹.

In summary, the latter models both allow efficient grafting of HSCs and show better NK cells numbers and function than NSG mice so they provide interesting preclinical models to study NK cell responses in the presence of additional immune cells. Nevertheless, in the NOG-FcγR^{-/-}-hIL-15 Tg mice antibody mediated NK cell responses can be studied while precluding the contribution of mouse FcγRs.

MISTRG mice

In MISTRG mice human M-CSF, IL-3, granulocyte-macrophage colony stimulating factor (GM-CSF) and thrombopoietin genes are knocked-in to the respective locus in the mouse genome in *Rag2*^{-/-} *Il2rg*^{-/-} 129×Balb/c (N2) mice and bear human SIRPα as a transgene on a bacterial artificial chromosome²⁷³. In HIS mice human M-CSF expression has been demonstrated to increase numbers of monocytes/macrophages in various tissues and augment their function²⁰⁴. The knock-in of IL-3 in combination with GM-CSF supports the development of alveolar macrophages²⁰⁷. Furthermore, thrombopoietin enhances maintenance of functional human HSCs^{286,292,293}. Fetal liver derived CD34⁺ HSCs have been shown to graft in humanized MISTRG mice as efficiently as in NSG mice but resulted in much higher human CD33⁺ myeloid cell numbers compared to NSG. In MISTRG mice, three subsets of monocytes (CD14⁺CD16⁻, CD14⁺CD16⁺ and CD14^{dim}CD16⁺) likewise to humans are present. The CD14⁺CD16⁻ and CD14⁺CD16⁺ subsets are able to produce TNFα and IL-6 *in vitro* and *in vivo*. Further, they can phagocytose *E. coli in vitro* and it has been shown that hIFN-β expression in the lung was increased upon influenza infection. In addition, NK cell numbers are also increased in MISTRG mice compared to NSG mice and are

functional, as they are able to degranulate, specifically lyse HLA class I negative cells and produce IFN γ following *Listeria* infection. The enhancement of NK cells is most likely due to the trans-presentation of IL-15 on IL-15R α as mRNA for both is expressed in CD33 $^+$ human myeloid cells, especially in the CD14 $^+$ CD16 $^+$ subset²⁷³.

Up to date several *in vivo* differentiation studies and disease models have been set up in MISTRG mice, for example an HIV model and patient derived xenograft (PDX) models of myelodysplastic syndromes, which do not graft well in other available mouse models^{294–296}. A drawback in these mice is the progressive destruction of mouse RBCs which leads to anemia within a few weeks post grafting, precluding long term studies. However, this obstacle can be delayed by not irradiating the mice prior to engraftment or reducing the cell numbers of engrafted fetal liver CD34 $^+$ HSCs or using adult human CD34 $^+$ HSCs²⁷³.

BRGSF mice

BRGSF mice have been generated by backcrossing BRGS mice with BRGF mice which are BRG-based mice with a *fms*-like tyrosine kinase 3 (Flt3) knock out²⁷⁴. BRGF mice mainly exhibit reduced numbers of mouse cDC and pDC in spleen and bone marrow. In humanized BRGF mice that are boosted by injections of human Flt3L, cell numbers and percentages of cDC and pDC are significantly increased and they produce high levels of IFN α , RANTES, IL-12 and TNF α after stimulation with CpG, PolyIC and R848, respectively. Furthermore, the NK cells and T cells are increased as well in Flt3L boosted BRGF mice²⁹⁷. In the combined BRGSF model, in addition to the DCs also monocytes are significantly increased the bone marrow and spleen of Flt3 boosted HIS mice. Further, NK cells are not only increased in numbers but also show higher degranulation and higher IFN γ production following poly (I:C) stimulation. In addition, the development of ILCs is enhanced in Flt3L boosted BRGSF mice with higher numbers and/or percentages found in spleen, lung, liver and gut. In the liver an ILC1 population distinct from NK cells was found, in the lung an ILC2 population and an ILC3 population in the gut which are more abundant in Flt3L boosted mice and capable of producing IFN γ , IL-13 and IL-17, respectively²⁷⁴. One disadvantage of this model is that the Flt3L has to be administered to the mice by multiple injections.

1.3 Anti-Tumor Immune Responses

General and EBV-associated prevalence of cancer

Based on the GLOBOCAN 2020 estimates by the International Agency for Research and Cancer an incidence of 19.3 million new cases of cancer worldwide occurred in 2020 and almost 10 million people died from cancer. In females, 24.5% of the new cases are breast cancers and in males the two most common cancers are lung cancer with 14.3% and prostate cancer with 14.1% of the cases, respectively. Across sexes female breast cancers (11.7%), lung cancers (11.4%) and colorectal cancers (10%) have the highest incidences with lung cancers causing the highest mortality (18%). There are major differences in the cumulative risk between the age of 0 to 74 years of cancer incidence between different areas of the world. In men as well as in women there is a higher risk in areas with a high or very high human development index (HDI) compared to areas with a low or medium HDI²⁹⁸. In the WHO report on cancer of 2020 distinct regional differences can be seen in the proportions of cancer attributable to infectious agents²⁹⁹. The Epstein Barr virus (EBV) is such an infectious agent which is associated with multiple malignancies. A study that compiled data of malignancies which are relatively highly associated with EBV (nasopharyngeal carcinoma, gastric carcinoma, Hodgkin lymphoma, Burkitt lymphoma, diffuse large B-cell lymphoma, nasal type of extranodal NK/T-cell lymphoma) estimated that among these malignancies 239,700 to 357,900 of the new cases and 137,900 to 208,700 of the deaths worldwide were EBV-related in 2020. So the EBV-related cases considered in the referred study make up 1.3-1.9% of the total worldwide incidences³⁰⁰.

Carcinogenesis, hallmarks and risk factors of cancer

Cancer is a disease in which cells proliferate in an uncontrolled manner and have the ability to invade other tissues³⁰¹. During carcinogenesis normal cells undergo genetic alterations in a multistep process and progressively evolve to a malignant state^{302,303}. A set of functional capabilities, the hallmarks of cancer, which are acquired during this process have been proposed to be crucial for the formation of malignant tumors and are common for the cellular phenotype of all types of cancers³⁰²⁻³⁰⁴. Currently the hallmarks comprise: sustaining proliferative signaling, evading growth suppressors, resisting cell death, enabling replicative immortality, deregulating cellular metabolism,

inducing of accessing vasculature, avoiding immune destruction, and activating invasion and metastasis. In addition, some cancer “enabling” traits have been identified, such as genome instability and mutation, tumor-promoting inflammation and non-mutational epigenetic reprogramming³⁰⁴.

Tumors are classified according to the cell type they arise from. For example lymphomas are derived from cells of the immune system and can be further distinguished by the specific immune cell type they originate from³⁰⁵.

The probability to develop cancer is influenced by different aspects, including an individual’s genetic predisposition, lifestyle, e.g., diet, physical activity, alcohol consumption, smoking, exposure to carcinogens and other exogenous factors like infections by pathogens^{301,306,307}. Genetic predisposition is mainly determined by inherited mutations that alter DNA repair, cell-cycle regulation and cell-death pathways³⁰⁶. Persistent infections with pathogens can induce cancer and three major mechanisms have been proposed on how infectious agents cause cancer. One is by chronic inflammation, which leads to increased cell proliferation, DNA, protein and membrane damage and consequently to changes in gene expression. Secondly, virus induced transformation through expression of active oncogenes in combination with inhibition of tumor suppressors which stimulates mitosis, for example in EBV associated malignancies. The third mechanism is the causation of immunosuppression like in the case of HIV infection which leads to a compromised immune control of aberrant cells³⁰⁸.

Anti-tumor immune responses

In humans, many mechanisms are in place to avoid the emergence of cancer, among them tumor suppressor genes which have functions such as inhibition of cell proliferation and induction of apoptosis. Furthermore, cancer immunosurveillance by innate and adaptive immunity eliminates cells which show abnormalities³⁰⁹. Yet, a dual role of the immune system in cancer development has been described with involvements not only in host protection but also in the facilitation of tumor escape. Therefore, the concept of immunoediting was introduced which comprises the 3 sequential phases of elimination, equilibrium and escape^{310,311}.

During the elimination phase the immunosurveillance may start with the recognition of transformed cells by innate immune cells including NKT, NK and $\gamma\delta$ T cells that kill

tumor cells, release IFN- γ and recruit further immune cells³¹⁰. These events are proposed to lead to the induction of the so-called cancer-immunity cycle which describes the uptake and processing of tumor cell debris by DCs which traffic to the lymph nodes where they present the tumor antigens to T cells³¹². Tumor antigens are classified into tumor-specific antigens (TSA) which are exclusive to tumors, such as proteins derived from mutated sequences or viral oncogenes, and into tumor associated antigens (TAA) which exist on other cells and are overexpressed on tumors³¹³. Tumor antigen specific T cells get activated through DC-T cell interactions, T effector cells traffic back and contribute to the immunosurveillance by eliminating transformed cells³¹². According to the immunoediting concept, this leads to an equilibrium whereby the transformed cells are kept under control. Nevertheless, during the equilibrium phase selective pressure may favor immunotolerant tumor variants which evade the immunosurveillance leading to the progressive outgrowth of malignant cells in the escape phase³¹¹.

Inferred from the characteristics of tumors and their microenvironment it has been recognized that tumor cells have different escape mechanisms. For example, some tumors downregulate MHC class I molecules to decrease antigenicity and become undetectable for the immune system³¹⁴. Some tumors become resistant to the signals of the immune system, e.g. tumors unresponsive to IFN- γ ³¹⁵. Further, tumors can upregulate ligands of immune checkpoint inhibitors like PD-L1 that binds to PD-1 on immune cells that effectively silence the cancer fighting immune cells^{316,317}.

These mechanisms can lead to “cold” (immune excluded) or “hot” (inflamed) tumors which differ in the composition of their TME. The TME encompasses immune cells, fibroblasts, blood vessels, extracellular matrix and signaling molecules³¹⁸. An array of different immune cells are found in the TME and while tumor infiltrating lymphocytes (TILs), are associated with positive clinical outcome, Treg cells, TAMs which are the most abundant immune population in the TME and MDSC are poor prognostic factors and associated with an immunosuppressive state^{319–323}.

Plenty of evidence exists that NK cell are involved in the anti-tumor response and their roles during this process of cancer initiation and progression are detailed in the cancer-natural killer cell immunity cycle³²⁴ (Figure 10).

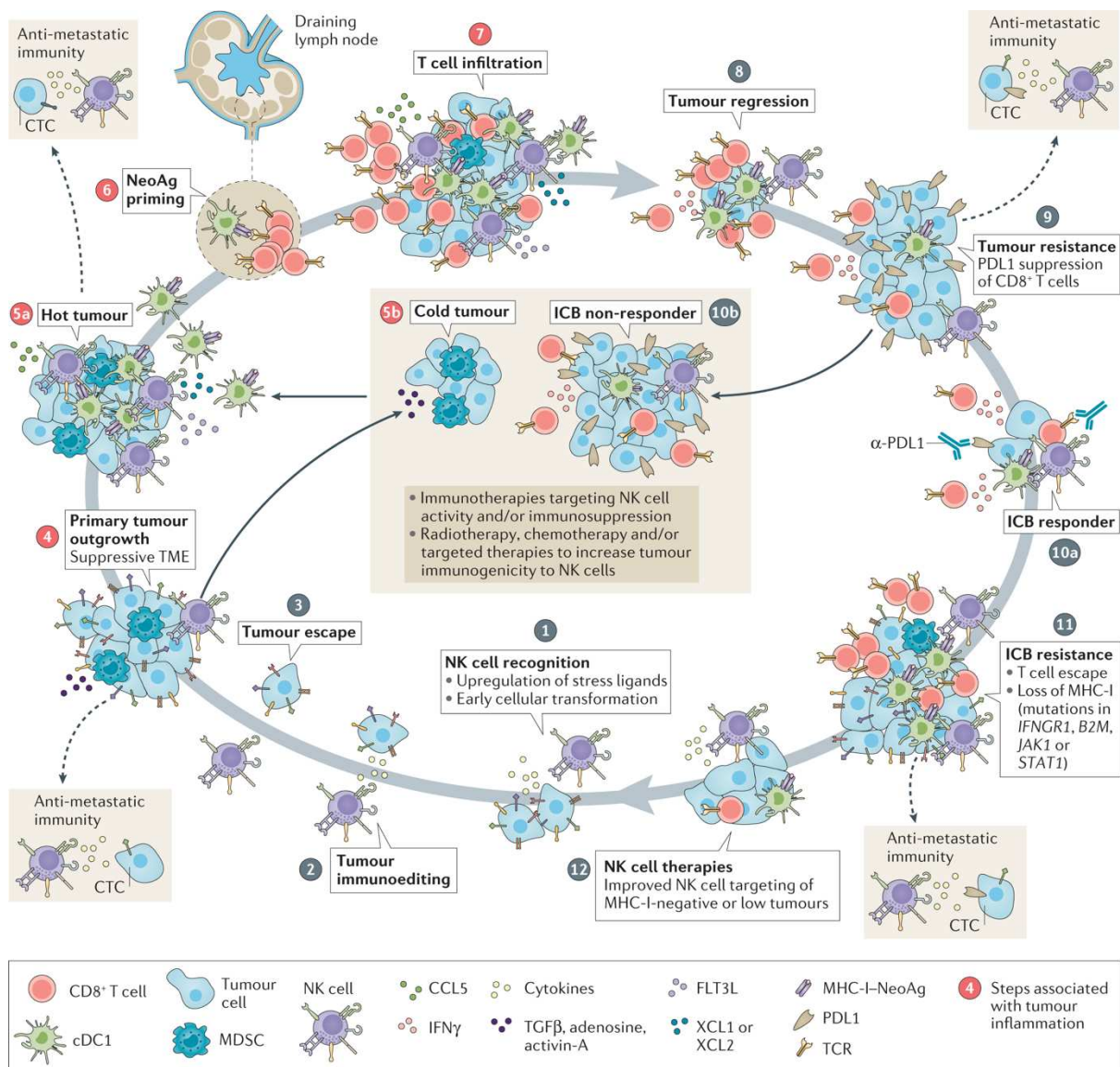


Figure 10. The cancer-natural killer cell immunity cycle (from Huntington et al.³²⁴)

As NK cells have mechanisms to recognize and eliminate transformed cells and predominantly kill sensitive cells, they are thought to be among the first cells involved in immunosurveillance and tumor immunoediting. Upon activation NK cells can release chemokines (e.g. XCL1 and XCL2) and cytokines which may result in “hot” tumors due to immune infiltration and activation^{325,326}. In this way they contribute further to elimination and tumor regression by coordinating antigen presenting DCs and effector cells like cytotoxic T cells. Further, NK cells have the capability to recognize cells with lower abundance of MHC class I molecules and can counteract the immune escape form T cells¹¹¹. In a preclinical model, the lack of NK cells is associated with higher burden of metastasis, consequently NK cells are likely also involved in the elimination

of metastatic cells which potentially evade at any point of the cancer- immunity cycle^{324,327,328}.

Modeling human anti-tumor immune responses *in vivo*

To model human tumors in mice, the transplantation of either human tumor cell lines or tumor biopsies of patients into immunodeficient mouse models are currently the main options. While human tumor cell lines graft robustly, they also show a more homogeneous, undifferentiated histology which is less representative of human cancers than PDX in which morphological and molecular markers are better retained. In addition, tumor cell lines lack human stromal and immune cells, which make up the tumor microenvironment. However, a disadvantage of PDX models is the variability in grafting efficiency^{329,330}. Besides the type of xenograft, the anatomical location has to be considered when generating tumor models *in vivo*, since the tumor cells can be introduced in an orthotopic or an ectopic way. For a mouse colon cancer model it has been demonstrated that the injection of the same tumor cells either into the colon wall or subcutaneously led to significant differences in the frequency of several infiltrating immune cell populations³³¹.

When directly grafting primary PDX, they may include some stroma and the immune cells of the pre-existing infiltrate can be studied. However, solely using a primary PDX model does not allow to study the recruitment and impact of leukocytes outside of the tumor^{330,332}. So, to study the human immune response, these tumor models have to be combined with HIS mouse models. The simplest method is to engraft immunodeficient mice with tumor cells and PBMCs from the same patient, which provides an autologous model. However, due to the PBMCs, such a model will develop GvHD within a few weeks³³². Yet, it has been shown in HLA transgenic “HUMAMICE” that in mice humanized with HLA-matched human PBMCs no signs of GvHD were evident for 3 months³³³. Therefore, longer studies of anti-tumor responses could be possible in such HLA-matched models. Another approach is the humanization of immunodeficient mice with CD34⁺ HSCs and later engraftment with PDX tumors. However, these are mostly allogeneic models in which the human immune system may cause not only anti-tumor effects but also xenograft-allograft rejection^{334,335}.

Recently, a novel HIS mouse model has been described which spontaneously develops B-cell acute lymphoblastic leukemia (B-ALL) due to retroviral transduction of

the CD34⁺ cells with a leukemia-associated fusion gene. This provides new opportunities to study autologous anti-tumor responses *in vivo* and the B-ALL cells from this model can further be transplanted into HIS mice with an autologous immune system³³⁵.

Human tumor models in mice allow *in vivo* testing of therapeutic agents and especially in combination with a human immune system they provide important pre-clinical model to test immunotherapies³³⁶. Notably, PDX models can also be used as a tool in personalized medicine since the efficacy of different therapies for a patient-specific tumor can be tested³³⁷.

Epstein Barr Virus – an oncogenic pathogen

The Epstein Barr Virus (EBV), also known as human herpes virus 4, is a double stranded DNA virus belonging to the human γ -herpesvirus subfamily³³⁸. Primary infection with EBV is usually asymptomatic but can occasionally cause infectious mononucleosis, which is characterized by pharyngitis, cervical lymph node enlargement, fatigue and fever. Most frequently such symptoms are reported in adolescents and young adults^{339,340}. The prevalence of EBV is very high in adult populations with more than 90% of individuals found to be seropositive for EBV specific antibodies^{341,342}. EBV is thought to be transmitted mainly by saliva and it has been proposed that it is shed there by lytically infected epithelial cells³⁴³. EBV can infect B cells as well as epithelial cells, T cells and NK cells^{344–346}. Cell entry is facilitated by viral envelope glycoproteins (gp) and relies on target cell specific mechanisms³⁴⁷. Attachment to B cells is mediated by gp350 which binds the B-cell specific complement receptor (CR2 or CD21) with high affinity³⁴⁸. It can also bind CR1 (or CD35) expressed on B cells³⁴⁹. Subsequently, fusion is triggered by the interaction of gp42 with HLA class II. Together with highly conserved glycoproteins within the herpesvirus family, namely gH/gL, a core fusion machinery is formed and the interaction with the gB leads to direct fusion with the plasma membrane^{350,351}. Generally, EBV establishes a lifelong persistent infection which is mostly asymptomatic in healthy individuals³⁵². In contrast to some new-world monkeys like cotton-top tamarins, common marmoset and owl monkeys and even rabbits which can experimentally be infected, humans are the only natural hosts of EBV^{353–357}.

Already the first description of EBV, which dates back to *in vitro* cultures of Burkitt lymphoma cell lines established in 1964 by Epstein, Achong and Barr³⁵⁸, points towards a link between EBV and tumorigenesis. Indeed, EBV was the first virus shown to cause cancer in humans. It is associated with various human cancers such as Burkitt, Hodgkin's and diffuse large B cell lymphoma originating from B cells, nasopharyngeal carcinoma originating from epithelial cells and T/NK cell lymphoproliferative disorders. Some lymphoproliferative disorders arise primarily in immunosuppressed individuals, mainly in post-transplant or HIV-infected patients³⁵⁹. These malignancies express distinct patterns of EBV latency genes encoded by the viral genome, termed Latency Programs I, II and III. Latency I is characteristic for Burkitt's lymphoma, while Latency II is found in Hodgkin's lymphoma, and Latency III genes are expressed in nasopharyngeal carcinoma and T/NK cell lymphoma and immunodeficiency related lymphomas³⁶⁰.

Further, EBV can infect mature, resting B cells *in vitro* and efficiently transform them into activated, proliferating B-lymphoblastoid cell lines (B-LCL)³⁶¹. B-LCL show high expression of B cell activation markers, like CD23, CD30, CD39 and CD70³⁴⁰ and display Latency III by expressing Epstein Barr nuclear antigen (EBNA) -1, -2, -3A, -3B, -3C, -leader protein (LP), Latent membrane protein (LMP) -1, -2A, -2B, Epstein-Barr virus encoded RNA (EBER) -1, -2, and BART RNA³⁶². This *in vitro* infection system together with the ability to genetically engineer the viral genome has allowed to decipher the roles of the different latency genes in the EBV-induced B-cell transformation process. Five of these latency genes, EBNA-2, -3A, -3B, -LP and LMP1 have shown to be essential for efficient B-cell transformation but also other latency antigens and non-coding RNAs are involved³⁶³. Manifold mechanisms of EBV latent transcripts, associated with growth transformation, causing aberrant cell proliferation have been identified and the major processes are depicted in Figure 11.

Taken together, *in vitro* infection of B cells with EBV provides a simple and efficient method to generate immortalized B-LCLs from various donors as desired. These B-LCL may be used as tumor models and most closely resemble B lymphoproliferative states in immunosuppressed patients, as their outgrowth is also initiated in the absence of T cell immunosurveillance and they share the latency III program³⁶⁴.

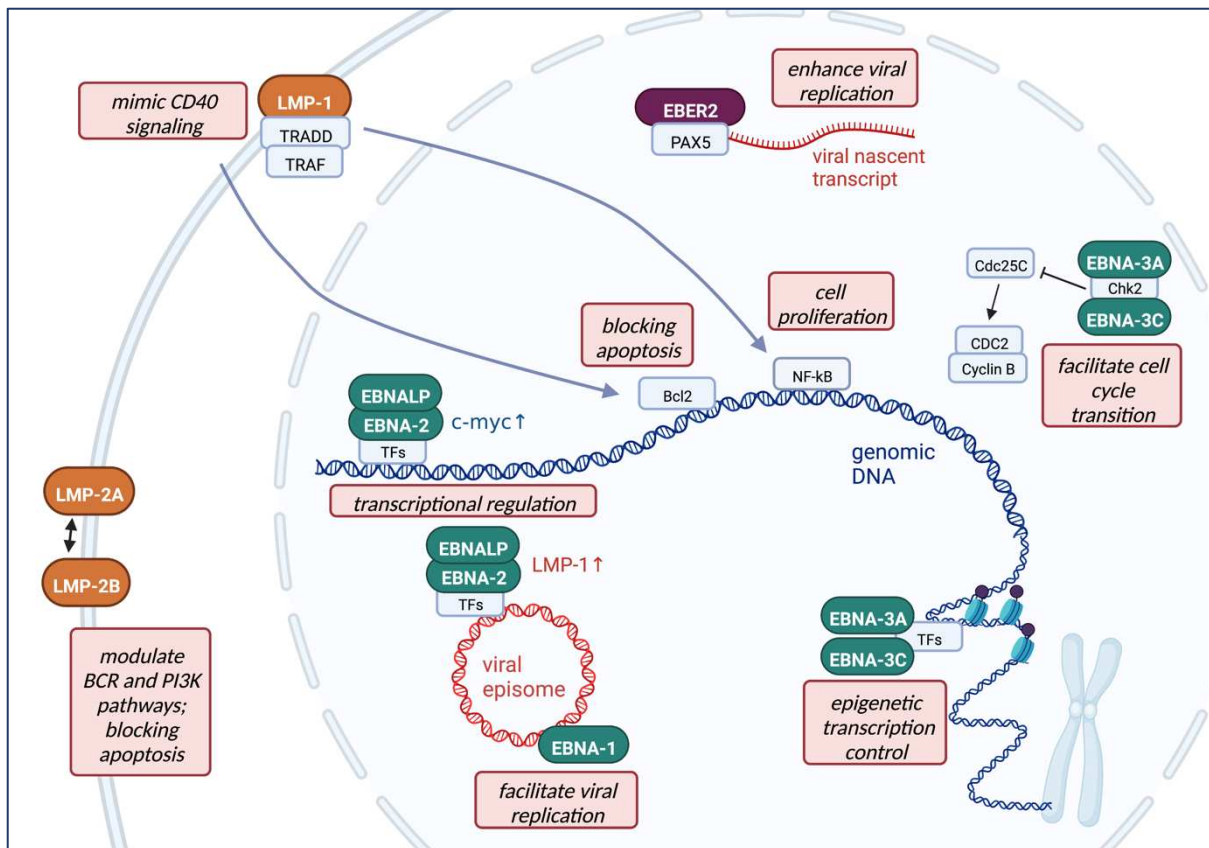


Figure 11. EBV oncogenic mechanisms (adapted from Saha and Robertson³⁶³) – Latent membrane proteins (orange), Epstein-Barr nuclear antigens (green) and Epstein-Barr virus encoded RNA (purple).

Classic cancer treatments and novel immunotherapies

Conventional methods to treat cancer include the surgical removal of tumors as well as radio- and chemotherapy, the latter induce strong DNA damage that leads to cell death³⁶⁵. These methods exhibit significant efficacy in eliminating primary tumors but tumor recurrence remains as a frequent problem which requires alternative strategies³⁶⁶.

In the last decades immunotherapies have revolutionized cancer treatment through approaches that enhance anti-tumor immune functions, for example by implementing cytokines, therapeutic antibodies, immune checkpoint inhibitors, cancer vaccines and cell based therapies³⁶⁷.

In the tumor microenvironment the presence of certain cytokines may be beneficial but others can have disadvantageous effects, e.g. by augmenting cytotoxic activity of immune cells or promoting tumor cell survival. Hence, cytokine and anti-cytokine approaches may provide effective cancer therapies³⁶⁸. Recombinant IL-15 (rIL-15) has

been tested in clinical trials to enhance NK and T cell responses and indeed, NK and T cell populations were expanded in patients³⁶⁹. In some patients a disease stabilization but no objective clinical response was observed³⁷⁰. Further, several IL-15/IL-15R α complexes which have greater bioavailability and stability than soluble rIL-15 are currently in clinical trials³⁷¹. N-803, a IL-15/IL-15R α complex fused with a hlgG1-Fc domain, showed promising results in clinical trials and mainly increased NK cell numbers. When N-803 was added to the therapeutic regimen in combination with either Bacillus Calmette-Guerin in non-muscle invasive bladder cancer (NMIBC) or with anti-PD-1 antibody in non-small cell lung cancer (NSCLC), some patients that had previously been unresponsive showed disease control^{371–373}.

Monoclonal antibodies (mAB) have become a main component of cancer therapy due to the diversity of their clinically relevant mechanisms of action. Clinical applications include direct tumor targeting, tumor microenvironment targeting, immune checkpoint inhibitor blocking, and antibody-drug conjugates. Tumor targeting antibodies are either directed against antigens which are unique or overexpressed on tumor cells. They can cause cell death by blockade of growth factor receptor signaling (e.g. anti-EGFR, anti-HER2) or indirectly by inducing ADCC, ADCP and CDC (e.g. anti-CD20)²⁴³. Various studies *in vitro*, in mice, as well as in patients, indicate that all three mechanisms (ADCC, ADCP and CDC) may be involved in the depletion of CD20⁺ tumor cells by the Rituximab^{374–376}. Rituximab is a chimeric mAB against the CD20 antigen which has been approved for therapeutic use more than 25 years ago. In numerous clinical trials it has been shown to improve prognosis of B cell lymphomas³⁷⁷. Recently, the blocking of checkpoint inhibitors through antibodies binding either to the inhibitory receptor or to its ligand has gained attention with the main focus on cytotoxic T-lymphocyte antigen-4 (CTLA-4) and programmed cell death protein 1 (PD-1). CTLA-4 and PD-1 act as negative regulators of effector cell functions when they are bound by their specific ligands³⁷⁸. Multiple antibodies against either PD-1, which is expressed on activated T cells, NK cells and other cell types, or against the programmed death ligand 1 (PD-L1) which is overexpressed in certain tumors, have been shown to disrupt the PD-1 pathway and enhance effector cell functions. They have made it to the clinic and are approved for the treatment of many different cancer types^{379,380}.

Moreover, antibody engineering has led to the generation of more complex formats, for example tri-specific killer engagers which are designed to mediate and improve specific anti-tumor NK cell responses. They bind to the activating CD16 receptor on

NK cells as well as to a tumor specific antigen and in addition induce NK cell expansion through a IL-15 moiety³⁸¹.

Another approach to fight cancer is by vaccination, which may be applied preventively or curatively. Cancer vaccination has the aim to stimulate the adaptive immune system against specific antigens, which can be mutant sequences, cancer or viral antigens to inhibit the emergence of tumors or to induce tumor regression^{382,383}. Especially personalized vaccines against patient-specific neoantigens are becoming feasible owing to new technologies and are currently being explored with some first trials in patients³⁸⁴.

A further research area with a large potential in cancer treatment is adoptive transfer of immune cells, mainly of endogenous or engineered T and NK cells. An important difference is that T cells have to be produced from autologous cells as they cause GvHD when binding to foreign antigens³⁶⁶. To generate tumor antigen specific chimeric antigen receptor (CAR) T cells, T cells are collected from the patient, purified and transduced with the CAR via a viral delivery vector³⁸⁵. In contrast, allogeneic NK cell infusions are not associated with severe reactions like GvHD. In fact, better responses are achieved in allogeneic stem cell transplantation when KIR genes were mismatched³⁸⁶. This makes NK cells better candidates for “off-the-shelf” products and current approaches are to retrieve them from umbilical cord blood, peripheral blood, established NK cell lines or differentiate them from induced pluripotent stem cells (iPSCs)^{387–390}. As for T cells, tumor specificity can also be achieved by introducing CARs into NK cells³⁹¹.

1.4 State of the Art

Cancer is a leading cause of death and worldwide one in five people are estimated to develop cancer during their life time. Immunotherapeutic agents have proven clinical efficacy and represent an important treatment for cancer patients. In recent years, NK cell-based cancer immunotherapies have gained considerable attention. However, cancer immunotherapy is associated with variable clinical responses and only a minority of patients experience a lifelong cure from it.

The development of pre-clinical tumor models that resemble human immunity and reliably predict treatment effects is currently a major challenge for progress in cancer immunotherapy. HIS mouse models co-engrafted with human tumors enable to recapitulate anti-tumor immune responses and test therapeutic agents *in vivo*. At present, a range of different HIS mouse and tumor models is available. Nevertheless, several limitations, such as (1) restricted development of mature myeloid and NK cells, (2) confounding effects of mouse immune components like Fc receptors and (3) allogeneity between immune and tumor graft are inherent to many of these human immuno-oncology models. In some models these constraints have been resolved. Myeloid and NK cell development could clearly be enhanced by administration or transgenic expression of human cytokines in HIS mice. The deficiency of mouse FcγRs abrogates the antibody mediated effects of FcγR-bearing mouse cells. Thereby the detection of therapeutic antibody mediated ADCC by human NK cells against engrafted tumor cell lines in mice was improved. To date, few autologous tumor models have been generated from human cells in HIS mice that do not depend on the availability of HSCs autologous to PDXs. These models have emerged over the last years. However, we propose a novel model that combines a FcγR deficient HIS mouse model, in which NK cells are boosted, with an autologous tumor model, to study therapeutic antibody mediated anti-tumor responses by NK cells.

1.5 Specific aims of the thesis

- 1) Characterization of a novel mFcγR deficient HIS mouse model to investigate antibody-mediated responses by human natural killer cells *in vivo*

- 2a) Establishment of a lymphoma model autologous to the human immune system in HIS mice and analysis of the immune responses against the tumor cells

- 2b) Testing immunotherapeutic reagents against cancer in next-generation HIS mouse models with a focus on the NK cell response

Chapter II

Delineating mechanisms underlying antibody-mediated effects via FcRs in Human Immune System (HIS) mice

Anna Louisa Thaller¹, Friederike Jönsson², Oriane Fiquet¹, Solenne Marie¹, Jean-Marc Doisne¹, Giulia Girelli-Zubani¹, Toshiki Eri¹, Priyanka Fernandes¹, Francina Langa-Vives³, Pierre Bruhns², Hélène Strick-Marchand¹ and James P. Di Santo^{1,*}

¹Institut Pasteur, Université Paris Cité, Inserm U1223, Innate Immunity Unit, Paris 75015, France

²Institut Pasteur, Université Paris Cité, Inserm U1222, Unit of Antibodies in Therapy and Pathology, Paris 75015, France

³Institut Pasteur, Université Paris Cité, Center for Murine Genetic Engineering, Paris 75015, France

*Correspondence:

Innate Immunity Unit, Inserm U1223

Institut Pasteur, 25 rue du Docteur Roux, 75724 Paris, France

Tel: +33 1 45 68 82 09

E-mail: james.di-santo@pasteur.fr

Keywords: Humanized mice, mAbs, Fc receptors

2.1 Abstract

Human immune system (HIS) mice provide a model to study human immune responses *in vivo*. Many currently available HIS mouse models harbor mouse hematopoietic Fc Receptor (FcR)-expressing cells that exert potent effector functions following administration of human Ig. Previous studies showed that ablation of the murine FcR gamma chain (FcR γ) results in loss of antibody-dependent cellular cytotoxicity (ADCC) and antibody-dependent cellular phagocytosis (ADCP) *in vivo*. We created BRGSA2DR2-based FcR γ -deficient HIS mice to delineate effector mechanisms that underlie antibody-mediated immune responses in this model. FcR γ -deficient HIS mice lack expression and function of activating FcRs and can be stably and robustly reconstituted with human immune cells after transfer of human hematopoietic stem cell (HSC) precursors. Using antibody-mediated cell depletion, we could assign specific effects to either endogenous mouse FcR $^{+}$ cells or engrafted human FcR $^{+}$ cells (including NK cells) depending on antibody subclass. We further reveal an unexpected role for mouse complement for antibody depletion in the absence of mouse FcR binding and activation. Our novel FcR γ -deficient HIS mice provide an additional relevant mouse model that can dissect the roles for human FcR $^{+}$ cells in effects mediated by exogenous administered human antibodies *in vivo*.

2.2 Introduction

Robust and relevant pre-clinical animal models remain essential tools to evaluate *in vivo* biological activities, pharmacodynamics as well as safety and efficacy of novel therapeutics for human disease. In this respect, human immune system (HIS) mice based on immunodeficient hosts (for example, NOD/LtSz-*scid Il2rg^{null}* (NSG), NOD/Shi-*scid Il2rg^{null}* (NOG) and Balb/c *Rag2^{null}Il2rg^{null} Sirpa^{NOD}* (BRGS) mice) have demonstrated their value for the study of candidate vaccines, treatments for viral infections like EBV or HIV and for novel cancer therapies¹⁻³. HIS mice harbor human innate and adaptive immune cells after engraftment and differentiation of human hematopoietic stem cells (HSCs) that generate functional cellular and humoral immune responses⁴⁻⁶ and can thus be used for pre-clinical testing of novel therapeutic strategies, while closely mirroring the situation in humans.

Monoclonal antibodies (mAbs) represent one category of therapeutic agents that have revolutionized disease treatment, in particular those involving viral infections and cancer; this is an extremely active area of research with >100 mAbs already approved for clinical use⁷. Antibodies function by modulating immune responses through several distinct modes of action that include blocking of receptor-ligand interactions, mimicking the binding of natural ligands, direct induction of apoptosis and mediating interactions with immune system components⁸⁻¹¹. In the latter, engagement of antibodies with the complement system leads to complement dependent cytotoxicity (CDC)¹² or complement dependent phagocytosis (CDP)¹³ while engagement with Fc Receptor-expressing (FcR+) immune cells such as natural killer (NK) cells, neutrophils and macrophages provokes antibody dependent cellular cytotoxicity (ADCC) or antibody dependent cellular phagocytosis (ADCP) through activation pathways involving the FcR γ chain (encoded by *Fcer1g*)¹⁴.

Therapeutic mAbs (Tx mAbs) are developed with human IgG isotypes (mostly IgG1, IgG4) which have differential binding to human (Fc γ R+) hematopoietic cells and abilities to activate complement^{15,16}. The analysis of these human mAbs in pre-clinical HIS models is further complicated as recipients harbor functional mouse macrophages and neutrophils¹⁷ and may retain a functional complement system¹⁸, which can confound the interpretation of exogenously administered Tx mAbs^{19,20}. Previous

studies have shown that human IgG-based mAbs bind to mouse FcR γ ⁺ cells *in vivo* 21,22.

To define the roles for human FcR γ ⁺ hematopoietic cells during Tx mAb administration *in vivo* more clearly, HIS mouse models have been developed where the contribution of activating mouse FcRs can be excluded. One approach made use of mAbs with Fc regions that have reduced or abolished binding to mouse FcRs^{14,21}. Still, these variant mAbs also show reduced or abolished human FcR binding so their ability to discriminate mouse versus human FcR activation was limited. HIS mouse models with ablation of *Fcer1g* (lacking expression of IgG activating receptors Fc γ RI, Fc γ RIII, Fc γ RIV and IgE receptor Fc ϵ RI) and *Fcgr2b* (lacking inhibitory receptor Fc γ RIIB) genes have been reported^{23,24}. These models provide 'cleaner' systems to assess Tx mAbs activities that interact with human FcR⁺ cells. Interestingly, hCD20⁺ tumor cell depletion was observed in one *Fcer1g*-deficient model²⁴ after Rituximab administration even in the absence of human immune cells suggesting additional host effector mechanisms.

In this study, we generated a novel *Fcer1g*-deficient BRGSA2DR2-based mouse strain using a CRIPSR/Cas9 approach that functionally ablates mouse activating FcRs (Fc γ RI, Fc γ RIII, Fc γ RIV) that bind human Ig^{14,25,26}. We further characterized HIS mice produced in BRGSA2DR2 *Fcer1g*^{-/-} recipients to identify the human FcR γ ⁺ cells and other effector mechanisms contributing to exogenous Tx mAbs responses *in vivo*.

2.3 Results

Generation and validation of BRGSA2DR2 Fcer1g^{-/-} mice

BALB/c *Rag2^{null}//2rg^{null} Sirpa^{NOD} HLA-A2^{Tg} HLA-DR2^{Tg}* (BRGSA2DR2) mice² were rendered *Fcer1g*-deficient using CRISPR/Cas9-mediated gene targeting (see Materials and Methods). Genomic DNA sequencing revealed a 66-base pair (bp) Exon 2 deletion (Supplementary Fig. 1A, C) resulting in Exon 2 skipping upon transcription (Supplementary Fig. 1B, C). *In silico* mRNA sequence analysis predicted a frameshift truncated protein of 27 amino acids (Supplementary Fig. 1D, E).

Fcer1g gene ablation impairs expression of murine CD16/CD32 (FcγRIII/FcγRII), CD64 (FcγRI) and the IgE receptor (FcεRI)²⁵. We observed no significant difference in CD16/CD32 expression in Gr-1⁺ neutrophils between *Fcer1g* wt or heterozygous BRGSA2DR2 mice, while CD16/CD32 expression in *Fcer1g*^{-/-} mice was significantly reduced (Fig. 1A). Moreover, CD64 and FcεRI staining was abrogated in CD11b⁺ and CD11b⁻ cells, respectively (Fig. 1B, C; Supplemental Fig. 2A) consistent with previous reports²⁵. Absence of mouse FcRγ chain protein in spleen cells was confirmed by intracellular staining (Supplemental Fig. 2B). We performed an IgG dependent passive systemic anaphylaxis (PSA) assay (Fig. 1D) to assess FcγRIII function²⁷. A significant drop in body temperature consistent with acute anaphylaxis was seen in *Fcer1g* wt and heterozygous mice, whereas *Fcer1g*-deficient mice maintained stable body temperature over time (Fig. 1E). Together, these results demonstrate successful inactivation of the FcRγ chain in BRGSA2DR2 mice at DNA, mRNA, protein and functional levels.

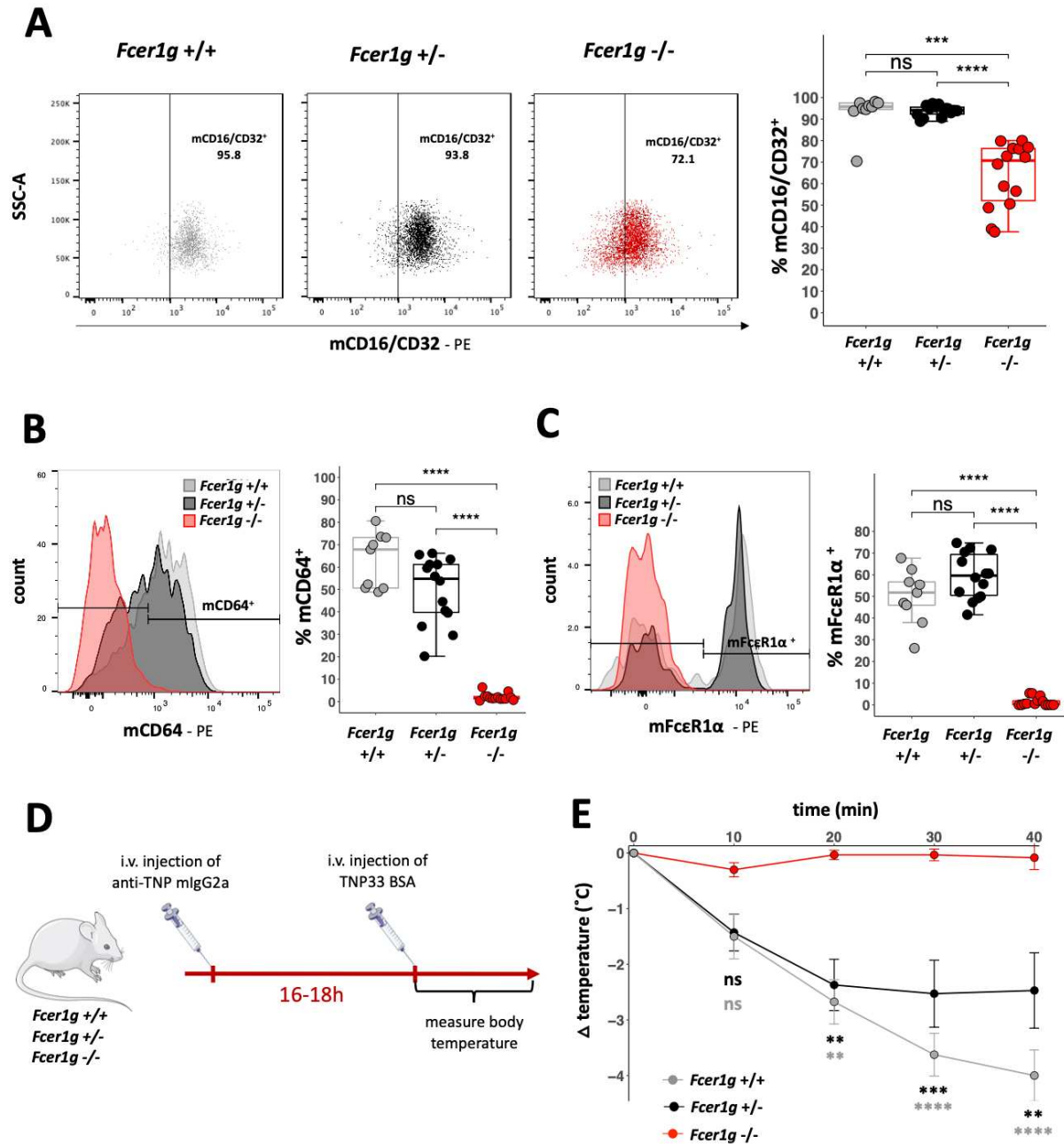


Figure 1 - Validation of Fcεr1g-deficient BRGSA2DR2 hosts

(A) - (C) Representative FACS staining in blood (left) and quantification of frequency of positive cells (right) in *Fcεr1g* wt (grey; n=9), *Fcεr1g* +/- (black; n=14), *Fcεr1g* -/- (red; n=14) BRGSA2DR2 mice for (A) CD16/32, (B) CD64, and (C) FcεR1α in monocytes, (CD11b⁺, SSC-A^{lo}, Gr1^{hi} neg), macrophages (CD11b⁺, SSC-A^{lo}, Gr1^{mid/-}) and CD11b⁻, Gr1⁻ cells, respectively; each dot represents one mouse and data includes results from 3 independent experiments. (D) Schematic diagram of passive systemic anaphylaxis (PSA) assay. (E) Body temperature difference $\Delta T = (T_{x\min} - T_{0\min})$

in °C over time in PSA assay after TNP₃₃-BSA mIgG2a injection in *Fcer1g* wt (grey; n=4), *Fcer1g* +/- (black; n=7), *Fcer1g* -/- (red; n=6) BRGSA2DR2 mice. Data are represented as mean ± SEM and representative of 2 independent experiments.

Efficient human immune cell engraftment in BRGSA2DR2 Fcer1g-/- mice

We assessed human cell reconstitution² after CD34⁺ HSC engraftment in this new BRGSA2DR2 strain. Human immune cell subset composition in the blood at 12 weeks post graft (wpg) and in the organs at 16 wpg was similar when comparing BRGSA2DR2 *Fcer1g* WT or heterozygous HIS mice (referred to as 'HIS') with BRGSA2DR2 *Fcer1g*-deficient HIS mice (referred to as 'HIS *Fcer1g*-/-'). There were no significant differences in the degree of humanization in the blood or in different organs in the absence of *Fcer1g* (Supplemental Fig. 3A, C). No significant differences in percentages or absolute numbers of total hCD45 (Fig. 2A, D), CD19⁺ B cells (Fig. 2B, E), CD3⁺ T cells (Fig. 2C, F), NKp46⁺CD94⁺ NK cells (Fig. 2G), CD4⁺ or CD8⁺ T cells (Fig. 2H, I), or ratio of CD4/CD8 T cells (Supplementary Fig. 3B) were observed in the blood, spleen, bone marrow and liver between HIS and HIS *Fcer1g*-/- mice, indicating normal human immune cell differentiation in this novel *Fcer1g*-deficient HIS mouse model.

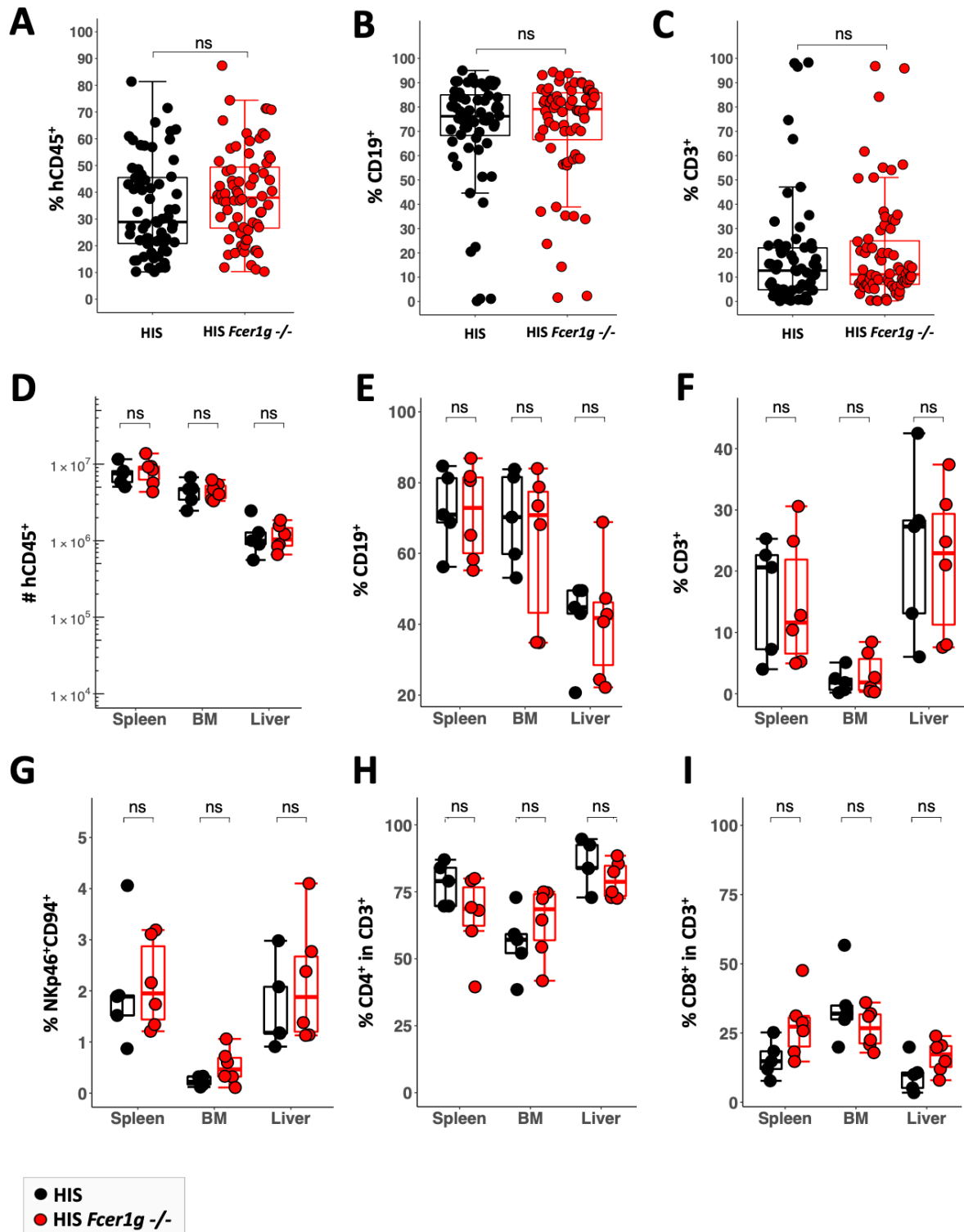


Figure 2 - Human immune cell reconstitution in BRGSA2DR2 *Fcεr1g*^{-/-} mice
 Quantification of human immune cell populations in human immune system (HIS) *Fcεr1g* wt or +/- mice (black) versus HIS *Fcεr1g*^{-/-} mice (red). (A)-(C) In blood at 12 weeks post grafting (wpg), (A) percentage of hCD45 calculated as %hCD45 cells = 100*hCD45/(hCD45+mCD45), (B) frequency of CD19⁺ B cells in hCD45 cells and

(C) frequency of CD3⁺ T cells in hCD45 cells. (D)-(I) For the spleen, bone marrow (BM) and liver at 16 wpg. (D) Absolute numbers of hCD45 per organ (for bone marrow for 1 femur and 1 tibia). Frequency of (E) CD19⁺ B cells, (F) CD3⁺ T cells, (G) NKp46⁺ and CD94⁺ NK cells in hCD45 and (H) CD4⁺ and (I) CD8⁺ in total CD3⁺ T cells. Each dot represents one mouse, data from the blood are representative > 6 independent experiments and from the organs for 2 independent experiments.

OKT8-mediated depletion of hCD8a⁺ cells in HIS mice requires FcγR1g

We next assessed exogenous antibody-mediated depletion in HIS *FcγR1g*^{-/-} mice. The anti-hCD8a antibody (OKT8) has been demonstrated to efficiently deplete human CD8a⁺ T cells in several HIS mouse models^{28,29}. This mIgG2a antibody binds murine FcγRs and can activate complement via C1q binding^{22,30}. OKT8 injection into HIS mice efficiently depleted hCD8a⁺ T cells in the blood, whereas only partial depletion was seen in HIS *FcγR1g*^{-/-} mice (Supplemental Fig. 4A, B), demonstrating the involvement of mouse *FcγR1g*-dependent as well as *FcγR1g*-independent mechanisms. We could exclude OKT8-mediated inhibition (masking) as an explanation for the observed hCD8a⁺ T cell loss as hCD8b (which forms heterodimers with the hCD8 alpha chain³¹ and is co-expressed on most hCD8a⁺ T cells in our HIS mice) was similarly depleted (Supplemental Fig. 4A, C). Frequencies of hCD19⁺ B cells (Supplemental Fig. 4D) were unaffected, confirming specificity of the OKT8-mediated depletion.

Deciphering mechanisms that contribute to Ig-mediated cell depletion in HIS mice

We next dissected the human FcR-dependent mechanisms underlying exogenous antibody-mediated depletion in HIS mice. For this, we studied depletion of human B cells following administration of the Tx anti-hCD20 mAb Rituximab (Fig. 3A). One advantage of this model is the availability of human IgG variants with different isotypes and capacities to bind and activate complement^{15,16,23,32}. In a fashion similar to that initially described by Lux et al.²³, we analyzed hCD19⁺ cells before and after Rituximab injection as hCD19 is co-expressed on the majority of hCD20⁺ B cells in the HIS mice (Supplementary Fig. 5A).

We first compared depletion mediated by hIgG1 and hIgG4 variants, the latter displaying limited affinity for human FcRs (except for CD64), while retaining strong binding to mouse FcRs and weakly activating complement^{16,22,33–38}. We found that the hIgG1 Rituximab variant could similarly reduce human B cells in both HIS and HIS *Fcer1g*^{-/-} mice (Fig. 3B, C) suggesting the involvement of human FcR⁺ effector cells and/or mouse complement in the depletion. In contrast, the hIgG4 Rituximab variant, while able to deplete human B cells in HIS mice, was significantly less efficient in HIS *Fcer1g*^{-/-} mice (Fig 3B, C) confirming earlier studies²³. These results demonstrate that hIgG4 mAbs can deplete target cells in HIS mouse models and this largely occurs through activating FcR⁺ mouse cells. Interestingly, partial hIgG4 antibody-mediated depletion still occurred in HIS *Fcer1g*^{-/-} mice (compared to control PBS injected mice; Fig. 3C) revealing a non-FcR γ -dependent mechanism that could include mouse complement.

In order to delineate effects mediated by Rituximab in HIS *Fcer1g*^{-/-} mice via human FcR⁺ cells from those involving complement, we analyzed the depletion capacity of a Rituximab variant (IgG1_K322A) which fails to bind complement or induce complement dependent cytotoxicity and has reduced binding to human Fc γ RIIA and Fc γ RIIIA with a roughly 2-fold reduction in ADCC compared to IgG1³⁹. Human B cell depletion by the Rituximab IgG1_KA variant was clearly reduced in HIS *Fcer1g*^{-/-} mice compared to Rituximab IgG1 control mAb (Fig. 3B, C). These results indicate that complement-dependent mAb depletion operates in HIS mice in the absence of activating mouse FcRs.

In most Rituximab IgG1_KA-injected HIS *Fcer1g*^{-/-} mice, little or no human B cell depletion was detected. Nevertheless, IgG1_KA-injected HIS *Fcer1g*^{-/-} mice had significantly higher depletion compared with PBS-injected HIS *Fcer1g*^{-/-} control mice (Fig. 3C) suggesting the involvement of human FcR⁺ cells. We verified the specificity of Rituximab treatment and found no significant differences in CD8a⁺ T cell numbers in HIS and HIS *Fcer1g*^{-/-} mice injected with Rituximab IgG1 or IgG1_KA versus controls (Supplemental Fig. 5C). We noticed that the degree of depletion in Rituximab IgG1_KA-injected HIS *Fcer1g*^{-/-} mice strongly correlated with the percentage of human NK cells present in individual HIS mice (Fig. 3D). We failed to find a similar correlation with other human immune cell subsets, for example CD8a⁺ T cells (Supplementary Fig. 5D).

To further test the potential role for human NK cells, we expanded these FcγR+ effector cells in HIS *Fcer1g*^{-/-} mice using exogenous IL-15. Previous work from our laboratory⁴⁰ showed that human IL-15 supplementation in HIS mice increases NK cell effector functions and human CD16 expression. We observed significantly higher levels of hCD19 B cell depletion in IL-15 boosted compared with control Rituximab IgG1_KA-treated HIS *Fcer1g*^{-/-} mice (Fig. 3C). Furthermore, human B cell depletion correlated strongly with enhanced CD16 expression on human NK cells in IL-15 boosted HIS mice (Fig. 3E), whereas FcR+ human macrophages were not affected by the IL-15 boost (Supplementary Fig. 5E). These results suggest that an inducible ADCC activity by human NK cells underlies the human B cell depletion in Rituximab IgG1_KA-treated HIS *Fcer1g*^{-/-} mice.

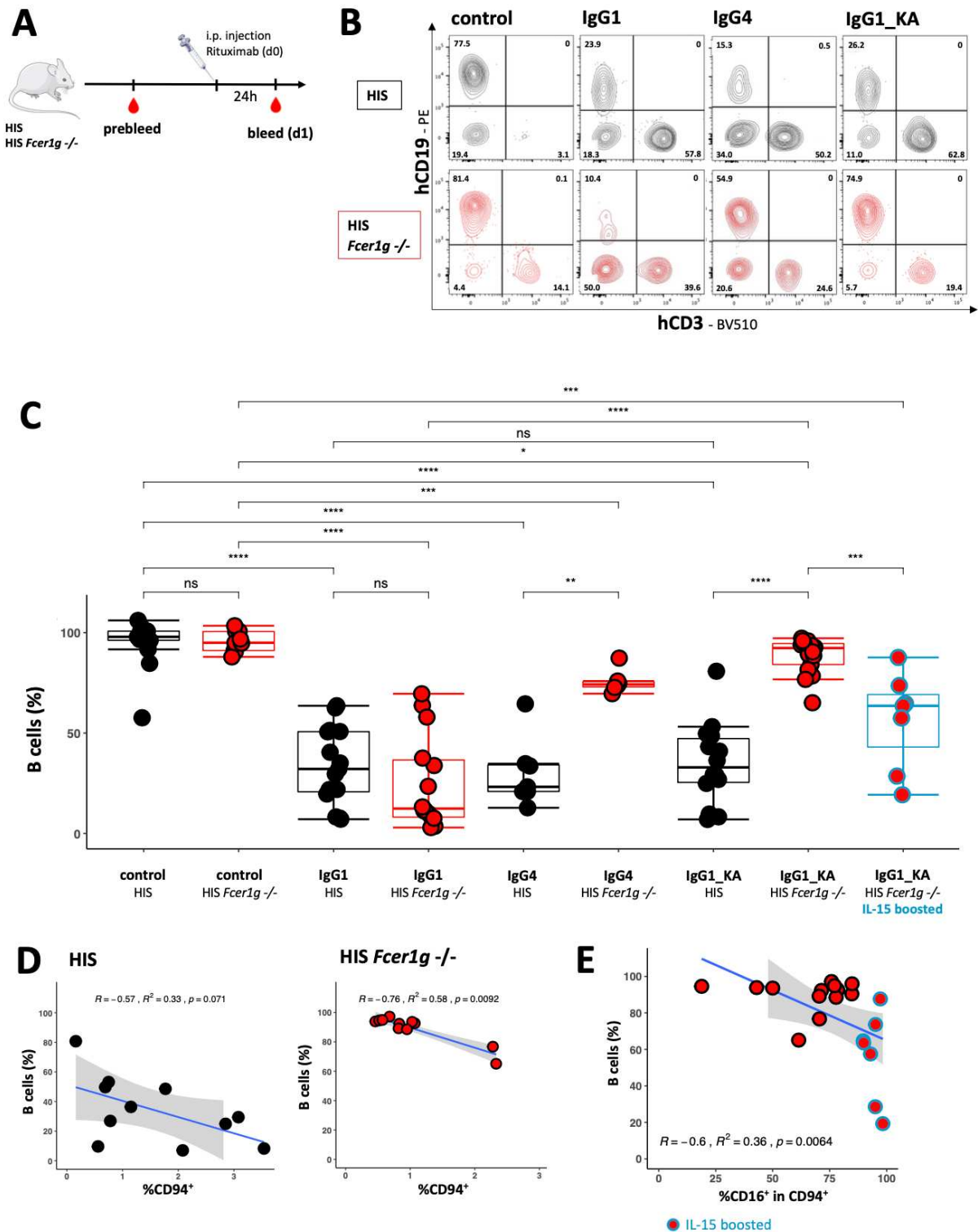


Figure 3. Human B cell depletion in HIS mice by Rituximab variants

(A) Scheme of hCD20 depletion by Rituximab injection. (B) Representative FACS plots of blood from HIS (top) and HIS *Fcer1g*^{-/-} (bottom) mice 24h after injection of each antibody variant. (C) B cell depletion (% B cells) = %CD19 (d1)/ %CD19*100 (pre-bleed) in HIS (black), HIS *Fcer1g*^{-/-} (red), and IL-15 boosted HIS *Fcer1g*^{-/-} (red; blue outline) mice injected with either NaCl (control) or variants of Rituximab with human

IgG1, IgG4 or IgG1_KA Fc fragment. (D) Spearman correlation analysis of %B cell depletion to %CD94⁺ NK cells in hCD45 at pre-bleed for Rituximab IgG1_KA injected HIS (left) and HIS *Fcer1g*^{-/-} (right) mice. (E) Spearman correlation analysis of %B cell depletion to %CD16⁺ NK cells (CD19⁻, CD3⁻, CD94⁺) at pre-bleed for Rituximab IgG1_KA injected HIS *Fcer1g*^{-/-} mice with or without IL-15 boost. Each dot represents one mouse and data includes results from ≥ 2 independent experiments for all conditions.

2.4 Discussion

Antibodies elicit diverse effects during immune responses as soluble Ig, complexed with antigens (immune complexes) or bound to relevant targets on the cell surface. Subsequent steps may involve activation of effector cells (via FcRs) or complement, leading to ADCC, ADCP, CDP or CDC^{12-14,41,42}. As many current HIS mouse models may possess endogenous mouse FcR-bearing hematopoietic cells and may retain a functional complement system^{18,43}, interpretation of effects elicited by Tx mAbs in reconstituted HIS mice is challenging^{19,20}. Recently, several FcRγ-deficient HIS mouse models based on NOG, NSG or *Rag2^{-/-}/Il2rg^{-/-}* backgrounds were reported^{23,24,44,45}. Here we describe a FcRγ-deficient BRGSA2DR2 strain that can be robustly reconstituted to generate HLA-educated human immune systems. Together, these new models have provided important insights into specific roles for mouse and human FcRγ⁺ cells as well as complement in HIS mice receiving exogenous Tx mAbs.

One consistent finding observed in these different FcRγ-deficient HIS models is the important role played by residual mouse FcR⁺ cells in effects mediated by Tx mAbs. This was first shown in immunocompetent and immunodeficient mouse models⁴³⁻⁴⁶ and subsequently in HIS mice^{23,24,47,48} in the context of tumor rejection. The differential effects mediated by hIgG1 and hIgG4 isotypes in HIS mice were initially revealed in FcRγ-deficient HIS mice using human B cell or mouse platelet-depleting antibodies^{23,47}; results we confirm here using B cell-depleting Rituximab. Katano and colleagues showed the important role for mouse FcR receptors (most likely involving activating forms) in human tumor rejection using a NOG-based model²⁴, confirming earlier work^{43,45,46}. Still the murine effector cells responsible for the biological effects varied in these reports, including circulating neutrophils and/or tissue macrophages.

Here we extend the list of potential host mechanisms responsible for Tx mAb effects in HIS mice to include mouse complement. We used an Fc mutant of Rituximab IgG1, which harbors the K₃₂₂A point mutation that abolishes C1q binding³⁹. B cell depletion was less efficient using the KA variant Rituximab in HIS *Fcer1g^{-/-}* mice, suggesting an important contribution of complement to cell depletion in our HIS mouse model. Still, a two-fold reduction in ADCC and binding of IgG1_KA via FcγRIIA and FcγRIIIA to human immune cells has been reported³⁹ suggesting that lower ADCC/ADCP mediated by human FcγR⁺ cells may also be involved.

FcR γ -deficient HIS mice may be useful in defining the contribution of human Fc γ R⁺ cells to effects mediated by exogenously delivered Tx mAbs or other immunomodulators that can bind FcRs (for example, Fc-fusion proteins⁴⁹). Katano et al.⁴⁸ used an adoptive cell transfer model in IL-15Tg FcR γ -deficient NOG mice to suggest that human NK cells could be involved in the elimination of human tumor xenografts, although the precise mechanism remained unclear. Here, we could show in fully reconstituted FcR γ -deficient BRGSA2DR2 HIS mice that NK cells were important effectors of Rituximab-mediated effects and that boosting human CD16⁺ NK cells (via exogenous IL-15) could amplify B cell depletion elicited by the IgG1_KA Rituximab variant. To our knowledge, this result represents the first direct demonstration of *in vivo* ADCC mediated by human NK cells.

Neutrophils, DCs and macrophages are the other main human FcR⁺ hematopoietic cells that develop in HIS mice and may also be involved in antibody-dependent effects. As such, use of BRGSA2DR2 *Fcer1g*^{-/-} HIS mice carrying a Flk2Flt3 mutation that develop human dendritic cells and innate lymphoid cells after hFlt3L administration^{17,50} may help clarify the role for human FcR⁺ DC in effects mediated by Tx mAbs in HIS mice. Identification of the precise human Fc γ R⁺ cell subsets involved in antibody-mediated cell effects *in vivo* will allow better characterization of the properties of Tx mAbs to tailor them to be most efficient in diverse disease settings.

2.5 Material and Methods

Ethics statement

Animals were housed in ventilated cages under specific-pathogen-free conditions with human care. Experiments were approved by an ethical committee (Ref. # 2007–006) at Institut Pasteur and validated by the French Ministry of Education and Research (Ref. MENESR # 02162.02).

Mice and generation of BRGSA2DR2 Fcer1g-deficient strain

BRGSF (BALB/c *Rag2*^{tm1Fwa} *Il2rg*^{tm1Cgn} *Sirpa*^{NOD} *Flt3*^{tm1Ir1}) and BRGSA2DR2 (BALB/c *Rag2*^{-/-} *Il2rg*^{-/-} *Sirpa*^{NOD} Tg(HLA-A/H2-D/B2M)^{1Bpe}, Tg(HLA-DRB1*1501)^{#Lfug}) have been previously described^{2,50}. BRGSA2DR2 mice were generated and used as hosts for CRISPR-mediated modification of the *Fcer1g* locus (Mouse Genetics

Engineering Center of Institut Pasteur). The following guide sequences were chosen by using the CRISPOR Web tool (<https://crispor.tefor.net/>)⁵¹, guide 1: TGA GTC GAC AGT AGA GTA GG and guide2: TCC AGG ATA TAG CAG AGC TG targeting exon 2 of the *FceR1g* gene were each cloned into a PX330 expression vector (a gift from F. Zhang, the Broad Institute of Massachusetts Institute of Technology and Harvard University, Cambridge, MA; plasmid 42230; Addgene⁵²). To generate a deletion in the *FceR1g* gene, zygotes were microinjected with pX330 as previously described⁵³.

PCR and Sequencing

Extraction of genomic DNA was done from biopsies by digestion with Proteinase K (Eurobio) at 56°C and subsequent precipitation and washing of the DNA with ethanol. Extraction of mRNA was done from blood with the QIAamp RNA Blood Mini Kit (Qiagen). Retro transcription of mRNA into cDNA was done using SuperScript™ III Reverse Transcriptase (Invitrogen) with Random Hexamers (Invitrogen). DNA or cDNA spanning the *Fcer1g* Exon 2 was amplified by PCR; primers for genomic DNA, forward (Fwd): 5'-TTT TCC CTT CAG ACC ATG GGG-3', reverse (Rev): 5'-CCC ATG GGC ACC CTG TAT C-3'; for cDNA, Fwd: 5'-CAG CTG CGC AGT TCT GTC A- 3', Rev: 5'-ATC TGC TTT CTC ACG GCT GG-3'. For sequencing the PCR product was run on an agarose gel, the respective bands were cut out, the DNA was purified with the NucleoSpin Gel and PCR clean-up kit (Macherey-Nagel) and sent for sequencing (Eurofins Genomics, Cologne). Analysis, primer design and protein prediction were done on <https://www.ncbi.nlm.nih.gov/>.

Passive systemic anaphylaxis assay (PSA)

Mice between 9-15 weeks old were sensitized by intravenous (i.v.) injection of 200µg mIgG2a-anti-trinitrophenyl (TNP) (clone Hy-1.2) per mouse. 24h later they were i.v. injected with 100µg BSA substituted with 33 molecules of TNP (TNP₃₃-BSA)/mouse and the body temperature was measured via a rectal thermometer before injection (t0) and at 10, 20, 30 and 40 min after injection²⁷.

Tissue/organ processing and cell isolation

To obtain single cell suspensions, spleens were dissociated using 40µm cell strainers (Falcon). To extract bone marrow cells, one femur and one tibia were crushed with a mortar and pestle and cells were filtered with a 100µm cell strainer (Falcon). Red blood

cells were lysed using ACK buffer (NH_4Cl , KHCO_3 , EDTA in H_2O ; pH 7.3). The liver was cut into small pieces, digested at 37°C with $25\mu\text{g/ml}$ Liberase TL (Roche) and $100\mu\text{g/ml}$ DNase I (Roche), passed through a $100\mu\text{m}$ cell strainer and mononuclear cells isolated by Percoll (GE Healthcare) density gradient centrifugation. All cell suspensions were filtered through cell-strainer caps (Falcon) before counting with trypan blue (Life Technologies) and staining for flow cytometry. For all organ processing steps RPMI Medium 1640 (Life Technologies) with 5% fetal calf serum (Eurobio) was used.

Flow cytometry

Flow cytometric analysis was performed in accordance with published guidelines⁵⁴. Whole blood collected in EDTA coated Microvettes (Sarstedt) was directly stained with fluorochrome-conjugated antibodies (Supporting Information Table 1) at 4°C for 30min, erythrocytes were lysed and samples fixed with FACS™ Lysing solution (BD). For the organ-derived cells a maximum of 2×10^6 cells were used for analysis, prior to staining they were incubated for 10min at RT with IgG from human serum (Sigma-Aldrich) and FcR blocking reagent Mouse (Miltenyi). For surface marker staining, respective fluorochrome-conjugated antibodies (Supporting Information Table 1), for dead cell exclusion Viability dye eFluor™ 506 (Invitrogen) and cell number determination CountBright™ absolute counting beads (Invitrogen) were diluted in brilliant stain buffer (BD). Staining was done at 4°C for 30min, after washing cells were fixed in 4% PFA (EMS) and resuspended for acquisition. Washing steps were done in FACS buffer (1x DPBS (Gibco) with 2% fetal calf serum (Eurobio), 2mM EDTA (Invitrogen)). For intra cellular (IC) staining cells were fixed by Cytofix/Cytoperm (BD) and subsequently incubated with IC antibody diluted in Perm/Wash (BD) for 30min at 4°C .

Generation of human immune system (HIS) mice

Human immune system (HIS) mice were generated in BRGSA2DR2 *FceR1g*^{+/-} and *FceR1g*^{-/-} mice as previously described^{2,17,50,55}. Briefly, human fetal liver (Advanced Bioscience Resources Inc.) $\text{CD}34^+$ cells were isolated using MicroBead Kits (Miltenyi). $\text{CD}34$, $\text{CD}38$, and HLA-A2 expression was phenotyped by FACS and the HLA class II allele haplotype analysis by PCR (LABType SSO, One Lambda). $7\text{-}15 \times 10^4$ $\text{CD}34^+\text{CD}38^-$ cells from HLA-A*02⁺ HLA-DRB1*15⁺ donors, or from 1:1 mixtures of

HLA-A*02⁺ and HLA-DRB1*15⁺ donors, were intra-hepatically injected into 2-to-10-day-old mice that had been sub-lethally irradiated (3Gy). The efficiency of humanization was assessed by flow cytometry on the blood and calculating the humanization with the following formula: $100 \times \frac{\%hCD45}{(\%hCD45 + \%mCD45)}$; only mice with humanization $\geq 10\%$ were used for experiments.

Antibody-mediated depletion of human cell subsets in vivo

For CD8a⁺ cell depletion, HIS mice were pre-bled 3 days before i.p. (intra-peritoneal) injection with 100µg/mouse of anti-human CD8a antibody OKT8 (BioXcell) in PBS, control mice were injected with only PBS, and bled at day 4 (d4) post injection. For CD20⁺ cell depletion HIS mice were pre-bled 6 days before i.p. injection with 25µg/mouse of anti-human CD20 antibody Rituximab in the IgG1, IgG4_{S228P} and IgG1_K322A format or saline solution and bled at day 1 (d1) post-injection. Tx Abs are generally used in the stabilized IgG4_{S228P} format to prevent Fab arm exchange of IgG4 hemi-molecules⁵⁶.

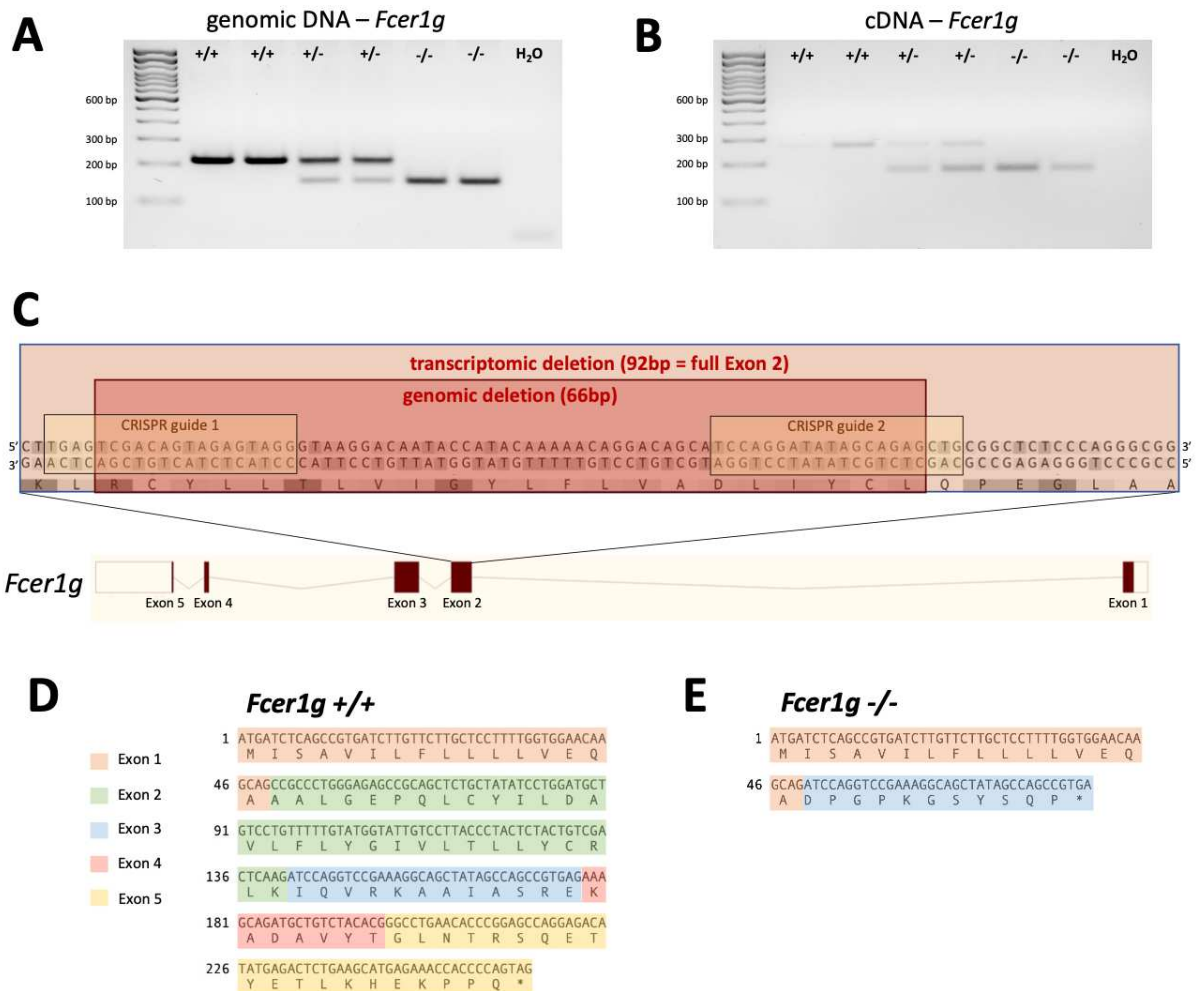
Human IL15 boost in vivo

HIS mice were injected 4 times i.p. with 100 µl of hIL-15Ra-Fc (7.5 µg) + hIL-15 (2.5 µg) (R&D Systems) every 3-4 days; 1 day after the last injection mice were pre-bled, injected with IgG1_KA and bled at d1 post antibody injection.

Statistical analysis

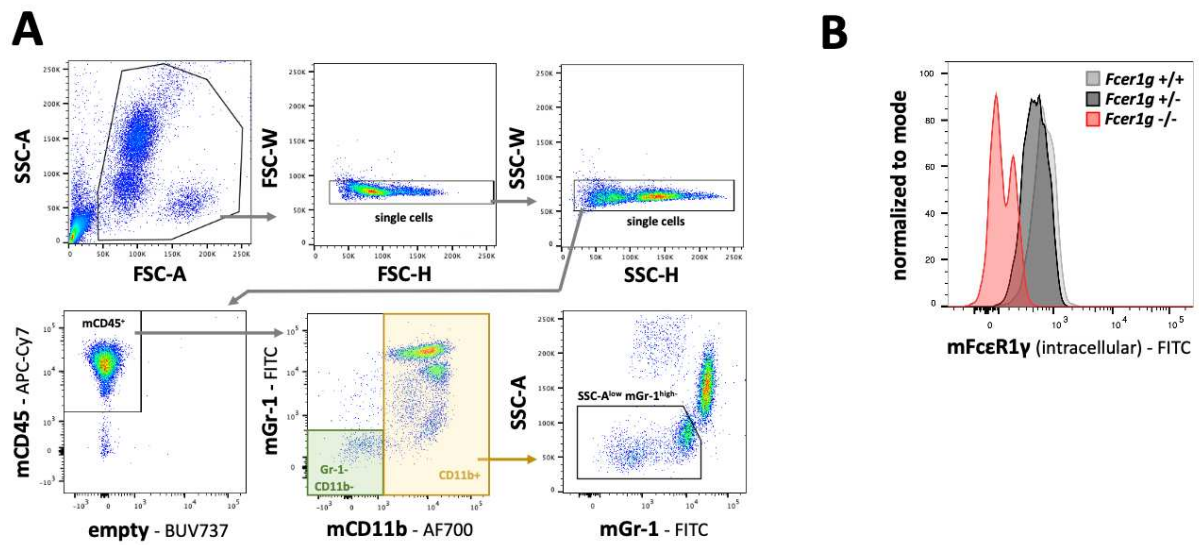
Data were compared with unpaired non-parametric tests, Mann Whitney Wilcoxon test for comparison between two groups, Kruskal-Wallis test for comparison of multiple groups, correlations were tested by Spearman correlation using RStudio (Version 1.4.1106). P values are indicated as: ns: $p > 0.05$, *: $p \leq 0.05$, **: $p \leq 0.01$, ***: $p \leq 0.001$, ****: $p \leq 0.0001$.

2.6 Supplementary Figures



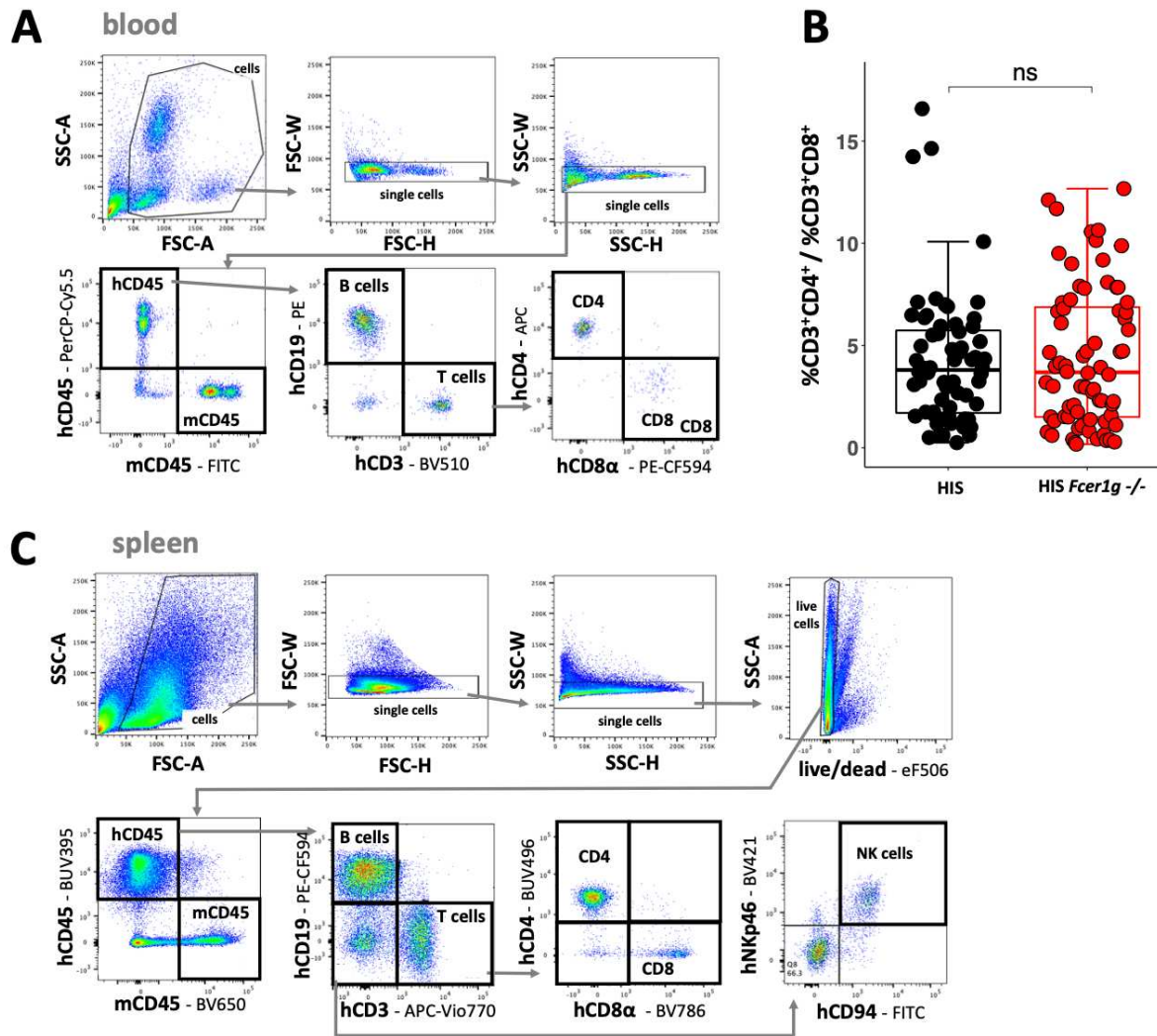
Supplementary Figure 1

(A)-(B) Ethidium bromide-stained agarose gel with 100bp ladder (left on gel) and PCR products with (A) genomic DNA as a template with *Fcer1g* wt band of 214 bp and *Fcer1g*^{-/-} band of 148 bp and (B) cDNA as template with *Fcer1g* wt band of 255 bp and *Fcer1g*^{-/-} band of 163 bp. (C) Scheme of the mouse *Fcer1g* gene with focus on Exon2 and CRISPR guide sequences and deletions on DNA and RNA level indicated. (D-E) *Fcer1g* protein coding mRNA sequence and predicted amino acid (AA) sequence for (D) *Fcer1g* wt and (E) *Fcer1g*^{-/-} mice.



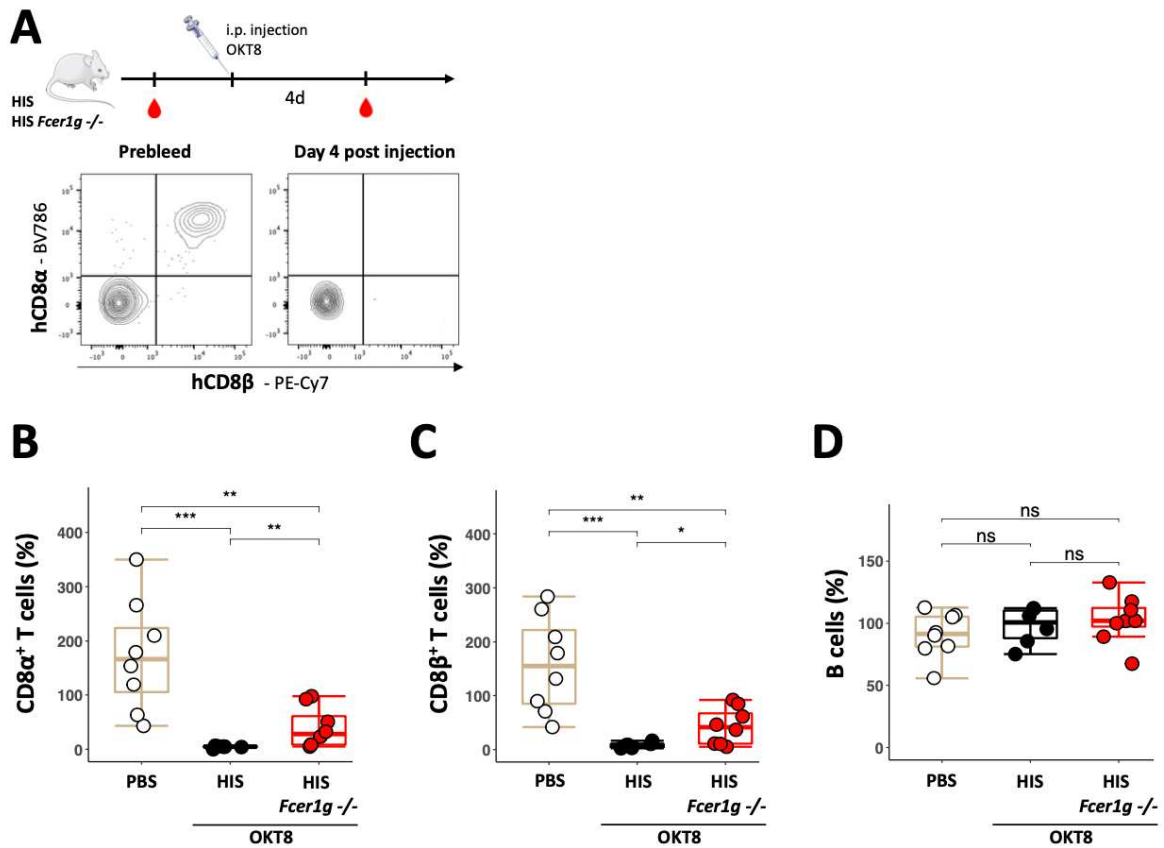
Supplementary Figure 2

(A) Gating strategy for FACS analysis of blood cells. (B) Representative FACS plots for intracellular FCER1G staining of splenocytes of *Fcεr1g* wt, *Fcεr1g*^{+/-} and *Fcεr1g*^{-/-} mice in CD11b⁺ splenocytes.



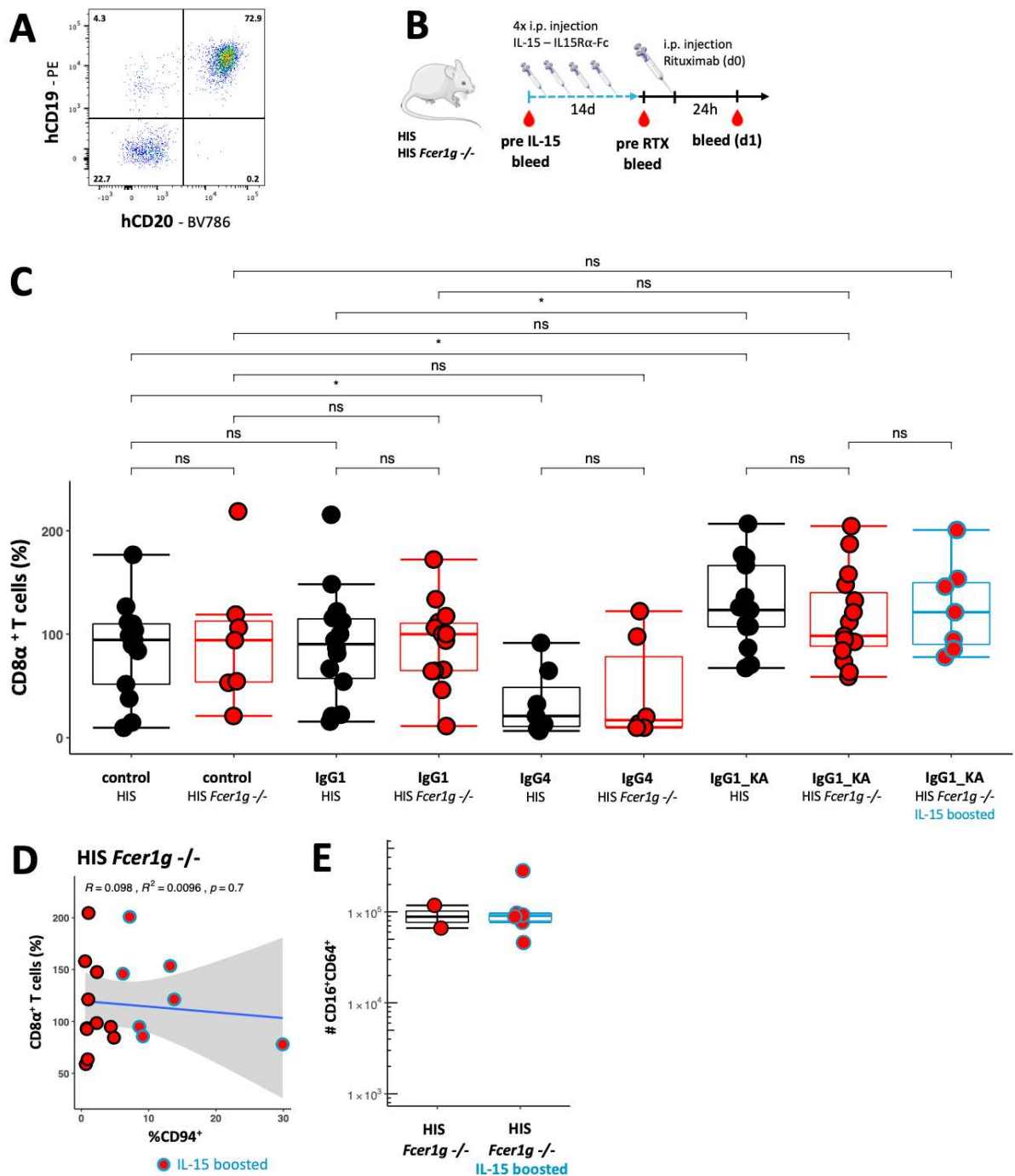
Supplementary Figure 3

(A) Gating strategy for FACS analysis of immune cell subsets in blood. (B) Ratio of CD4/CD8 T cells in blood at 12 wpg in HIS mice (black) versus HIS *Fcεr1g*^{-/-} mice (red). (C) Gating strategy for FACS analysis of immune cell subsets in spleen.



Supplementary Figure 4 - CD8⁺ T cell depletion in *Fcer1g*^{-/-} HIS mice

(A) Scheme of hCD8a depletion by OKT8 injection with representative FACS plots of CD8a and CD8b staining at pre-bleed (left) and bleeding at d4 post injection (right) of a HIS mouse. (B)-(D) Ratio (%(d4)/%(pre-bleed)) of immune cell populations in blood of PBS injected control mice (beige) and OKT8 antibody injected HIS (black) and HIS *Fcer1g*^{-/-} (red) mice for (B) CD8a⁺ T cells, (C) CD8b⁺ T cells, (D) CD19⁺ B cells. Each dot represents one mouse and data are representative of 2 independent experiments.



Supplementary Figure 5

(A) Representative FACS plot for CD19 and CD20 staining in blood of HIS mice. (B) Scheme of IL-15 boost and hCD20 depletion by Rituximab injection. (C) %CD8 α ⁺ T cell depletion (%) (= %CD8 α in CD3 (d1)/%CD8 α in CD3 (pre-bleed) in percent) in HIS (black), HIS *Fcγ1g*^{-/-} (red), and IL-15 boosted HIS *Fcγ1g*^{-/-} (red; blue outline) mice injected with either NaCl (control) or variants of Rituximab with human IgG1, IgG4 or IgG1_KA Fc regions. (D) Correlation of %CD8 α ⁺ T cell depletion with %CD94⁺ NK cells in hCD45 at pre-bleed for Rituximab IgG1_KA injected HIS *Fcγ1g*^{-/-} mice. (E)

Total numbers of CD16⁺ CD64⁺ macrophages in liver of HIS *Fcer1g*^{-/-} control and IL-15 boosted mice.

antigen	fluorochrome	clone	reactivity	supplier	catalog number
CD3	BV510	SK7	human	BioLegend	344828
CD3	APC-Vio770	REA613	human	Miltenyi Biotec	130-113-136
CD4	APC	RPA-T4	human	BD	555349
CD4	BUV496	SK3	human	BD	612936
CD11b	AF700	M1/70	mouse/human	eBioscience	56-0112-82
CD16	BUV737	3G8	human	BD	564434
CD16	BUV805	3G8	human	BD	748850
CD16/CD32	PE	2.4G2	mouse	BD	561727
CD19	PE	HIB19	human	BioLegend	302208
CD19	PE-CF594	HIB19	human	BD	562294
CD20	BV786	2H7	human	BioLegend	302356
CD45	APC-Cy7	30-F11	mouse	BD	557659
CD45	PerCP-Cy5.5	HI30	human	BD	564105
CD45	FITC	30-F11	mouse	BioLegend	103108
CD45	BUV395	HI30	human	BD	563792
CD45	BV650	30-F11	mouse	BD	563410
CD45	BUV805	HI30	human	BD	612891
CD64	PE	X54-5/7.1	mouse	BD	558455
CD8a	PE-CF594	RPA-T8	human	BD	562282
CD8a	BV786	RPA-T8	human	BioLegend	301046
CD8b	PE-Cy7	SID18BEE	human	eBioscience	25-5273-42
CD94	FITC	DX22	human	BioLegend	305504
CD94	PerCP-Vio700	REA113	human	Miltenyi Biotec	130-119-763
FCER1A	PE	MAR-1	mouse	eBioscience	12-5898-82
FCER1G	FITC		human/mouse	Merck-Millipore	FCABS400F
Gr-1	FITC	RB6-8C5	mouse	BD	553127
NKp46	BV421	9E2/NKp46	human	BD	564065

Table 1 - List of antibodies

2.7 References

1. Zyl, D. G. van *et al.* Immunogenic particles with a broad antigenic spectrum stimulate cytolytic T cells and offer increased protection against EBV infection *ex vivo* and in mice. *PLoS Pathog.* **14**, e1007464 (2018).
2. Masse-Ranson, G. *et al.* Accelerated thymopoiesis and improved T-cell responses in HLA-A2/-DR2 transgenic BRGS-based human immune system mice. *Eur. J. Immunol.* **49**, 954–965 (2019).
3. Capasso, A. *et al.* Characterization of immune responses to anti-PD-1 mono and combination immunotherapy in hematopoietic humanized mice implanted with tumor xenografts. *J. Immunother. Cancer* **7**, 37 (2019).
4. Shultz, L. D. *et al.* Human Lymphoid and Myeloid Cell Development in NOD/LtSz- *scid* IL2R γ ^{null} Mice Engrafted with Mobilized Human Hemopoietic Stem Cells. *J. Immunol.* **174**, 6477–6489 (2005).
5. Ito, M. *et al.* NOD/SCID/ γ cnul mouse: an excellent recipient mouse model for engraftment of human cells. *Blood* **100**, 3175–3182 (2002).
6. Legrand, N. *et al.* Functional CD47/signal regulatory protein alpha (SIRP α) interaction is required for optimal human T- and natural killer- (NK) cell homeostasis *in vivo*. *Proc. Natl. Acad. Sci.* **108**, 13224–13229 (2011).
7. Mullard, A. FDA approves 100th monoclonal antibody product. *Nat. Rev. Drug Discov.* **20**, 491–495 (2021).
8. Reinherz, E. L., Hussey, R. E. & Schlossman, S. F. A monoclonal antibody blocking human T cell function. *Eur. J. Immunol.* **10**, 758–762 (1980).
9. Kaye, J., Porcelli, S., Tite, J., Jones, B. & Janeway, C. A. Both a monoclonal antibody and antisera specific for determinants unique to individual cloned helper T cell lines can substitute for antigen and antigen-presenting cells in the activation of T cells. *J. Exp. Med.* **158**, 836–856 (1983).
10. Reff, M.E. *et al.* Depletion of B Cells *In Vivo* by a Chimeric Mouse Human Monoclonal Antibody to CD20. *Blood* **15**, 435–45 (1994).
11. Könitzer, J. D., Sieron, A., Wacker, A. & Enenkel, B. Reformatting Rituximab into Human IgG2 and IgG4 Isotypes Dramatically Improves Apoptosis Induction *In Vitro*. *PLoS One* **10**: e0145633 (2015).
12. Di Gaetano, N. *et al.* Complement Activation Determines the Therapeutic Activity of Rituximab *In Vivo*. *J. Immunol.* **171**, 1581–1587 (2003).
13. Walbaum, S. *et al.* Complement receptor 3 mediates both sinking phagocytosis and phagocytic cup formation via distinct mechanisms. *J. Biol. Chem.* **296**: 100256 (2021).
14. Bruhns, P. & Jönsson, F. Mouse and human FcR effector functions. *Immunol. Rev.* **268**, 25–51 (2015).
15. Yu, J., Song, Y. & Tian, W. How to select IgG subclasses in developing anti-tumor therapeutic antibodies. *J Hematol Oncol* **13**, 45 (2020).
16. Bruhns, P. *et al.* Specificity and affinity of human Fc γ receptors and their polymorphic variants for human IgG subclasses. *Blood* **113**, 3716–3725 (2009).
17. Li, Y. *et al.* A novel Flt3-deficient HIS mouse model with selective enhancement of human DC development. *Eur. J. Immunol.* **46**, 1291–1299 (2016).
18. Yamauchi, T. *et al.* Polymorphic Sirpa is the genetic determinant for NOD-based mouse lines to achieve efficient human cell engraftment. *Blood* **121**, 1316–1325 (2013).
19. Lux, A. & Nimmerjahn, F. Of mice and men: the need for humanized mouse models to study human IgG activity *in vivo*. *J. Clin. Immunol.* 2013 **33**, S4-8 (2013).

20. Bournazos, S., DiLillo, D.J. & Ravetch, J.V. Humanized mice to study Fc γ R function. *Curr. Top. Microbiol. Immunol.* **382**, 237-48 (2014).
21. Overdijk, M. B. *et al.* Crosstalk between human IgG isotypes and murine effector cells. *J. Immunol.* **189**, 3430–3438 (2012).
22. Wang, Y. *et al.* Specificity of mouse and human Fc γ receptors and their polymorphic variants for IgG subclasses of different species. *Eur. J. Immunol.* **52**, 753–759 (2022).
23. Lux, A. *et al.* A humanized mouse identifies the bone marrow as a niche with low therapeutic IgG activity. *Cell Reports* **7**, 236–48 (2014).
24. Katano, I., Ito, R., Kawai, K. & Takahashi, T. Improved Detection of in vivo Human NK Cell-Mediated Antibody-Dependent Cellular Cytotoxicity Using a Novel NOG-Fc γ R-Deficient Human IL-15 Transgenic Mouse. *Front. Immunol.* **11**:532684 (2020).
25. Takai, T., Li, M., Sylvestre, D., Clynes, R. & Ravetch, J. V. FcR γ chain deletion results in pleiotropic effector cell defects. *Cell* **76**, 519–529 (1994).
26. Nimmerjahn, F., Bruhns, P., Horiuchi, K. & Ravetch, J. V. Fc γ RIV: A Novel FcR with Distinct IgG Subclass Specificity. *Immunity* **23**, 41–51 (2005).
27. Beutier, H. *et al.* IgG subclasses determine pathways of anaphylaxis in mice. *J. Allergy Clin. Immunol.* **139**, 269-280.e7 (2017).
28. Strowig, T. *et al.* Priming of protective T cell responses against virus-induced tumors in mice with human immune system components. *J. Exp. Med.* **206**, 1423–1434 (2009).
29. Chijioke, O. *et al.* Human natural killer cells prevent infectious mononucleosis features by targeting lytic Epstein-Barr virus infection. *Cell Rep.* **5**, 1489–1498 (2013).
30. Leatherbarrow, R. J. & Dwek, R. A. Binding of complement subcomponent C1q to mouse IgG1, IgG2a AND IgG2b: A novel C1q binding assay. *Mol. Immunol.* **21**, 321–327 (1984).
31. Terry, L. A., DiSanto, J. P., Small, T. N. & Flomenberg, N. Differential expression and regulation of the human CD8 α and CD8 β chains. *Tissue Antigens* **35**, 82–91 (1990).
32. Peschke, B., Keller, C. W., Weber, P., Quast, I. & Lünemann, J. D. Fc-Galactosylation of Human Immunoglobulin Gamma Isotypes Improves C1q Binding and Enhances Complement-Dependent Cytotoxicity. *Front. Immunol.* **8**:646 (2017).
33. de Taeye, S. W. *et al.* Fc γ R Binding and ADCC Activity of Human IgG Allotypes. *Front. Immunol.* **11**, 740 (2020).
34. Stepkowski, Z. *et al.* Biological activity of human-mouse IgG1, IgG2, IgG3, and IgG4 chimeric monoclonal antibodies with antitumor specificity. *Proc. Natl. Acad. Sci.* **85**, 4852–4856 (1988).
35. Tao, M. H., Smith, R. I. & Morrison, S. L. Structural features of human immunoglobulin G that determine isotype-specific differences in complement activation. *J. Exp. Med.* **178**, 661–667 (1993).
36. Brüggemann, M. *et al.* Comparison of the effector functions of human immunoglobulins using a matched set of chimeric antibodies. *J. Exp. Med.* **166**, 1351–1361 (1987).
37. Derebe, M. G., Nanjunda, R. K., Gilliland, G. L., Lacy, E. R. & Chiu, M. L. Human IgG subclass cross-species reactivity to mouse and cynomolgus monkey Fc γ receptors. *Immunol. Lett.* **197**, 1–8 (2018).
38. Dekkers, G. *et al.* Affinity of human IgG subclasses to mouse Fc gamma receptors. *mAbs* **9**, 767–773 (2017).

39. Hezareh, M., Hessel, A.J., Jensen, R.C., van de Winkel, J.G., Parren, P.W. Effector Function Activities of a Panel of Mutants of a Broadly Neutralizing Antibody against Human Immunodeficiency Virus Type 1. *J. Virol.* **75**, 12161–8 (2001).
40. Huntington, N. D. *et al.* IL-15 trans-presentation promotes human NK cell development and differentiation in vivo. *J. Exp. Med.* **206**, 25–34 (2009).
41. Titus, J. A., Perez, P., Kaubisch, A., Garrido, M. A. & Segal, D. M. Human K/natural killer cells targeted with hetero-cross-linked antibodies specifically lyse tumor cells in vitro and prevent tumor growth in vivo. *J. Immunol.* **139**, 3153–3158 (1987).
42. Anderson, C. L., Shen, L., Eicher, D. M., Wewers, M. D. & Gill, J. K. Phagocytosis is mediated by three distinct Fc γ receptor classes on human leukocytes. *J. Exp. Med.* **171**, 1333–45 (1990).
43. Clynes, R., Takechi, Y., Moroi, Y., Houghton, A. & Ravetch, J. V. Fc receptors are required in passive and active immunity to melanoma. *Proc. Natl. Acad. Sci.* **95**, 652–656 (1998).
44. Uchida, J. *et al.* The Innate Mononuclear Phagocyte Network Depletes B Lymphocytes through Fc Receptor–dependent Mechanisms during Anti-CD20 Antibody Immunotherapy. *J. Exp. Med.* **199**, 1659–1669 (2004).
45. Albanesi, M. *et al.* Neutrophils mediate antibody-induced antitumor effects in mice. *Blood* **122**, 3160–3164 (2013).
46. Montalvao, F. *et al.* The mechanism of anti-CD20–mediated B cell depletion revealed by intravital imaging. *J. Clin. Invest.* **123**, 5098–5103 (2013).
47. Schwab, I., Lux, A. & Nimmerjahn, F. Pathways Responsible for Human Autoantibody and Therapeutic Intravenous IgG Activity in Humanized Mice. *Cell Rep.* **13**, 610–620 (2015).
48. Katano, I. *et al.* Development of a novel humanized mouse model for improved evaluation of in vivo anti-cancer effects of anti-PD-1 antibody. *Sci. Rep.* **11**, 21087 (2021).
49. Czajkowsky, D. M., Hu, J., Shao, Z. & Pleass, R. J. Fc-fusion proteins: new developments and future perspectives. *EMBO Mol. Med.* **4**, 1015–1028 (2012).
50. Lopez-Lastra, S. *et al.* A functional DC cross talk promotes human ILC homeostasis in humanized mice. *Blood Adv.* **1**, 601–614 (2017).
51. Haeussler, M. *et al.* Evaluation of off-target and on-target scoring algorithms and integration into the guide RNA selection tool CRISPOR. *Genome Biol.* **17**, 148 (2016).
52. Ran, F. A. *et al.* Genome engineering using the CRISPR-Cas9 system. *Nat. Protoc.* **8**, 2281–2308 (2013).
53. Mashiko, D. *et al.* Generation of mutant mice by pronuclear injection of circular plasmid expressing Cas9 and single guided RNA. *Sci. Rep.* **3**, 3355 (2013).
54. Cossarizza A. *et al.* Guidelines for the use of flow cytometry and cell sorting in immunological studies (third edition). *Eur. J. Immunol.* **51**, 2708–3145 (2021).
55. Li, Y. *et al.* A human immune system mouse model with robust lymph node development. *Nat. Methods* **15**, 623–630 (2018).
56. Silva, J.-P., Vetterlein, O., Jose, J., Peters, S. & Kirby, H. The S228P mutation prevents in vivo and in vitro IgG4 Fab-arm exchange as demonstrated using a combination of novel quantitative immunoassays and physiological matrix preparation. *J. Biol. Chem.* **290**, 5462–5469 (2015).

2.8 Acknowledgements

We thank the UTechS Cytometry and Biomarkers, the Center for Murine Genetic Engineering, and the Central Animal Facility of the Institut Pasteur. We thank P. Bouso (Institut Pasteur) for providing FcRg-deficient B6 mice. JPD receives financial support from the Institut Pasteur, the Institut National de la Santé et de la Recherche Médicale (INSERM), and the Vaccine Research Institute (to GG-Z). PB acknowledges funding from the French National Research Agency grants ANR-18-CE15-0001 project Autoimmuni-B, from the Institut Carnot Pasteur Microbes et Santé, from the Institut Pasteur and from the Institut National de la Santé et de la Recherche Médicale (INSERM). FJ is employed by the Centre National de la Recherche Scientifique (CNRS). AT received funding from the European Union's Horizon 2020 research and innovation programme under the Marie Skłodowska-Curie (Grant Agreement No. 765104).

Chapter III

A novel lymphoma model to study human anti-tumor immune responses in HIS mice

3.1 Introduction

In the fight against cancer, immunotherapies are important further applications to conventional therapies. One of the major challenges in the development of immunotherapies is the availability of pre-clinical models that mimic human immunity³⁹². A vast number of mouse tumor models exists but immunotherapies must target human proteins that may differ from the mouse equivalents. Since mouse immune responses are significantly different from those in humans, more human-specific models are needed³³². The combination of human immune system (HIS) and human tumor models in immunodeficient mice may present a step in the right direction, but to date many limitations still exist. While autologous models with patient derived peripheral blood mononuclear cells (PBMCs) and patient derived xenografts (PDXs) allow only a short experimental window due to the development of graft versus host disease (GvHD), access of hematopoietic stem cells (HSCs) autologous to PDX is highly limited and in allogeneic settings the distinction between the anti-tumor and the alloantigen response is challenging.

Novel models are in sight, recently an autologous HIS-leukemia model was described³⁹³. Here we report the generation of B lymphoblastoid cell lines (B-LCLs) from human B cells of HIS mice transformed by Epstein Barr virus (EBV) which may be used in an autologous setting in the future (Figure 1). The B-LCL cells efficiently engrafted and proliferated in immunodeficient and partially HLA-matched HIS mice and showed tumorigenicity. They had immunogenic potential, as immune cells were recruited to the site of injection in HIS mice following intraperitoneal injection of partially HLA-matched B-LCL. Moreover, we combined this tumor model with our novel BRGSA2DR2 Fcer1g^{-/-} HIS mouse model described in chapter II and tested the effects of antibody treatment and injection of 15-IL-15R α complex on B-LCL depletion.

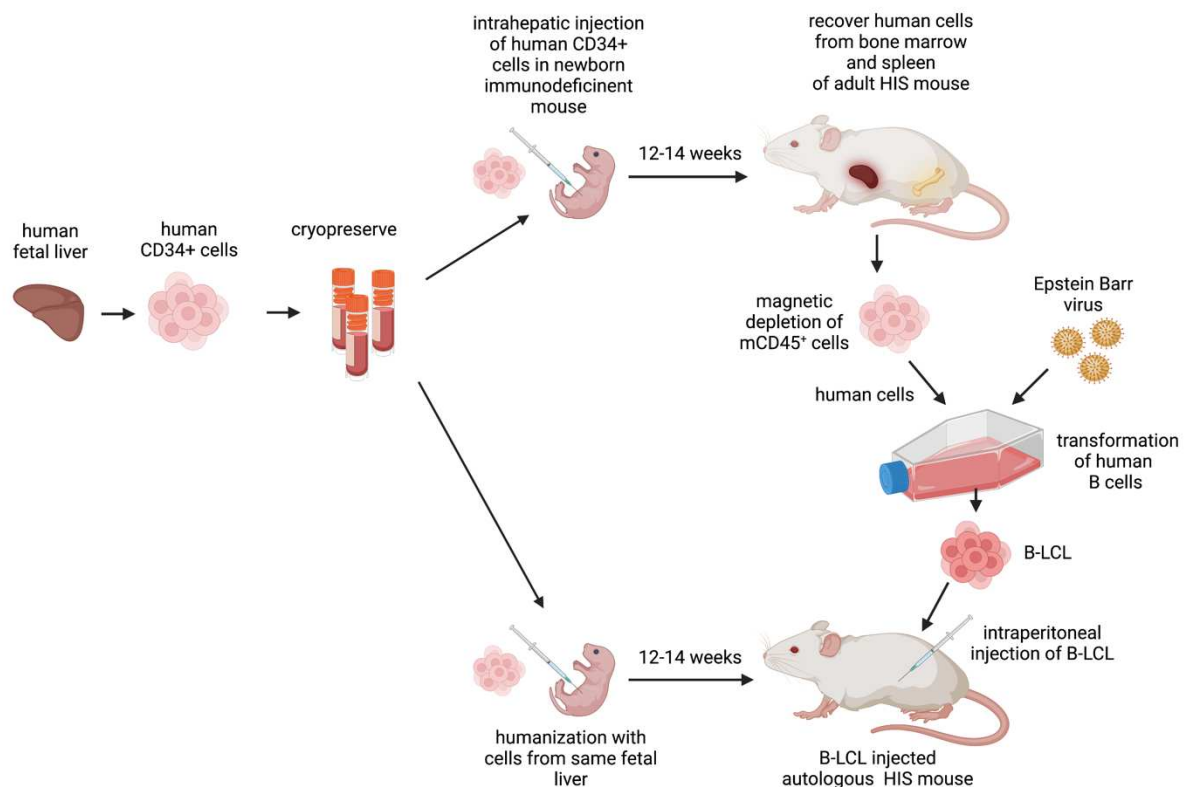


Figure 1. Scheme for the generation of an autologous tumor model by *in vitro* EBV transformation

3.2 Results

Phenotypic characterization of B lymphoblastoid cell lines generated by *in vitro* transformation of HIS mouse derived human B cells with Epstein Barr Virus

To generate an autologous B-LCL HIS mouse model we envisaged a two-step protocol: B-LCL lines were produced from a cohort of HIS mice and then injected into naïve HIS hosts. To produce the B-LCL line, HIS mice were generated by engraftment of fetal liver derived human CD34⁺ HLA-A2⁺ HSCs into newborn immunodeficient BRGSA2DR2 mice. To enrich for human cells, we extracted spleen and bone marrow cells of adult HIS mice, and mouse CD45⁺ cells were removed by magnetic bead depletion. Subsequently the cells were cultured *in vitro* and transformed by EBV infection, resulting in immortalized B-LCLs which proliferated robustly *in vitro*. The B-LCLs were characterized by flow cytometric analysis, confirming a B cell phenotype,

as the majority of cells express CD19, CD20 and CD21 and no T cell (CD3) or NK cell (CD16, CD94) markers (Figure 2). All the generated cell lines expressed B-LCL characteristic markers, such as CD39, CD70 and CD23³⁴⁰, which were found to be expressed on the majority of cells as well as HLA-A2. The largest differences in terms of marker expression between the cell lines was observed in the B-LCL stemming from the #2 bone marrow. The B cell markers CD19, CD20 and especially CD21 were expressed at lower levels, which may indicate that more immature B cells gave rise to this B-LCL³⁹⁴.

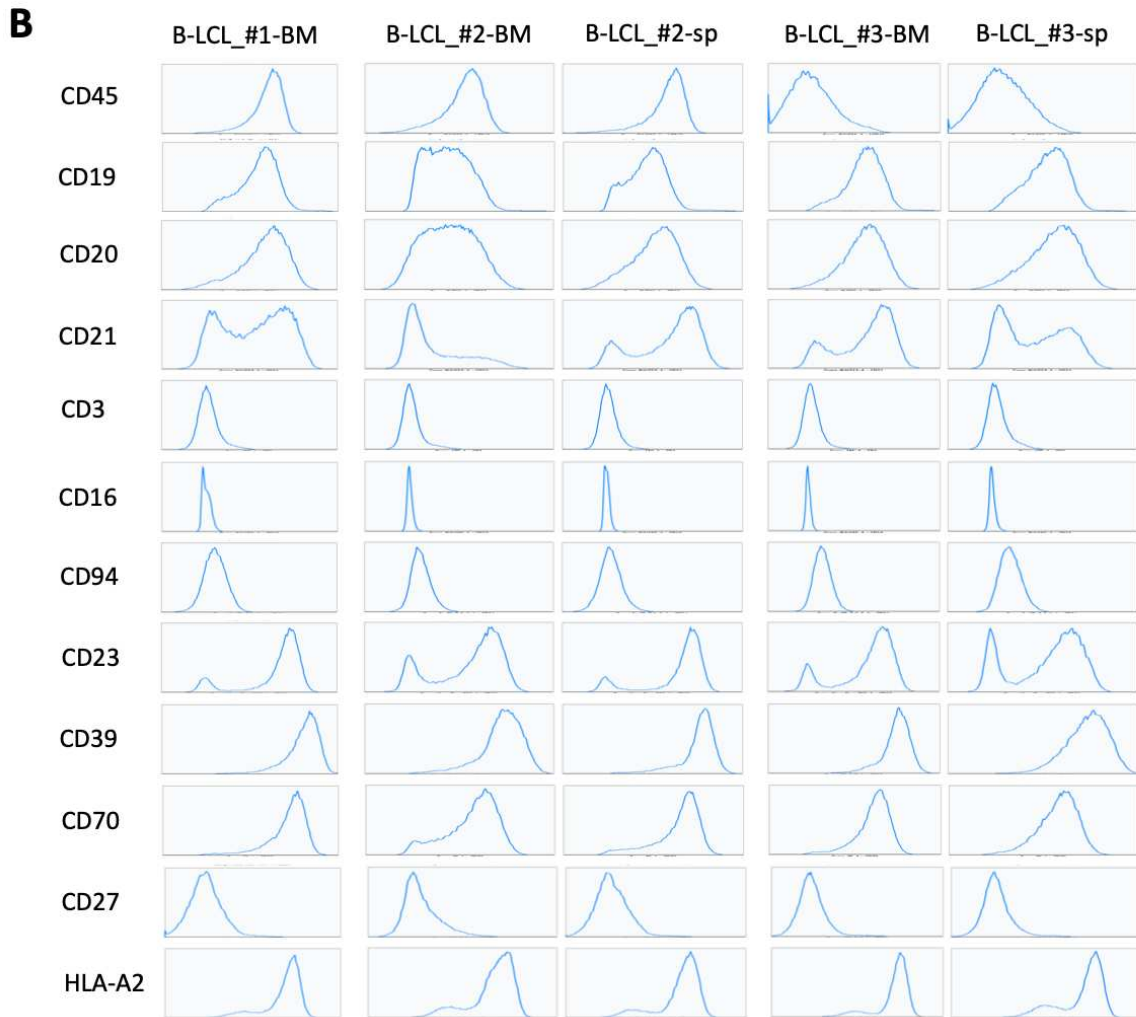
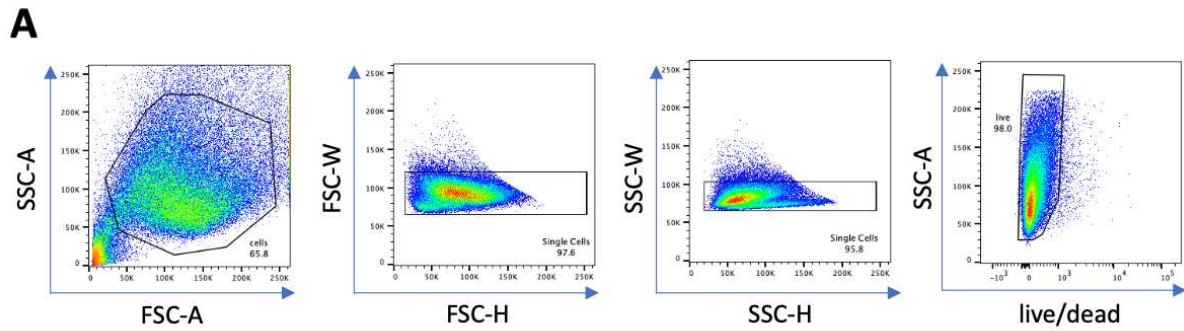


Figure 2. Phenotypic characteristics of B-LCLs generated by *in vitro* EBV infection of cells from the bone marrow (BM) or spleen (sp) of three HIS mice by flow cytometry. (A) gating strategy (B) Distribution of expression profiles for different cell surface markers.

Assessment of the tumorigenic potential of newly generated B-LCL in immunodeficient BRGSA2DR2 mice

In order to assess the potential of the B-LCLs to engraft and expand *in vivo*, we injected 10^6 and 10^7 B-LCL intraperitoneally (i.p.) into immunodeficient BRGSA2DR2 mice and analyzed them one- and two-weeks post injection. For this and all subsequent experiments B-LCL_#1_BM was used which was generated from the bone marrow of a HIS mouse that had been humanized with HLA-A2⁺ HLA-DR2⁺ HSCs from fetal liver #1.

B-LCL were detected in the peritoneal cavity of all mice at week 1 and consistently, higher cell numbers were found for mice injected with 10^7 than for mice injected with 10^6 B-LCL. At week 2, higher cell numbers were observed for both doses, showing that B-LCL cells are able to expand *in vivo*. In the blood and in the spleen much lower numbers of B-LCL were found at week one and two and only in the spleen an increase in B-LCL numbers is evident from week one to week two (Figure 3). This finding indicates, that a large proportion of B-LCL cells remains in the peritoneal cavity when injected i.p..

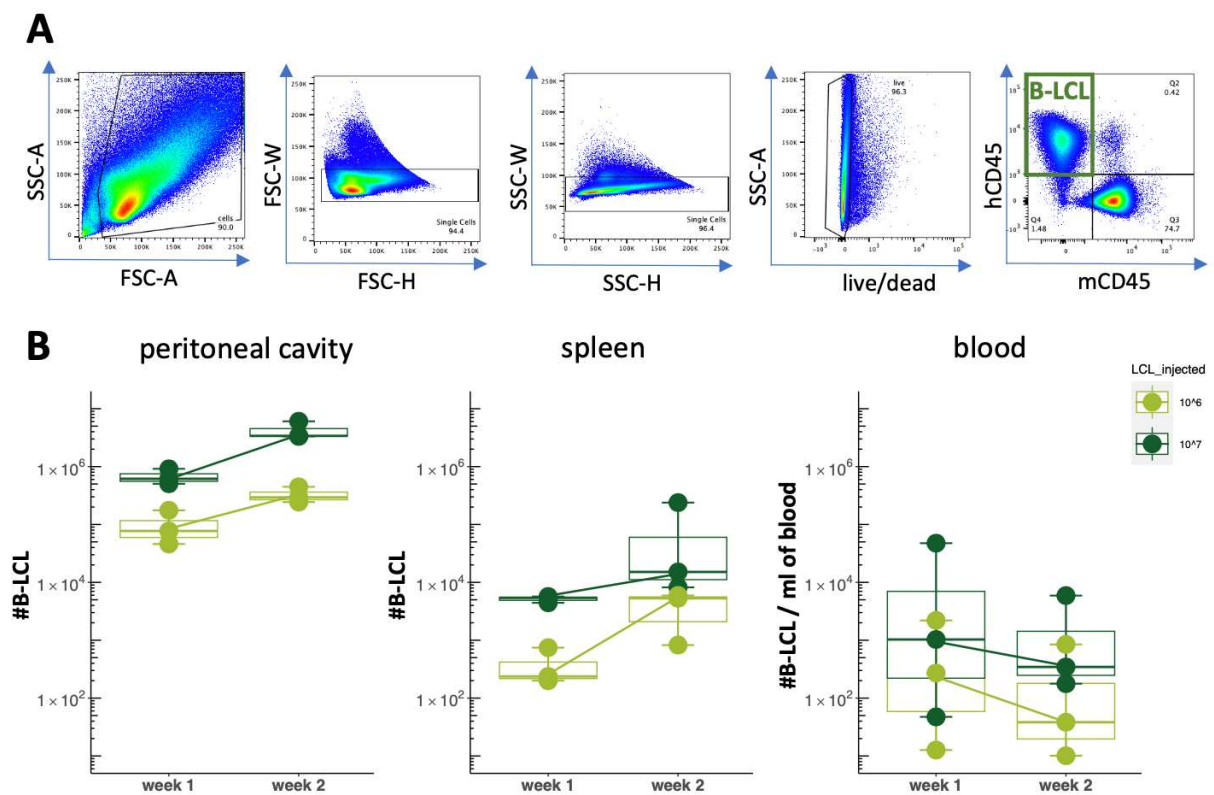


Figure 3. Grafting of B-LCL in non-HIS BRGSA2DR2 mice

(A) Gating strategy (B) Numbers of B-LCL found in the peritoneal cavity, spleen and blood at 1- and 2-weeks post i.p. injection of B-LCL.

To determine whether B-LCL cells are harmful and lethal for the host, we injected 10^6 B-LCL or for control just medium i.p. into immunodeficient BRGSA2DR2 mice and screened them by regularly measuring the bodyweight, checking their physical appearance and bleeding them. For up to 23 days post injection the bodyweight of the mice was mostly stable but quickly dropped in most B-LCL injected mice between day 23 and 33 post injection. All B-LCL injected animals died or had to be sacrificed following the regulations between day 33 and 40 post injection (Figure 4). B-LCL cell numbers in the blood increased steadily and mice with higher B-LCL cell numbers in the blood at day 30 died earlier. Control mice showed no weight loss or signs of pain and survived several weeks longer. At the endpoint, dissection of B-LCL injected mice revealed solid tumor masses in the peritoneal cavity and high numbers of B-LCL were found in the liver, spleen and peritoneal cavity (Figure 4). Thus, the newly generated B-LCL_#1-BM efficiently grafts in immunodeficient mice and is lethal in immunodeficient hosts, making them an applicable tumor model as they consistently formed tumors.

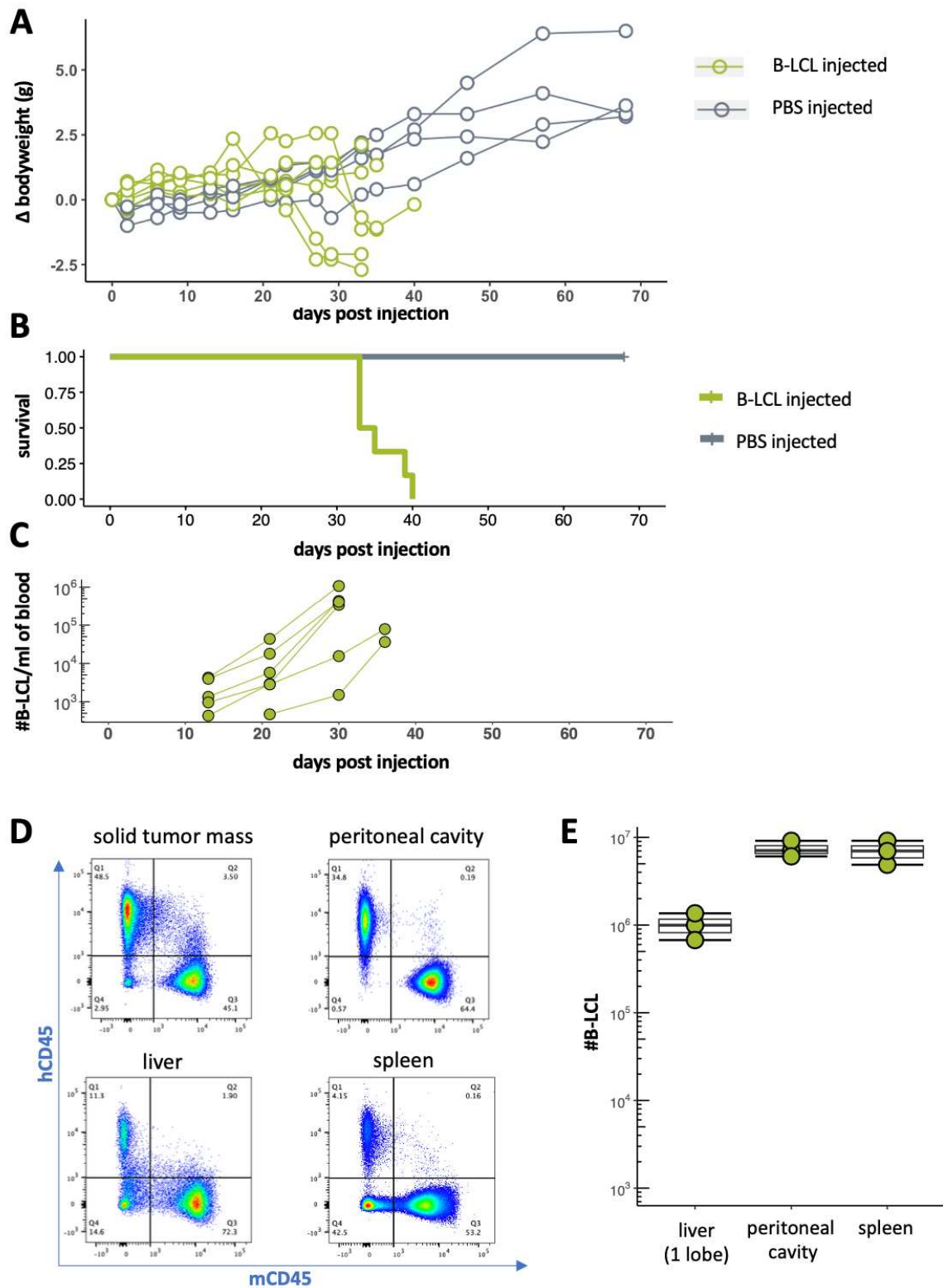


Figure 4. Development of lethal tumors in B-LCL injected non-HIS BRGSA2DR2 mice. (A) Difference of bodyweight to d0 for over time, each line corresponds to one mouse. (B) Survival of mice over time. (C) Number of B-LCL cells per ml of blood measured at different timepoints. (D) representative FACS plots and (E) total number of B-LCL cells in different tissues at sacrifice.

Identifying immune cell responses against novel B-LCL in the peritoneal cavity of BRGSA2DR2 HIS mice

To characterize the immune cell responses, we injected 10^6 B-LCL i.p. into BRGSA2DR2 HIS mice that had been previously humanized with partially HLA-matched HSCs to the B-LCL cell line (both HLA-A2⁺ and HLA-DR2⁺). The cells were then analyzed in the peritoneal cavity at one- and two-weeks post injection. For the distinction between the HIS cells and the transformed B-LCL cells we used CD23 as a marker which is expressed on most B-LCL cells (Figure 2) and only very few hCD45⁺ cells in HIS mice express CD23 in HIS mice (Figure 5B).

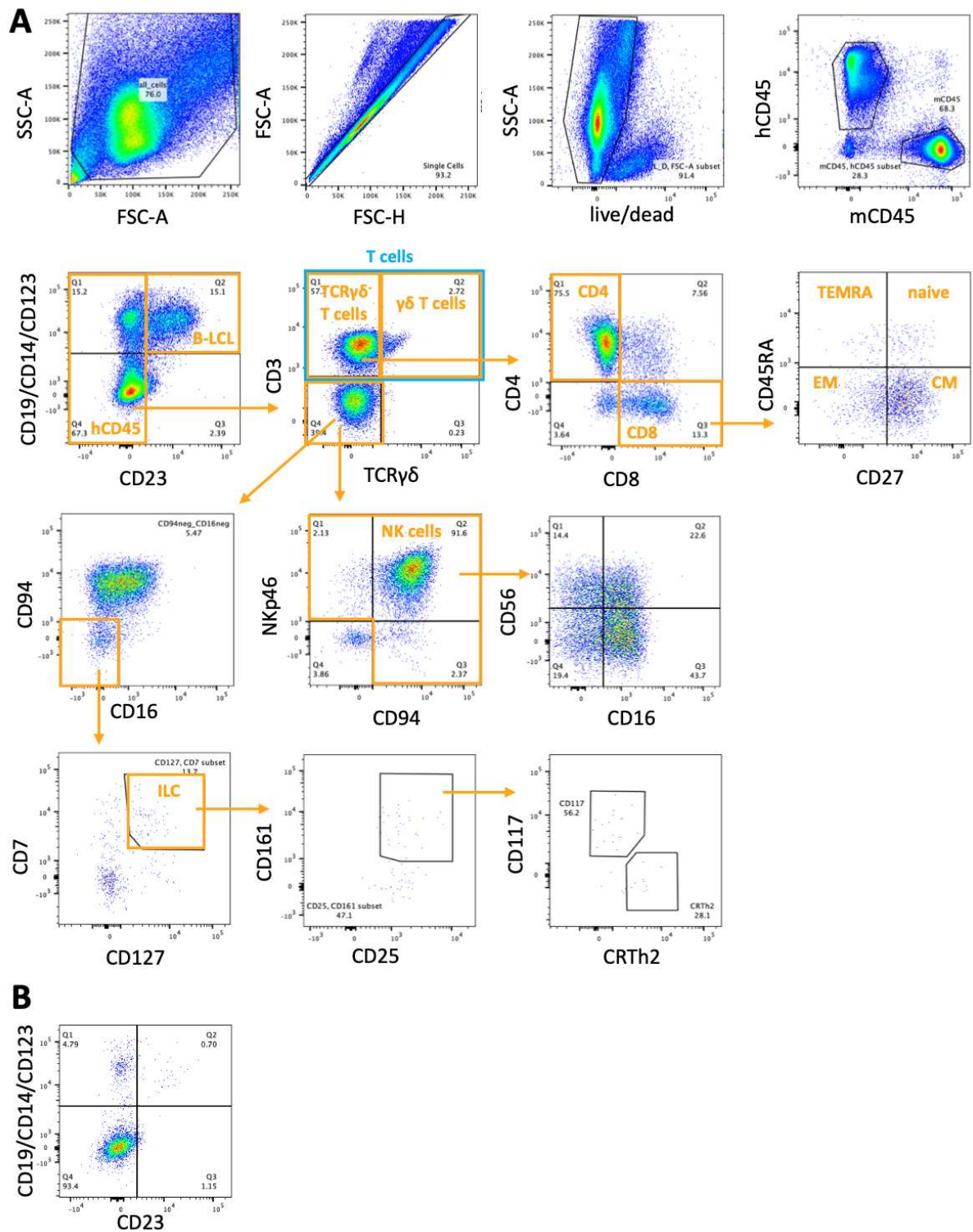


Figure 5. (A) Gating strategy of human immune cell subsets in the peritoneal cavity of B-LCL injected BRGSA2DR2 HIS mice (B) FACS plot of hCD45 cells in the peritoneal cavity of HIS mice not injected with B-LCL cells

In the peritoneal cavity of HIS mice lower numbers of B-LCL cells were found than in non-HIS control mice. Whereas B-LCL numbers increased in non-HIS mice from week

one to week two, they decreased in HIS mice (Figure 6A), which indicated the elimination of B-LCL cells through the HIS. In B-LCL injected HIS mice, the total numbers of hCD45 cells in the peritoneal cavity increased both at week one and week two compared to the respective control HIS mice with no B-LCL cells injected (Figure 6B) and a high amount of T cells were found (Figure 6C). Interestingly, at week one the mice with the lowest B-LCL numbers detected (mouse #21140 and #21298) are mice with the highest amounts of total hCD45 as well as T cells. This relationship is inverse in week two where mice with higher B-LCL numbers correspond to the mice with higher hCD45 cell numbers. This could mean that at week one the infiltrating cells are eliminating the B-LCL cells and with more immune cells infiltrating the B-LCL depletion is stronger. The difference at week two may be due to higher death of cells that efficiently reduced B-LCL numbers. Alternatively, lower B-LCL cell numbers, may result in reduced recruitment of hCD45 to the peritoneal cavity.

In several mice an increased frequency of CD8⁺ T cells compared to non-B-LCL injected HIS mice was evident at week one and week two. Especially in mouse #21140, the CD8⁺ T cells constitute more than half of all TCR $\gamma\delta$ - T cells (Figure 6D). The CD8⁺ T cells found in the peritoneal cavity are mostly central memory (CM) T cells and these make up a particularly high proportion in mouse #21140 (Figure 6E). We also detected other lymphocyte populations in the peritoneal cavity, such as NK cells (Figure 7A) and $\gamma\delta$ T cells (Figure 7B) which are largely increased in the B-LCL injected HIS mice. Hence, the i.p. injection of B-LCL cells into HIS mice seems to result in the infiltration and/or expansion of multiple immune cell subsets in the peritoneal cavity. Further, we also observed low numbers of ILCs which are only slightly increased compared to control mice (Figure 7C), suggesting that there is no strong infiltration of ILCs due to B-LCL injection. The analysis of NK cell subsets reveals that at both timepoints there is a higher frequency of CD56⁺CD16⁺ NK cells in the peritoneal cavity of B-LCL injected mice, mainly at the cost of the CD56⁺CD16⁻ NK cell population (Figure 7D). This indicates a shift in frequency of NK cells subsets in B-LCL injected mice. The numbers of immune cells in the peritoneal cavity for all the analyzed populations decreased between week one and week two after B-LCL injection. However, this is also the case for the cell numbers in the control mice. The control mouse at week 2 already had lower humanization in the blood at the pre-bleed before the experiment so this could explain the difference. However, the difference in the

blood was only by a factor of two (data not shown), whereas the difference observed in the peritoneal cavity accounts for two orders of magnitude.

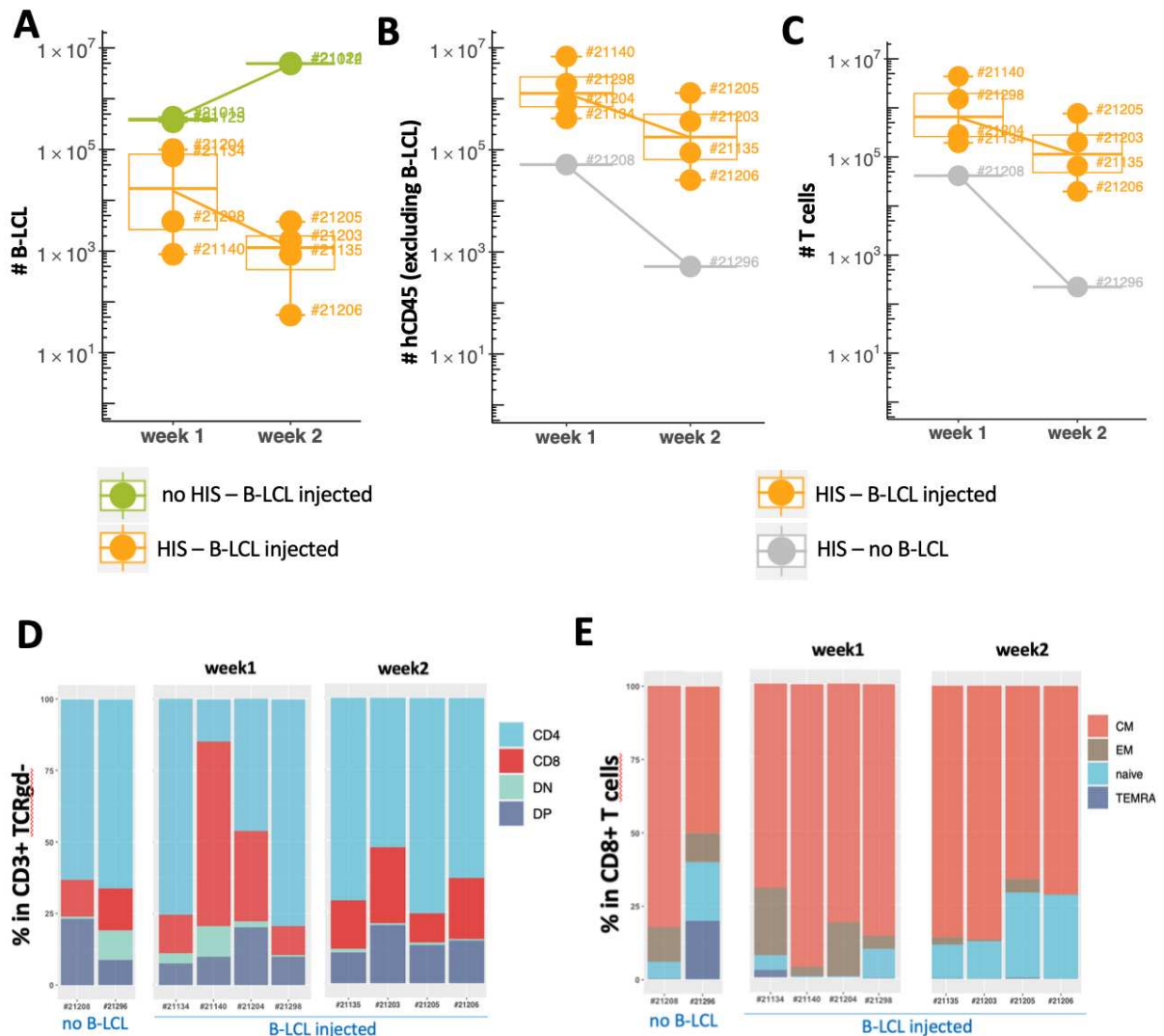


Figure 6. Cell numbers and frequencies of immune cell subsets in the peritoneal cavity of B-LCL injected HIS mice and control mice at week 1 and week 2 after injection. (A-C) each dot corresponds to one mouse and its number is indicated next to each dot. Number of (A) B-LCL cells (B) human CD45 cells (C) human T cells. (D-E) Each column corresponds to one mouse and its number of the mouse is indicated at the bottom of the column, in non B-LCL injected mice left column corresponds to the control mouse at week 1 and right column to the control mouse at week 2. (D) Frequencies of CD4⁺, CD8⁺, double negative (DN) and double positive (DP) T cells within TCRγδ⁻ T cells. (E) Frequencies of naïve, central memory (CM), effector memory (EM) and CD45RA⁺ EM (TEMRA) T cells within CD8⁺ T cells.

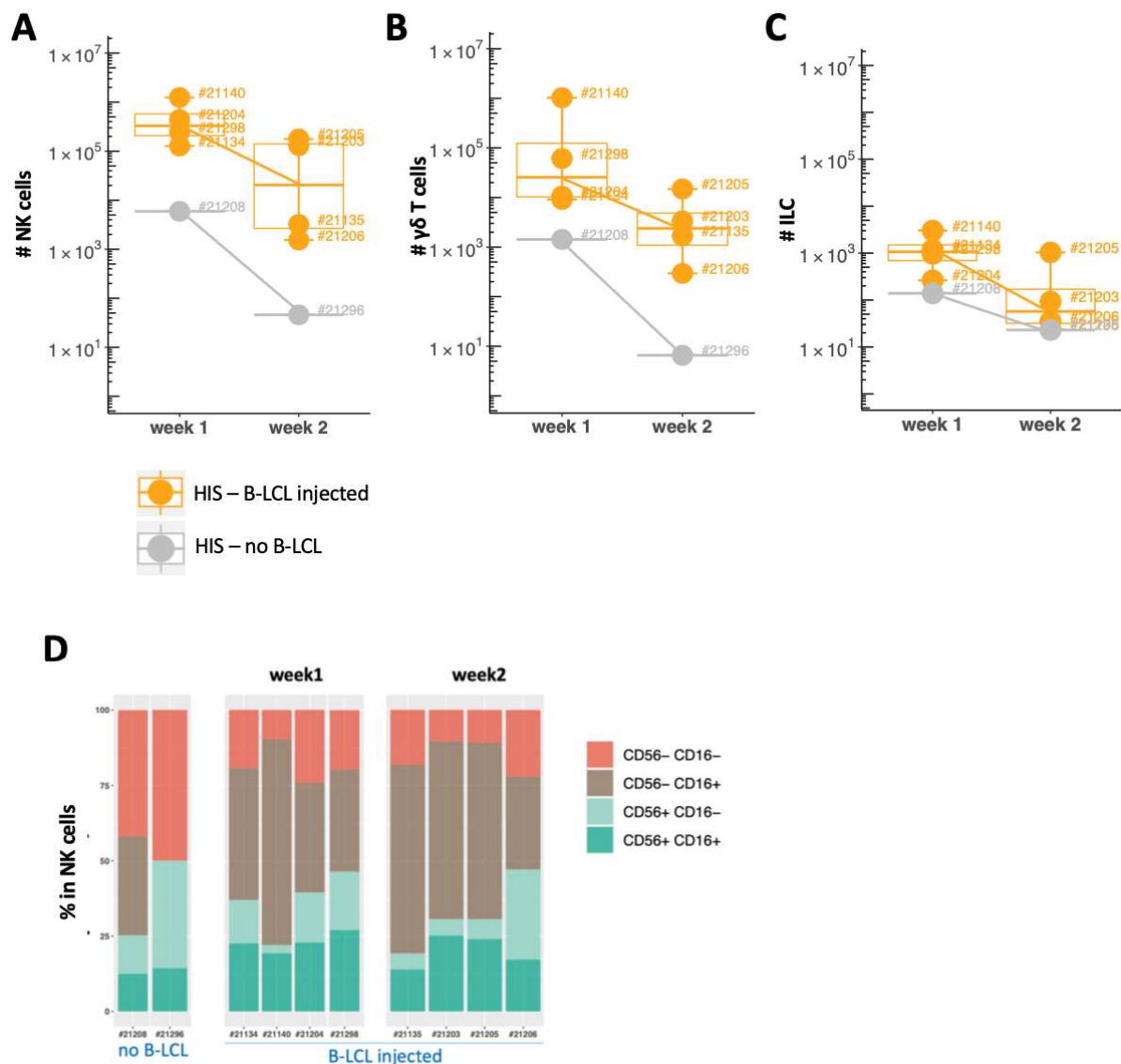


Figure 7. Lymphocyte numbers and frequencies of immune cell subsets in the peritoneal cavity of B-LCL injected HIS mice and non-injected control mice at week 1 and week 2 after injection. (A-C) each dot corresponds to one mouse and its number is indicated next to each dot. (A) NK cell numbers (B) $\gamma\delta$ T cell numbers (C) ILC numbers. (D) Frequencies of NK cell subsets, each column corresponds to one mouse and its number is indicated at the bottom of the column, in no B-LCL injected mice left column corresponds to the control mouse at week 1 and right column to the control mouse at week 2.

Taken together, this experiment suggests that the newly generated B-LCL cells are immunogenic because increased immune cell numbers are detected in the peritoneal cavity of B-LCL injected mice. This finding may result from proliferation and infiltration of immune cells. Furthermore, B-LCL cells appear to be sensitive to depletion by human immune cells *in vivo*, as B-LCL cell numbers are decreased in HIS mice compared to immunodeficient mice. Various human immune cell populations, such as cytotoxic T and NK cells which were abundantly found in the peritoneal cavity of B-LCL injected HIS mice may contribute to the B-LCL elimination. Whether this is due to alloreactivity or whether the B-LCL are also immunogenic and get depleted in an autologous setting remains to be determined.

B-LCL depletion in immunocompetent mice and allogeneic HIS mice

Further, we investigated to which extent the B-LCL cells get depleted in immunocompetent mice and whether there is a difference between HIS mice either with an immune system partially HLA-matched to the B-LCL, versus those with an HLA-mismatched immune system. We compared B-LCL numbers in the peritoneal cavity one week after i.p. injection of 10^6 B-LCL cells in (1) BALB/c mice, (2) BRGS mice with an HLA-A2⁻ HLA-DR2⁻ HIS, (3) BRGSA2DR2 mice with an HLA-A2⁺ HLA-DR2⁺ HIS and (4) immunodeficient BRGSA2DR2 mice with no HIS (Figure 8). This revealed that HIS mice with an allogeneic HIS (2) can deplete the B-LCL cells to similar levels as immunocompetent BALB/c mice (1). In HLA-mismatched HIS mice (2), lower B-LCL cell numbers were detected than in some of the HLA-matched HIS mice (3), which may indicate an alloreactive response in addition to an anti-tumor response. However, no statistically significant difference was detected between these groups. Overall, B-LCL cell numbers were decreased in immunocompetent and HIS mice compared to immunodeficient mice. Hence, the B-LCL cells were depleted in immunocompetent and HIS mice, indicating that the B-LCL cells are immunogenic.

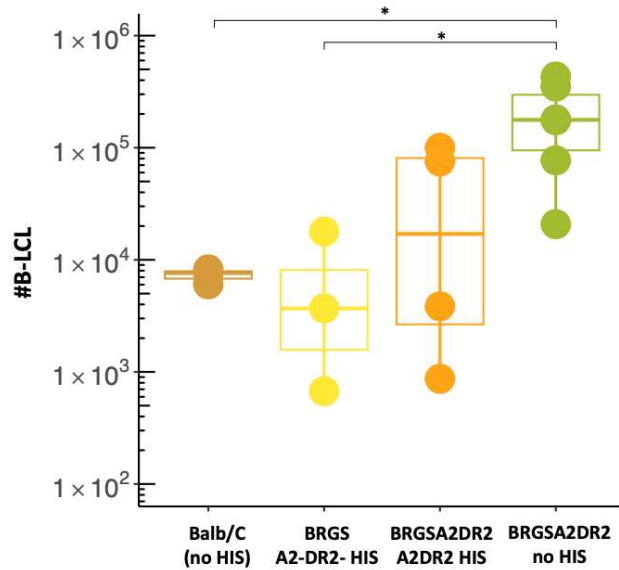


Figure 8. Numbers of B-LCL cells in the peritoneal cavity at week 1 after i.p. injection of 10^6 HLA-A2⁺ HLA-DR2⁺ B-LCL cells per mouse into immunocompetent mice (BALB/c), HLA-mismatched HIS mice (BRGS with A2-DR2- HIS), HLA-matched (BRGSA2DR2 with A2⁺DR2⁺ HIS) and immunodeficient mice (BRGSA2DR2 with no HIS). Statistical analysis by Wilcoxon test, * $p < 0.05$.

Longer survival of humanized BRGSA2DR2 mice after B-LCL injection

Next, we assessed whether mice with a HIS are able to fully reject the injected B-LCL cells or whether the B-LCL cells eventually expand, form tumors and are lethal similar to immunodeficient mice. 10^6 B-LCL cells were injected i.p. into HLA-matched HIS mice and the bodyweight as well as the physical appearance were regularly monitored. Compared to non-HIS mice, bodyweight loss in HIS mice occurred a few days later and at day 27 post injection the B-LCL cell numbers in the blood of most HIS mice were lower (Figure 9). Furthermore, some HIS mice survived up to 12 days longer than the non-HIS mice. However, there is no statistically significant difference between LCL injected groups and all HIS mice died or had to be sacrificed according to the regulations within 43 days post B-LCL injection whereas PBS-injected control mice showed no signs of stress or pain, had no weight loss and all survived beyond 43 days. Similar to the non-HIS BRGSA2DR2 mice, large tumor masses were found in the peritoneal cavity of BRGSA2DR2 HIS mice. Even though some HIS mice are able to deplete B-LCL cells (Figure 6) none of the HIS mice in this long-term experiment were

able to fully reject the B-LCL cells or keep them from outgrowing and consequently the B-LCL injection was lethal for the HIS mice.

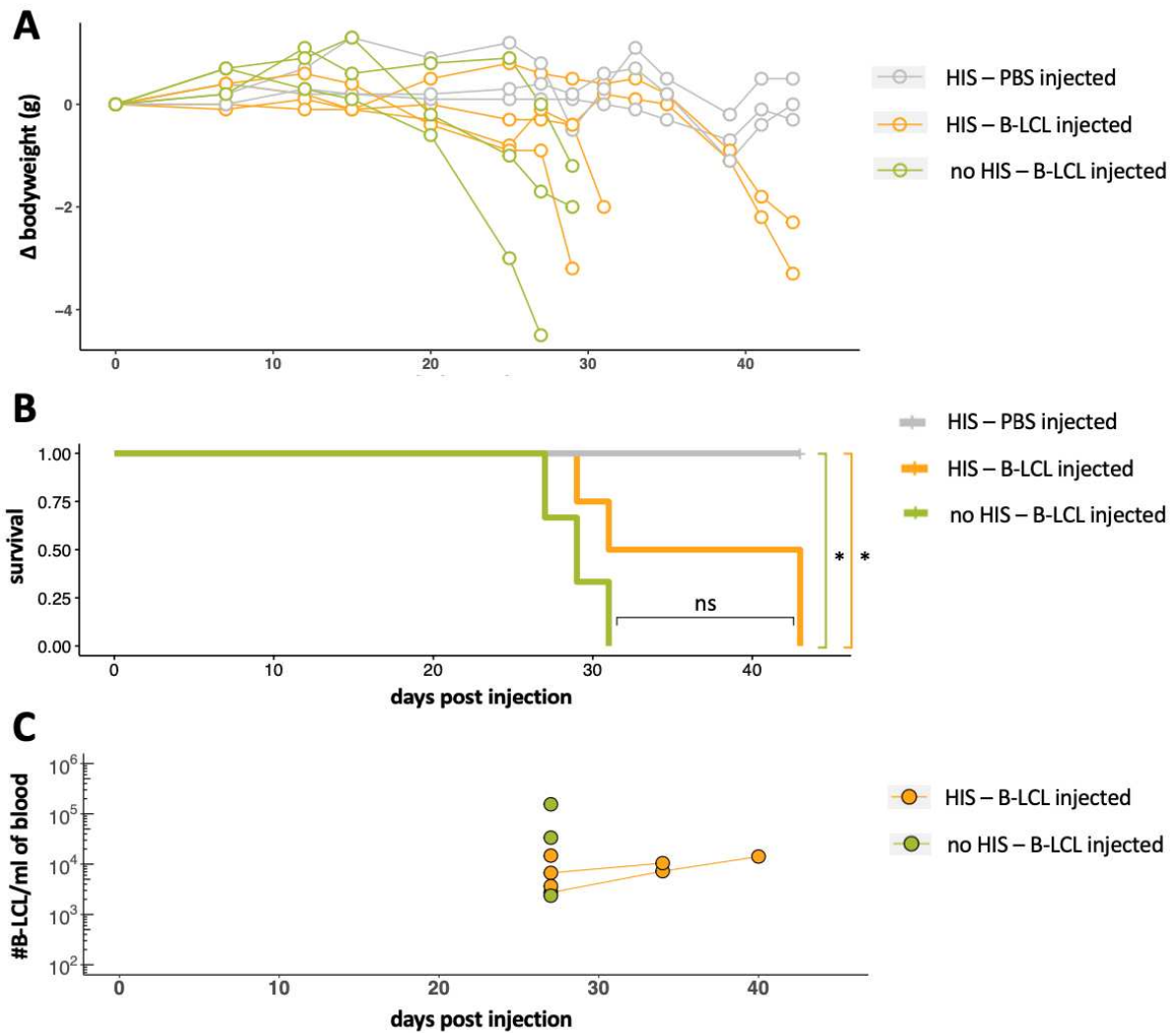


Figure 9. Progression of tumors in B-LCL injected HIS BRGSA2DR2 mice

(A) Longitudinal difference of bodyweight to d0 for over time, each line corresponds to one mouse (B) Survival of mice over time (C) Number of B-LCL cells per ml of blood measured at different timepoints. Statistical analysis by Mantel-Cox test, ns: $p > 0.05$, * $p < 0.05$.

Testing of therapeutic antibodies in IL-15 boosted FcγR deficient HIS mice

Finally, we combined our novel BRGSA2DR2 Fcγ1g^{-/-} model with the B-LCL tumor model to test the anti-CD20 antibody Rituximab mediated depletion of B-LCL cells, which express the B cell marker CD20 on their surface. Furthermore, we tested whether the boosting of human NK cells by injection of an IL-15-IL-15Rα complex (IL-15 boost) would increase the B-LCL depletion efficiency in HIS mice. We boosted BRGSA2DR2 mice that were humanized with HLA-A2⁺ and HLA-DR2⁺ HSCs by injecting IL-15-IL-15Rα complex over the course of 2 weeks. Subsequently, we injected the mice with 8x10⁵ B-LCL cells and IgG1-Rituximab (RTX) and sacrificed them 48h later (Figure 10A). At this early timepoint, the effects of innate immune cells rather than the adaptive immune response can be measured in the peritoneal cavity. The B-LCL cells were stained with violet trace prior to injection for improved distinction from HIS cells. Moreover, we included controls of mice (1) without a HIS (no HIS) injected with B-LCL, (2) HIS mice without IL-15 boost, B-LCL and RTX injection, (3) HIS mice without IL-15 boost and with B-LCL injection, (4) HIS mice without IL-15 boost injected with B-LCL and RTX and (5) IL-15 boosted mice injected with B-LCL but without RTX injection. In each group, except for the HIS only group, we included BRGSA2DR2 Fcγ1g^{+/-} and BRGSA2DR2 Fcγ1g^{-/-} mice.

To determine the efficiency of the IL-15 boost we compared the numbers of NK cells in the blood between the prebleed at day 1 (d1) and the bleed at day 14 (d14) (gating strategy in Figure 10B). Whereas in some IL-15 boosted mice the NK cell numbers in the blood increased, surprisingly it decreased in others, so the NK cells numbers in the blood between d1 and d14 were not significantly different. In the PBS injected control mice, the NK cell numbers mostly stayed stable between the two timepoints (Figure 10C). However, in the IL-15 boosted mice the percentage of CD16⁺ cells (Figure 10D) within total NK cells increased as well as the percentage of CD57⁺ (Figure 10E) and CD69⁺ (Figure 10F) NK cells with a statistically significant difference for all these markers. This was not the case in PBS injected mice. In this experiment the IL-15 boost did not robustly increase NK cells numbers in the blood. Nevertheless, the NK cells appear to be more activated.

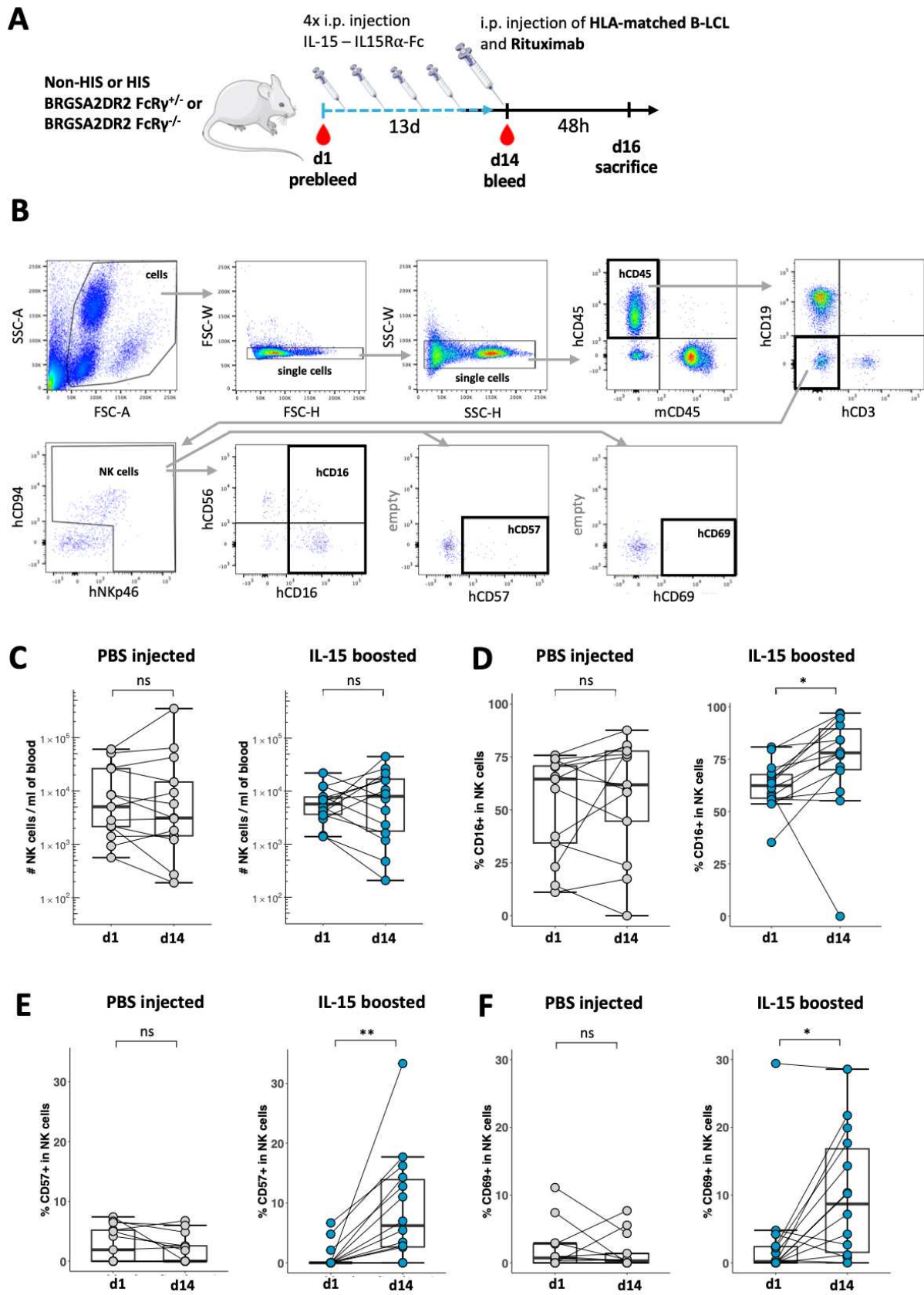


Figure 10. NK cells in the blood of IL-15-IL-15Ra complex injected mice. (A) Scheme of the experiment (B) Gating strategy of NK cells in the blood of HIS mice. (C-F) Cell numbers or frequencies between d1 and d14 of PBS and IL-15-IL-15Ra complex

injected mice, each dot corresponds to one mouse and lines connect the same mice. (C) Number of NK cells per ml of blood. (D-F) Percentage of CD16⁺ (D), CD57⁺ (E), CD69⁺ (F) cells within NK cells. Statistical analysis by Wilcoxon test, ns: $p > 0.05$, * $p < 0.05$, ** $p < 0.01$.

Next, we analyzed the NK cells numbers in the peritoneal cavity at the sacrifice on day 16 (d16). In the majority of IL-15 boosted mice, both in the group with and without RTX injection, the number of NK cells is clearly higher than in the HIS mice without the boost, however the differences are not statistically significant (Figure 11B). As there are only few NK cells in the peritoneal cavity of non-boosted HIS mice a precise analysis of NK cell subsets in each group is challenging. Nevertheless, the uniform manifold approximation and projection (UMAP) on the total NK cells in the peritoneal cavity reveals that the NK cells seem similarly distributed within non-IL-15 boosted HIS mice whereas differences were observed compared to IL-15 boosted mice (Figure 11C). Between the two IL-15 boosted groups (with or without RTX) the NK cell subsets in the peritoneal cavity were mostly overlapping except for a small subset which was CD56^{low}, NKG2A^{-/low} and had a slightly higher PD-1 signal than the other NK cells. This subset was mainly present in the IL-15 boosted, B-LCL and RTX injected HIS mice and not in the IL-15 boosted, B-LCL injected HIS mice without RTX treatment. These results indicate that IL-15 boost efficiently increases the numbers of NK cells in the peritoneal cavity either due to expansion of the NK cells and/or recruitment of NK cells.

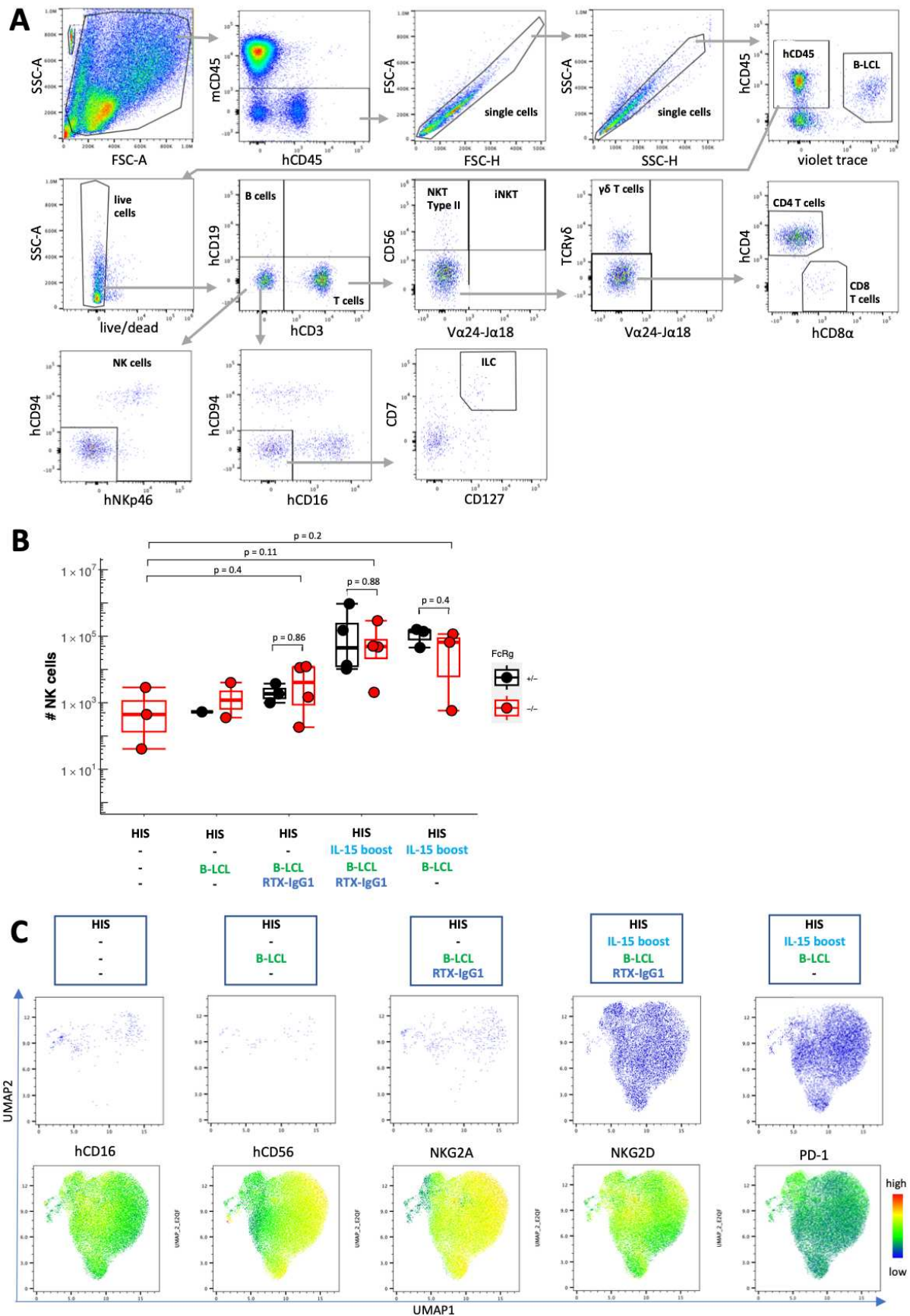


Figure 11. Increased NK cell numbers in the peritoneal cavity of IL-15 boosted HIS mice; (A) Gating strategy for B-LCL and human lymphocytes in the peritoneal cavity

of HIS mice (B) Number of NK cells in the peritoneal cavity at d16 (C) UMAP of total NK cells, upper row: NK cells according to different groups, lower row: heatmap statistic for expression of different markers on NK cells. Wilcoxon test was used for statistical analysis, indicated p-values are not corrected for multiple comparison, for Bonferroni corrected p-values no statistical significance was observed.

Furthermore, we quantified the number of B-LCL cells present in the peritoneal cavity at the sacrifice on d16 of mice that had been injected with B-LCL 48h prior to sacrifice. Compared to the mice with no HIS B-LCL cell numbers are lower in the majority of HIS mice (Figure 12B). However, this did not reach statistical significance for any group. Due to a large variation of B-LCL numbers within the different groups of HIS mice, more mice per group are needed to determine further differences. Nevertheless, in the RTX injected groups, more than half of the mice show B-LCL numbers which are lower than the lowest value in the HIS-only group. This suggests that the RTX treatment leads to B-LCL depletion in these mice. In the IL-15 boosted group without RTX treatment a few mice showed lower B-LCL cell numbers than HIS mice injected with B-LCL cells which may be caused by the IL-15 boost. This indicates that B-LCLs are sensitive to RTX treatment and IL-15 boost may enhance the elimination of B-LCL in HIS mice. The lack of explicit differences between Fc γ 1g $^{+/-}$ and Fc γ 1g $^{-/-}$ mice in the RTX injected groups suggests a role of mouse complement in the antibody mediated B-LCL depletion, as demonstrated in the blood for B-cell depletion (Chapter II)

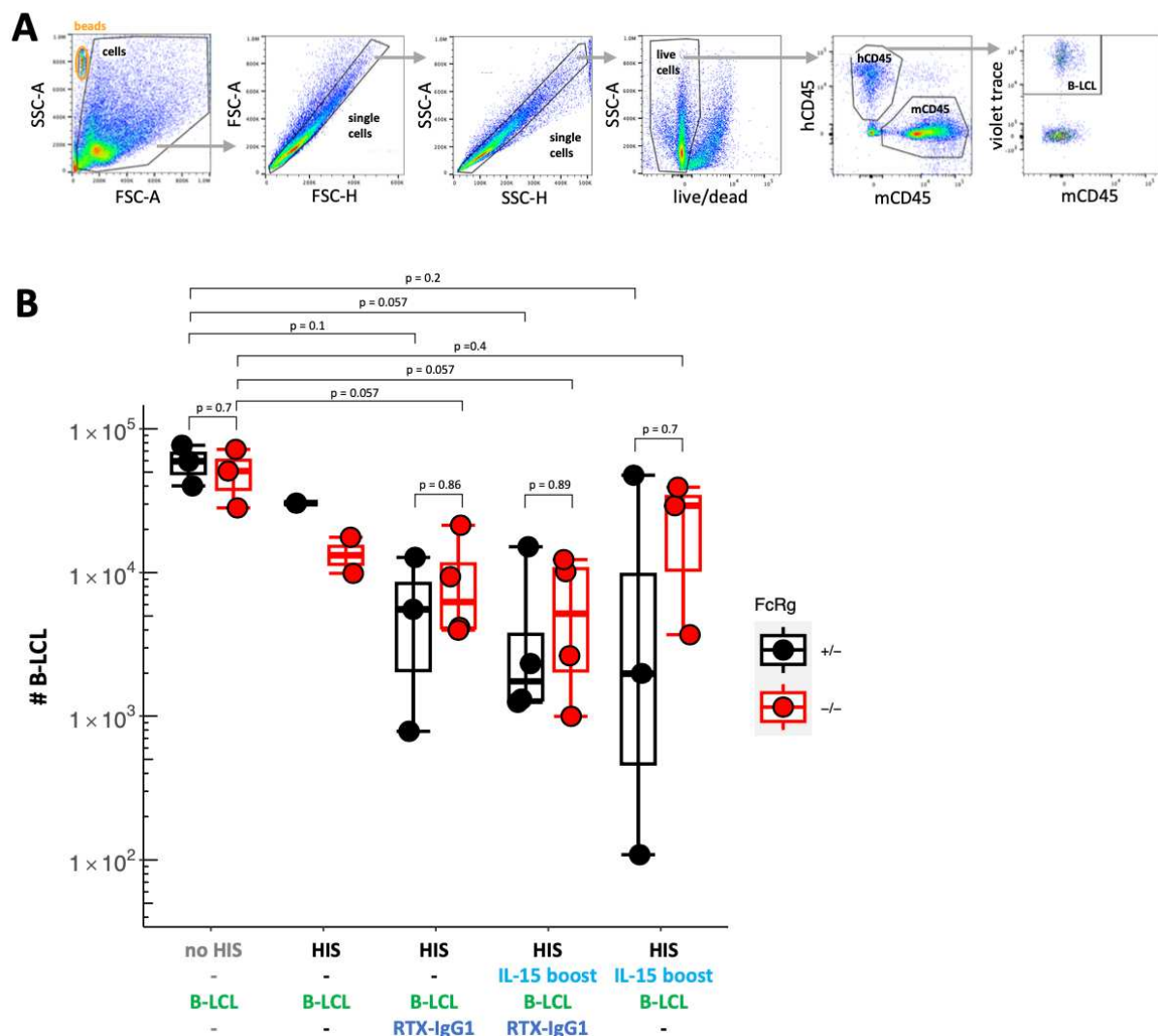


Figure 12. B-LCL in the peritoneal cavity at day 16 (A) Gating strategy for B-LCL (B) Number of B-LCL cells. Wilcoxon test was used for statistical analysis, indicated p-values are not corrected for multiple comparison, for Bonferroni corrected p-values no statistical significance was observed.

We further analyzed other human lymphocyte populations and human as well as mouse myeloid cells in the peritoneal cavity for the different groups of mice at sacrifice. Human CD8 α T cells were more abundant in the peritoneal cavity of B-LCL injected mice and further increased in IL-15 boosted mice (Figure 13A). Low numbers of human ILCs were identified in all HIS mice without evident differences between the experimental groups (Figure 13B). In most HIS mice boosted with IL-15-IL-15R α complex and/or treated with RTX the $\gamma\delta$ T cells (Figure 13C), as well as CD3⁺ CD56⁺ Va24-J α 18⁻ type II NKT cells (Figure 13D), were elevated compared to non-injected

or only B-LCL injected HIS mice. Whereas CD8 α T cells are not expected to impact the B-LCL depletion two days after B-LCL injection, $\gamma\delta$ T cells and type II NKT cells belong to the innate arm of the immune system and can be activated early on in the immune response. Hence, they may be involved in the elimination of B-LCL cells.

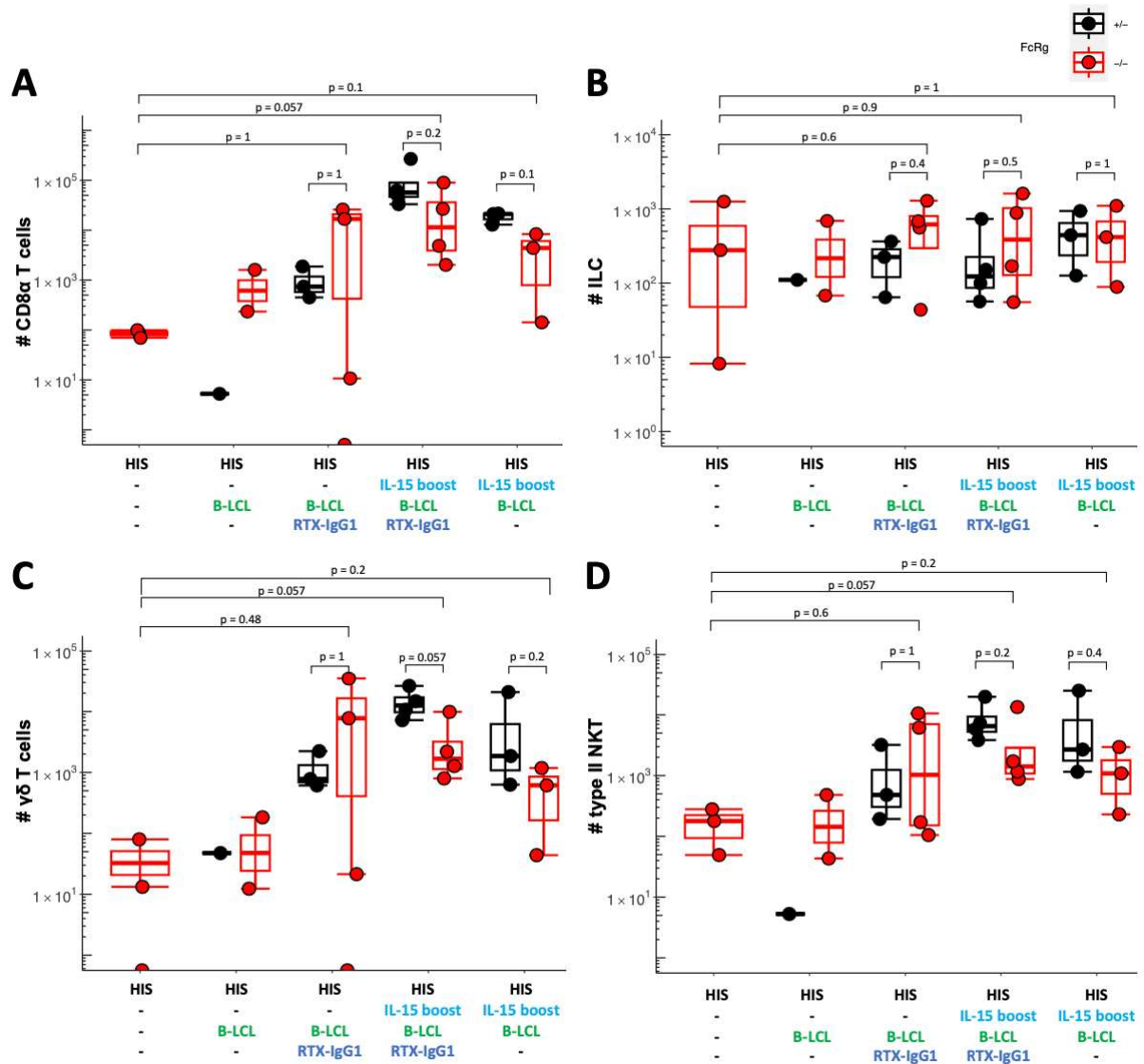


Figure 13. Human lymphoid cell subsets in the peritoneal cavity at d16; Numbers of (A) CD8 α ⁺ T cells, (B) ILCs, (C) $\gamma\delta$ T cells and (D) Type II NKT cells. Wilcoxon test was used for statistical analysis, indicated p-values are not corrected for multiple comparison, for Bonferroni corrected p-values no statistical significance was observed.

Human myeloid cells were found at low levels in the peritoneal cavity (Figure 14B) and in all groups some DCs (CD11c⁺ HLA-DR^{high}) and pDCs (CD123⁺) are present (Figure

14C). Whereas in the HIS-only mice barely any human macrophages (CD86⁺ CD64⁺) were observed, these were present in all B-LCL injected HIS mouse groups and seem to be most abundant in the B-LCL injected, RTX treated group. Especially on the macrophages, several activating FcγRs were expressed, FcγRI (CD64), FcγRIIA (CD32a) and FcγRIII (CD16), which may contribute to the antibody dependent depletion. No human CD66abce⁺ granulocytes were found in the peritoneal cavity of HIS mice. Consequently, human myeloid cells represent a further group of effector cells which could be involved in the elimination of B-LCL cells within the peritoneal cavity.

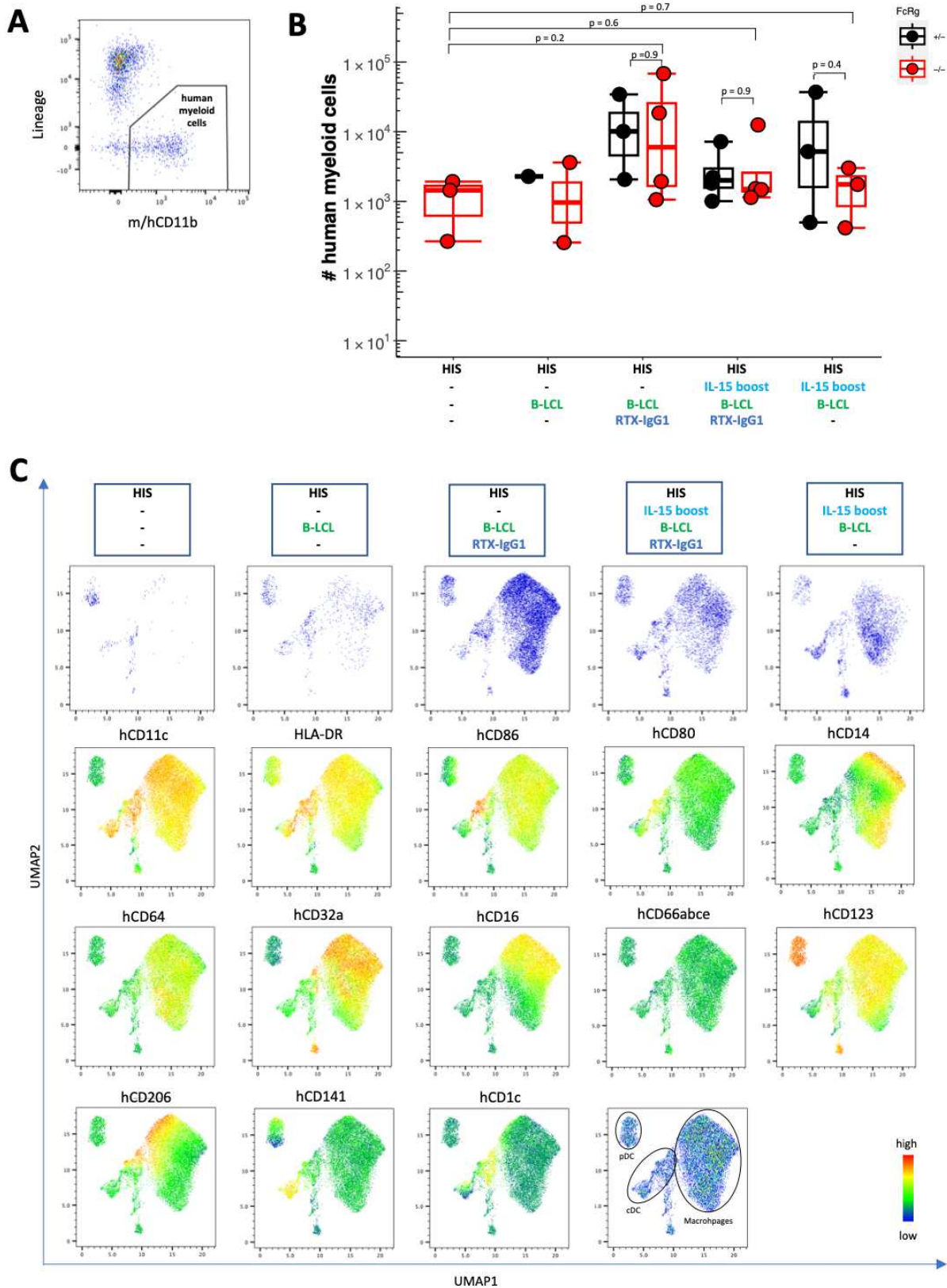


Figure 14. Human myeloid cells in the peritoneal cavity at day 16. (A) Gating strategy for human myeloid cells on hCD45⁺ cells (see Figure 12A), lineage includes hCD3, hCD7, hCD19, hCD94 and hNKp46. (B) Number of total human myeloid cells. (C) UMAP of total human myeloid cells, upper row: human myeloid cells according to

different groups, lower rows: heatmap statistics for expression of different markers on human myeloid cells. Wilcoxon test was used for statistical analysis, indicated p-values are not corrected for multiple comparison, for Bonferroni corrected p-values no statistical significance was observed.

Lastly, we compared mouse myeloid cell numbers between the different groups. High numbers of mouse myeloid cells were found in the peritoneal cavity for the majority of mice (Figure 15B). The mouse myeloid cells in all mice comprised granulocytes (Gr1⁺), macrophages (F4/80⁺) and DCs with altered proportions between the different groups (Figure 15C). In mice with no HIS the macrophage populations was most dominant in the peritoneal cavity. In HIS mice without injection of B-LCL a macrophage population with low mF4/80 expression is observed which not very present in other groups. Whereas in HIS mice only injected with B-LCL the different myeloid cell populations seem quite balanced, HIS mice treated with either RTX-IgG1 and/or IL-15 boost had a more prominent granulocyte population than other groups. Mouse myeloid cells could impact the immune response against B-LCL, for example by cytokine secretion. While in Fc ϵ 1g^{+/-} mice the mouse myeloid cells may contribute to the antibody mediated B-LCL depletion, this is precluded in the Fc ϵ 1g^{-/-} mice.

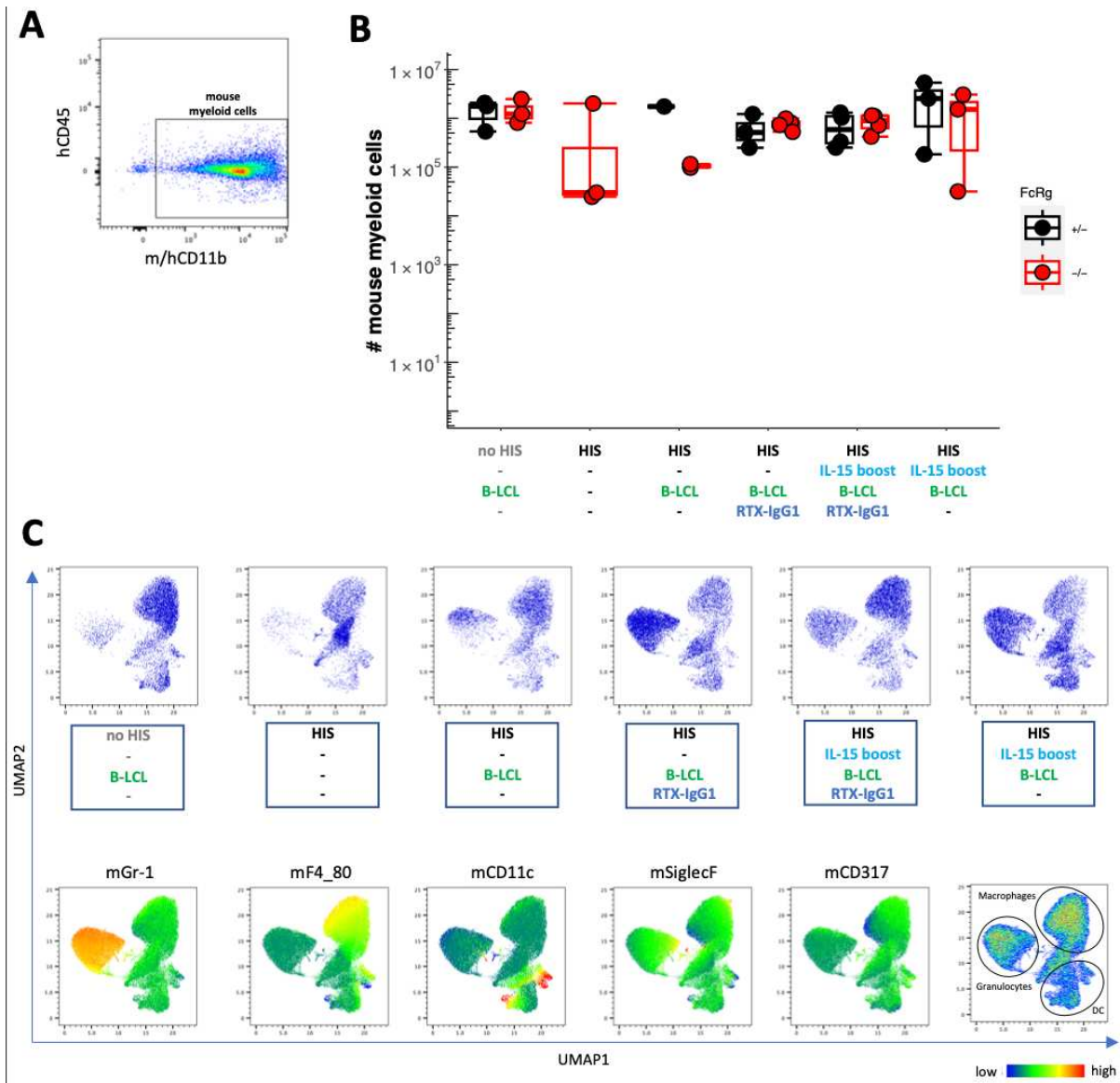


Figure 15. Mouse myeloid cells peritoneal cavity at day 16 (A) Gating strategy for mouse myeloid cells on mCD45⁺ cells (see Figure 12A) (B) Number of total mouse myeloid cells (C) UMAP of total mouse myeloid cells, upper row: mouse myeloid cells according to different groups, lower rows: heatmap statistic for expression of different markers on mouse myeloid cells.

3.3 Conclusion

By employing in vitro EBV transformation of B cells extracted from the spleen and bone marrow of HIS mice, we have successfully generated immortalized cell lines autologous to fetal liver CD34⁺ HCS that can be used to graft HIS mice which will allow to establish a fully autologous model. These immortalized cells have a B cell phenotype and express B-LCL characteristic markers. The B-LCL cells efficiently graft and expand in immunodeficient mice upon i.p. injection and have tumorigenic potential. In these mice solid tumor masses were found within the peritoneal cavity and substantial amounts of B-LCL were also detected in the spleen and liver. Further, the B-LCL cells showed immunogenic potential, since human immune cells were recruited to the peritoneal cavity of B-LCL injected HIS mice and B-LCL numbers decreased in partially HLA-matched HIS mice from week 1 to week 2 after B-LCL injection. Higher elimination of B-LCL was found in HLA-mismatched HIS mice compared to HIS mice that had been humanized with partially HLA-matched HSCs, indicating lower alloreactivity in the latter setting.

By combining the B-LCL tumor model with our novel BRGSA2DR2 FcγR1^{-/-} model we aimed to evaluate the antibody mediated depletion in the absence of mouse myeloid cell effector mechanisms, which are mediated through activating FcγRs. In addition, we administered an IL-15-IL-15Rα complex to boost human NK cells to determine whether these cells improved antibody mediated depletion of B-LCL. While NK cell numbers in the blood of HIS mice were not higher after the IL15 boost in the majority of mice, NK cell numbers in the peritoneal cavity were found to be increased in most IL-15 boosted mice. In addition, CD8α T cells were particularly increased in the peritoneal cavity of IL-15 boosted HIS mice but as we chose a very short timeline of 48h after B-LCL injection to analyze the mice, the detected effects should be mainly mediated by innate immune cells.

Our B-LCL cells seem to be sensitive to RTX treatment and the IL15 boost also seems to improve the B-LCL depletion in some mice. However, no additive effects of RTX treatment in combination with the IL15 boost were evident and no clear differences in RTX mediated B-LCL depletion between FcγR1^{-/-} and FcγR1^{+/-} mice were visible. The reason for this might be that we used the IgG1 variant of Rituximab in these experiments, which can also be bound by complement. Hence, the complement system may contribute to depletion of B-LCL cells and, as shown in Chapter II, be

responsible for the depletion of B cells. Therefore, it may be necessary to use a non-complement binding Rituximab variant like the IgG1_KA to see a clear difference between the Fc γ 1g $^{-/-}$ and Fc γ 1g $^{+/-}$ mice to preclude the contribution of mouse complement and mouse Fc γ R bearing cells to the Rituximab mediated depletion of B-LCL cells. In addition, more mice per treatment are needed to clearly evaluate whether statistically significant differences exist between the groups due to the large individual variation within some groups.

In summary, we have established a haplotype matched model to evaluate the anti-tumoral mechanisms of immunotherapeutic antibodies by the human immune system.

3.4 Material and Methods

Mice

Refer to Material and Methods in chapter II.

B-LCL generation and culture

Cells were isolated from the spleen and bone marrow and depleted for mCD45⁺ cells by labelling with a biotin conjugated anti-mCD45 antibody, subsequent incubation with anti-biotin microbeads (Miltenyi Biotech) and separation on LS columns (Miltenyi Biotech) following manufacturer's instructions. EBV transformation was done in collaboration with Sylvain Latour (Institut Imagine), cells were given to the Necker DNA biobank of Institut Imagine. B-LCL were cultured under sterile conditions in tissue culture flasks (TPP) at 37°C, 5% CO₂ in RPMI 1640 + Glutamax (gibco) supplemented with 10% fetal calf serum (FCS) (eurobio), 1% Penicillin and Streptomycin, 1% Non-essential amino acids, 1% Sodium-Pyruvate (gibco). B-LCL were frozen in FCS with 10% DMSO (Sigma-Aldrich) and thawed 1-3 weeks before injection.

***In vivo* injection of B-LCL**

B-LCL were washed and resuspended in PBS and injected intraperitoneally (i.p.) using 29G insulin syringes. Mice were euthanized one week or two weeks after injection or at endpoint (>20% of weight loss or according to signs of pain) as indicated in the experiment.

IL-15 boost, B-LCL, Rituximab experiment in BRGSA2DR2 Fcer1g^{+/-} and BRGSA2DR2 Fcer1g^{-/-} HIS mice

Mice were pre-bled on d1 and subsequently injected with IL-15 complex (25µg hIL-15 + 75µg hIL-15R alpha Fc Chimera Protein (biotechne) per mouse in PBS and incubated at room temperature (RT) for 30min before injection) or PBS for control mice on d2, d6, d9, d13. On d14 mice were first bled and then injected with 8x10⁵ B-LCL in 100µl of PBS per mouse and 50µg Rituximab (IgG1) per mouse according to the treatment group. Injected B-LCL had been stained with 0,5µM CellTrace Violet (Thermo Fisher Scientific) in PBS prior to injection, following manufacturer's

instructions. Mice with less than 10% of hCD45+ cells or with more than 80% human T cells within hCD45+ cells in the blood at prebleed were excluded from analysis.

Cell isolation

To recover the cells from the peritoneal cavity mice were sacrificed by cervical dislocation, the skin in the abdominal area was opened and 12ml of FACS buffer (PBS (gibco) with 2%FCS and 2mM EDTA (invitrogen)) were injected with a 20ml syringe (BD bioscience) and the cell suspension was subsequently aspirated from the peritoneal cavity with the same syringe and collected in a 15 ml tube.

Flow cytometry analysis

Whole blood or isolated cells were incubated with IgG from human serum (Sigma-Aldrich) and mouse Fc blocking reagent (Miltenyi Biotech) for 10min at RT 2,5µl or 5µl of absolute counting beads (invitrogen) were added respectively. Subsequently, biotin-conjugated antibodies in FACS buffer or fluorochrome-conjugated antibodies in Brilliant Stain Buffer (BD bioscience) for extracellular staining and live/dead stain were added and cells incubated at 4°C for 30min. For whole blood FACS™ lysing solution (BD) was directly added to lyse red blood cells and fix the samples, other cells were washed twice with FACS buffer. Cells stained with biotin antibodies were afterwards stained with fluorochrome-conjugated streptavidin and antibodies for 30min at 4°C and washed. If no intracellular staining was done cells were fixed with 2% PFA (EMS) for 10min at 4°C. For intracellular staining cells were fixed and permeabilized with Cytotfix/Cytoperm™ (BD Bioscience) for 20min at 4°C, washed twice with Perm Buffer (BD), incubated with antibodies diluted in Perm Buffer for 30min at RT and washed with Perm Buffer. All samples were resuspended in FACS buffer for flow cytometric analysis. Samples were either run on a LSRFortessa™ (BD) or Spectral ID7000™ Spectral Analyzer (Sony).

antigen	fluorochrome/conjugate	clone	reactivity	supplier	catalog number
CD1c	BV786	L161	human	BioLegend	331544
CD3	APC	BW264/56	human	Miltenyi Biotec	130-091-373
CD3	BB790	UCHT1	human	BD	624296
CD3	Biotin	OKT3	human	eBioscience	13-0037-82
CD3	BV510	SK7	human	BioLegend	344828
CD4	NovaFluor Blue 660-120S	SK3	human	eBioscience	H001T03B08
CD7	Biotin	eBio124-D1	human	eBioscience	13-0079-82
CD7	BV510	M-T701	human	BD	563650
CD7	PerCP-eFluor710	4H9	human	eBioscience	46-0078-42
CD11b	PerCP-Cy5.5	M1/70	human/mouse	BioLegend	101228
CD11c	BV480	B-ly6	human	BD	566135
CD11c	PE-Cy7	N418	mouse	BioLegend	117318
CD14	BV570	M5E2	human	BioLegend	301832
CD14	PE-Cy5	M5E2	human	BioLegend	301864
CD16	BUV496	3G8	human	BD	564653
CD16	BUV737	3G8	human	BD	564434
CD16	BV570	3G8	human	BioLegend	302036
CD16	BV650	3G8	human	BioLegend	302042
CD19	Biotin	HIB19	human	eBioscience	13-0199-82
CD19	BV605	HIB19	human	BioLegend	B206070
CD19	PE	HIB19	human	BioLegend	302208
CD19	PE-Cy5	HIB19	human	BioLegend	302210
CD20	BV786	2H7	human	BioLegend	302356
CD21	BUV737	B-ly4	human	BD	564595
CD23	AF700	M-L233	human	BD	563673
CD25	BV711	BC96	human	BioLegend	302635
CD27	APC-eFluor780	O323	human	eBioscience	47-0279-42
CD27	BUV737	L128	human	BD	564301
CD32a	AF647	FUN-2	human	SONY	2116060
CD39	PE-Cy7	eBioA1	human	eBioscience	25-0399-42
CD45	APC-Vio770	5B1	human	Miltenyi Biotec	130-096-609
CD45	BB630	30-F11	mouse	BD	
CD45	BUV395	HI30	human	BD	563792
CD45	BUV805	HI30	human	BD	612891
CD45	BV650	30-F11	mouse	BD	563410
CD45	BV711	30-F11	mouse	BD	563709
CD45	NovaFluor Blue 610-70S	30-F11	mouse	eBioscience	M005T02806
CD45RA	BUV563	HI100	human	BD	565702
CD56	BB755	NCAM16.2	human	BD	624391
CD56	BUV395	NCAM16.2	human	BD	563554
CD56	PE-CF594	B159	human	BD	562289
CD57	BV605	QA17A04	human	BioLegend	393304
CD64	BUV737	10.1	human	BD	612778
CD66abce	PE	REA1230	human	Miltenyi Biotec	130-124-503
CD69	AF700	FN50	human	BD	560739
CD70	PE	113-16	human	BioLegend	355104
CD80	BV750	L307.4	human	BD	747001
CD86	BUV563	BU63	human	BD	748377
CD8a	BV786	RPA-T8	human	BioLegend	301046
CD94	APC-Fire750	DX22	human	BioLegend	305518
CD94	Biotin	REA113	human	Miltenyi Biotec	130-098-966
CD94	BUV661	HP-3D9	human	BD	750231
CD94	BV750	HP-3D9	human	BD	747394
CD94	PerCP-Vio700	REA113	human	Miltenyi Biotec	130-119-763
CD117	BB790	104D2	human	BD	624296
CD123	PE-Cy5	6H6	human	BioLegend	306008
CD127	PE-Cy7	eBioRDR5	human	eBioscience	25-1278-42

antigen	fluorochrome/conjugate	clone	reactivity	supplier	catalog number
CD141	BV711	1A4	human	BD	563155
CD159a (NKG2A)	APC-Fire750	S19004C	human	BioLegend	375116
CD161	BUV395	HP-3G10	human	BD	748280
CD206	BV605	19.2	human	BD	740417
CD279 (PD-1)	BUV615	EH12.1	human	BD	612991
CD294 (CRTh2)	AF647	BM16	human	BD	558042
CD314 (NKG2D)	BV711	1D11	human	BD	563688
CD317	BUV661	BST2	mouse	BD	750635
F4/80	BUV805	T45-2342	mouse	BD	749282
Gr-1	AF700	RB6-8C5	mouse	BD	557979
HLA-A2	FITC	BB7.2	human	BD	551285
HLA-DR	APC-Fire750	L243	human	BioLegend	980412
MHCII	BUV496	M5/114.15.2	mouse	BD	750281
NKp46	BB515	9E2/NKp46	human	BD	564536
NKp46	Biotin	9E2/NKp46	human	BioLegend	331906
NKp46	BV421	9E2/NKp46	human	BD	564065
SiglecF	PE-CF594	E50-2440	mouse	BD	562757
TCRgd	BUV661	11F2	human	BD	750019
TCRgd	PE	B1	human	BD	555717
Va24Ja18	PerCP-eFluor710	6B11	human	BioLegend	46-5806-42

Table 1 – List of antibodies

Chapter IV

Discussion

Human immune system (HIS) mice provide valuable preclinical models to study human immune cells and HIS responses *in vivo*. HIS mice may further be engrafted with human tumor models which allows to investigate human specific immune system–tumor interactions and to test anti-tumor immunotherapies in an *in vivo* setting. Over the last decades various HIS mouse models with different characteristic properties have been generated. However, in the currently available humanized mouse models for immuno-oncology research, several limitations exist and it is important to understand those relevant to the respective research question. The knowledge of these restrictions allows a more accurate interpretation of the results obtained and may subsequently foster the generation of more advanced models which overcome these limitations.

In this thesis, a novel BRGSA2DR2 Fcer1g^{-/-} HIS mouse model has been characterized which allows to determine the effectors involved in antibody mediated cell depletion when administering therapeutic antibodies. Further, we aimed at generating an autologous tumor model in HIS mice to be able to study human anti-tumor responses *in vivo* in the absence of alloreactive effects. The final goal was to combine the BRGSA2DR2 Fcer1g^{-/-} HIS mouse model with the autologous tumor model in order to investigate the contribution of human natural killer (NK) cells in antibody mediated anti-tumor responses *in vivo*.

Key findings

In the BRGSA2DR2 HIS mouse model we identified three types of effectors that contribute to antibody mediated depletion, which include (1) the mouse FcγR bearing cells, (2) the complement system and (3) human immune cells. For BRGSA2DR2 Fcer1g^{-/-} mice we demonstrated their deficiency in expression of FcγRs and the concomitant loss of function in activating FcγRs. Further, BRGSA2DR2 Fcer1g^{-/-} mice robustly engraft with human hematopoietic stem cells (HSCs) and develop a HIS. By

using an antibody variant (IgG1_KA) which cannot bind complement in the BRGSA2DR2 FcγR1g^{-/-} HIS mice we were able to investigate the antibody dependent depletion effects of the HIS while excluding the contribution of mouse effectors. In this experimental setting, the number of human NK cells in blood clearly correlated with the antibody mediated depletion efficiency.

Moreover, we generated an autologous lymphoma model by transforming HIS mouse derived human B cells via EBV infection. The resulting B lymphoblastoid cell line (B-LCL) cells were able to engraft upon intraperitoneal (i.p.) injection in immunodeficient mice as well as partially HLA-matched HIS mice, developing lethal tumors in these hosts. Further, the B-LCL cells are immunogenic and the HIS in our mice leads to decreased B-LCL cell numbers compared to immunodeficient mice. In addition, the boosting of HIS mice with IL-15-IL15Rα complex and/or treatment with Rituximab seems to improve the depletion of B-LCL cells in most mice compared to non-treated HIS mice.

In the following sections I firstly highlight evidence for human NK cells as main effectors in antibody mediated depletion in our HIS mouse model and elaborate on how HIS mouse models could be improved to study antibody dependent cellular cytotoxicity (ADCC) of NK cells. Secondly, I indicate options to ameliorate innate lymphoid cells (ILCs) and myeloid cell compartments in HIS mouse models. Thirdly, I will discuss the achievements I have made in generating an autologous tumor model and disclose its potentials as well as limitations. Lastly, I emphasize the perspectives for both, the BRGSA2DR2 FcγR1g^{-/-} HIS mouse model and the autologous tumor model as preclinical models for immunotherapeutic approaches.

Are the human NK cells the effectors that mediate antibody dependent depletion in our HIS mouse model?

Katano *et al.* (2020) established a NOG-FcγR^{-/-}-hIL-15 Tg model with adoptively transferred human NK cells which were expanded *in vitro*. Their results suggested that human NK cells were able to contribute to antibody mediated depletion *in vivo*. However, they also acknowledged that other effectors such as the complement may partly cause antibody dependent cytotoxicity in their model²⁸⁸. In our FcγR deficient model we found a statistically significant correlation between the percentage of NK

cells and the decrease of B cells in the blood when using a non-complement binding antibody variant which strongly indicates the involvement of NK cells in antibody mediated depletion (Chapter II). The fact that B cell depletion was absent in HIS mice lacking NK cells detected in the blood further suggests that human NK cells may be the major effectors of antibody-mediated depletion in our model. While we are impairing the contribution of complement and mouse FcγRs in the antibody mediated depletion, our model is complicated by the presence of other human immune cell subsets. Many human immune cells, other than NK cells, expressing activating FcγRs could potentially contribute in the antibody mediated depletion, such as macrophages, dendritic cells (DCs), neutrophils and other granulocytes²⁵⁰. However, myeloid cells develop poorly in HIS mice when not adding cytokines that specifically boost them. This is also the case for BRG and BRGS HIS mice on which our model is based^{274,297}. Thus, the contribution of human myeloid cells is likely to be limited but it cannot be fully excluded. The role of NK cells in the antibody mediated depletion is further supported by its increase when boosting with human IL15-IL15Rα complex. NK cell frequencies are elevated in the blood of boosted mice whereas numbers of macrophages, as shown for the liver, remain constant. Nevertheless, we have not determined the cell numbers for all activating FcγR bearing human cells in every organ and tissue and do not definitively know whether other immune cell frequencies also correlate with depletion efficiency.

Specific elimination of NK cells might underline the role of NK cells in antibody dependent depletion in our HIS mouse model in which other immune cells are present. In other HIS mouse models, NK cells have been depleted by administration of an anti-human NKp46 antibody but not all NK cells got depleted thereby, as some CD56⁺ CD3⁻ cells remained³⁹⁵. In addition, the depletion of NK cells using this mouse IgG1 antibody most likely depends on Fc binding effectors including mouse activating FcγRs which are not functional in our mouse model. Therefore, it needs to be carefully analyzed whether this antibody can efficiently deplete human NK cells in FcγR deficient HIS mouse models. A recently published anti-human NKp46 antibody that gets internalized upon NKp46 binding has been conjugated with a toxin and was shown to inhibit cell growth *in vitro*³⁹⁶. This antibody may be an alternative for NK cell depletion that does not depend on Fc binding effectors.

All pieces of evidence essentially support the involvement of NK cells in the antibody dependent depletion in our model. However, to provide a more explicit proof is challenging due the complexity of the model and to technical limitations.

How well adapted is our model system to study ADCC of human NK cell responses?

An difficulty in many HIS mouse models is the poor development of human NK cells. To increase the total number of NK cells and the proportion of CD16 expressing NK cells in our experiments, we administered a IL15-IL15R α complex to our mice which had been shown to augment NK cells in HIS mice²⁸⁴. In accordance, we observed an increase of NK cells and, similarly to humans, NK cells in the blood of IL-15 boosted HIS mice are mostly in the range of 5% to 15% of total hCD45. Further, antibody dependent B cell depletion is significantly improved in IL-15 boosted mice (Chapter II). Consequently, our experimental setup allows us to study human ADCC upon exogenous antibody injection.

However, I would like to point out that even in the IL-15 boosted NK cells in our HIS mice, we did not identify the same NK cells subsets in the peripheral blood as reported in humans. Instead, we identified a CD56⁺CD16⁻ but not a CD56^{bright} NK cell population. CD16⁺ cells were present in our HIS mice but rather than a CD56^{dim} population we observed a CD56⁺CD16⁺ as well as a CD56⁻CD16⁺ subpopulation, respectively. Hence, it might be worthwhile to also consider other methods available to enhance NK cells in HIS mice. Those alternatives could either boost the development of myeloid cells which subsequently enhances the NK cell development (MISTRG, BRGSF mice) or directly improve the NK cell development by expression of human IL-15 by a transgene or a knock-in (SRG-15, NSG-Tg(Hu-IL15) mice)^{273,290,291,297,397}. To optimize the experimental conditions for studying NK cells in HIS mice, it would be of interest to understand which method or model gives rise to NK cells which resemble NK cells in the human to a highest degree. Herndler-Brandstetter *et al.* (2017) directly compared NK cell numbers in blood as well as spleen between MISTRG and SRG-15 mice. Especially in the blood, NK cells were more abundant in SRG-15 mice. Further, circulating NK cells in SRG-15 mice were also compared to human NK cells by mass cytometry showing that they overlapped phenotypically to a large extent. However, NK cell subsets stimulated with an MHC-I-

deficient tumor cell line (K562) or phorbol 12-myristate 13-acetate (PMA) plus ionomycin revealed partial differences in expression of perforin, CD107a, IFN- γ , MIP-1 β and GM-CSF compared with humans²⁹⁰. Side-by-side comparisons are challenging as published studies differ in their use of mouse strains, antibodies, gating strategies and analysis techniques. To determine in which setting NK cells are best developed it would be instrumental to perform functional profiling on the NK cell subsets in the HIS mice in comparison to human blood and other tissues if possible.

Besides the cellular component, the antibody which mediates the killing in ADCC needs to be considered as well. In the setting in which we identified a correlation between the abundance of NK cells and the depletion efficiency we used an IgG1_KA variant of Rituximab. This IgG1_KA variant is characterized by a non-synonymous base substitution in the Fc region of the antibody causing a K322A mutation at the N-terminal end of the CH2 domain. We specifically selected this variant due to its inability to bind to complement, to remove this mechanism of action from the antibody mediated depletion. However, not only the complement binding is affected but also the binding to Fc γ RIIa and Fc γ RIIIa which causes a reduction of ADCC by about two-fold³⁹⁸. Consequently, by using the IgG1_KA variant of Rituximab, the ADCC potential of the NK cells is most likely underestimated in our experiment. Inhibitors of the complement cascade may provide an alternative to disable the contribution of the complement in antibody mediated depletion and could allow to use the conventional IgG1 Rituximab. For example, with the ANX-M1.21 C1q-blocking antibody, the complement cascade could be directly inhibited at the initiation of the classical pathway³⁹⁹. A further possibility to avoid the effects of complement is the knockout of crucial genes in the complement cascade, as proposed by Katano *et al.* (2020)²⁸⁸. The establishment of a model in which the contribution of complement can be circumvented without altering the Fc portion of the antibody would largely facilitate the testing of further antibodies of interest using our model as they could stay in their native form.

Studying the effects of human ILCs in anti-tumor responses

In the tumor experiments (Chapter III) I have also analyzed the cell numbers of helper innate lymphoid cells (ILCs) in the peritoneal cavity of HIS mice. Only low numbers of Lin⁻CD16⁻CD94⁻CD7⁺CD127⁺ ILCs were present (<10³ cells). Neither for different

conditions at 48h, nor at week one or week two post B-LCL injection, were any major alterations in cell numbers detected. Due to the low amount of ILCs I did not investigate further details such as identifying ILC subsets and their cytokine production profiles. However, as the role of human ILCs in cancer is not well understood to date, it would be extremely interesting to study the effects of ILCs in our HIS mouse tumor model. There are several options to adapt the model system that may facilitate the study of ILCs in the context of cancer. In the BRGSF model, increased numbers of human ILCs were observed in multiple organs of Flt3L boosted HIS mice. In addition, the production of the respective signature cytokines was demonstrated for ILC1 from the liver, ILC2 from the lung and for ILC3 from the gut²⁷⁴. Whether Flt3L boosting would increase the ILC abundance in the peritoneal cavity remains to be assessed. In humans, the distribution of ILC subsets varies largely between different tissues and organs⁴⁰⁰. And whereas NK cells are abundant in the circulation and can infiltrate into tissues, ILCs are mainly tissue resident. Moreover, ILCs are highly plastic and change their phenotype and function based on environmental signals¹⁶⁸. Therefore, to study ILC-tumor interactions it might be essential to establish tumor models in anatomical locations in which ILCs reside. For example, to study ILC3s which are abundant in the intestine, B-LCL cells could be injected into intestinal tissue. Another possibility to achieve higher numbers of ILCs could be the adoptive transfer of *in vitro* expanded ILCs. Protocols which allow the expansion of mature ILCs as well as ILC precursors *in vitro* have already been established^{84,401}. Also, human ILCPs from the fetal liver have been expanded *in vitro*⁸⁴. Since we retrieve the human CD34⁺ HSCs that we use for the humanization of HIS mice from fetal livers we actually have autologous ILCPs available. I have therefore conducted some experiments in which I expanded ILC3s from fetal liver ILCPs and injected them *i.p.* into immunodeficient mice. I was able to recover ILCs up to two weeks after injection (data not shown). Alternatively, HIS mice could be directly administered with cytokines, such as human IL-2, IL-7, IL-1 β , IL-23 and IL-25 to enhance the development of ILCs *in vivo*. Some of these approaches could also be combined and may provide exciting opportunities to study the effects of ILCs on tumors.

Improvement of myeloid cell compartments in HIS mice

Immune responses result from a complex interplay between innate immune cells, adaptive immune cells and their environment. Hence, to get a comprehensive view of immune responses in a model system all these components should be reproduced at its best. During an immune response, myeloid cells are active at many stages, such as the initiation and coordination of immune responses, antigen presentation and execution of effector mechanisms. In most HIS models mouse myeloid cells are abundantly present but human myeloid cells develop poorly and are strongly underrepresented^{273,297}. This is also true in the peritoneal cavity where mouse myeloid cells outnumbered the human myeloid cells by far (Chapter III). Furthermore, a high infiltration of mCD45⁺ cells was observed in the solid tumor mass formed by B-LCL cells (Chapter III). The presence of mouse myeloid cells may on the one hand compete with the human myeloid cells and preclude them from the immune response, and, on the other hand may confound immune effects. Certain mouse chemokines and cytokines can cross-react with the respective human receptors whereas others are not able to do so⁴⁰². Consequently, it would be ideal if the mouse myeloid cells in HIS mice could be completely replaced by a full range of human myeloid cells. Specifically in the models I have set up, this would firstly facilitate the study of antibody dependent effector mechanisms by human myeloid cells *in vivo*, and secondly result in a more representative TME. Over the last decade, considerable advances have been made in this respect and in some models, such as the BRGSF and MISTRG HIS mice, the numbers of mouse myeloid cells are reduced whereas several human myeloid cell populations are increased^{273,274,297}. Recently, a HIS mouse model (MISTRGGR) which supports the development of human neutrophils has been generated. However, in these MISTRGGR HIS mice the frequency of circulatory neutrophils did not reach similar levels compared to human blood and a next major deficiencies of this model include the short lifespan of mice (14 weeks), poor breeding of females and necessity to maintain the colony on antibiotics⁴⁰³. Therefore, further advances are needed to optimize the human immune cell compartment in HIS mice for being able to study anti-tumor responses in a TME which is composed of mostly human immune cells including granulocytes instead of mouse myeloid cells. Nevertheless, the BRGSA2DR2 Fcγ1g-/- mice in which we demonstrated antibody dependent depletion by NK cells were created in a strain with a Flt3 knockout as reported in BRGSF mice^{274,297}. So, it could

be expected that in the BRGSFA2DR2 Fc ϵ r1g^{-/-} mice administration of Flt3L will equally boost dendritic cells and macrophages. Experiments in these HIS mice boosted with Flt3L may be instructive with respect to the *in vivo* contribution of human macrophages and DCs in antibody mediated depletion and anti-tumor responses.

Relevance, challenges and perspectives of autologous tumor models

Autologous tumor models are crucial to adequately mimic the situation in patients, since in an allogeneic setting, the immune system mounts an allogeneic response in addition to an anti-tumor response against the introduced tumor cells. This leads to higher tumor cell rejection which has also been demonstrated for a HIS mouse tumor model³³⁵. Allograft rejection is mainly controlled by T and B cells but innate immune cells are involved in this process as well⁴⁰⁴. A cause for allograft rejections is the expression of the highly diverse human leukocyte antigens (HLAs) which allows the immune system to distinguish between self and non-self cells⁴⁰⁵. HLA class I protein interactions with killer cell immunoglobulin-like receptors (KIRs) as well as with CD94/NKG2 receptors strongly impact the development of NK cells and codetermine their function¹²⁵. Even though we have generated B-LCLs which are autologous to fetal liver HSCs, I only could perform the tumor experiments in HLA-matched and not in autologous HIS mice to date. These mice were only partially matched for HLA-A2 and HLA-DR2, but human cells in addition also express other HLAs, such as HLA-B, HLA-C and HLA-DQ. Further, the HLA alleles are highly polymorph. Therefore, although there may be an improvement in partially HLA matched HIS mice compared to HLA mis-matched HIS mice in terms of alloreactivity (Chapter III), it would be beneficial to repeat these experiments in a truly autologous setting to achieve more convincing results. This would avoid that the responsiveness of NK cells is altered by not recognizing all the HLA class I proteins expressed on the B-LCL cells. For example, it has been clearly demonstrated that NK cells show less inhibition against B-LCL cells that do not express the full array of self HLA class I molecules⁴⁰⁶.

A major limitation in the generation of HIS mice is the paucity of HSCs which is even more restrictive in an autologous tumor model, where only a few cohorts of HIS mice can be produced from autologous HSCs. Further, the generation of new autologous cell lines is highly time consuming as mice need to be humanized, have to grow up,

then the cells need to be transformed and expanded before autologous experiments can be performed. With our current protocol this process takes at least 4 months. Therefore, it would be desirable to obtain HSCs from a less limited source to be able to perform more experiments with the same autologous cell line. In this context, an area of research with very high potential is the generation and differentiation of induced pluripotent stem cells (iPSCs). HSCs stemming from iPSCs could not only provide an “unlimited” source of HSCs but would also open up further possibilities, such as the generation of HSCs autologous to patient derived tumor samples. However, the generation of engraftable HSCs derived from iPSCs is currently in an early stage and the protocols to obtain HSCs need to be further improved to make these techniques applicable⁴⁰⁷.

Suitability of the peritoneal cavity as a B-LCL injection site

It has been shown that the anatomical location at which tumor models are established impacts various relevant aspects, such as the growth rate and invasiveness of the tumor as well as the immune infiltration, immune response and sensitivity to therapies^{331,408}. Therefore, tumor models in an orthotopic location may seem to be more representative of the respective tumor which is studied. The B-LCL cells that we generated are derived from B lymphocytes, which means that they resemble a lymphoma model. Most lymphomas are so called nodal lymphomas which are found within organs of the lymphatic system, such as lymph nodes, tonsils, spleen and thymus⁴⁰⁹. However, extranodal lymphomas can be found throughout the body and make up about 40% of all lymphoma cases^{410,411}. Although a few case reports of lymphomas with peritoneal location exist, the peritoneal cavity is rarely affected by lymphomas⁴¹¹. Consequently, the injection of B-LCL cells into the peritoneal cavity, as performed in our experiments, presents an ectopic rather than orthotopic location and may be less representative for lymphomas.

Nevertheless, the primary aim of our study has to be kept in mind. We envisaged to demonstrate that an autologous human tumor model in HIS mice can be generated by *in vitro* transformation of HIS mice derived B cells. Further, this model should allow to study human NK cell and ILC immune responses and effects of immunotherapies. To achieve these goals, the peritoneal cavity overall seems well suited. We could assess the usefulness of this approach, as we demonstrated the grafting and tumorigenicity

of the B-LCL cells. Further, human NK cells are present in the peritoneal cavity of HIS mice and even more so in IL-15 boosted HIS mice. In a next step it could be of interest to choose a more lymphoma-typical injection site as well. However, there are some major constraints in setting up an orthotopic lymphoma model. Firstly, a typical location of lymphomas are lymph nodes. But the deficiency of IL-7 signaling resulting from the common γ chain (IL2RG) knockout in most current HIS mouse models leads to severe defects in lymph node development⁴¹², which is also the case in our model. This deficiency has been overcome in some HIS mouse models with restored lymph node development, such as BRGST HIS mice^{275,413}. BRGST mice are transgenic for mouse thymic-stromal-cell-derived lymphopoietin (TSLP) which exhibits functional homology to IL-7 but is IL-2R γ independent²⁷⁵. TSLP expression has been demonstrated to rescue fetal LTi function in *Il2ry*^{-/-} mice⁴¹². In BRGST HIS mice robust development of compartmentalized lymph nodes has been observed²⁷⁵. As the BRGST model is based on the same strain as our BRGSA2DR2 Fc ϵ 1g^{-/-} model, the TSLP transgene can be crossed in rather easily to obtain lymph nodes which would solve this obstacle. Secondly, it is *per se* possible to perform injections into the lymph nodes or alternatively into the spleen of mice. This however requires a surgical procedure for which the mice need to be anaesthetized and at least the skin has to be opened. Thus, the generation of an orthotopic lymphoma model is technically more challenging, more stressful for the mice and the surgical procedure bears a risk of inflammation and immune cell stimulation. Such reactions could in turn impact the study of anti-tumor immune responses³³¹. Although an orthotopic lymphoma model may be biologically more relevant, the described impediments are critical. Other potential tumor injection sites are much easier to access, neither intraperitoneal, nor subcutaneous, nor intravenous injections require anesthesia or a surgical procedure.

The BRGSA2DR2 Fc ϵ 1g^{-/-} HIS mouse model in combination with autologous tumor cell lines – a versatile preclinical model for immunotherapeutic applications

Beyond the testing of target cell depleting antibodies, the knockout of the mFc ϵ 1g gene should presumably facilitate the *in vivo* testing of any therapeutic agent that can be bound by activating mouse Fc γ Rs, such as blocking antibodies and Fc-fusion proteins. For the blocking of immune checkpoint receptors, mainly IgG4 antibodies are

used, since IgG4 do not trigger depleting effector mechanisms in humans⁴¹⁴. In contrast, human IgG4 antibodies can be bound by mouse FcγRs and our data confirm that IgG4 antibodies can cause strong mouse FcγR-dependent depletion of the targeted cells (Chapter II). Even in FcγR1g^{-/-} HIS mice we observed some residual depletion with IgG4 and it remains to be determined whether this depletion is due to mouse complement, human immune cells or effector independent. In any case, the BRGSA2DR2 FcγR1g^{-/-} mice should serve as a superior preclinical model for IgG4 blocking antibodies than HIS mice with functional mFcγRs. This is supported by a recent publication in which the effects of an anti-PD-1 blocking antibody were compared between NOG and NOG-FcγR^{-/-} mice HIS mice⁴¹⁵. The authors demonstrated a higher T-cell infiltration in the tumors of anti-PD-1 treated NOG-FcγR^{-/-} HIS mice and a decrease in tumor volume for several of the tested allogeneic tumor cell lines. Whether this holds in the absence of allo-HLA could be investigated with the autologous tumor model we generated.

Overall, our BRGSA2DR2 FcγR1g^{-/-} HIS mouse model combines multiple beneficial properties to study immunotherapeutic effects, such as efficient engraftment with HSCs, a long lifespan, improved T cell responses due to the HLA-A2 and HLA-DR2 transgenes as well as deficient antibody binding by mouse cells. Most likely, an enhanced development of human DCs, macrophages, NK cells and ILCs could be achieved in these mice by administering Flt3L as demonstrated in BRGSF mice²⁷⁴. Thus, together with the autologous tumor model, these mice provide an outstanding preclinical model to test and explore a large range of anti-tumor immunotherapies, including, but not limited to, bi-/tri-specific antibodies, blocking antibodies, cytokines, adoptive cell therapies, cancer vaccines, gene therapies and combinations thereof. Moreover, this HIS mouse model is also applicable for setting up further disease models, such as viral infections (e.g. HIV, EBV) and likewise test immunotherapeutic approaches.

Concluding remarks

Harnessing NK cells for anti-cancer therapies currently constitutes a major focus of innovations in immunotherapies and over the last years a plethora of NK cell related treatments have been developed. A constraint in evaluating the efficacy of new treatment options is the availability of adequate preclinical models. These are essential to facilitate the selection of the most promising therapeutic candidates which proceed into clinical trials.

The BRGSA2DR2 Fc γ 1g $^{-/-}$ HIS mice characterized in this thesis are adapted for studying antibody-based treatment options. In combination with the B-LCL autologous tumor model, they provide advanced tools to test a versatile range of immunology treatments, including NK cell specific applications. Since these models overcome the confounding effects of activating mouse Fc γ R s as well as alloreactive effects, they comprise tremendous potential to extend the knowledge on therapeutic applications *in vivo* and could assist the development of clinically relevant anti-cancer treatments to leverage their transition to the clinic.

References

1. Parham, P. *The Immune System*. (Garland Science, 2014).
2. Sattler, S. The Role of the Immune System Beyond the Fight Against Infection. in *The Immunology of Cardiovascular Homeostasis and Pathology* (eds. Sattler, S. & Kennedy-Lydon, T.) 3–14 (Springer International Publishing, 2017). doi:10.1007/978-3-319-57613-8_1.
3. Elsaid, R. *et al.* Hematopoiesis: A Layered Organization Across Chordate Species. *Front. Cell Dev. Biol.* **8**, 606642 (2020).
4. Palis, J., Robertson, S., Kennedy, M., Wall, C. & Keller, G. Development of erythroid and myeloid progenitors in the yolk sac and embryo proper of the mouse. *Development* **126**, 5073–5084 (1999).
5. Tober, J. *et al.* The megakaryocyte lineage originates from hemangioblast precursors and is an integral component both of primitive and of definitive hematopoiesis. *Blood* **109**, 1433–1441 (2006).
6. Frame, J. M., Fegan, K. H., Conway, S. J., McGrath, K. E. & Palis, J. Definitive Hematopoiesis in the Yolk Sac Emerges from Wnt-Responsive Hemogenic Endothelium Independently of Circulation and Arterial Identity. *Stem Cells* **34**, 431–444 (2016).
7. Cumano, A., Dieterlen-Lievre, F. & Godin, I. Lymphoid Potential, Probed before Circulation in Mouse, Is Restricted to Caudal Intraembryonic Splanchnopleura. *Cell* **86**, 907–916 (1996).
8. Neo, W. H., Lie-A-Ling, M., Fadlullah, M. Z. H. & Lacaud, G. Contributions of Embryonic HSC-Independent Hematopoiesis to Organogenesis and the Adult Hematopoietic System. *Front. Cell Dev. Biol.* **9**, (2021).
9. Ginhoux, F. *et al.* Fate mapping analysis reveals that adult microglia derive from primitive macrophages. *Science* **330**, 841–845 (2010).
10. Gomez Perdiguero, E. *et al.* Tissue-resident macrophages originate from yolk-sac-derived erythro-myeloid progenitors. *Nature* **518**, 547–551 (2015).
11. Hoeffel, G. *et al.* C-Myb(+) erythro-myeloid progenitor-derived fetal monocytes give rise to adult tissue-resident macrophages. *Immunity* **42**, 665–678 (2015).
12. Sawai, C. M. *et al.* Hematopoietic Stem Cells Are the Major Source of Multilineage Hematopoiesis in Adult Animals. *Immunity* **45**, 597–609 (2016).
13. Biasco, L. *et al.* In Vivo Tracking of Human Hematopoiesis Reveals Patterns of Clonal Dynamics during Early and Steady-State Reconstitution Phases. *Cell Stem Cell* **19**, 107–119 (2016).
14. Wilkinson, A. C., Igarashi, K. J. & Nakauchi, H. Haematopoietic stem cell self-renewal in vivo and ex vivo. *Nat. Rev. Genet.* **21**, 541–554 (2020).
15. Lewis, K., Yoshimoto, M. & Takebe, T. Fetal liver hematopoiesis: from development to delivery. *Stem Cell Res. Ther.* **12**, 139 (2021).
16. Ciriza, J., Thompson, H., Petrosian, R., Manilay, J. O. & García-Ojeda, M. E. The migration of hematopoietic progenitors from the fetal liver to the fetal bone marrow: Lessons learned and possible clinical applications. *Exp. Hematol.* **41**, 411–423 (2013).
17. Ding, L., Saunders, T. L., Enikolopov, G. & Morrison, S. J. Endothelial and perivascular cells maintain haematopoietic stem cells. *Nature* **481**, 457–462 (2012).
18. Kunisaki, Y. *et al.* Arteriolar niches maintain haematopoietic stem cell quiescence. *Nature* **502**, 637–643 (2013).

19. Bhatia, M., Wang, J. C., Kapp, U., Bonnet, D. & Dick, J. E. Purification of primitive human hematopoietic cells capable of repopulating immune-deficient mice. *Proc. Natl. Acad. Sci. U. S. A.* **94**, 5320–5325 (1997).
20. Majeti, R., Park, C. Y. & Weissman, I. L. Identification of a hierarchy of multipotent hematopoietic progenitors in human cord blood. *Cell Stem Cell* **1**, 635–645 (2007).
21. Manz, M. G., Miyamoto, T., Akashi, K. & Weissman, I. L. Prospective isolation of human clonogenic common myeloid progenitors. *Proc. Natl. Acad. Sci.* **99**, 11872–11877 (2002).
22. Höfer, T. & Rodewald, H.-R. Differentiation-based model of hematopoietic stem cell functions and lineage pathways. *Blood* **132**, 1106–1113 (2018).
23. Pei, W. *et al.* Polylox barcoding reveals haematopoietic stem cell fates realized in vivo. *Nature* **548**, 456–460 (2017).
24. Zhu, J. & Emerson, S. G. Hematopoietic cytokines, transcription factors and lineage commitment. *Oncogene* **21**, 3295–3313 (2002).
25. Kärre, K., Ljunggren, H. G., Piontek, G. & Kiessling, R. Selective rejection of H-2-deficient lymphoma variants suggests alternative immune defence strategy. *Nature* **319**, 675–678 (1986).
26. van den Berg, T. K. & van der Schoot, C. E. Innate immune ‘self’ recognition: a role for CD47–SIRP α interactions in hematopoietic stem cell transplantation. *Trends Immunol.* **29**, 203–206 (2008).
27. Cruvinel, W. de M., Júnior, D. M., Araújo, J. A. P. & Catelan, T. T. T. Immune system – Part I Fundamentals of innate immunity with emphasis on molecular and cellular mechanisms of inflammatory response.
28. Iwasaki, A. & Medzhitov, R. Control of adaptive immunity by the innate immune system. *Nat. Immunol.* **16**, 343–353 (2015).
29. Vénéreau, E., Ceriotti, C. & Bianchi, M. E. DAMPs from Cell Death to New Life. *Front. Immunol.* **6**, (2015).
30. El-Zayat, S. R., Sibaii, H. & Mannaa, F. A. Toll-like receptors activation, signaling, and targeting: an overview. *Bull. Natl. Res. Cent.* **43**, 187 (2019).
31. Sheu, K. M., Luecke, S. & Hoffmann, A. Stimulus-specificity in the responses of immune sentinel cells. *Curr. Opin. Syst. Biol.* **18**, 53–61 (2019).
32. Reis e Sousa, C. Activation of dendritic cells: translating innate into adaptive immunity. *Curr. Opin. Immunol.* **16**, 21–25 (2004).
33. Dress, R. J., Wong, A. Y. & Ginhoux, F. Homeostatic control of dendritic cell numbers and differentiation. *Immunol. Cell Biol.* **96**, 463–476 (2018).
34. Dress, R. J. *et al.* Plasmacytoid dendritic cells develop from Ly6D⁺ lymphoid progenitors distinct from the myeloid lineage. *Nat. Immunol.* **20**, 852–864 (2019).
35. Collin, M. & Bigley, V. Human dendritic cell subsets: an update. *Immunology* **154**, 3–20 (2018).
36. Spranger, S., Dai, D., Horton, B. & Gajewski, T. F. Tumor-Residing Batf3 Dendritic Cells Are Required for Effector T Cell Trafficking and Adoptive T Cell Therapy. *Cancer Cell* **31**, 711–723.e4 (2017).
37. Hildner, K. *et al.* Batf3 Deficiency Reveals a Critical Role for CD8 α ⁺ Dendritic Cells in Cytotoxic T Cell Immunity. *Science* **322**, 1097–1100 (2008).
38. Wculek, S. K. *et al.* Dendritic cells in cancer immunology and immunotherapy. *Nat. Rev. Immunol.* **20**, 7–24 (2020).
39. Swiecki, M. & Colonna, M. The multifaceted biology of plasmacytoid dendritic cells. *Nat. Rev. Immunol.* **15**, 471–485 (2015).

40. Saitoh, T. *et al.* Antiviral Protein Viperin Promotes Toll-like Receptor 7- and Toll-like Receptor 9-Mediated Type I Interferon Production in Plasmacytoid Dendritic Cells. *Immunity* **34**, 352–363 (2011).
41. Moses, K. & Brandau, S. Human neutrophils: Their role in cancer and relation to myeloid-derived suppressor cells. *Semin. Immunol.* **28**, 187–196 (2016).
42. Kolaczowska, E. & Kubes, P. Neutrophil recruitment and function in health and inflammation. *Nat. Rev. Immunol.* **13**, 159–175 (2013).
43. Naish, E. *et al.* The formation and function of the neutrophil phagosome. *Immunol. Rev.* (2022) doi:10.1111/imr.13173.
44. Eichelberger, K. R. & Goldman, W. E. Manipulating neutrophil degranulation as a bacterial virulence strategy. *PLOS Pathog.* **16**, e1009054 (2020).
45. Tamassia, N. *et al.* Cytokine production by human neutrophils: Revisiting the “dark side of the moon”. *Eur. J. Clin. Invest.* **48**, e12952 (2018).
46. Brinkmann, V. *et al.* Neutrophil Extracellular Traps Kill Bacteria. *Science* **303**, 1532–1535 (2004).
47. Herrero-Cervera, A., Soehnlein, O. & Kenne, E. Neutrophils in chronic inflammatory diseases. *Cell. Mol. Immunol.* **19**, 177–191 (2022).
48. Németh, T. & Mócsai, A. The role of neutrophils in autoimmune diseases. *Immunol. Lett.* **143**, 9–19 (2012).
49. Howard, R., Kanetsky, P. A. & Egan, K. M. Exploring the prognostic value of the neutrophil-to-lymphocyte ratio in cancer. *Sci. Rep.* **9**, 19673 (2019).
50. Rao, H.-L. *et al.* Increased Intratumoral Neutrophil in Colorectal Carcinomas Correlates Closely with Malignant Phenotype and Predicts Patients’ Adverse Prognosis. *PLOS ONE* **7**, e30806 (2012).
51. Ring, N. G. *et al.* Anti-SIRP α antibody immunotherapy enhances neutrophil and macrophage antitumor activity. *Proc. Natl. Acad. Sci.* **114**, E10578–E10585 (2017).
52. Matlung, H. L. *et al.* Neutrophils Kill Antibody-Opsonized Cancer Cells by Trogoptosis. *Cell Rep.* **23**, 3946–3959.e6 (2018).
53. Grecian, R., Whyte, M. K. B. & Walmsley, S. R. The role of neutrophils in cancer. *Br. Med. Bull.* **128**, 5–14 (2018).
54. Breedveld, A., Groot Kormelink, T., van Egmond, M. & de Jong, E. C. Granulocytes as modulators of dendritic cell function. *J. Leukoc. Biol.* **102**, 1003–1016 (2017).
55. Sastre, B., Rodrigo-Muñoz, J., Garcia-Sanchez, D., Cañas, J. & del Pozo, V. Eosinophils: Old Players in a New Game. *J. Investig. Allergol. Clin. Immunol.* **28**, 289–304 (2018).
56. Galli, S. J., Gaudenzio, N. & Tsai, M. Mast Cells in Inflammation and Disease: Recent Progress and Ongoing Concerns. *Annu. Rev. Immunol.* **38**, 49–77 (2020).
57. Miyake, K., Shibata, S., Yoshikawa, S. & Karasuyama, H. Basophils and their effector molecules in allergic disorders. *Allergy* **76**, 1693–1706 (2021).
58. Gordon, S. Phagocytosis: An Immunobiologic Process. *Immunity* **44**, 463–475 (2016).
59. Kulle, A., Thanabalasuriar, A., Cohen, T. S. & Szydlowska, M. Resident macrophages of the lung and liver: The guardians of our tissues. *Front. Immunol.* **13**, 1029085 (2022).
60. Locati, M., Curtale, G. & Mantovani, A. Diversity, Mechanisms and Significance of Macrophage Plasticity. *Annu. Rev. Pathol.* **15**, 123–147 (2020).
61. Evren, E. *et al.* CD116+ fetal precursors migrate to the perinatal lung and give rise to human alveolar macrophages. *J. Exp. Med.* **219**, e20210987 (2022).

62. Gordon, S. & Martinez, F. O. Alternative Activation of Macrophages: Mechanism and Functions. *Immunity* **32**, 593–604 (2010).
63. Pittoni, V. & Valesini, G. The clearance of apoptotic cells: implications for autoimmunity. *Autoimmun. Rev.* **1**, 154–161 (2002).
64. Djaldetti, M., Salman, H., Bergman, M., Djaldetti, R. & Bessler, H. Phagocytosis—The mighty weapon of the silent warriors. *Microsc. Res. Tech.* **57**, 421–431 (2002).
65. Overdijk, M. B. *et al.* Antibody-mediated phagocytosis contributes to the anti-tumor activity of the therapeutic antibody daratumumab in lymphoma and multiple myeloma. *mAbs* **7**, 311–320 (2015).
66. Grandjean, C. L., Garcia, Z., Lemaître, F., Bréart, B. & Bousso, P. Imaging the mechanisms of anti-CD20 therapy in vivo uncovers spatiotemporal bottlenecks in antibody-dependent phagocytosis. *Sci. Adv.* **7**, eabd6167 (2021).
67. Shapouri-Moghaddam, A. *et al.* Macrophage plasticity, polarization, and function in health and disease. *J. Cell. Physiol.* **233**, 6425–6440 (2018).
68. Kosmac, K. *et al.* Immunohistochemical Identification of Human Skeletal Muscle Macrophages. *Bio-Protoc.* **8**, e2883 (2018).
69. Nahrendorf, M. & Swirski, F. K. Abandoning M1/M2 for a Network Model of Macrophage Function. *Circ. Res.* **119**, 414–417 (2016).
70. Liu, J. *et al.* Tumor-Associated Macrophages Recruit CCR6+ Regulatory T Cells and Promote the Development of Colorectal Cancer via Enhancing CCL20 Production in Mice. *PLOS ONE* **6**, e19495 (2011).
71. Biswas, S. K. *et al.* A distinct and unique transcriptional program expressed by tumor-associated macrophages (defective NF- κ B and enhanced IRF-3/STAT1 activation). *Blood* **107**, 2112–2122 (2006).
72. Torroella-Kouri, M. *et al.* Identification of a Subpopulation of Macrophages in Mammary Tumor-Bearing Mice That Are Neither M1 nor M2 and Are Less Differentiated. *Cancer Res.* **69**, 4800–4809 (2009).
73. Ostuni, R., Kratochvill, F., Murray, P. J. & Natoli, G. Macrophages and cancer: from mechanisms to therapeutic implications. *Trends Immunol.* **36**, 229–239 (2015).
74. Chao, M. P. *et al.* Therapeutic Targeting of the Macrophage Immune Checkpoint CD47 in Myeloid Malignancies. *Front. Oncol.* **9**, (2020).
75. Advani, R. *et al.* CD47 Blockade by Hu5F9-G4 and Rituximab in Non-Hodgkin's Lymphoma. *N. Engl. J. Med.* **379**, 1711–1721 (2018).
76. Jalil, A. R., Andrechak, J. C. & Discher, D. E. Macrophage checkpoint blockade: results from initial clinical trials, binding analyses, and CD47-SIRP α structure–function. *Antib. Ther.* **3**, 80–94 (2020).
77. Spits, H. *et al.* Innate lymphoid cells — a proposal for uniform nomenclature. *Nat. Rev. Immunol.* **13**, 145–149 (2013).
78. Spits, H. & Cupedo, T. Innate Lymphoid Cells: Emerging Insights in Development, Lineage Relationships, and Function. *Annu. Rev. Immunol.* **30**, 647–675 (2012).
79. Yang, Q. *et al.* TCF-1 upregulation identifies early innate lymphoid progenitors in the bone marrow. *Nat. Immunol.* **16**, 1044–1050 (2015).
80. Klose, C. S. N. *et al.* Differentiation of Type 1 ILCs from a Common Progenitor to All Helper-like Innate Lymphoid Cell Lineages. *Cell* **157**, 340–356 (2014).
81. Constantinides, M. G., McDonald, B. D., Verhoef, P. A. & Bendelac, A. A committed precursor to innate lymphoid cells. *Nature* **508**, 397–401 (2014).

82. Scoville, S. D. *et al.* A Progenitor Cell Expressing Transcription Factor ROR γ t Generates All Human Innate Lymphoid Cell Subsets. *Immunity* **44**, 1140–1150 (2016).
83. Scoville, S. D., Freud, A. G. & Caligiuri, M. A. Cellular pathways in the development of human and murine innate lymphoid cells. *Curr. Opin. Immunol.* **56**, 100–106 (2019).
84. Lim, A. I. *et al.* Systemic Human ILC Precursors Provide a Substrate for Tissue ILC Differentiation. *Cell* **168**, 1086–1100.e10 (2017).
85. Kennedy, M. K. *et al.* Reversible Defects in Natural Killer and Memory Cd8 T Cell Lineages in Interleukin 15–Deficient Mice. *J. Exp. Med.* **191**, 771–780 (2000).
86. Vonarbourg, C. & Diefenbach, A. Multifaceted roles of interleukin-7 signaling for the development and function of innate lymphoid cells. *Semin. Immunol.* **24**, 165–174 (2012).
87. Cherrier, D. E., Serafini, N. & Di Santo, J. P. Innate Lymphoid Cell Development: A T Cell Perspective. *Immunity* **48**, 1091–1103 (2018).
88. Bal, S. M., Golebski, K. & Spits, H. Plasticity of innate lymphoid cell subsets. *Nat. Rev. Immunol.* **20**, 552–565 (2020).
89. Murphy, K. M. & Stockinger, B. Effector T cell plasticity: flexibility in the face of changing circumstances. *Nat. Immunol.* **11**, 674–680 (2010).
90. Vonarbourg, C. *et al.* Regulated Expression of Nuclear Receptor ROR γ t Confers Distinct Functional Fates to NK Cell Receptor-Expressing ROR γ t+ Innate Lymphocytes. *Immunity* **33**, 736–751 (2010).
91. Bernink, J. H. *et al.* Interleukin-12 and -23 Control Plasticity of CD127+ Group 1 and Group 3 Innate Lymphoid Cells in the Intestinal Lamina Propria. *Immunity* **43**, 146–160 (2015).
92. Gordon, S. M. *et al.* The Transcription Factors T-bet and Eomes Control Key Checkpoints of Natural Killer Cell Maturation. *Immunity* **36**, 55–67 (2012).
93. Natural Killer Cells: Their Roles in Defenses Against Disease. <https://www.science.org/doi/10.1126/science.7025208>
doi:10.1126/science.7025208.
94. Perera Molligoda Arachchige, A. S. Human NK cells: From development to effector functions. *Innate Immun.* **27**, 212–229 (2021).
95. Imai, K., Matsuyama, S., Miyake, S., Suga, K. & Nakachi, K. Natural cytotoxic activity of peripheral-blood lymphocytes and cancer incidence: an 11-year follow-up study of a general population. *The Lancet* **356**, 1795–1799 (2000).
96. Pross, H. F. & Lotzová, E. Role of natural killer cells in cancer. *Nat. Immun.* **12**, 279–292 (1993).
97. Schantz, S. P., Shillitoe, E. J., Brown, B. & Campbell, B. Natural Killer Cell Activity and Head and Neck Cancer: A Clinical Assessment². *JNCI J. Natl. Cancer Inst.* **77**, 869–875 (1986).
98. Prager, I. & Watzl, C. Mechanisms of natural killer cell-mediated cellular cytotoxicity. *J. Leukoc. Biol.* **105**, 1319–1329 (2019).
99. Mace, E. M. *et al.* Cell biological steps and checkpoints in accessing NK cell cytotoxicity. *Immunol. Cell Biol.* **92**, 245–255 (2014).
100. Fauriat, C., Long, E. O., Ljunggren, H.-G. & Bryceson, Y. T. Regulation of human NK-cell cytokine and chemokine production by target cell recognition. *Blood* **115**, 2167–2176 (2010).
101. Lusty, E. *et al.* IL-18/IL-15/IL-12 synergy induces elevated and prolonged IFN- γ production by ex vivo expanded NK cells which is not due to enhanced STAT4 activation. *Mol. Immunol.* **88**, 138–147 (2017).

102. Tugues, S. *et al.* New insights into IL-12-mediated tumor suppression. *Cell Death Differ.* **22**, 237–246 (2015).
103. Lee, N. *et al.* Human monocytes have increased IFN- γ -mediated IL-15 production with age alongside altered IFN- γ receptor signaling. *Clin. Immunol. Orlando Fla* **152**, 101–110 (2014).
104. Stoll, S. *et al.* Production of functional IL-18 by different subtypes of murine and human dendritic cells (DC): DC-derived IL-18 enhances IL-12-dependent Th1 development. *Eur. J. Immunol.* **28**, 3231–3239 (1998).
105. Vankayalapati, R. *et al.* NK Cells Regulate CD8⁺ T Cell Effector Function in Response to an Intracellular Pathogen 1. *J. Immunol.* **172**, 130–137 (2004).
106. Regis, S., Dondero, A., Caliendo, F., Bottino, C. & Castriconi, R. NK Cell Function Regulation by TGF- β -Induced Epigenetic Mechanisms. *Front. Immunol.* **11**, (2020).
107. Barthelemy-Brichant, N. *et al.* Increased TGF β ₁ plasma level in patients with lung cancer: potential mechanisms: Increased TGF β 1 in lung cancer. *Eur. J. Clin. Invest.* **32**, 193–198 (2002).
108. Narai, S. *et al.* Significance of transforming growth factor β 1 as a new tumor marker for colorectal cancer. *Int. J. Cancer* **97**, 508–511 (2002).
109. Lee, J.-C., Lee, K.-M., Kim, D.-W. & Heo, D. S. Elevated TGF- β 1 Secretion and Down-Modulation of NKG2D Underlies Impaired NK Cytotoxicity in Cancer Patients1. *J. Immunol.* **172**, 7335–7340 (2004).
110. Viel, S. *et al.* TGF- β inhibits the activation and functions of NK cells by repressing the mTOR pathway. *Sci. Signal.* **9**, ra19–ra19 (2016).
111. Long, E. O., Sik Kim, H., Liu, D., Peterson, M. E. & Rajagopalan, S. Controlling Natural Killer Cell Responses: Integration of Signals for Activation and Inhibition. *Annu. Rev. Immunol.* **31**, 227–258 (2013).
112. Chiossone, L., Dumas, P.-Y., Vienne, M. & Vivier, E. Natural killer cells and other innate lymphoid cells in cancer. *Nat. Rev. Immunol.* **18**, 671–688 (2018).
113. Manser, A. R., Weinhold, S. & Uhrberg, M. Human KIR repertoires: shaped by genetic diversity and evolution. *Immunol. Rev.* **267**, 178–196 (2015).
114. HLA-E is a major ligand for the natural killer inhibitory receptor CD94/NKG2A. <https://www.pnas.org/doi/10.1073/pnas.95.9.5199> doi:10.1073/pnas.95.9.5199.
115. Sullivan, L. C. *et al.* The Heterodimeric Assembly of the CD94-NKG2 Receptor Family and Implications for Human Leukocyte Antigen-E Recognition. *Immunity* **27**, 900–911 (2007).
116. Zingoni, A. *et al.* NKG2D and Its Ligands: “One for All, All for One”. *Front. Immunol.* **9**, (2018).
117. Champsaur, M. & Lanier, L. L. Effect of NKG2D ligand expression on host immune responses. *Immunol. Rev.* **235**, 267–285 (2010).
118. Hecht, M.-L. *et al.* Natural Cytotoxicity Receptors NKp30, NKp44 and NKp46 Bind to Different Heparan Sulfate/Heparin Sequences. *J. Proteome Res.* **8**, 712–720 (2009).
119. Brandt, C. S. *et al.* The B7 family member B7-H6 is a tumor cell ligand for the activating natural killer cell receptor NKp30 in humans. *J. Exp. Med.* **206**, 1495–1503 (2009).
120. Koch, J., Steinle, A., Watzl, C. & Mandelboim, O. Activating natural cytotoxicity receptors of natural killer cells in cancer and infection. *Trends Immunol.* **34**, 182–191 (2013).
121. Kumar, S. Natural killer cell cytotoxicity and its regulation by inhibitory receptors. *Immunology* **154**, 383–393 (2018).

122. Cooper, M. A., Fehniger, T. A. & Caligiuri, M. A. The biology of human natural killer-cell subsets. *Trends Immunol.* **22**, 633–640 (2001).
123. Morvan, M. G. & Lanier, L. L. NK cells and cancer: you can teach innate cells new tricks. *Nat. Rev. Cancer* **16**, 7–19 (2016).
124. Brodin, P., Kärre, K. & Höglund, P. NK cell education: not an on-off switch but a tunable rheostat. *Trends Immunol.* **30**, 143–149 (2009).
125. Höglund, P. & Brodin, P. Current perspectives of natural killer cell education by MHC class I molecules. *Nat. Rev. Immunol.* **10**, 724–734 (2010).
126. Kadri, N., Luu Thanh, T. & Höglund, P. Selection, tuning, and adaptation in mouse NK cell education. *Immunol. Rev.* **267**, 167–177 (2015).
127. Elliott, J. M. & Yokoyama, W. M. Unifying concepts of MHC-dependent natural killer cell education. *Trends Immunol.* **32**, 364–372 (2011).
128. Zhang, X., Feng, J., Chen, S., Yang, H. & Dong, Z. Synergized regulation of NK cell education by NKG2A and specific Ly49 family members. *Nat. Commun.* **10**, 5010 (2019).
129. Caligiuri, M. A. Human natural killer cells. *Blood* **112**, 461–469 (2008).
130. Melsen, J. E., Lugthart, G., Lankester, A. C. & Schilham, M. W. Human Circulating and Tissue-Resident CD56bright Natural Killer Cell Populations. *Front. Immunol.* **7**, (2016).
131. Carrega, P. *et al.* CD56brightPerforinlow Noncytotoxic Human NK Cells Are Abundant in Both Healthy and Neoplastic Solid Tissues and Recirculate to Secondary Lymphoid Organs via Afferent Lymph. *J. Immunol.* **192**, 3805–3815 (2014).
132. Montaldo, E. *et al.* Unique Eomes+ NK Cell Subsets Are Present in Uterus and Decidua During Early Pregnancy. *Front. Immunol.* **6**, (2016).
133. Chiossone, L. *et al.* Maturation of mouse NK cells is a 4-stage developmental program. *Blood* **113**, 5488–5496 (2009).
134. Renoux, V. M. *et al.* Identification of a Human Natural Killer Cell Lineage-Restricted Progenitor in Fetal and Adult Tissues. *Immunity* **43**, 394–407 (2015).
135. Cichocki, F., Grzywacz, B. & Miller, J. S. Human NK Cell Development: One Road or Many? *Front. Immunol.* **10**, (2019).
136. Dulphy, N. *et al.* An Unusual CD56brightCD16low NK Cell Subset Dominates the Early Posttransplant Period following HLA-Matched Hematopoietic Stem Cell Transplantation1. *J. Immunol.* **181**, 2227–2237 (2008).
137. Chan, A. *et al.* CD56bright Human NK Cells Differentiate into CD56dim Cells: Role of Contact with Peripheral Fibroblasts. *J. Immunol.* **179**, 89–94 (2007).
138. Wu, C. *et al.* Clonal Tracking of Rhesus Macaque Hematopoiesis Highlights a Distinct Lineage Origin for Natural Killer Cells. *Cell Stem Cell* **14**, 486–499 (2014).
139. Clonal expansion and compartmentalized maintenance of rhesus macaque NK cell subsets | Science Immunology. <https://www.science.org/doi/full/10.1126/sciimmunol.aat9781>.
140. Gumá, M. *et al.* Imprint of human cytomegalovirus infection on the NK cell receptor repertoire. *Blood* **104**, 3664–3671 (2004).
141. Sun, J. C., Lopez-Verges, S., Kim, C. C., DeRisi, J. L. & Lanier, L. L. NK Cells and Immune “Memory”. *J. Immunol.* **186**, 1891–1897 (2011).
142. Cerwenka, A. & Lanier, L. L. Natural killer cell memory in infection, inflammation and cancer. *Nat. Rev. Immunol.* **16**, 112–123 (2016).
143. Sun, J. C. & Lanier, L. L. Natural killer cells remember: An evolutionary bridge between innate and adaptive immunity? *Eur. J. Immunol.* **39**, 2059–2064 (2009).

144. Riggan, L., Freud, A. G. & O'Sullivan, T. E. True Detective: Unraveling Group 1 Innate Lymphocyte Heterogeneity. *Trends Immunol.* **40**, 909–921 (2019).
145. Björklund, Å. K. *et al.* The heterogeneity of human CD127+ innate lymphoid cells revealed by single-cell RNA sequencing. *Nat. Immunol.* **17**, 451–460 (2016).
146. Fuchs, A. *et al.* Intraepithelial Type 1 Innate Lymphoid Cells Are a Unique Subset of IL-12- and IL-15-Responsive IFN- γ -Producing Cells. *Immunity* **38**, 769–781 (2013).
147. Yudanin, N. A. *et al.* Spatial and Temporal Mapping of Human Innate Lymphoid Cells Reveals Elements of Tissue Specificity. *Immunity* **50**, 505–519.e4 (2019).
148. Carrega, P. *et al.* NCR+ILC3 concentrate in human lung cancer and associate with intratumoral lymphoid structures. *Nat. Commun.* **6**, 8280 (2015).
149. Salimi, M. *et al.* Activated innate lymphoid cell populations accumulate in human tumour tissues. *BMC Cancer* **18**, 341 (2018).
150. Gao, Y. *et al.* Tumor immunoevasion by the conversion of effector NK cells into type 1 innate lymphoid cells. *Nat. Immunol.* **18**, 1004–1015 (2017).
151. Neill, D. R. *et al.* Nuocytes represent a new innate effector leukocyte that mediates type-2 immunity. *Nature* **464**, 1367–1370 (2010).
152. Klose, C. S. N. *et al.* The neuropeptide neuromedin U stimulates innate lymphoid cells and type 2 inflammation. *Nature* **549**, 282–286 (2017).
153. Mjösberg, J. *et al.* The Transcription Factor GATA3 Is Essential for the Function of Human Type 2 Innate Lymphoid Cells. *Immunity* **37**, 649–659 (2012).
154. Wong, S. H. *et al.* Transcription factor ROR α is critical for nuocyte development. *Nat. Immunol.* **13**, 229–236 (2012).
155. Moro, K. *et al.* Innate production of TH2 cytokines by adipose tissue-associated c-Kit+Sca-1+ lymphoid cells. *Nature* **463**, 540–544 (2010).
156. Halim, T. Y. F., Krauß, R. H., Sun, A. C. & Takei, F. Lung Natural Helper Cells Are a Critical Source of Th2 Cell-Type Cytokines in Protease Allergen-Induced Airway Inflammation. *Immunity* **36**, 451–463 (2012).
157. Oliphant, C. J. *et al.* MHCII-Mediated Dialog between Group 2 Innate Lymphoid Cells and CD4+ T Cells Potentiates Type 2 Immunity and Promotes Parasitic Helminth Expulsion. *Immunity* **41**, 283–295 (2014).
158. Roediger, B. *et al.* Cutaneous immunosurveillance and regulation of inflammation by group 2 innate lymphoid cells. *Nat. Immunol.* **14**, 564–573 (2013).
159. Imai, Y. *et al.* IL-33-Induced Atopic Dermatitis-Like Inflammation in Mice Is Mediated by Group 2 Innate Lymphoid Cells in Concert with Basophils. *J. Invest. Dermatol.* **139**, 2185–2194.e3 (2019).
160. Christianson, C. A. *et al.* Persistence of asthma requires multiple feedback circuits involving type 2 innate lymphoid cells and IL-33. *J. Allergy Clin. Immunol.* **136**, 59–68.e14 (2015).
161. Brestoff, J. R. *et al.* Group 2 innate lymphoid cells promote beiging of white adipose tissue and limit obesity. *Nature* **519**, 242–246 (2015).
162. Monticelli, L. A. *et al.* Innate lymphoid cells promote lung-tissue homeostasis after infection with influenza virus. *Nat. Immunol.* **12**, 1045–1054 (2011).
163. Trabanelli, S. *et al.* Tumour-derived PGD2 and NKp30-B7H6 engagement drives an immunosuppressive ILC2-MDSC axis. *Nat. Commun.* **8**, 593 (2017).
164. Chevalier, M. F. *et al.* ILC2-modulated T cell-to-MDSC balance is associated with bladder cancer recurrence. <https://www.jci.org/articles/view/89717/pdf> (2017) doi:10.1172/JCI89717.
165. Moral, J. A. *et al.* ILC2s amplify PD-1 blockade by activating tissue-specific cancer immunity. *Nature* **579**, 130–135 (2020).

166. Grisaru-Tal, S., Rothenberg, M. E. & Munitz, A. Eosinophil–lymphocyte interactions in the tumor microenvironment and cancer immunotherapy. *Nat. Immunol.* **23**, 1309–1316 (2022).
167. Jacquelot, N. *et al.* Blockade of the co-inhibitory molecule PD-1 unleashes ILC2-dependent antitumor immunity in melanoma. *Nat. Immunol.* **22**, 851–864 (2021).
168. Bruchard, M. & Spits, H. The role of ILC subsets in cancer. *Semin. Immunol.* **61–64**, 101654 (2022).
169. Eberl, G. *et al.* An essential function for the nuclear receptor ROR γ t in the generation of fetal lymphoid tissue inducer cells. *Nat. Immunol.* **5**, 64–73 (2004).
170. Montaldo, E., Juelke, K. & Romagnani, C. Group 3 innate lymphoid cells (ILC3s): Origin, differentiation, and plasticity in humans and mice. *Eur. J. Immunol.* **45**, 2171–2182 (2015).
171. Cella, M. *et al.* A human natural killer cell subset provides an innate source of IL-22 for mucosal immunity. *Nature* **457**, 722–725 (2009).
172. Magri, G. *et al.* Innate lymphoid cells integrate stromal and immunological signals to enhance antibody production by splenic marginal zone B cells. *Nat. Immunol.* **15**, 354–364 (2014).
173. Vacca, P. *et al.* Identification of diverse innate lymphoid cells in human decidua. *Mucosal Immunol.* **8**, 254–264 (2015).
174. Teunissen, M. B. M. *et al.* Composition of Innate Lymphoid Cell Subsets in the Human Skin: Enrichment of NCR $^{+}$ ILC3 in Lesional Skin and Blood of Psoriasis Patients. *J. Invest. Dermatol.* **134**, 2351–2360 (2014).
175. Matsumoto, A. *et al.* IL-22-Producing ROR γ t-Dependent Innate Lymphoid Cells Play a Novel Protective Role in Murine Acute Hepatitis. *PLOS ONE* **8**, e62853 (2013).
176. Taube, C. *et al.* IL-22 Is Produced by Innate Lymphoid Cells and Limits Inflammation in Allergic Airway Disease. *PLOS ONE* **6**, e21799 (2011).
177. Dudakov, J. A., Hanash, A. M. & van den Brink, M. R. M. Interleukin-22: immunobiology and pathology. *Annu. Rev. Immunol.* **33**, 747–785 (2015).
178. Zheng, Y. *et al.* Interleukin-22 mediates early host defense against attaching and effacing bacterial pathogens. *Nat. Med.* **14**, 282–289 (2008).
179. Schmalzl, A. *et al.* Interferon regulatory factor 1 (IRF-1) promotes intestinal group 3 innate lymphoid responses during *Citrobacter rodentium* infection. *Nat. Commun.* **13**, 5730 (2022).
180. Pantelyushin, S. *et al.* Ror γ t $^{+}$ innate lymphocytes and $\gamma\delta$ T cells initiate psoriasiform plaque formation in mice. *J. Clin. Invest.* **122**, 2252–2256 (2012).
181. Zeng, B. *et al.* ILC3 function as a double-edged sword in inflammatory bowel diseases. *Cell Death Dis.* **10**, 1–12 (2019).
182. Siegler, J.-J. *et al.* Human ILC3 Exert TRAIL-Mediated Cytotoxicity Towards Cancer Cells. *Front. Immunol.* **13**, 742571 (2022).
183. Rao, A. *et al.* Cytokines regulate the antigen-presenting characteristics of human circulating and tissue-resident intestinal ILCs. *Nat. Commun.* **11**, 2049 (2020).
184. Irshad, S. *et al.* ROR γ t $^{+}$ Innate Lymphoid Cells Promote Lymph Node Metastasis of Breast Cancers. *Cancer Res.* **77**, 1083–1096 (2017).
185. Godfrey, D. I., Uldrich, A. P., McCluskey, J., Rossjohn, J. & Moody, D. B. The burgeoning family of unconventional T cells. *Nat. Immunol.* **16**, 1114–1123 (2015).
186. Mayassi, T., Barreiro, L. B., Rossjohn, J. & Jabri, B. A multilayered immune system through the lens of unconventional T cells. *Nature* **595**, 501–510 (2021).

187. Khan, M. A. & Khan, A. Role of NKT Cells during Viral Infection and the Development of NKT Cell-Based Nanovaccines. *Vaccines* **9**, 949 (2021).
188. Li, Y.-R. *et al.* Tumor-Localized Administration of α -GalCer to Recruit Invariant Natural Killer T Cells and Enhance Their Antitumor Activity against Solid Tumors. *Int. J. Mol. Sci.* **23**, 7547 (2022).
189. Kitamura, H. *et al.* The Natural Killer T (NKT) Cell Ligand α -Galactosylceramide Demonstrates Its Immunopotentiating Effect by Inducing Interleukin (IL)-12 Production by Dendritic Cells and IL-12 Receptor Expression on NKT Cells. *J. Exp. Med.* **189**, 1121–1128 (1999).
190. Kjer-Nielsen, L. *et al.* MR1 presents microbial vitamin B metabolites to MAIT cells. *Nature* **491**, 717–723 (2012).
191. Le Bourhis, L. *et al.* Antimicrobial activity of mucosal-associated invariant T cells. *Nat. Immunol.* **11**, 701–708 (2010).
192. Couzi, L. *et al.* Antibody-dependent anti-cytomegalovirus activity of human $\gamma\delta$ T cells expressing CD16 (Fc γ RIIIa). *Blood* **119**, 1418–1427 (2012).
193. Yazdanifar, M., Barbarito, G., Bertaina, A. & Airoidi, I. $\gamma\delta$ T Cells: The Ideal Tool for Cancer Immunotherapy. *Cells* **9**, 1305 (2020).
194. Nielsen, M. M., Witherden, D. A. & Havran, W. L. $\gamma\delta$ T cells in homeostasis and host defence of epithelial barrier tissues. *Nat. Rev. Immunol.* **17**, 733–745 (2017).
195. Imbert, C. & Olive, D. $\gamma\delta$ T Cells in Tumor Microenvironment. in *Tumor Microenvironment: Hematopoietic Cells – Part B* (ed. Birbrair, A.) 91–104 (Springer International Publishing, 2020). doi:10.1007/978-3-030-49270-0_5.
196. Halary, F. *et al.* Shared reactivity of V δ 2(neg) $\gamma\delta$ T cells against cytomegalovirus-infected cells and tumor intestinal epithelial cells. *J. Exp. Med.* **201**, 1567–1578 (2005).
197. Bonilla, F. A. & Oettgen, H. C. Adaptive immunity. *J. Allergy Clin. Immunol.* **125**, S33–S40 (2010).
198. Schatz, D. G. & Ji, Y. Recombination centres and the orchestration of V(D)J recombination. *Nat. Rev. Immunol.* **11**, 251–263 (2011).
199. Rock, E. P., Sibbald, P. R., Davis, M. M. & Chien, Y. H. CDR3 length in antigen-specific immune receptors. *J. Exp. Med.* **179**, 323–328 (1994).
200. Schatz, D. G. Antigen receptor genes and the evolution of a recombinase. *Semin. Immunol.* **16**, 245–256 (2004).
201. Amendt, T. & Jumaa, H. Adaptive tolerance: Protection through self-recognition. *BioEssays* **44**, 2100236 (2022).
202. Chaudhry, M. S., Velardi, E., Dudakov, J. A. & van den Brink, M. R. M. Thymus: the next (re)generation. *Immunol. Rev.* **271**, 56–71 (2016).
203. Neely, H. R. & Flajnik, M. F. Emergence and Evolution of Secondary Lymphoid Organs. *Annu. Rev. Cell Dev. Biol.* **32**, 693–711 (2016).
204. Kumar, B. V., Connors, T. J. & Farber, D. L. Human T Cell Development, Localization, and Function throughout Life. *Immunity* **48**, 202–213 (2018).
205. Sprent, J. & Surh, C. D. Normal T cell homeostasis: the conversion of naive cells into memory-phenotype cells. *Nat. Immunol.* **12**, 478–484 (2011).
206. van den Broek, T., Borghans, J. A. M. & van Wijk, F. The full spectrum of human naive T cells. *Nat. Rev. Immunol.* **18**, 363–373 (2018).
207. Trifari, S., Kaplan, C. D., Tran, E. H., Crellin, N. K. & Spits, H. Identification of a human helper T cell population that has abundant production of interleukin 22 and is distinct from TH-17, TH1 and TH2 cells. *Nat. Immunol.* **10**, 864–871 (2009).
208. Zhu, J., Yamane, H. & Paul, W. E. Differentiation of Effector CD4 T Cell Populations. *Annu. Rev. Immunol.* **28**, 445–489 (2010).

209. Pearce, E. L. & Shen, H. Generation of CD8 T Cell Memory Is Regulated by IL-121. *J. Immunol.* **179**, 2074–2081 (2007).
210. Mahmoud, S. M. A. *et al.* Tumor-Infiltrating CD8⁺ Lymphocytes Predict Clinical Outcome in Breast Cancer. *J. Clin. Oncol.* **29**, 1949–1955 (2011).
211. Kawai, O. *et al.* Predominant infiltration of macrophages and CD8⁺ T Cells in cancer nests is a significant predictor of survival in stage IV nonsmall cell lung cancer. *Cancer* **113**, 1387–1395 (2008).
212. Pagès, F. *et al.* In Situ Cytotoxic and Memory T Cells Predict Outcome in Patients With Early-Stage Colorectal Cancer. *J. Clin. Oncol.* **27**, 5944–5951 (2009).
213. Thomas, D. A. & Massagué, J. TGF- β directly targets cytotoxic T cell functions during tumor evasion of immune surveillance. *Cancer Cell* **8**, 369–380 (2005).
214. Jiang, Y., Li, Y. & Zhu, B. T-cell exhaustion in the tumor microenvironment. *Cell Death Dis.* **6**, e1792–e1792 (2015).
215. Hargadon, K. M., Johnson, C. E. & Williams, C. J. Immune checkpoint blockade therapy for cancer: An overview of FDA-approved immune checkpoint inhibitors. *Int. Immunopharmacol.* **62**, 29–39 (2018).
216. Owen, D. L., Sjaastad, L. E. & Farrar, M. A. Regulatory T Cell Development in the Thymus. *J. Immunol.* **203**, 2031–2041 (2019).
217. Rudensky, A. Y. Regulatory T cells and Foxp3. *Immunol. Rev.* **241**, 260–268 (2011).
218. Shang, B., Liu, Y., Jiang, S. & Liu, Y. Prognostic value of tumor-infiltrating FoxP3⁺ regulatory T cells in cancers: a systematic review and meta-analysis. *Sci. Rep.* **5**, 15179 (2015).
219. Saleh, R. & Elkord, E. FoxP3⁺ T regulatory cells in cancer: Prognostic biomarkers and therapeutic targets. *Cancer Lett.* **490**, 174–185 (2020).
220. Crotty, S. T Follicular Helper Cell Biology: A Decade of Discovery and Diseases. *Immunity* **50**, 1132–1148 (2019).
221. Hoffman, W., Lakkis, F. G. & Chalasani, G. B Cells, Antibodies, and More. *Clin. J. Am. Soc. Nephrol. CJASN* **11**, 137–154 (2016).
222. Young, C. & Brink, R. The unique biology of germinal center B cells. *Immunity* **54**, 1652–1664 (2021).
223. Pilzecker, B. & Jacobs, H. Mutating for Good: DNA Damage Responses During Somatic Hypermutation. *Front. Immunol.* **10**, (2019).
224. Shinnakasu, R. & Kurosaki, T. Regulation of memory B and plasma cell differentiation. *Curr. Opin. Immunol.* **45**, 126–131 (2017).
225. Roco, J. A. *et al.* Class-Switch Recombination Occurs Infrequently in Germinal Centers. *Immunity* **51**, 337–350.e7 (2019).
226. Suan, D., Sundling, C. & Brink, R. Plasma cell and memory B cell differentiation from the germinal center. *Curr. Opin. Immunol.* **45**, 97–102 (2017).
227. Fridman, W. H. *et al.* B cells and cancer: To B or not to B? *J. Exp. Med.* **218**, e20200851 (2020).
228. Lin, J.-X. & Leonard, W. J. Fine-Tuning Cytokine Signals. *Annu. Rev. Immunol.* **37**, 295–324 (2019).
229. Mishra, A., Sullivan, L. & Caligiuri, M. A. Molecular Pathways: Interleukin-15 Signaling in Health and in Cancer. *Clin. Cancer Res.* **20**, 2044–2050 (2014).
230. Habib, T., Senadheera, S., Weinberg, K. & Kaushansky, K. The Common γ Chain (γ c) Is a Required Signaling Component of the IL-21 Receptor and Supports IL-21-Induced Cell Proliferation via JAK3. *Biochemistry* **41**, 8725–8731 (2002).

231. Schett, G., Elewaut, D., McInnes, I. B., Dayer, J.-M. & Neurath, M. F. How Cytokine Networks Fuel Inflammation: Toward a cytokine-based disease taxonomy. *Nat. Med.* **19**, 822–824 (2013).
232. Shimabukuro-Vornhagen, A. *et al.* Cytokine release syndrome. *J. Immunother. Cancer* **6**, 56 (2018).
233. Hughes, C. E. & Nibbs, R. J. B. A guide to chemokines and their receptors. *Febs J.* **285**, 2944–2971 (2018).
234. López-Cotarelo, P., Gómez-Moreira, C., Criado-García, O., Sánchez, L. & Rodríguez-Fernández, J. L. Beyond Chemoattraction: Multifunctionality of Chemokine Receptors in Leukocytes. *Trends Immunol.* **38**, 927–941 (2017).
235. Kohli, K., Pillarisetty, V. G. & Kim, T. S. Key chemokines direct migration of immune cells in solid tumors. *Cancer Gene Ther.* **29**, 10–21 (2022).
236. Mlecnik, B. *et al.* Biomolecular Network Reconstruction Identifies T-Cell Homing Factors Associated With Survival in Colorectal Cancer. *Gastroenterology* **138**, 1429–1440 (2010).
237. Buss, N. A., Henderson, S. J., McFarlane, M., Shenton, J. M. & de Haan, L. Monoclonal antibody therapeutics: history and future. *Curr. Opin. Pharmacol.* **12**, 615–622 (2012).
238. Rubinstein, N. D. *et al.* Computational characterization of B-cell epitopes. *Mol. Immunol.* **45**, 3477–3489 (2008).
239. Chiu, M. L., Goulet, D. R., Teplyakov, A. & Gilliland, G. L. Antibody Structure and Function: The Basis for Engineering Therapeutics. *Antibodies* **8**, 55 (2019).
240. Rogers, L. M., Veeramani, S. & Weiner, G. J. Complement in monoclonal antibody therapy of cancer. *Immunol. Res.* **59**, 203–210 (2014).
241. Forthal, D. N. Functions of Antibodies. *Microbiol. Spectr.* **2**, 2.4.21 (2014).
242. Mullard, A. FDA approves 100th monoclonal antibody product. *Nat. Rev. Drug Discov.* **20**, 491–495 (2021).
243. Zahavi, D. & Weiner, L. Monoclonal Antibodies in Cancer Therapy. *Antibodies* **9**, 34 (2020).
244. Yu, J., Song, Y. & Tian, W. How to select IgG subclasses in developing anti-tumor therapeutic antibodies. *J. Hematol. Oncol. J Hematol Oncol* **13**, 45 (2020).
245. Tay, S. S., Carol, H. & Biro, M. TriKEs and BiKEs join CARs on the cancer immunotherapy highway. *Hum. Vaccines Immunother.* **12**, 2790–2796 (2016).
246. Daëron, M. Fc Receptors as Adaptive Immunoreceptors. *Fc Recept.* **382**, 131–164 (2014).
247. Cleary, K. L. S., Chan, H. T. C., James, S., Glennie, M. J. & Cragg, M. S. Antibody Distance from the Cell Membrane Regulates Antibody Effector Mechanisms. *J. Immunol.* **198**, 3999–4011 (2017).
248. Baselga, J. & Albanell, J. Mechanism of action of anti-HER2 monoclonal antibodies. *Ann. Oncol.* **12**, S35–S41 (2001).
249. Weiner, G. J. Rituximab: Mechanism of Action. *Semin. Hematol.* **47**, 115–123 (2010).
250. Bruhns, P. & Jönsson, F. Mouse and human FcR effector functions. *Immunol. Rev.* **268**, 25–51 (2015).
251. de Taeye, S. W. *et al.* FcγR Binding and ADCC Activity of Human IgG Allotypes. *Front. Immunol.* **11**, 740 (2020).
252. Kaifu, T. & Nakamura, A. Polymorphisms of immunoglobulin receptors and the effects on clinical outcome in cancer immunotherapy and other immune diseases: a general review. *Int. Immunol.* **29**, 319–325 (2017).

253. Wang, Y. *et al.* Specificity of mouse and human Fcγ receptors and their polymorphic variants for IgG subclasses of different species. *Eur. J. Immunol.* **n/a**.
254. Hajishengallis, G., Reis, E. S., Mastellos, D. C., Ricklin, D. & Lambris, J. D. Novel mechanisms and functions of complement. *Nat. Immunol.* **18**, 1288–1298 (2017).
255. Arbore, G., Kemper, C. & Kolev, M. Intracellular complement – the complosome – in immune cell regulation. *Mol. Immunol.* **89**, 2–9 (2017).
256. Rus, H., Cudrici, C. & Niculescu, F. The Role of the Complement System in Innate Immunity. *Immunol. Res.* **33**, 103–112 (2005).
257. Cook, E. M. *et al.* Antibodies That Efficiently Form Hexamers upon Antigen Binding Can Induce Complement-Dependent Cytotoxicity under Complement-Limiting Conditions. *J. Immunol.* **197**, 1762–1775 (2016).
258. Charbonneau, B. *et al.* Germline variation in complement genes and event-free survival in follicular and diffuse large B-cell lymphoma. *Am. J. Hematol.* **87**, 880–885 (2012).
259. Mestas, J. & Hughes, C. C. W. Of Mice and Not Men: Differences between Mouse and Human Immunology. *J. Immunol.* **172**, 2731–2738 (2004).
260. Lux, A. & Nimmerjahn, F. Of Mice and Men: The Need for Humanized Mouse Models to Study Human IgG Activity in Vivo. *J. Clin. Immunol.* **33**, 4–8 (2013).
261. Rongvaux, A. *et al.* Human Hemato-Lymphoid System Mice: Current Use and Future Potential for Medicine. *Annu. Rev. Immunol.* **31**, 635–674 (2013).
262. Allen, T. M. *et al.* Humanized immune system mouse models: progress, challenges and opportunities. *Nat. Immunol.* **20**, 770–774 (2019).
263. Mombaerts, P. *et al.* RAG-1-deficient mice have no mature B and T lymphocytes. *Cell* **68**, 869–877 (1992).
264. Bosma, G. C., Custer, R. P. & Bosma, M. J. A severe combined immunodeficiency mutation in the mouse. *Nature* **301**, 527–530 (1983).
265. DiSanto, J. P., Müller, W., Guy-Grand, D., Fischer, A. & Rajewsky, K. Lymphoid development in mice with a targeted deletion of the interleukin 2 receptor gamma chain. *Proc. Natl. Acad. Sci.* **92**, 377–381 (1995).
266. Ishikawa, F. *et al.* Development of functional human blood and immune systems in NOD/SCID/IL2 receptor γ chainnull mice. *Blood* **106**, 1565–1573 (2005).
267. Walsh, N. C. *et al.* Humanized Mouse Models of Clinical Disease. *Annu. Rev. Pathol. Mech. Dis.* **12**, 187–215 (2017).
268. Takenaka, K. *et al.* Polymorphism in Sirpa modulates engraftment of human hematopoietic stem cells. *Nat. Immunol.* **8**, 1313–1323 (2007).
269. Legrand, N. *et al.* Functional CD47/signal regulatory protein alpha (SIRPα) interaction is required for optimal human T- and natural killer- (NK) cell homeostasis in vivo. *Proc. Natl. Acad. Sci.* **108**, 13224–13229 (2011).
270. Shultz, L. D. *et al.* Humanized mouse models of immunological diseases and precision medicine. *Mamm. Genome* **30**, 123–142 (2019).
271. Theodorides, A. P. A., Rongvaux, A., Fritsch, K., Flavell, R. A. & Manz, M. G. Humanized hemato-lymphoid system mice. *Haematologica* **101**, 5–19 (2016).
272. Karpel, M. E., Boutwell, C. L. & Allen, T. M. BLT Humanized Mice as a Small Animal Model of HIV Infection. *Curr. Opin. Virol.* **13**, 75–80 (2015).
273. Rongvaux, A. *et al.* Development and function of human innate immune cells in a humanized mouse model. *Nat. Biotechnol.* **32**, 364–372 (2014).
274. Lopez-Lastra, S. *et al.* A functional DC cross talk promotes human ILC homeostasis in humanized mice. *Blood Adv.* **1**, 601–614 (2017).

275. Li, Y. *et al.* A human immune system mouse model with robust lymph node development. *Nat. Methods* **15**, 623–630 (2018).
276. Masse-Ranson, G. *et al.* Accelerated thymopoiesis and improved T-cell responses in HLA-A2/-DR2 transgenic BRGS-based human immune system mice. *Eur. J. Immunol.* **49**, 954–965 (2019).
277. Strick-Marchand, H. *et al.* A Novel Mouse Model for Stable Engraftment of a Human Immune System and Human Hepatocytes. *PLOS ONE* **10**, e0119820 (2015).
278. A Double Humanized Blt-Mice Model Featuring A Stable Human-Like Gut Microbiome And Human Immune System - Video. <https://www.jove.com/t/59773/a-double-humanized-blt-mice-model-featuring-stable-human-like-gut>.
279. Long, B. R. & Stoddart, C. A. Alpha Interferon and HIV Infection Cause Activation of Human T Cells in NSG-BLT Mice. *J. Virol.* **86**, 3327–3336 (2012).
280. White, R. E. *et al.* EBNA3B-deficient EBV promotes B cell lymphomagenesis in humanized mice and is found in human tumors. *J. Clin. Invest.* **122**, (2012).
281. Meraz, I. M. *et al.* An Improved Patient-Derived Xenograft Humanized Mouse Model for Evaluation of Lung Cancer Immune Responses. *Cancer Immunol. Res.* **7**, 1267–1279 (2019).
282. Dusséaux, M. *et al.* Viral Load Affects the Immune Response to HBV in Mice With Humanized Immune System and Liver. *Gastroenterology* **153**, 1647-1661.e9 (2017).
283. Manz, M. G. Human-Hemato-Lymphoid-System Mice: Opportunities and Challenges. *Immunity* **26**, 537–541 (2007).
284. Huntington, N. D. *et al.* IL-15 trans-presentation promotes human NK cell development and differentiation in vivo. *J. Exp. Med.* **206**, 25–34 (2009).
285. Chen, Q., Khoury, M. & Chen, J. Expression of human cytokines dramatically improves reconstitution of specific human-blood lineage cells in humanized mice. *Proc. Natl. Acad. Sci.* **106**, 21783–21788 (2009).
286. Willinger, T. *et al.* Human IL-3/GM-CSF knock-in mice support human alveolar macrophage development and human immune responses in the lung. *Proc. Natl. Acad. Sci.* **108**, 2390–2395 (2011).
287. Schwab, I., Lux, A. & Nimmerjahn, F. Pathways Responsible for Human Autoantibody and Therapeutic Intravenous IgG Activity in Humanized Mice. *Cell Rep.* **13**, 610–620 (2015).
288. Katano, I., Ito, R., Kawai, K. & Takahashi, T. Improved Detection of in vivo Human NK Cell-Mediated Antibody-Dependent Cellular Cytotoxicity Using a Novel NOG-FcγR-Deficient Human IL-15 Transgenic Mouse. *Front. Immunol.* **11**, (2020).
289. Katano, I. *et al.* Long-term maintenance of peripheral blood derived human NK cells in a novel human IL-15- transgenic NOG mouse. *Sci. Rep.* **7**, 17230 (2017).
290. Herndler-Brandstetter, D. *et al.* Humanized mouse model supports development, function, and tissue residency of human natural killer cells. *Proc. Natl. Acad. Sci.* **114**, E9626–E9634 (2017).
291. Aryee, K.-E. *et al.* Enhanced development of functional human NK cells in NOD-scid-IL2rgnull mice expressing human IL15. *FASEB J.* **36**, e22476 (2022).
292. Rathinam, C. *et al.* Efficient differentiation and function of human macrophages in humanized CSF-1 mice. *Blood* **118**, 3119–3128 (2011).
293. Rongvaux, A. *et al.* Human thrombopoietin knockin mice efficiently support human hematopoiesis in vivo. *Proc. Natl. Acad. Sci.* **108**, 2378–2383 (2011).
294. Astle, J. *et al.* Developing a Model of Human Pluripotent to Hematopoietic Stem Cell Development in Mistrg Mice. *Blood* **126**, 4755 (2015).

295. Ivic, S. *et al.* Differential Dynamics of HIV Infection in Humanized MISTRG versus MITRG Mice. *ImmunoHorizons* **1**, 162–175 (2017).
296. Song, Y. *et al.* A highly efficient and faithful MDS patient-derived xenotransplantation model for pre-clinical studies. *Nat. Commun.* **10**, 366 (2019).
297. Li, Y. *et al.* A novel Flt3-deficient HIS mouse model with selective enhancement of human DC development. *Eur. J. Immunol.* **46**, 1291–1299 (2016).
298. Sung, H. *et al.* Global Cancer Statistics 2020: GLOBOCAN Estimates of Incidence and Mortality Worldwide for 36 Cancers in 185 Countries. *CA. Cancer J. Clin.* **71**, 209–249 (2021).
299. World Health Organization. *WHO report on cancer: setting priorities, investing wisely and providing care for all.* (World Health Organization, 2020).
300. Wong, Y., Meehan, M. T., Burrows, S. R., Doolan, D. L. & Miles, J. J. Estimating the global burden of Epstein–Barr virus-related cancers. *J. Cancer Res. Clin. Oncol.* **148**, 31–46 (2022).
301. Hatta, M. N. A., Mohamad Hanif, E. A., Chin, S.-F. & Neoh, H. Pathogens and Carcinogenesis: A Review. *Biology* **10**, 533 (2021).
302. Hanahan, D. & Weinberg, R. A. The Hallmarks of Cancer. *Cell* **100**, 57–70 (2000).
303. Hanahan, D. & Weinberg, R. A. Hallmarks of Cancer: The Next Generation. *Cell* **144**, 646–674 (2011).
304. Hanahan, D. Hallmarks of Cancer: New Dimensions. *Cancer Discov.* **12**, 31–46 (2022).
305. Cooper, G. M. *The Development and Causes of Cancer. Cell Mol. Approach 2nd Ed.* (2000).
306. Frank, S. A. Genetic predisposition to cancer — insights from population genetics. *Nat. Rev. Genet.* **5**, 764–772 (2004).
307. Weiderpass, E. Lifestyle and Cancer Risk. *J. Prev. Med. Pub. Health* **43**, 459–471 (2010).
308. Dalton-Griffin, L. & Kellam, P. Infectious causes of cancer and their detection. *J. Biol.* **8**, 67 (2009).
309. Jakóbiśiak, M., Lasek, W. & Gołąb, J. Natural mechanisms protecting against cancer. *Immunol. Lett.* **90**, 103–122 (2003).
310. Dunn, G. P., Bruce, A. T., Ikeda, H., Old, L. J. & Schreiber, R. D. Cancer immunoediting: from immunosurveillance to tumor escape. *Nat. Immunol.* **3**, 991–998 (2002).
311. Dunn, G. P., Old, L. J. & Schreiber, R. D. The Three Es of Cancer Immunoediting. *Annu. Rev. Immunol.* **22**, 329–360 (2004).
312. Chen, D. S. & Mellman, I. Oncology Meets Immunology: The Cancer-Immunity Cycle. *Immunity* **39**, 1–10 (2013).
313. Munhoz, R. R. & Postow, M. A. Recent advances in understanding antitumor immunity. *F1000Research* **5**, 2545 (2016).
314. Vitale, M. *et al.* HLA Class I Antigen Down-Regulation in Primary Ovary Carcinoma Lesions: Association with Disease Stage. *Clin. Cancer Res.* **11**, 67–72 (2005).
315. Gao, J. *et al.* Loss of IFN- γ Pathway Genes in Tumor Cells as a Mechanism of Resistance to Anti-CTLA-4 Therapy. *Cell* **167**, 397-404.e9 (2016).
316. Ghebeh, H. *et al.* The B7-H1 (PD-L1) T Lymphocyte-Inhibitory Molecule Is Expressed in Breast Cancer Patients with Infiltrating Ductal Carcinoma: Correlation with Important High-Risk Prognostic Factors. *Neoplasia* **8**, 190–198 (2006).

317. Swaika, A., Hammond, W. A. & Joseph, R. W. Current state of anti-PD-L1 and anti-PD-1 agents in cancer therapy. *Mol. Immunol.* **67**, 4–17 (2015).
318. Arneth, B. Tumor Microenvironment. *Medicina (Mex.)* **56**, 15 (2020).
319. Wang, K., Xu, J., Zhang, T. & Xue, D. Tumor-infiltrating lymphocytes in breast cancer predict the response to chemotherapy and survival outcome: A meta-analysis. *Oncotarget* **7**, 44288–44298 (2016).
320. Nguyen, N. *et al.* Tumor infiltrating lymphocytes and survival in patients with head and neck squamous cell carcinoma. *Head Neck* **38**, 1074–1084 (2016).
321. Waniczek, D. *et al.* Tumor-Associated Macrophages and Regulatory T Cells Infiltration and the Clinical Outcome in Colorectal Cancer. *Arch. Immunol. Ther. Exp. (Warsz.)* **65**, 445–454 (2017).
322. Mizukoshi, E. *et al.* Myeloid-derived suppressor cells correlate with patient outcomes in hepatic arterial infusion chemotherapy for hepatocellular carcinoma. *Cancer Immunol. Immunother.* **65**, 715–725 (2016).
323. Shimizu, K., Iyoda, T., Okada, M., Yamasaki, S. & Fujii, S. Immune suppression and reversal of the suppressive tumor microenvironment. *Int. Immunol.* **30**, 445–455 (2018).
324. Huntington, N. D., Cursons, J. & Rautela, J. The cancer–natural killer cell immunity cycle. *Nat. Rev. Cancer* **20**, 437–454 (2020).
325. Böttcher, J. P. *et al.* NK Cells Stimulate Recruitment of cDC1 into the Tumor Microenvironment Promoting Cancer Immune Control. *Cell* **172**, 1022-1037.e14 (2018).
326. Barry, K. C. *et al.* A natural killer–dendritic cell axis defines checkpoint therapy–responsive tumor microenvironments. *Nat. Med.* **24**, 1178–1191 (2018).
327. López-Soto, A., Gonzalez, S., Smyth, M. J. & Galluzzi, L. Control of Metastasis by NK Cells. *Cancer Cell* **32**, 135–154 (2017).
328. Laughney, A. M. *et al.* Regenerative lineages and immune-mediated pruning in lung cancer metastasis. *Nat. Med.* **26**, 259–269 (2020).
329. De La Rochere, P. *et al.* Humanized Mice for the Study of Immuno-Oncology. *Trends Immunol.* **39**, 748–763 (2018).
330. Rubio-Viqueira, B. & Hidalgo, M. Direct In Vivo Xenograft Tumor Model for Predicting Chemotherapeutic Drug Response in Cancer Patients. *Clin. Pharmacol. Ther.* **85**, 217–221 (2009).
331. Zhao, X., Li, L., Starr, T. K. & Subramanian, S. Tumor location impacts immune response in mouse models of colon cancer. *Oncotarget* **8**, 54775–54787 (2017).
332. Zitvogel, L., Pitt, J. M., Daillère, R., Smyth, M. J. & Kroemer, G. Mouse models in oncoimmunology. *Nat. Rev. Cancer* **16**, 759–773 (2016).
333. Zeng, Y. *et al.* Creation of an immunodeficient HLA-transgenic mouse (HUMAMICE) and functional validation of human immunity after transfer of HLA-matched human cells. *PLOS ONE* **12**, e0173754 (2017).
334. Wege, A. K. *et al.* Humanized tumor mice—A new model to study and manipulate the immune response in advanced cancer therapy. *Int. J. Cancer* **129**, 2194–2206 (2011).
335. Xia, J. *et al.* Modeling Human Leukemia Immunotherapy in Humanized Mice. *eBioMedicine* **10**, 101–108 (2016).
336. Chuprin, J. *et al.* Humanized mouse models for immuno-oncology research. *Nat. Rev. Clin. Oncol.* 1–15 (2023) doi:10.1038/s41571-022-00721-2.
337. Gerstein, R. *et al.* Patient-Derived Xenografts (PDX) of B Cell Lymphoma in NSG Mice: A Mouse Avatar for Developing Personalized Medicine. *Blood* **126**, 5408 (2015).

338. Zhang, N. *et al.* Epstein-Barr Virus and Neurological Diseases. *Front. Mol. Biosci.* **8**, (2022).
339. Balfour Jr, H. H., Dunmire, S. K. & Hogquist, K. A. Infectious mononucleosis. *Clin. Transl. Immunol.* **4**, e33 (2015).
340. Young, L. S. & Rickinson, A. B. Epstein–Barr virus: 40 years on. *Nat. Rev. Cancer* **4**, 757–768 (2004).
341. Levin, L. I., Munger, K. L., O’Reilly, E. J., Falk, K. I. & Ascherio, A. Primary infection with the Epstein-Barr virus and risk of multiple sclerosis. *Ann. Neurol.* **67**, 824–830 (2010).
342. Kuri, A. *et al.* Epidemiology of Epstein-Barr virus infection and infectious mononucleosis in the United Kingdom. *BMC Public Health* **20**, 912 (2020).
343. Hadinoto, V., Shapiro, M., Sun, C. C. & Thorley-Lawson, D. A. The Dynamics of EBV Shedding Implicate a Central Role for Epithelial Cells in Amplifying Viral Output. *PLOS Pathog.* **5**, e1000496 (2009).
344. Pegtel, D. M., Middeldorp, J. & Thorley-Lawson, D. A. Epstein-Barr Virus Infection in Ex Vivo Tonsil Epithelial Cell Cultures of Asymptomatic Carriers. *J. Virol.* **78**, 12613–12624 (2004).
345. Coleman, C. B. *et al.* Epstein-Barr Virus Type 2 Latently Infects T Cells, Inducing an Atypical Activation Characterized by Expression of Lymphotactic Cytokines. *J. Virol.* **89**, 2301–2312 (2014).
346. Isobe, Y. *et al.* Epstein-Barr Virus Infection of Human Natural Killer Cell Lines and Peripheral Blood Natural Killer Cells. *Cancer Res.* **64**, 2167–2174 (2004).
347. Shannon-Lowe, C. & Rowe, M. Epstein Barr virus entry; kissing and conjugation. *Curr. Opin. Virol.* **4**, 78–84 (2014).
348. Tanner, J., Weis, J., Fearon, D., Whang, Y. & Kieff, E. Epstein-barr virus gp350/220 binding to the B lymphocyte C3d receptor mediates adsorption, capping, and endocytosis. *Cell* **50**, 203–213 (1987).
349. Ogembo, J. G. *et al.* Human Complement Receptor Type 1/CD35 Is an Epstein-Barr Virus Receptor. *Cell Rep.* **3**, 371–385 (2013).
350. Li, Q. *et al.* Epstein-Barr virus uses HLA class II as a cofactor for infection of B lymphocytes. *J. Virol.* **71**, 4657–4662 (1997).
351. Backovic, M., Jardetzky, T. S. & Longnecker, R. Hydrophobic Residues That Form Putative Fusion Loops of Epstein-Barr Virus Glycoprotein B Are Critical for Fusion Activity. *J. Virol.* **81**, 9596–9600 (2007).
352. Kurth, J. *et al.* EBV-Infected B Cells in Infectious Mononucleosis: Viral Strategies for Spreading in the B Cell Compartment and Establishing Latency. *Immunity* **13**, 485–495 (2000).
353. Fujiwara, S., Imadome, K.-I. & Takei, M. Modeling EBV infection and pathogenesis in new-generation humanized mice. *Exp. Mol. Med.* **47**, e135–e135 (2015).
354. Malignant Lymphoma in Cottontop Marmosets after Inoculation with Epstein-Barr Virus. <https://www.pnas.org/doi/10.1073/pnas.70.9.2487>
doi:10.1073/pnas.70.9.2487.
355. Epstein, M. A., Zur Hausen, H., Ball, G. & Rabin, H. Pilot experiments with eb virus in owl monkeys (*aotus trivirgatus*). III. Serological and biochemical findings in an animal with reticuloproliferative disease. *Int. J. Cancer* **15**, 17–22 (1975).
356. Cox, C., Chang, S., Karran, L., Griffin, B. & Wedderburn, N. Y. 1996. Persistent Epstein–Barr virus infection in the common marmoset (*Callithrix jacchus*). *J. Gen. Virol.* **77**, 1173–1180.

357. Takashima, K. *et al.* A new animal model for primary and persistent Epstein–Barr virus infection: Human EBV-infected rabbit characteristics determined using sequential imaging and pathological analysis. *J. Med. Virol.* **80**, 455–466 (2008).
358. Epstein, M. A., Achong, B. G. & Barr, Y. M. VIRUS PARTICLES IN CULTURED LYMPHOBLASTS FROM BURKITT'S LYMPHOMA. *The Lancet* **283**, 702–703 (1964).
359. Ocheni, S. *et al.* EBV-Associated Malignancies. *Open Infect. Dis. J.* **4**, 101–112 (2010).
360. Hsu, J. L. & Glaser, S. L. Epstein–Barr virus-associated malignancies: epidemiologic patterns and etiologic implications. *Crit. Rev. Oncol. Hematol.* **34**, 27–53 (2000).
361. Mrozek-Gorska, P. *et al.* Epstein–Barr virus reprograms human B lymphocytes immediately in the prelatent phase of infection. *Proc. Natl. Acad. Sci.* **116**, 16046–16055 (2019).
362. Kang, M.-S. & Kieff, E. Epstein–Barr virus latent genes. *Exp. Mol. Med.* **47**, e131–e131 (2015).
363. Saha, A. & Robertson, E. S. Mechanisms of B-Cell Oncogenesis Induced by Epstein-Barr Virus. *J. Virol.* **93**, e00238-19 (2019).
364. Gottschalk, S. *et al.* An Epstein-Barr virus deletion mutant associated with fatal lymphoproliferative disease unresponsive to therapy with virus-specific CTLs. *Blood* **97**, 835–843 (2001).
365. Yum, S., Li, M. & Chen, Z. J. Old dogs, new trick: classic cancer therapies activate cGAS. *Cell Res.* **30**, 639–648 (2020).
366. Shin, M. H. *et al.* NK Cell-Based Immunotherapies in Cancer. *Immune Netw.* **20**, e14 (2020).
367. Ventola, C. L. Cancer Immunotherapy, Part 1: Current Strategies and Agents. *Pharm. Ther.* **42**, 375–383 (2017).
368. Propper, D. J. & Balkwill, F. R. Harnessing cytokines and chemokines for cancer therapy. *Nat. Rev. Clin. Oncol.* **19**, 237–253 (2022).
369. Conlon, K. C. *et al.* Redistribution, Hyperproliferation, Activation of Natural Killer Cells and CD8 T Cells, and Cytokine Production During First-in-Human Clinical Trial of Recombinant Human Interleukin-15 in Patients With Cancer. *J. Clin. Oncol.* **33**, 74–82 (2015).
370. Miller, J. S. *et al.* A First-in-Human Phase I Study of Subcutaneous Outpatient Recombinant Human IL15 (rhIL15) in Adults with Advanced Solid Tumors. *Clin. Cancer Res.* **24**, 1525–1535 (2018).
371. Knudson, K. M., Hodge, J. W., Schlom, J. & Gameiro, S. R. Rationale for IL-15 superagonists in cancer immunotherapy. *Expert Opin. Biol. Ther.* **20**, 705–709 (2020).
372. Wrangle, J. M. *et al.* ALT-803, an IL-15 superagonist, in combination with nivolumab in patients with metastatic non-small cell lung cancer: a non-randomised, open-label, phase 1b trial. *Lancet Oncol.* **19**, 694–704 (2018).
373. Chamie, K. *et al.* Phase II/III clinical results of IL-15R α Fc superagonist N-803 with BCG in BCG-unresponsive non-muscle invasive bladder cancer (NMIBC) carcinoma in situ (CIS) patients. *J. Clin. Oncol.* **39**, 510–510 (2021).
374. Manches, O. *et al.* In vitro mechanisms of action of rituximab on primary non-Hodgkin lymphomas. *Blood* **101**, 949–954 (2003).
375. Shiokawa, M. *et al.* In vivo assay of human NK-dependent ADCC using NOD/SCID/ γ cnnull (NOG) mice. *Biochem. Biophys. Res. Commun.* **399**, 733–737 (2010).

376. Weng, W.-K. & Levy, R. Two Immunoglobulin G Fragment C Receptor Polymorphisms Independently Predict Response to Rituximab in Patients With Follicular Lymphoma. *J. Clin. Oncol.* **21**, 3940–3947 (2003).
377. Mohammed, R., Milne, A., Kayani, K. & Ojha, U. How the discovery of rituximab impacted the treatment of B-cell non-Hodgkin's lymphomas. *J. Blood Med.* **10**, 71–84 (2019).
378. Webb, E. S. *et al.* Immune checkpoint inhibitors in cancer therapy. *J. Biomed. Res.* **32**, 317–326 (2018).
379. Bagchi, S., Yuan, R. & Engleman, E. G. Immune Checkpoint Inhibitors for the Treatment of Cancer: Clinical Impact and Mechanisms of Response and Resistance. *Annu. Rev. Pathol. Mech. Dis.* **16**, 223–249 (2021).
380. Quatrini, L. *et al.* The Immune Checkpoint PD-1 in Natural Killer Cells: Expression, Function and Targeting in Tumour Immunotherapy. *Cancers* **12**, 3285 (2020).
381. Felices, M. *et al.* Potent Cytolytic Activity and Specific IL15 Delivery in a Second-Generation Trispecific Killer Engager. *Cancer Immunol. Res.* **8**, 1139–1149 (2020).
382. Melief, C. J. M., Hall, T. van, Arens, R., Ossendorp, F. & Burg, S. H. van der. Therapeutic cancer vaccines. *J. Clin. Invest.* **125**, 3401–3412 (2015).
383. Saxena, M., van der Burg, S. H., Melief, C. J. M. & Bhardwaj, N. Therapeutic cancer vaccines. *Nat. Rev. Cancer* **21**, 360–378 (2021).
384. Sahin, U. & Türeci, Ö. Personalized vaccines for cancer immunotherapy. *Science* **359**, 1355–1360 (2018).
385. Abou-el-Enin, M. *et al.* Scalable Manufacturing of CAR T Cells for Cancer Immunotherapy. *Blood Cancer Discov.* **2**, 408–422 (2021).
386. Symons, H. J. *et al.* Improved Survival with Inhibitory Killer Immunoglobulin Receptor (KIR) Gene Mismatches and KIR Haplotype B Donors after Nonmyeloablative, HLA-Haploidentical Bone Marrow Transplantation. *Biol. Blood Marrow Transplant.* **16**, 533–542 (2010).
387. Dolstra, H. *et al.* Successful Transfer of Umbilical Cord Blood CD34+ Hematopoietic Stem and Progenitor-derived NK Cells in Older Acute Myeloid Leukemia Patients. *Clin. Cancer Res.* **23**, 4107–4118 (2017).
388. Tonn, T. *et al.* Treatment of patients with advanced cancer with the natural killer cell line NK-92. *Cytotherapy* **15**, 1563–1570 (2013).
389. Lim, S. A. *et al.* Ex Vivo Expansion of Highly Cytotoxic Human NK Cells by Cocultivation with Irradiated Tumor Cells for Adoptive Immunotherapy. *Cancer Res.* **73**, 2598–2607 (2013).
390. Knorr, D. A. *et al.* Clinical-Scale Derivation of Natural Killer Cells From Human Pluripotent Stem Cells for Cancer Therapy. *Stem Cells Transl. Med.* **2**, 274–283 (2013).
391. Mantesso, S., Geerts, D., Spanholtz, J. & Kučerová, L. Genetic Engineering of Natural Killer Cells for Enhanced Antitumor Function. *Front. Immunol.* **11**, (2020).
392. Hegde, P. S. & Chen, D. S. Top 10 Challenges in Cancer Immunotherapy. *Immunity* **52**, 17–35 (2020).
393. Sun, L., Jin, C.-H., Tan, S., Liu, W. & Yang, Y.-G. Human Immune System Mice With Autologous Tumor for Modeling Cancer Immunotherapies. *Front. Immunol.* **11**, (2020).
394. Schroeder, H. W., Radbruch, A. & Berek, C. 7 - B-Cell Development and Differentiation. in *Clinical Immunology (Fifth Edition)* (eds. Rich, R. R. *et al.*) 107–118.e1 (Elsevier, 2019). doi:10.1016/B978-0-7020-6896-6.00007-7.

395. Chijioke, O. *et al.* Human natural killer cells prevent infectious mononucleosis features by targeting lytic Epstein-Barr virus infection. *Cell Rep.* **5**, 1489–1498 (2013).
396. Berhani, O. *et al.* Human anti-NKp46 antibody for studies of NKp46-dependent NK cell function and its applications for type 1 diabetes and cancer research. *Eur. J. Immunol.* **49**, 228–241 (2019).
397. Shan, L., Flavell, R. A. & Herndler-Brandstetter, D. Development of Humanized Mouse Models for Studying Human NK Cells in Health and Disease. in *Natural Killer (NK) Cells: Methods and Protocols* (ed. Shimasaki, N.) 53–66 (Springer US, 2022). doi:10.1007/978-1-0716-2160-8_5.
398. Hezareh, M., Hessel, A. J., Jensen, R. C., van de Winkel, J. G. J. & Parren, P. W. H. I. Effector Function Activities of a Panel of Mutants of a Broadly Neutralizing Antibody against Human Immunodeficiency Virus Type 1. *J. Virol.* **75**, 12161–12168 (2001).
399. Absinta, M. *et al.* A lymphocyte–microglia–astrocyte axis in chronic active multiple sclerosis. *Nature* **597**, 709–714 (2021).
400. Simoni, Y. & Newell, E. W. Dissecting human ILC heterogeneity: more than just three subsets. *Immunology* **153**, 297–303 (2018).
401. Mjösberg, J. M. *et al.* Human IL-25- and IL-33-responsive type 2 innate lymphoid cells are defined by expression of CRTH2 and CD161. *Nat. Immunol.* **12**, 1055–1062 (2011).
402. Garcia-Beltran, W. F. *et al.* Innate Immune Reconstitution in Humanized Bone Marrow-Liver-Thymus (HuBLT) Mice Governs Adaptive Cellular Immune Function and Responses to HIV-1 Infection. *Front. Immunol.* **12**, (2021).
403. Zheng, Y. *et al.* Human neutrophil development and functionality are enabled in a humanized mouse model. *Proc. Natl. Acad. Sci.* **119**, e2121077119 (2022).
404. Moreau, A., Varey, E., Anegon, I. & Cuturi, M.-C. Effector Mechanisms of Rejection. *Cold Spring Harb. Perspect. Med.* **3**, a015461 (2013).
405. Marino, J., Paster, J. & Benichou, G. Allorecognition by T Lymphocytes and Allograft Rejection. *Front. Immunol.* **7**, (2016).
406. Valiante, N. M. *et al.* Functionally and Structurally Distinct NK Cell Receptor Repertoires in the Peripheral Blood of Two Human Donors. *Immunity* **7**, 739–751 (1997).
407. Demirci, S., Leonard, A. & Tisdale, J. F. Hematopoietic stem cells from pluripotent stem cells: Clinical potential, challenges, and future perspectives. *STEM CELLS Transl. Med.* **9**, 1549–1557 (2020).
408. Igarashi, K. *et al.* Patient-derived orthotopic xenograft (PDOX) mouse model of adult rhabdomyosarcoma invades and recurs after resection in contrast to the subcutaneous ectopic model. *Cell Cycle* **16**, 91–94 (2017).
409. Newton, R., Ferlay, J., Beral, V. & Devesa, S. S. The epidemiology of non-Hodgkin's lymphoma: Comparison of nodal and extra-nodal sites. *Int. J. Cancer* **72**, 923–930 (1997).
410. Møller, M. B., Pedersen, N. T. & Christensen, B. E. Diffuse large B-cell lymphoma: clinical implications of extranodal versus nodal presentation – a population-based study of 1575 cases. *Br. J. Haematol.* **124**, 151–159 (2004).
411. Curakova, E. *et al.* NonHodgkin's Lymphoma with Peritoneal Localization. *Case Rep. Gastrointest. Med.* **2014**, e723473 (2014).
412. Chappaz, S. & Finke, D. The IL-7 Signaling Pathway Regulates Lymph Node Development Independent of Peripheral Lymphocytes. *J. Immunol.* **184**, 3562–3569 (2010).

413. Takahashi, T. *et al.* Enhanced Antibody Responses in a Novel NOG Transgenic Mouse with Restored Lymph Node Organogenesis. *Front. Immunol.* **8**, (2018).
414. Davies, A. M. & Sutton, B. J. Human IgG4: a structural perspective. *Immunol. Rev.* **268**, 139–159 (2015).
415. Katano, I. *et al.* Development of a novel humanized mouse model for improved evaluation of in vivo anti-cancer effects of anti-PD-1 antibody. *Sci. Rep.* **11**, 21087 (2021).

Résumé substantiel en français

Le cancer est un fléau majeur pour la santé humaine, il a été estimé que près de 10 millions de personnes sont mortes du cancer dans le monde en 2020. En complément des options de traitement classiques, de nouvelles approches immunothérapeutiques, ont permis une amélioration des résultats pour les patients dont les anticorps thérapeutiques, l'administration de cytokines et le transfert adoptif de lymphocytes T. Par conséquent, l'utilisation du système immunitaire pour combattre le cancer est une stratégie thérapeutique prometteuse. Les cellules lymphoïdes innées, y compris les lymphocytes tueuses naturelles (NK) font partie du système immunitaire inné. Bien que les effets antitumoraux des lymphocytes NK ont été démontrés, le rôle des cellules lymphoïdes innées auxiliaires dans la réponse immunitaire antitumorale est moins clair.

Pour explorer le potentiel des lymphocytes NK et des cellules lymphoïdes innées dans l'immunothérapie, les modèles précliniques sont essentiels. Les souris avec un système immunitaire humain (HIS) constituent des modèles *in vivo* précieux pour étudier le développement et la fonction des cellules immunitaires humaines. Divers modèles de tumeurs ont été établis dans des souris HIS pour étudier les réponses immunitaires anti-tumorales humaines. Cependant, ces modèles présentent des limites, car les cellules immunitaires innées humaines se développent peu dans la plupart des modèles de souris HIS, et les modèles de tumeurs qui sont autologues du système immunitaire humain sont rares. De plus, chez les souris HIS, plusieurs composants du système immunitaire de la souris, comme les cellules myéloïdes et les protéines du complément, sont présents et fonctionnels, ce qui peut perturber les effets observés chez les souris HIS.

Dans cette thèse, j'ai caractérisé un nouveau modèle de souris HIS déficient en FcR, développé pour améliorer les tests d'anticorps thérapeutiques. De plus, j'ai établi un modèle de tumeur autologue en générant des lignées de cellules lymphoblastoïdes B (B-LCL) par transformation avec le virus d'Epstein Barr des cellules B isolées de souris HIS. Enfin, j'ai combiné ces deux modèles pour étudier l'effet des cellules NK humaines dans les réponses anti-tumorales médiées par les anticorps *in vivo*.

Pour générer un modèle de souris HIS déficient pour les FcγRs activateurs, une délétion de l'Exon 2 du gène *FcεR1g* a été introduite dans la souche de souris BRGSFA2DR2 par CRISPR/Cas9. La délétion dans *FcεR1g* a été vérifiée par PCR et séquençage de l'ADN et de l'ARN. L'analyse par cytométrie a révélé l'expression réduite du mFcεR1γ (chaîne FcRγ) et des récepteurs dépendants de la chaîne FcRγ (mCD16/CD32, mCD64 et mFcεR1α). La déficience fonctionnelle du FcγR activateur a été validée par un test d'anaphylaxie systémique passive pour lequel les souris ont été sensibilisées par injection d'anti-TNP et stimulés avec l'allergène TNP33 BSA 16-

18h plus tard. La réaction anaphylactique a été analysée en mesurant la température corporelle : les souris de type sauvage (Fcer1g +/+) et hétérozygotes (Fcer1g +/-) ont présenté une chute nette de la température corporelle, tandis que les souris knock-out (Fcer1g -/-) n'ont montré aucun signe d'anaphylaxie et leur température corporelle est restée stable. Par conséquent, nous avons confirmé que les souris BRGSA2DR2 Fcer1g-/- sont déficientes de la chaîne γ du FcR au niveau de l'ADN, des protéines et de la fonction. Ensuite, nous avons analysé la capacité des souris BRGSA2DR2 Fcer1g-/- à être greffées par des cellules souches hématopoïétiques (CSH) humaines pour établir un modèle HIS.

En comparant les souris HIS BRGSA2DR2 Fcer1g-/- et BRGSA2R2 Fcer1g+/- à 12 semaines, aucune différence significative n'a été observé par rapport au nombre ou à la fréquence des cellules hCD45+, des cellules T, des cellules B ou des cellules NK dans le sang. Ces mêmes résultats s'observent à 16 semaines dans la rate, la moelle osseuse, ou le foie.

Les souris BRGSA2DR2 Fcer1g-/- peuvent donc être efficacement greffées avec des CSH humaines. De plus, nous avons testé comment l'inactivation de Fcer1g affecte la déplétion des cellules T CD8+ médiée par les anticorps en utilisant un anticorps anti-hCD8a mIgG2a (OKT8) que nous avons injecté par voie intrapéritonéale aux souris HIS. Le nombre de cellules T CD8+ dans le sang des souris HIS a été déterminé 4 jours après l'injection de l'anticorps. Chez les souris HIS BRGSA2DR2 Fcer1g+/-, les cellules T CD8+ étaient absentes, alors que chez les souris HIS BRGSA2DR2 Fcer1g-/-, les cellules T CD8+ étaient partiellement déplétées, ce qui démontre l'implication de mécanismes dépendants et indépendants de Fcer1g dans la déplétion. Nous avons ensuite étudié les mécanismes dépendants du FcR humain impliqués dans la déplétion cellulaire médiée par les anticorps exogènes chez les souris HIS. Pour cela, nous avons étudié la déplétion des cellules B humaines après l'administration de l'anticorps monoclonal thérapeutique anti-hCD20, le Rituximab. Nous avons utilisé différents variants d'IgG humaines qui présentent des affinités de liaison différentes pour les récepteurs Fc et le complément. Avec la hIgG1, aucune différence de déplétion n'était évidente entre les souris Fcer1g+/- et Fcer1g-/- HIS, alors qu'une déplétion plus faible a été observée chez les souris Fcer1g-/- HIS avec la hIgG4 qui a une liaison plus faible aux Fc γ R humains et au complément. De plus, nous avons testé une variante d'anticorps IgG1_KA qui ne se lie pas au complément et conserve sa liaison aux Fc γ R, bien que cette liaison et la cytotoxicité cellulaire dépendante des anticorps (ADCC) soient réduites par rapport à l'IgG1. La déplétion des cellules B humaines par la variante IgG1_KA du Rituximab était clairement réduite chez les souris HIS Fcer1g-/- par rapport à l'IgG1 du Rituximab. Ces résultats indiquent que la déplétion d'anticorps dépendante du complément fonctionne chez les souris HIS en l'absence de FcRs activateurs. Dans la plupart des souris HIS Fcer1g-/- injectées par Rituximab IgG1_KA, peu ou pas de déplétion des cellules B humaines a été détectée. Néanmoins, les souris HIS Fcer1g-/- injectées par IgG1_KA présentaient une déplétion significativement plus élevée par rapport aux souris témoins HIS Fcer1g-/- injectées par PBS, ce qui suggère l'implication des cellules FcR+ humaines dans la déplétion cellulaire. Nous avons remarqué que le degré de

déplétion chez les souris HIS Fc γ R1g $^{-/-}$ injectées par Rituximab IgG1_KA était fortement corrélé au pourcentage de cellules NK humaines présentes dans chaque souris HIS, ce qui indique que les cellules NK sont des effecteurs dans la déplétion médiée par les anticorps. Pour approfondir le rôle potentiel des cellules NK humaines, nous avons enrichi ces cellules effectrices Fc γ R+ chez les souris HIS Fc γ R1g $^{-/-}$ en injectant de l'IL-15, qui augmente la fonction effectrice des cellules NK et l'expression de CD16 (Fc γ RIII). L'amplification des cellules NK par l'IL-15 a considérablement augmenté la déplétion des cellules B chez les souris HIS Fc γ R1g $^{-/-}$ traitées par IgG1_KA, ce qui suggère que les cellules NK humaines jouent un rôle important dans la déplétion médiée par les anticorps. En résumé, nos données révèlent de multiples effecteurs dans la déplétion dépendante des anticorps chez les souris HIS, y compris le Fc γ R et le complément murin, ainsi que les cellules NK humaines.

Afin d'étudier les réponses anti-tumorales en excluant les effets allogéniques, nous avons généré un modèle de tumeur autologue chez les souris HIS. Dans ce but, des cellules CD45+ humaines ont été isolées de la rate et de la moelle osseuse de souris HIS, puis infectées avec le virus d'Epstein Barr in vitro, transformant les cellules B en LCL B prolifératives. Dans un premier temps, les cellules B-LCL ont été injectées par voie intrapéritonéale à des souris immunodéficientes, les cellules B-LCL ont proliféré entre la première à la deuxième semaine après l'injection, ce qui montre que ces cellules peuvent se greffer et se développer in vivo. Dans un deuxième temps, nous avons démontré le caractère tumorigène des cellules B-LCL en suivant pendant plusieurs semaines des souris immunodéficientes auxquelles on avait injecté des B-LCL : les souris ont développé des masses tumorales solides et ont dû être sacrifiées dans les 40 jours suivant l'injection. Les B-LCL étaient également capables de se greffer à des souris HIS histocompatibles (HLA-A2 et HLA-DR15). Cependant, par rapport aux souris immunodéficientes, un nombre inférieur de B-LCL s'est développé chez les souris HIS à la première et à la deuxième semaine après l'injection ; de plus bien que cela ne soit pas significatif, les souris HIS histocompatibles ont survécu quelques jours de plus que les souris immunodéficientes. Nous avons observé dans le péritoine une augmentation du nombre de cellules immunitaires humaines, des cellules T et NK, par rapport aux souris HIS non injectées de B-LCL, ce qui suggère qu'elles sont immunogènes. Il est intéressant de noter qu'à la première semaine, les souris HIS avec un nombre plus faible de cellules B-LCL avaient la plus grande quantité de cellules immunitaires humaines, en particulier des cellules T CD8+, alors que ce rapport était inversé à la deuxième semaine. Cela peut être dû à la mort des cellules immunitaires induite par l'activation ou à une infiltration plus faible lorsque le nombre de B-LCL diminue. Ainsi, nous avons mis en place un modèle de tumeur autologue qui a montré un potentiel tumorigène et immunogène chez les souris HIS.

Nous avons combiné le modèle de tumeur B-LCL avec les souris HIS BRGSA2DR2 Fc γ R1g $^{-/-}$ afin d'étudier les effets anti-tumoraux des cellules NK médiés par les anticorps thérapeutiques in vivo. Pour augmenter les cellules NK humaines dans les souris HIS, certaines ont été injectées avec le complexe IL-15-IL-15R α puis avec les

B-LCL et certaines d'entre elles ont été traitées avec du Rituximab (IgG1). Chez les souris stimulées par l'IL-15, nous avons détecté une augmentation de l'expression des marqueurs des cellules NK, notamment CD16, CD57 et CD69 dans le sang et un nombre plus élevé de cellules NK dans la cavité péritonéale par rapport aux souris témoins comme attendu. Le nombre de cellules B-LCL était plus faible chez les souris HIS que chez les souris non-HIS et diminuait chez les souris traitées à l'IL-15 et/ou au Rituximab par rapport aux souris HIS non traitées, bien que ces différences n'étaient pas statistiquement significatives. Aucune différence claire n'a été observée entre les souris HIS Fc γ 1g $^{+/-}$ et Fc γ 1g $^{-/-}$ dans les groupes de traitement. Alors que le nombre d'ILC dans la cavité péritonéale reste pratiquement inchangé dans les différents groupes, plusieurs sous-ensembles de cellules immunitaires, tels que les cellules T CD8a $^{+}$, les cellules T $\gamma\delta$ et les cellules NKT de type II, augmentent chez les souris traitées par IL-15 et/ou Rituximab. De plus, des cellules myéloïdes humaines étaient présentes dans la cavité péritonéale, y compris des macrophages et des sous-ensembles de cellules dendritiques, mais aucun granulocyte humain n'a été détecté. Un nombre élevé de cellules myéloïdes de souris a été trouvé dans la cavité péritonéale dans tous les groupes de souris. Les sous-ensembles de cellules myéloïdes de souris, tels que les granulocytes, les macrophages et les cellules présentatrices d'antigènes, présentaient des proportions modifiées entre les différents groupes. Par exemple, les granulocytes de souris sont plus abondants chez les souris traitées par l'IL-15 et/ou le Rituximab que chez les souris non traitées.

En conclusion, j'ai établi un modèle pour étudier les réponses des cellules immunitaires autologues anti-tumorales humaines in vivo, ce qui permet de tester des anticorps thérapeutiques tout en excluant les effets des Fc γ R s activateurs de souris. De plus, nous avons démontré que les cellules NK humaines contribuent à la déplétion cellulaire médiée par les anticorps in vivo. Ainsi, nous fournissons un modèle préclinique particulièrement adapté pour tester l'effet anti-tumoral des cellules NK lors de l'utilisation de nouveaux agents immunothérapeutiques, tels que les anticorps. Cela pourrait favoriser le développement de thérapies anticancéreuses susceptibles d'améliorer le soin des patients à l'avenir.

Annex 1

Notch, RORC and IL-23 signals cooperate to promote multi-lineage human innate lymphoid cell differentiation

Carys A. Croft, Anna Thaller, Solenne Marie, Jean-Marc Doisne, Laura Surace, Rui Yang, Anne Puel, Jacinta Bustamante, Jean-Laurent Casanova & James P. Di Santo

Published on the 27th of July 2022

Journal: Nature Communications

Notch, RORC and IL-23 signals cooperate to promote multi-lineage human innate lymphoid cell differentiation

Received: 18 December 2021

Accepted: 13 July 2022

Published online: 27 July 2022

 Check for updatesCarys A. Croft¹, Anna Thaller¹, Solenne Marie¹, Jean-Marc Doisne¹, Laura Surace¹, Rui Yang², Anne Puel^{3,4,5}, Jacinta Bustamante^{3,4,5}, Jean-Laurent Casanova^{2,3,4,5,6} & James P. Di Santo¹✉

Innate lymphoid cells (ILCs) include cytotoxic natural killer cells and distinct groups of cytokine-producing innate helper cells which participate in immune defense and promote tissue homeostasis. Circulating human ILC precursors (ILCP) able to generate all canonical ILC subsets via multi-potent or uni-potent intermediates according to our previous work. Here we show potential cooperative roles for the Notch and IL-23 signaling pathways for human ILC differentiation from blood ILCP using single cell cloning analyses and validate these findings in patient samples with rare genetic deficiencies in *IL12RB1* and *RORC*. Mechanistically, Notch signaling promotes upregulation of the transcription factor *RORC*, enabling acquisition of Group 1 (IFN- γ) and Group 3 (IL-17A, IL-22) effector functions in multi-potent and uni-potent ILCP. Interfering with RORC or signaling through its target IL-23R compromises ILC3 effector functions but also generally suppresses ILC production from multi-potent ILCP. Our results identify a Notch->RORC->IL-23R pathway which operates during human ILC differentiation. These observations may help guide protocols to expand functional ILC subsets in vitro with an aim towards novel ILC therapies for human disease.

Innate lymphoid cells (ILC) are a family of lymphoid effector cells with notable similarities to T cells but lacking rearranged antigen receptors. ILCs can rapidly produce soluble factors (cytokines, chemokines) in response to environmental stimuli and actively participate in steady-state immune homeostasis as well as in the early immune response to infection, inflammation and tissue stress¹⁻³. Based on expression of transcription factors and cytokine production, ILCs in both mice and man have been categorized into five functional groups that mirror known helper and cytotoxic T cell subsets^{4,5}. NK cells, which express Eomesodermin (EOMES) and T-box transcription factor 21 (TBX21 encoding T-BET), are highly cytotoxic effector cells that also produce interferon gamma (IFN- γ) and tumour necrosis factor (TNF) and

thereby represent innate counterparts of CD8⁺ cytotoxic T-cells⁶. Related ILC1 are a non-cytotoxic subset of TNF and IFN- γ producing innate cells that also depend on T-BET (but not EOMES) and may represent innate homologues of Th1 cells^{7,8}. Group 2 ILCs require GATA-binding protein 3 (GATA-3) for development and are able to produce type 2 cytokines (interleukin (IL)-5, IL-9, IL-13) as well as the EGF-related factor amphiregulin and can be considered as innate homologues of Th2 cells⁹⁻¹². Group 3 ILCs are ROR related orphan receptor gamma t (ROR γ T)-dependent cells which produce IL-17A and IL-22 and are functionally analogous to Th17/22 cells^{13,14}. Lastly, lymphoid tissue inducer cells (LTi) are a distinct fetal ILC3 subset that promote secondary lymphoid tissue development in the embryo^{15,16}.

¹Institut Pasteur, Université Paris Cité, Inserm U1223, Innate Immunity Unit, Paris, France. ²St. Giles Laboratory of Human Genetics of Infectious Diseases, Rockefeller Branch, Rockefeller University, New York, NY, USA. ³Laboratory of Human Genetics of Infectious Diseases, Necker Branch, INSERM, UMR 1163 Paris, France. ⁴Imagine Institute, Université Paris Cité, Paris, France. ⁵Study Center for Primary Immunodeficiencies, Necker Hospital for Sick Children, AP-HP, Paris, France. ⁶Howard Hughes Medical Institute, New York, NY, USA. ✉e-mail: james.di-santo@pasteur.fr

The signals that drive primary cell fate decisions from mouse or human ILCP remain poorly defined^{17,18}. Earlier studies characterized CD34⁺ hematopoietic cells from human secondary lymphoid tissues and defined distinct NK/ILC-lineage precursors that could give rise to mature ILCs in vitro^{19–21}. We identified a circulating human ILC precursor (ILCP) with a Lineage⁺CD34⁺CD7⁺CD117⁺CRTh2⁻ phenotype which could generate all ILC subsets in vitro (using single cell cloning assays and bulk culture), as well as in vivo in a humanized mouse model²². At steady state, human ILCP lack expression of ILC group-defining transcription factors and do not produce cytokines, even following activation²². Nevertheless, human ILCP are present in numerous lymphoid and non-lymphoid tissues, existing in an epigenetically “poised” state ready for further expansion and differentiation to mature functional ILCs²². Based on these observations, we proposed an ‘ILC-poiesis’ model whereby circulating ILC precursors might enter tissues, and undergo a process of activation, proliferation and differentiation dictated by signals present in the tissue environment^{22,23}. While ILC-poiesis can help explain some characteristics of distinct ILC ‘repertoires’ found under steady-state conditions and after infection²⁴, the roles for identified signaling pathways (Notch, RORC, cytokines) that promote Group 1, Group 2 or Group 3 ILC differentiation from blood ILCP remain to be fully characterized.

The transcription factor ROR γ T and the cytokine IL-23 are important drivers of type 3 T cell differentiation (involving Th17 and Th22 cells)^{25,26}. Th17 cells are absent in *RORC*-deficient mice, and interestingly ILC3 generation is also ablated, highlighting the developmental similarities of mouse ILC3 and Th17 cells^{13,15}. Similarly, patients with genetic deficiencies in *RORC*, or in IL-23 signaling via loss of function (LOF) mutations in *IL12RB1* or *TYK2*, have defects in Th17 cell generation and function, and consequently are susceptible to infections with fungal pathogens^{26,27}. Additionally, IL-23 signaling in humans promotes type 1 immunity, as *IL23R*^{-/-} patients have reduced IFN- γ expression, clinically manifesting as Mendelian susceptibility to mycobacterial disease (MSMD)^{28–30}. Concerning human ILC generation, mutations in *RORC* have been previously reported to impair ILC3 development in human and have severe effects on the development of peripheral lymph nodes^{22,27}, while mutations in the IL-12/IL-23 signaling axis impair the ability of ILC2 to acquire IFN- γ expression upon IL-12 signaling³¹.

The precise contributions of these factors to ILC development have not been clearly defined. Here we identify an essential role for *RORC* in the generation of human ILC3, and an important contribution of downstream IL-23 signaling in the acquisition of type 1 and type 3 effector functions during human ILC differentiation from circulating ILCP. Our results further refine our understanding of the regulation of human ILC differentiation and the roles Notch and IL-23 signaling play in this process.

Results

Notch signaling and IL-23 promote ILC differentiation from human ILC precursors

We previously showed that peripheral blood human ILCP can give rise to diverse mature ILC subsets in vitro following bulk culture or single cell cloning on OP9 stromal cells in the presence of cytokines²². ILCP were identified in the peripheral blood as Lin⁻CD7⁺CD94⁻NKG2A⁻CD16⁻CD127⁺CRTh2⁻CD117⁺ (Supplementary Fig. 1a) and while the majority were uniformly CD25⁺, CD45RA⁺ and CD200R1⁺ (in line with previous reports^{22,32,33}), human ILCP were heterogeneous for CD56, CD62L and CD161 expression (Supplementary Fig. 1b). To better understand the individual roles for stromal-derived signals (Notch) and cytokines (IL-23) in promoting ILC differentiation, we analyzed progeny from short-term bulk cultures of human ILCP. Blood ILCP were cultured in wells pre-seeded with either OP9 or OP9-DLL4 stroma in media containing IL-2, IL-7 and IL-1 β with or without IL-23. After 5–7 days, expanded cells were electronically gated to exclude

NK cells and remaining cells were tested for transcription factors associated with development of ILC1 (T-BET), ILC2 (GATA-3) and ILC3 (RORC) as well as for their ability to produce cytokines upon short-term pharmacological stimulation with phorbol 12-myristate acetate/ionomycin (P/I).

Concerning ILC1 differentiation, IL-23 boosted IFN- γ production in cells cultured on OP9 or OP9-DLL4 stroma, with the highest percentage of IFN- γ -producing cells under IL-23/DLL4 conditions (Fig. 1a, Supplementary Fig. 2a, Supplementary Table 1). Interestingly, this was not associated with significant increases in T-BET (Fig. 1b, c, Supplementary Fig. 2b, Supplementary Table 1) and is consistent with the ability of IL-23 to promote IFN- γ production in humans^{29,34}. For ILC2 differentiation, IL-13 production varied greatly between healthy donors but was not significantly modulated by exposure to either DLL4, while a small but significant decrease was observed with the addition of IL-23 only in the absence of Notch signaling (Fig. 1d, Supplementary Fig. 2c, Supplementary Table 1). In contrast, GATA-3 levels were significantly higher in cultures grown on OP9-DLL4 (Fig. 1e, f, Supplementary Fig. 2d, Supplementary Tables 1–2). Concerning ILC3-associated cytokines, IL-17A was produced at low levels in most donors and was only appreciably expressed in OP9-DLL4 cultures in the presence of IL-23 (Fig. 1g, Supplementary Fig. 2e, Supplementary Table 1). In contrast, IL-22 production was significantly increased in bulks cultured on OP9-DLL4 and was highest in bulk cultures on OP9-DLL4 in the presence of IL-23 (Fig. 1h, Supplementary Fig. 2f, Supplementary Table 1). ILC3-related ROR γ T expression was also significantly higher in ILCP cultured on OP9-DLL4 (Fig. 1i, Fig. Supplementary Fig. 2g, Supplementary Table 1), with an average 3-fold increase in the percentage of ROR γ T⁺ cells between ILCP from the same donor cultured on OP9-DLL4 as compared to OP9 cells (Fig. 1j, Supplementary Table 2). Taken together, these results suggest an effect of Notch signaling via DLL4 on RORC/ROR γ T expression in developing ILC and a synergistic role for IL-23 and Notch signaling for the generation of Group ILC1 and ILC3 from peripheral blood ILCP.

Human ILCP differentiation in *RORC*-deficient patients

As DLL4 signaling could increase frequencies of ROR γ T⁺ cells generated from ILCP in bulk culture irrespective of cytokine combinations (Fig. 1i, j), we hypothesized that Notch-induced RORC expression might facilitate generation of certain ILC subsets (especially ILC3) from ILCP. We analyzed two MSMD patients with genetic deficiencies in the transcription factor RORC (encoding ROR γ T) (Supplementary Table 3)^{26,27}. We first characterized circulating ILC populations in *RORC*^{-/-} patients and were able to identify ILCP, ILC2 and NK cells (Fig. 2a, Supplementary Fig. 3a). While the frequency of NK cell subsets and total CD127⁺ILCs were within the normal range (Fig. 2b, Supplementary Fig. 3b), both patients had reduced ILCP frequencies (Fig. 2c, f), with increased proportions of blood ILC2 (Fig. 2d, g), resulting in an altered ratio of ILCP/ILC2 compared to healthy controls (Fig. 2e).

We examined the cell surface phenotype of ILCP in *RORC*^{-/-} patients using CD56, CD161, CD25, CD200R, CD45RA and CD62L. While ILCP from *RORC*^{-/-} donors did cluster with healthy donor ILCP following uniform manifold approximation and projection (UMAP) analyses (Fig. 2h–i)³⁵, they could be differentiated based on several markers including lower levels of CD117 and higher levels of CD56 (Supplementary Fig. 3c–d). In contrast, CD161, CD45RA, CD25, CD62L and CD200R1 expression on ILCP from *RORC*^{-/-} patients paralleled observations made on control ILCP in previous reports^{22,32,33} (Fig. 2h–i).

As ILC differentiation from *RORC*^{-/-} patients had been previously assessed solely in bulk cultures, we next sought to clarify the role of *RORC* in the determination of primary cell fate. We therefore employed a previously described in vitro cell cloning system²² based on OP9 stromal cells with exogenous cytokines, including IL-1 β , IL-2, IL-7 and IL-23, to examine the developmental potential of single ILCs

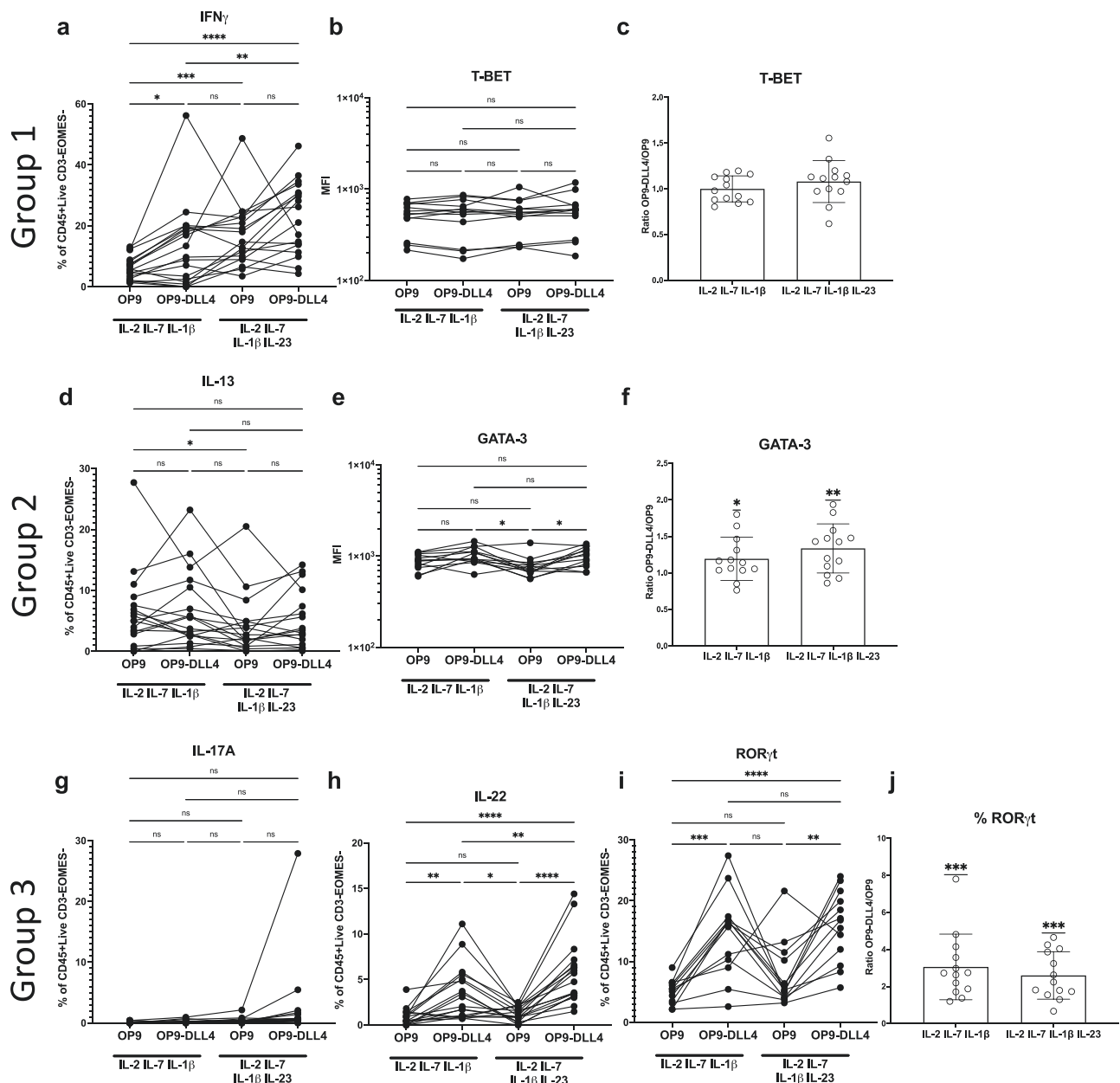


Fig. 1 | Effects of Notch and IL-23 signaling for human ILCP differentiation. ILCP Group 1, 2 and 3 cytokine expression ($n = 18$; after P/I stimulation) and transcription factors ($n = 13$) were assessed in bulk ILCP cultures (Supplementary Fig. 2). Expression of Group 1 ILC associated factors (a) IFN γ (b) T-BET (c) and relative quantity of T-BET on OP9-DLL4 vs OP9. Expression of Group 2 ILC associated factors (d) IL-13 (e) GATA-3 (f) and relative quantity of GATA-3 on OP9-DLL4 vs OP9. Expression of Group 3 ILC associated factors (g) IL-17A (h) IL-22 (i) ROR γ t (j) and relative quantity of ROR γ t on OP9-DLL4 vs OP9. Data compared using

(a–b, d–e, g–i) one-way repeated measures ANOVA using Tukey’s multiple comparison’s test, details in Supplementary Table 1 or (c, f, j) one sample T and Wilcoxon test, details in Supplementary Table 2. ns = not significant, * $p \leq 0.05$, ** $p \leq 0.01$, *** $p \leq 0.001$, **** $p < 0.001$. Data are presented as (a–b, d–e, g–i) individual unique donors matched across conditions or (c, f, j) mean with SD of ratios of individual donors. Results from from 6 (a, d, g–h) or 4 (b–c, e–f, i–j) independent experiments. Source Data are provided as a Source Data file.

(Supplementary Fig. 4a). ILC clones were then classified based on cytokine expression. Group 1 ILCs, comprising both NK cells (EOMES $^{+}$) or ILC1 (EOMES $^{-}$) produced IFN- γ , ILC2 clones as IL-13-producers and ILC3 as IL-17A- and/or IL-22-producing clones (Supplementary Fig. 4b–f). As previously reported²², some ILCP ‘clones’ harbored independent subsets of cells producing cytokines associated with different ILC groups; these ‘multi-potent’ clones were further designated as either IFN- γ and IL-13 producing Group 1/ILC2, IFN- γ and either IL-17A or IL-22 producing Group 1/ILC3, IL-13 and either IL-17A or IL-22 producing ILC2/ILC3, or IFN- γ , IL-13 and either IL-17A or IL-22 producing Group 1/ILC2/ILC3 (Supplementary Fig. 4h–k). As previously reported by us and others^{22,32}, a variable fraction of ILC clones

did not produce any cytokines after stimulation and were considered as ‘non-producers’ (Supplementary Fig. 4g).

We analyzed ILCP-derived ILC clones from the above-described *RORC* $^{-/-}$ patients. Although cloning efficiencies from *RORC* $^{-/-}$ ILCP were severely reduced compared to healthy donors (Fig. 2j), the few *RORC* $^{-/-}$ clones that were generated on OP9-DLL4 stroma with IL-23 expressed exclusively IFN- γ or IL-13; none produced IL-17A or IL-22, in contrast to clones from healthy donors (Fig. 2k), consistent with our previous report²². These results confirm a RORC-independent pathway of human ILC1, ILC2 and NK cell development and an essential role for RORC in the differentiation of human ILCs that produce ILC3-signature cytokines.

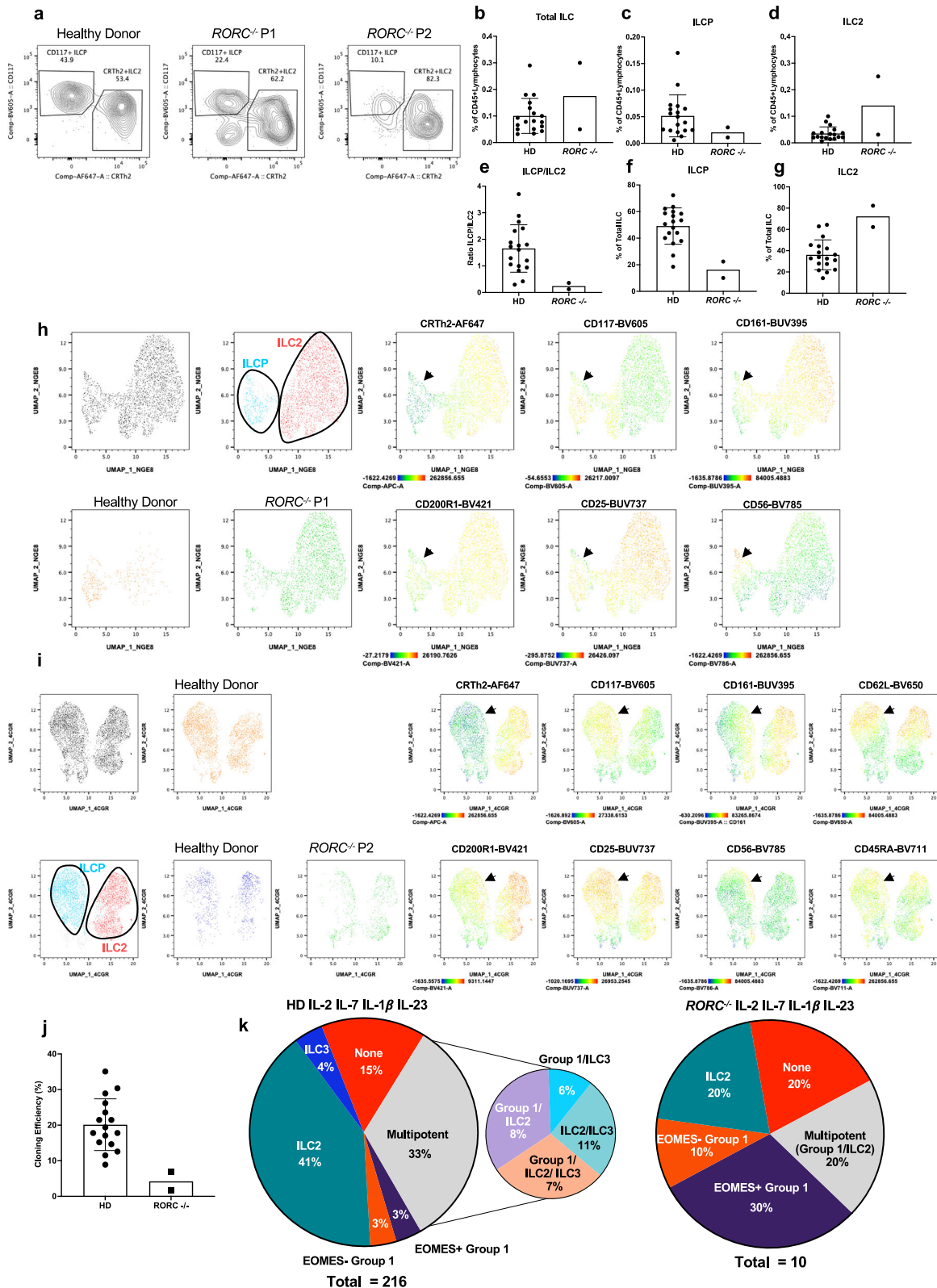


Fig. 2 | Human ILC differentiation in *RORC*^{-/-} patients. **a** Flow cytometric analysis of ILCs from a healthy donor and two *RORC*^{-/-} patients (gating strategy in Supplementary Fig. 1). Relative frequencies of **b** total ILC (**c**) ILCP (**d**) and ILC2 in CD45⁺ live lymphocytes. **e** Ratio of ILCP to ILC2. Relative frequencies of **f** ILCP and **g** ILC2 in total ILCs. **h**–**i** Uniform manifold projection (UMAP) analyses on healthy donors and *RORC*^{-/-} patients. **h** UMAP of experiment with P1 and healthy donor and **i** UMAP of

experiment with P2 and healthy donors. Representative plots of staining can be found in Supplementary Fig. 3. **j** Cloning efficiency of healthy donors and *RORC*^{-/-} patients. **k** Clone distributions of *RORC*^{-/-} patients and healthy donors analyzed concurrently. **b**–**g**, **j** Data are represented as mean with SD, with each point corresponding to an individual unique donor. Results compiled from healthy donors (*n* = 18) and *RORC*^{-/-} patients (*n* = 2). Source Data are provided as a Source Data file.

Pharmacological RORC inhibition alters ILC differentiation in bulk and clonal ILCP cultures

As access to ILCP from RORC-deficient patients was limited, we used an orthogonal approach to better understand how ROR γ T conditions ILC fate. We used the RORC inhibitor SR2211, which has been shown to modulate IL-23R and IL-17A expression in differentiating T cells³⁶. We included this inhibitor in bulk ILCP cultures on OP9-DLL4 with IL-1 β , IL-2, IL-7 and IL-23 and assessed its effects on transcription factor expression as well as P/I-induced cytokine expression. Addition of SR2211 did not significantly affect T-BET or GATA-3 expression, (Fig. 3b, d, Supplementary Fig. 5b, d, Supplementary Table 4) or the production of IL-13 from bulk cultured ILCP (Fig. 3c, Supplementary Fig. 5c, Supplementary Table 4). In contrast, the frequencies of mature ILCs producing IFN- γ or IL-22, or expressing ROR γ T were significantly reduced by SR2211 (Fig. 3a, f, g, Supplementary Fig. 5a, f–h, Supplementary Table 4). These results suggest that RORC inhibition modifies the generation of Group 1 and Group 3 ILCs in bulk cultured human ILCP.

We next assessed the impact of SR2211 on clonal ILCP differentiation. RORC inhibition increased (average of 15%) the frequency of uni-potent ILC2 clones, while it decreased (average of 20%) the generation of multi-potent ILC clones (Fig. 4a, Supplementary Table 5). Concerning the diversity of multi-potent clones generated, exposure

to SR2211 significantly decreased the frequency of ILC2/ILC3 clones and almost completely ablated the generation of ILC1/ILC3 clones, with only 1 donor able to generate any ILC1/ILC3 clones when cloned with SR2211, while a majority of donor ILCP (12 of 16) generated ILC1/ILC3 clones in control DMSO clonal cultures (Fig. 4b, Supplementary Table 5). While differentiation of uni-potent ILC1 was not obviously impacted by SR2211, and unipotent ILC3 were reduced only modestly (Fig. 4a, Supplementary Table 5), the overall frequency of IL-17A and IL-22 producing ILC clones was significantly reduced (Fig. 4d, Supplementary Table 5), reflecting the strong decrease at the level of multi-potent progenitors. The cumulative distributions of ILC clones generated from all donors were significantly different in the presence or absence of SR2211 (Fig. 4c, Supplementary Table 6). In line with results RORC^{-/-} patients (Fig. 2j), SR2211 significantly reduced ILCP cloning efficiency in healthy donors (Fig. 4e, Supplementary Table 4). Collectively, these results identify multiple roles for ROR γ T in the generation of mature ILC3 from Notch plus IL-23-stimulated multi-potent ILCP.

Effects of Notch signaling and IL-23 on clonal ILC differentiation from blood ILCP

As RORC promotes Th17 T cell differentiation through up-regulation of IL-23R^{36–38}, we hypothesized that IL-23 signals might represent the

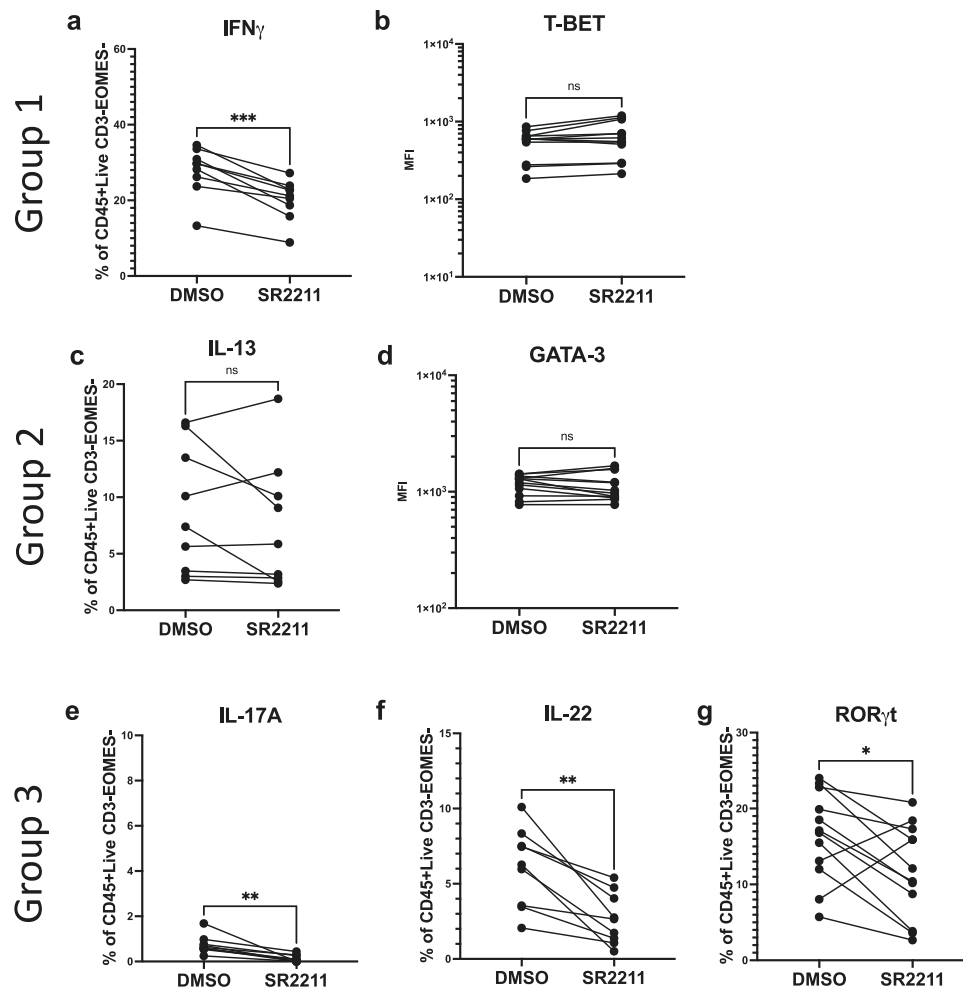


Fig. 3 | Impact of RORC inhibition for ILCP differentiation. Analysis of cytokine ($n = 9$) and transcription factor ($n = 12$) expression in differentiated human ILCP after addition of either 0.01% DMSO or SR2211 (10 μ M) was assessed as described in Fig. 1. Representative plots in Supplementary Fig. 4. Expression of Group 1 ILC associated factors (a) IFN γ and (b) T-BET. Expression of Group 2 ILC associated factors (c) IL-13 (d) and GATA-3. Expression of Group 3 ILC associated factors (e) IL-

17A and f IL-22 (g) ROR γ T. Data compared using paired T-tests (two-tailed), details in Supplementary Table 4. ns = not significant, * $p \leq 0.05$, ** $p \leq 0.01$, *** $p \leq 0.001$, **** $p < 0.001$. Data are presented as individual unique donors matched across conditions. Results from 3 (a, c, e, f) or 4 (b, d, g) independent experiments. Source Data are provided as a Source Data file.

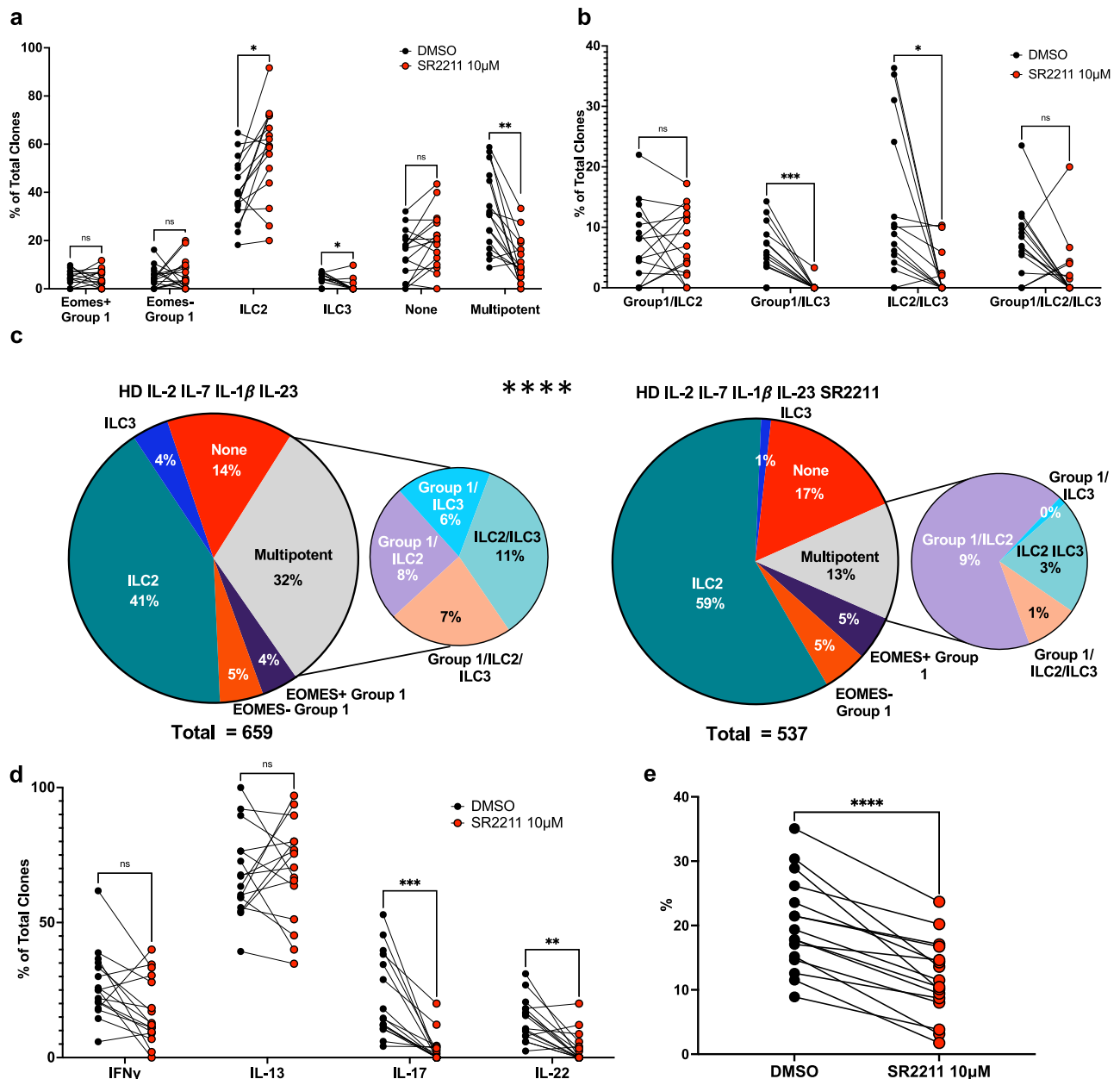


Fig. 4 | Impact of SR2211 on clonal ILCP differentiation. Single ILCP from healthy donors ($n = 16$) were cultured with either 0.01% DMSO (black circles) or SR2211 (10 μ M) (red). **a** Frequencies of unipotent (EOMES + ILC1, EOMES-ILC1, ILC2, ILC3, None) and total multipotent clones per individual healthy donor. **b** Frequencies of types of multipotent clones. **c** Overall distributions of clones grown in either DMSO alone or SR2211. **d** Overall frequencies of all clones expressing IFN γ , IL-13, IL-17A and IL-22. **e** Cloning efficiency of donors grown in either DMSO or SR2211. Comparisons performed using (a–b, d) Two-way ANOVA with matching using Šidák’s multiple comparisons tests, (details in Supplementary Table 5) (c) chi-square test (observed vs expected; details in Supplementary Table 6) and **e** paired t-test (two-tailed) (details in Supplementary Table 4). ns = not significant, * $p \leq 0.05$, ** $p \leq 0.01$, *** $p \leq 0.001$, **** $p < 0.0001$. Data represented as individual donors matched across conditions, compiled from 7 experiments. Source Data are provided as a Source Data file.

primary mechanism by which Notch-induced RORC exerts its effects in human ILCP differentiation. To test this hypothesis, we cloned healthy donor ILCP on OP9 ($n = 20$) or OP9-DLL4 ($n = 19$) stroma with or without IL-23. By analyzing the frequencies of different ILCs arising from single ILCP in multiple healthy donors, we could make some generalizations about the independent roles for IL-23 and Notch signaling in human ILCP differentiation.

When culturing blood ILCP on OP9 stroma, we found that ILC2 was the dominant ILC subset generated irrespective of the presence or absence of IL-23 or Notch signaling (Fig. 5a, Supplementary Table 5). However, the overall frequency of ILC2 arising from ILCP was clearly reduced (average of 16%) when ILCP were cloned on OP9 stroma in the

presence of IL-23, and the frequency of multi-potent clones increased (average of 6%) in the presence of IL-23 (Fig. 5a, Supplementary Table 5). The types of multi-potent clones most influenced by IL-23 were those producing ILC3-related cytokines IL-17A or IL-22 (Fig. 5b, Supplementary Table 5), and the overall frequency of clones producing IL-17A was substantially increased (Supplementary Fig. 6a, Supplementary Table 5). The cumulative difference in the distributions of ILC clones generated on OP9 stroma with or without IL-23 was statistically significant (Fig. 5c, Supplementary Table 6; chi-squared = $p < 0.0001$). Importantly, IL-23 had no effect on cloning efficiency (total # clones obtained/total # of ILCP wells seeded; Supplementary Fig. 6i, Supplementary Table 4).

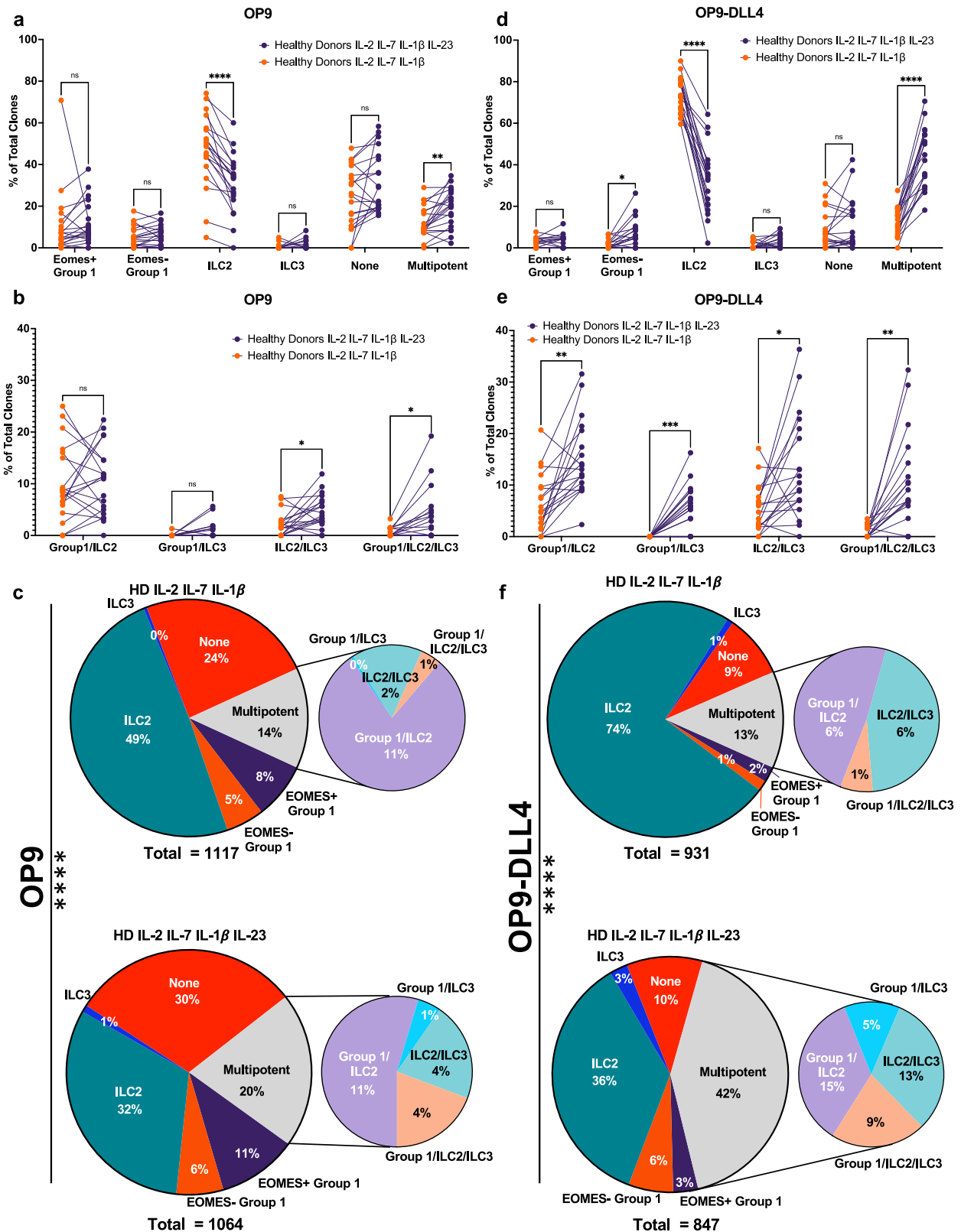


Fig. 5 | Effects of Notch signaling and IL-23 on clonal ILC differentiation from blood ILCP. Human ILCP cloning on OP9 ($n = 20$) or OP9-DLL4 ($n = 19$) stroma with (purple circles) or without (orange circles) IL-23 supplementation. **a** Frequencies of unipotent (EOMES + ILC1, EOMES-ILC1, ILC2, ILC3, None) and total multipotent clones per individual healthy donor, **b** Frequencies of types of multipotent clones and **c** Overall distributions of clones grown in the presence or absence of IL-23 on OP9 stroma. **d** Frequencies of unipotent and total multipotent clones per individual healthy donor, **e** Frequencies of types of multipotent clones and **f** Overall

distributions of clones grown in the presence or absence of IL-23 on OP9-DLL4 stroma. Data represented as individual matched values; each point corresponds to an individual donor. Comparisons performed using **(a–d)** Two-way ANOVA with matching using Šidák’s multiple comparisons test, details in Supplementary Table 5 and **e, f** chi-square test (observed vs expected; details in Supplementary Table 6). ns = not significant, * $p \leq 0.05$, *** $p \leq 0.01$, **** $p \leq 0.001$, ***** $p < 0.001$. Data represented as a Source Data file.

These results suggest that IL-23 promotes the growth of multi-potent ILC clones producing ILC3 cytokines at the expense of uni-potent ILC2 clones. Still, the frequencies of IL-17A and IL-22 ILC clones on OP9 were quite low (Supplementary Fig. 6a, Supplementary Table 5). As ILCP bulk culture on OP9-DLL4 increased both ROR γ T expression and IL-22 production (Fig. 1g–j, Supplementary Table 1), we reasoned that enhanced Notch signaling might facilitate Group 3 features during ILCP differentiation, especially in the presence of IL-23. ILCP cloned on OP9-DLL4 stroma with IL-23 showed increased frequencies (average of 23%) of multi-potent clones producing ILC3-related cytokines and showed significantly decreased frequencies of ILC2 clones (average of 41%; Fig. 5d–f, Supplementary Table 6). Thus, the effect of IL-23 to promote multi-potent ILC clones and reduce ILC2 clones (as seen on OP9 stroma) was retained in the presence of DLL4 stimulation. Moreover, cloning of DLL4-stimulated ILCP in the presence of IL-23 showed an increased (>3-fold) frequency of total IL-17A and IL-22 producing clones (Supplementary Fig. 6b, Supplementary Table 5). Interestingly, OP9-DLL4 cultures with IL-23 generated a modest (average of 5%) but significant increase in EOMES⁺Group 1 clones (Fig. 5d, Supplementary Table 5). Finally, Notch signaling with IL-23 resulted in a significant reduction in ILC ‘non-producer’ clones (Supplementary Fig. 6d, Supplementary Table 5). These results suggest that combined Notch and IL-23 generate synergistic effects on differentiation of mature ILC subsets from multi-potent as well as uni-potent ILCP.

To understand unique effects of Notch signaling in our system, we compared clonal ILC outcomes on OP9 versus OP9-DLL4 stroma. In the absence of IL-23, DLL4 promoted significantly more ILC2 (mean increase of 27%) (Supplementary Fig. 6c, Supplementary Table 5), matching the increase frequency of total IL-13 producing clones (27%) (Supplementary Fig. 6g, Supplementary Table 5). While overall frequencies of multi-potent clones did not change (Supplementary Fig. 6c, Supplementary Table 5), a modest but significant increase in ILC2/ILC3 clones (mean of 3%) was observed in the presence of DLL4 (Supplementary Fig. 6e, Supplementary Table 5).

We next assessed effects of Notch signaling in the presence of IL-23. Notch signaling resulted in a mean increase of 24% in the frequency of multipotent clones (Supplementary Fig. 6d, Supplementary Table 5), due to increases in multipotent clones containing ILC3 (mean increase of 4, 8 and 6% for Group 1/ILC3, ILC2/ILC3, Group 1/ILC2/ILC3 respectively, overall increase of 20%) (Supplementary Fig. 6f, Supplementary Table 5). Notch signaling in the presence of IL-23 also resulted in an average reduction of 9% in the frequency of EOMES⁺Group1 clones (Supplementary Fig. 6d, Supplementary Table 5). Irrespective of the presence or absence of IL-23, Notch signaling itself reduced the efficiency of cloning by an average of 15% (Supplementary Fig. 6j, Supplementary Table 7), as well as the frequency of the ‘non-producers’, by 15% in the absence of IL-23 (Supplementary Fig. 6c, Supplementary Table 5) and 19% in the presence of IL-23 (Supplementary Fig. 6d, Supplementary Table 5). Notch signaling therefore appears to selectively permit efficient generation of multi-potent ILCP and additionally promotes ILC2 differentiation. The presence or absence of IL-23 had no effect on ILCP cloning efficiency (Supplementary Fig. 6i, Supplementary Table 7), suggesting that it does not enhance the proliferation of specific biased ILC precursors, but promotes their acquisition of effector functions.

Human ILCP development and differentiation in *IL12RB1* deficient patients

To confirm the important role for IL-23 signaling in ILCP differentiation, we studied *IL12RB1*^{-/-} patients^{28–30,39}. Previous reports have shown that mutations in *IL12RB1* impair Th1 differentiation and IFN- γ production in response to IL-12 and IL-23, resulting in MSMD and increased susceptibility to intracellular pathogens including *Salmonella* spp., but can also impair Th17 cell development and immunity to fungal pathogens such as *Candida albicans*^{26,40}. We first analyzed

peripheral blood ILC subsets in patients lacking *IL12RB1* and were able to identify ILCP, ILC2 and NK cells that were present at similar (ILCP, NK cells) or slightly increased levels (ILC2) compared to healthy donors (Fig. 6a–d, Supplementary Fig. 7a, b, Supplementary Table 8). As a proportion of total CD127⁺ ILC, both ILCP and ILC2 were present at frequencies comparable to healthy donors (Fig. 6f, g, Supplementary Table 8). ILCP from *IL12RB1*^{-/-} patients had a normal phenotype with typical CD25, CD200R1, CD62L, CD161, CD45RA and CD56 expression (Fig. 6h, Supplementary Fig. 7c) and clustered with healthy donor ILCP after UMAP analyses (Fig. 6i).

ILCP cloning from *IL12RB1*^{-/-} patients on OP9 and OP9-DLL4 stroma with IL-23 gave rise to significantly fewer (average of 10%) EOMES⁺Group 1 ILC clones and significantly more ILC2 clones in both conditions, (average of 21% on OP9, average of 28% on OP9-DLL4) compared to healthy donors (Fig. 7a, b, Supplementary Table 5). Moreover, no Group 1/ILC3 were generated from any *IL12RB1*^{-/-} patient (Fig. 7c, d), and the cumulative distributions of all clones generated from healthy donors in comparison to *IL12RB1*^{-/-} patients were significantly different (Fig. 7e, f, Supplementary Table 6; chi-squared test = $p > 0.0001$). ILCP from *IL12RB1* patients were unable to generate significant proportions of IL-17A or IL-22 producing clones even in the presence of Notch signaling (Supplementary Fig. 8a, b, Supplementary Table 5). Finally, ILCP cloning efficiency from *IL12RB1*^{-/-} patients was similar to that observed using ILCP from healthy donors (Supplementary Fig. 8c, Supplementary Table 7). Taken together, our results suggest that Notch signaling alone does not appear to be sufficient for the generation of ILC3 fate but requires integration of IL-23 signaling to promote multi-lineage ILC differentiation from ILCP.

Discussion

The unique and cooperative roles for Notch and IL-23 signaling in promoting human ILCP differentiation remain poorly defined and here we provide evidence that the transcription factor ROR γ T plays a key intermediary role in this process. Previous studies have shown that murine Th17 and ILC3 differentiation both require ROR γ T^{13,26,27}, although the precise mechanisms have not been elucidated. RORC controls IL-23R expression^{41,42} but mice lacking IL-23 signaling retain gut ILC3 subsets, suggesting alternative regulatory pathways. Pharmacological inhibition of RORC has also produced conflicting results with ablation of Th17 function but little effect on ILC3 differentiation⁴³. Our results using RORC-deficient patients and ROR γ T inhibitors clearly point to an important role for RORC-dependent signals in generating mature functional human ILC3. This included not only IL-17A-producing ILCs but also extended to IL-22-producing ILC3, albeit to a lesser extent. The distinct impact of RORC inhibition for IL-17A versus IL-22 production in human ILC3 may involve alternative regulators of IL-22 expression, such as AHR, which also promotes IL-22 expression in ILC3^{44–46}. Moreover, we found an important impact of RORC inhibition on differentiation of multi-potent ILC clones. These results suggest a broader role for ROR γ T in early human hematopoietic precursors as previously proposed^{20,27,47}.

Notch signaling plays a key role in T cell development in the thymus and T cell differentiation in secondary lymphoid tissues, where specific Notch ligands act as instructors and/or amplifiers of T cell fate and function⁴⁸. DLL4 has been reported to enhance Th1 differentiation and inhibit Th2 differentiation^{49,50}, and may also promote Th17 differentiation through ROR γ T stabilization^{51–53}. However, other reports have documented that Notch signaling can simultaneously enhance Th1, Th2 and Th17 differentiation in the absence of polarizing cytokines⁵⁴. Concerning ILC differentiation, Notch signaling has been implicated in promoting ILC2 and ILC3 development in mice, and in human hematopoietic precursors isolated from secondary lymphoid tissues^{55–59}. Still, how Notch signaling operates, as either a general enhancer of ILC differentiation or as a promoter of particular ILC subsets remains unclear. Our finding that Notch stimulation up-

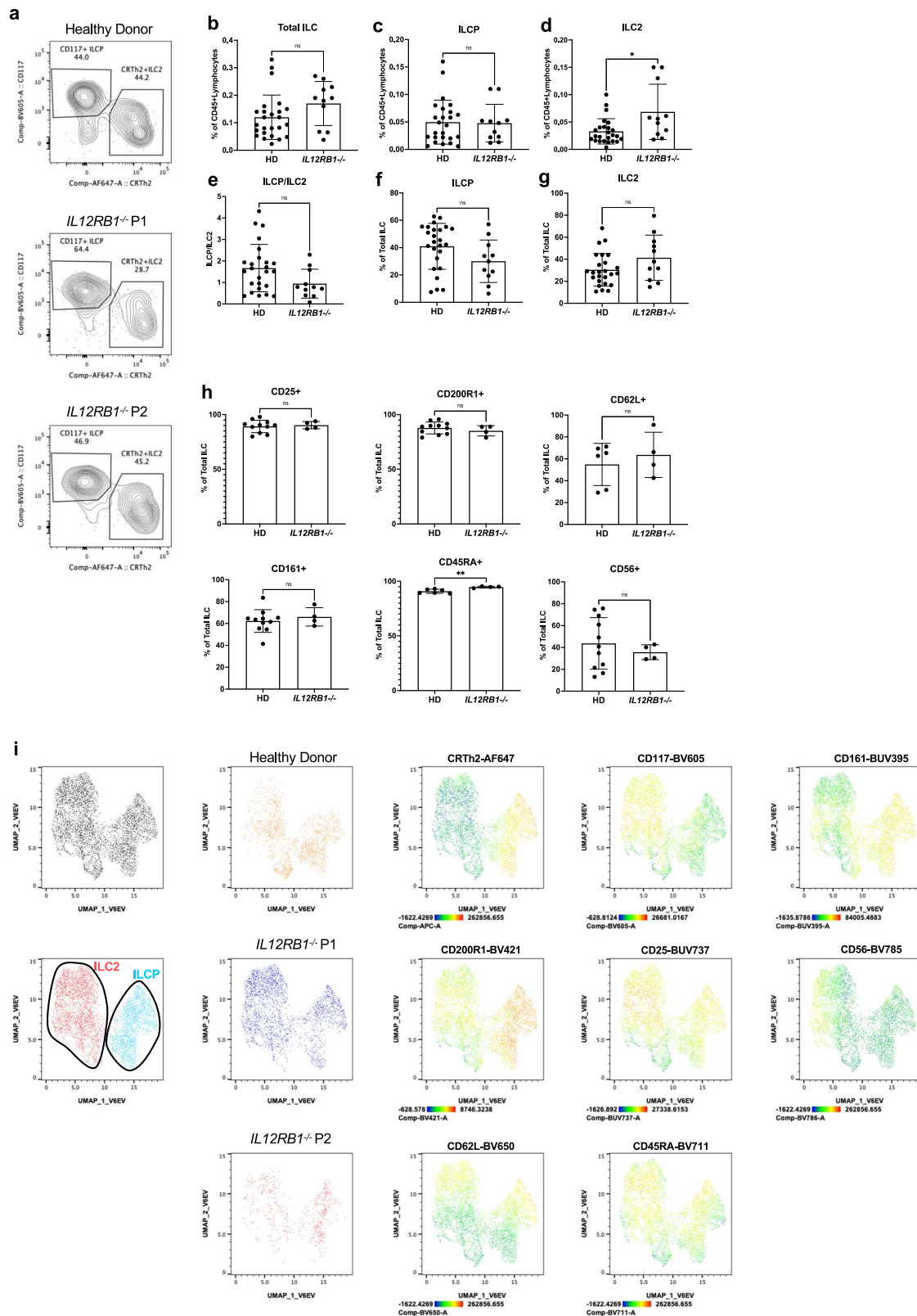


Fig. 6 | Human ILC differentiation in *IL12RB1*^{-/-} patients. **a** Flow cytometric analysis of ILCs from a healthy donor and two *IL12RB1*^{-/-} patients (gating strategy in Supplementary Fig. 1). Relative frequencies of **b** total ILC (**c**) ILCP (**d**) and ILC2 in CD45⁺ live lymphocytes. **e** Ratio of ILCP to ILC2. Relative frequencies of **f** ILCP and **g** ILC2 in total ILCs. **h** Expression of markers CD25, CD200R1, CD62L, CD161, CD45RA and CD56 on ILCP of healthy donors and *IL12RB1*^{-/-} patients. **b–g** Comparisons done using two-tailed Mann–Whitney test. ns = not significant,

* $p \leq 0.05$, ** $p \leq 0.01$, *** $p \leq 0.001$, **** $p < 0.001$. **i** Uniform manifold projection (UMAP) analyses on one healthy donor and two *IL12RB1*^{-/-} patients. Representative plots of staining can be found in Supplementary Fig. 7 (**b–h**). Data are represented as Mean with SD and each point corresponds to an individual donor or patient. **b–g** $n = 25$ healthy donors and $n = 11$ *IL12RB1*^{-/-} patients, **h** $n = 6$ or 11 healthy donors and $n = 4$ *IL12RB1*^{-/-} patients. Details for each test are found in Supplementary Table 8. Source Data are provided as a Source Data file.

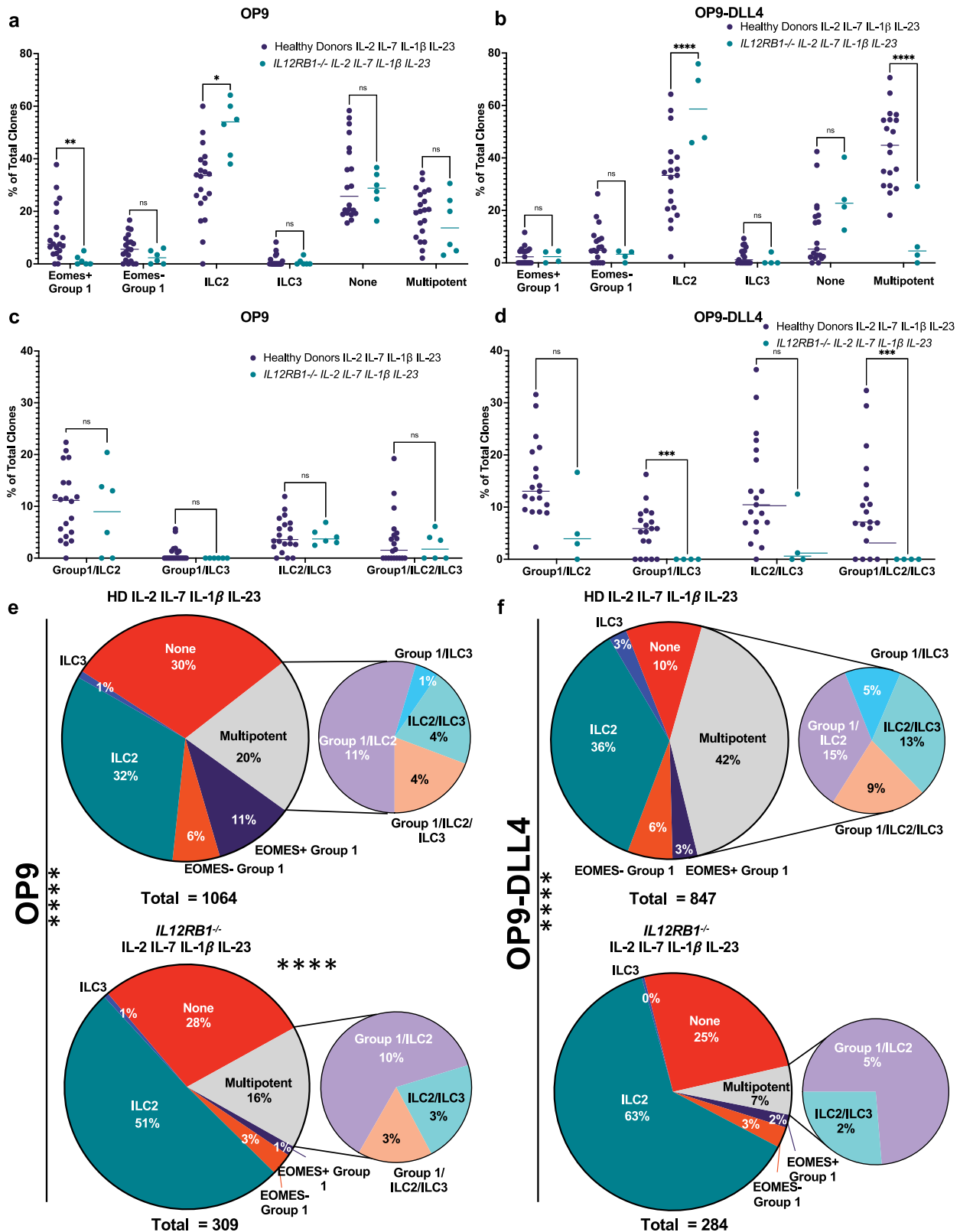


Fig. 7 | *IL12RB1* deficiency results in reduced frequency of multipotent and ILC3 cytokine producing ILC clones. ILC3 from healthy donors (purple circles) or *IL12RB1*^{-/-} patients (green circles) were cloned on OP9 (HD, *n* = 20; *IL12RB1*^{-/-}, *n* = 6) or OP9-DLL4 (HD, *n* = 19; *IL12RB1*^{-/-}, *n* = 4) stroma. Frequencies of unipotent (EOMES + ILC1, EOMES-ILC1, ILC2, ILC3, None) and total multipotent clones per individual healthy donor on **a** OP9 **b** or OP9-DLL4 stroma. Frequencies of types of multipotent clones on **c** OP9 **d** or OP9-DLL4 stroma. Data represented as individual matched values; each point corresponds to an individual donor. Overall

distributions of clones grown in the presence or absence of IL-23 on **e** OP9 or **f** OP9-DLL4 stroma. Comparisons performed using (a-d) Two-way ANOVA with no matching using Sidak's multiple comparisons test, details in Supplementary Table 5 and **e**, **f** chi-square test (observed vs expected; details in Supplementary Table 6). Data are compiled from a minimum of 3 independent experiments. ns = not significant, **p* ≤ 0.05, ***p* ≤ 0.01, ****p* ≤ 0.001, *****p* < 0.001. Source Data are provided as a Source Data file.

regulated RORC expression in human ILCP offers an explanation for the broad effects of Notch stimulation on human ILC differentiation.

Interestingly, IL-23 signaling enhanced the differentiation of Group 1 and Group 3 ILC from human ILCP, independent of Notch signaling. The impact on IFN- γ expressing Group 1 ILCs is relevant considering that defects in IFN- γ -dependent anti-mycobacterial immunity is observed in patients with mutations in *IL23R*, *IL12RB1* and *RORC*^{27,28}. Further, ILCP from *IL12RB1*^{-/-} patients primarily gave rise to ILC2 and had clear reductions in the generation of ILC3. While IL-23 affected ILCP differentiation irrespective of the presence of DLL4, Notch signaling clearly enhanced IL-23 mediated effects. That ROR γ T is required for the action of IL-23 to promote ILC3 differentiation is supported by both its upregulation by Notch signaling and the decline in ILC3 development during RORC inhibition. Effects on ILC3s parallel Th17 differentiation, during which ROR γ T upregulates *IL23R*; IL-23 signaling and the phosphorylation and activation of STAT3 is subsequently essential for the differentiation and function of Th17 cells, as evidenced by defects in Th17 differentiation and immunity in patients with mutations in *IL23R*, *IL12RB1* and *STAT3*^{26,28,40}. Still, Notch signals exhibit additional effects through stabilization of ROR γ T expression and IL-23 responsiveness that maintains ILCP multipotency. These data therefore identify a core Notch \rightarrow RORC \rightarrow IL-23R pathway that regulates human ILC differentiation at multiple stages.

We previously proposed an 'ILC-poiesis' model in which circulating ILCP are poised for further differentiation with ILC maturation relying on tissue signals that will vary depending on the state of stress, infection or inflammation^{22,23}. Our data here identify IL-23 as one such environmental factor that can modify ILC fate from ILCP by promoting multi-potent ILCP differentiation. We did observe that a proportion of ILCP in all conditions gave rise exclusively to a single fate, primarily ILC2, which may indicate that a proportion of ILCP are unipotent ILC2P³². Alternatively, ILC2 may represent a 'default' ILC maturation pathway when certain environmental signals are lacking. Such 'homeostatic' ILC2 may be important in the maintenance of tissues under steady-state conditions and during repair after inflammatory insults.

Multi-potent ILCP may have enhanced capacity to adapt to the tissue environment into which they are recruited. The tissue distribution of Notch ligands (and DLL4 in particular) may represent an important factor in generating tissue-specific repertoires of ILCs. ILC3 are not found in the circulation, and are also rare in many non-mucosal tissues^{22,60}. Tonsils are enriched in Notch ligands, and are one of the tissues in which ILC3 have been most studied in humans, in part due to their relative abundance, DLL4 is also highly expressed in the human small intestine and other tissues of the digestive system^{58,61}. This is notably also one of the tissues in which ILC3 are most abundant, both in human and in mice^{13,60,62}, and where they have been demonstrated to act in the maintenance of gut homeostasis and responses to pathogenic bacteria. A synergistic effect for IL-23 and Notch signaling may be particularly relevant in the intestine. IL-23 is expressed by dendritic cells and antigen presenting cells in the intestine and is important in the maintenance and homeostasis of epithelial barrier function^{3,63}. Thus, Notch and IL-23 signaling may act as tissue specific signals which direct the development of ILC upon entry into the tissue and may thereby promote the generation of ILC3.

The ability of ILCP to flexibly generate ILC subsets dictated by external signals may also have important consequences in the early immune response to infection. Notably, patients with LOF mutations in *IL12RB1* or *RORC* both are susceptible to chronic mucocutaneous candidiasis (CMC) resulting from infection with the common opportunistic fungal pathogen *Candida albicans*^{40,64}. Th17 generation and function is impacted in these patients as well; this defect in T cell differentiation is likely a key factor in the development of fungal disease in these patients²⁶. ILC3 have also been demonstrated to exhibit anti-fungal immunity through the expression of IL-17A, and due to

their localization in mucosal barrier tissues where pathogen exposure typically occurs, may play important roles in the initial immune response⁶⁵. While the relative distributions of ILCs in tissues from both *RORC* and *IL12RB1* patients is not known, the observed defects in their generation of Group 3 ILCs from ILCP may contribute to their susceptibility to fungal infections. It is also interesting to note that while a significant proportion of *IL12RB1* patients develop candidiasis, it is relatively more common, severe and chronic in patients with *RORC* deficiencies^{22,26-28}; this may correlate with the greater impacts on both ILCP and ILC3 generation seen in ROR γ T-deficient patients compared to *IL12RB1*-deficient patients. While the differences in ILC3s were the most striking in our investigation of the *RORC*/IL-23 axis, we also observed clear impacts on the generation of IFN- γ -producing Group 1 ILCs. This is in line with research demonstrating that mutations in *RORC* as well as both the IL-12 and IL-23 signaling axes are also strongly associated with MSMD as a result of impaired IFN γ -dependent immunity to mycobacteria²⁷⁻²⁹. The roles of ILCs and of ILCP differentiation in the context of mycobacterial infection are not well defined, however impairment of the generation or function of IFN- γ -producing Group 1 ILCs may further permit mycobacterial proliferation early in MSMD.

In summary, we have demonstrated key roles for Notch DLL4 signals, RORC and IL-23 in promoting multi-potent ILC fate, and for the generation of IL-17A and IL-22-producing ILC3. While future work will be required to define the precise molecular mechanisms underlying these processes, our results demonstrate that manipulation of these pathways can profoundly modify ILC differentiation, providing a potential path to harness the therapeutic potential of these novel effector cells in the clinic.

Methods

Human samples and cell isolation

All studies required ethics approval from the institutional ethics committees. Patient recruitment was done under the ID-RCB 2010-A00650-39 and 2010-A00636-33 delivered by EC IDF-II, France. Healthy donors were recruited by Etablissement Français du Sang (EFS, Paris, France) and samples given to the Institut Pasteur (Paris, France) under the agreement N°18/EFS/041. Healthy donors were provided without preselection and ranged in age from 19–61 with a 60–40 ratio of males to females. Essential information regarding patients with autosomal recessive complete *IL-12R β 1* and ROR γ T deficiency are included in Supplementary Table 3 and has been previously described^{27,39,64,66-68}. Informed consent was obtained from all patients, including protocols approved by the institutional review boards. A Ficoll-Paque gradient (GE Healthcare) was used for PBMC isolation. Cells from patients and healthy donors were studied after cryopreservation unless fresh samples were available.

Isolation and phenotyping of ILCP

For bulk sorting, PBMCs were first depleted of T cells, B cells, and residual monocytes, eosinophils, pDCs, and erythrocytes by incubation with biotinylated antibodies (anti-CD3, anti-CD14, anti-CD19, anti-CD123, anti-CD235a) for 20–30 min at room temperature, followed by incubation with MojoSort anti-biotin magnetic nanobeads (Stemcell) according to the manufacturer's instructions. Samples used for single cell cloning were thawed directly from cryopreserved PBMCs. Samples were stained for 15 min at room temperature in 2%FCS-PBS for lineage markers (anti-CD3, anti-CD4, anti-CD5, anti-CD14, anti-CD19, anti-TCR $\alpha\beta$, anti-TCR δ), anti-CD45, anti-CD7, anti-CD127, anti-CD16, anti-CD94, anti-NKG2A, anti-CD117, anti-CRTh2, as well as other markers used for surface phenotyping. A complete list of antibodies can be found in Supplementary Table 9. Cells were sorted and samples acquired simultaneously using a FACS Aria II (BD) using BD FACS DIVA version 6 (BD), or FACS Aria Fusion (BD) using BD FACS DIVA version 8 (BD). Bulks were sorted to >99% purity and single cell cloning was performed using single cell purity and index sorting.

Cell culture

All experiments performed in vitro were performed using Yssel's media: IMDM + Glutamax (ThermoFisher scientific), BSA 0.25% (w/v) (Sigma), 2-aminoethanol (1.8 µg/L) (Sigma), Apo-transferrin (40 µg/L) (Sigma), Insulin (5 µg/L) (Sigma), supplemented with 2% human AB serum (EFS), in wells pre-seeded the night before with ~2000 OP9 or OP9-DLL4 stromal cells²². The cytokines IL-2, IL-7 (Miltenyi Biotec), IL-1β and IL-23 (Peprotech) were added in the combinations indicated at 50 ng/ml for bulk culture and 10 ng/ml for single cell cloning. For bulk culture, 1000–3000 FACS sorted cells were plated onto stromal cells. For cloning, cells were directly sorted into the 96-well plates using index sorting. Media was changed every 2–3 days for bulk cultures and every 4–5 days for single cell cloning. Bulk cultures were analyzed after 5–7 days and cloning experiments after 13 days.

RORC inhibition

The specific RORC inhibitor SR2211³⁶ was purchased commercially (Tocris/Biotechne) and resuspended in DMSO at a stock of 100 mM. SR2211 was added at a final concentration of 10 µM in both bulk and single cell cultures; controls were treated with the equivalent concentration of DMSO (0.01%). SR2211 toxicity was tested on growing ILC cultures using a range of 5–100 µM; no effect was seen at 10 µM which was the dose previously reported³⁶. SR2211 and control DMSO were replenished every 2–3 days for bulk cultures and every 4–5 days for single cell cloning.

Intracellular staining and functional analysis

Analysis of ILC cytokine production was performed by intracellular staining after 3 h of pharmacological stimulation with PMA (10 ng/ml; Sigma), ionomycin (1 µg/ml; Sigma) and Golgi Plug (Brefeldin A; BD)²². Samples taken for transcription factor and phenotype analysis were taken directly for staining. Cells were stained for extracellular markers with Fc block and viability dye eFluor 506 (ThermoFisher Scientific) for 30 min at 4 °C in Brilliant Stain Buffer (BD). Fixation and permeabilization was performed using the FoxP3/Transcription Factor staining kit (ThermoFisher Scientific) as per the manufacturer's instructions. Cells were then stained for 30 min at room temperature for intracellular and intranuclear markers as indicated in Supplementary Table 9. Samples were acquired on an LSR Fortessa (BD) using BD FACS DIVA version 8 (BD) and analyzed using FlowJo (BD).

Antibodies

All antibodies used in this study are pre-conjugated and commercially available. A complete list of antibodies can be found in Supplementary Table 9.

Statistical and data analysis

Statistical analysis was performed using GraphPad Prism version 9.2.0 for Mac OS X, GraphPad Software, San Diego, California USA, www.graphpad.com. Unless otherwise detailed, all tests are two tailed; details of all multiple comparison tests including degrees of freedom, number of individuals per condition and either F or t statistics are included in Supplementary Tables 1, 2, 4–8. The details and assumptions of all tests are described in the relevant figure legends or in the referenced supplementary tables. The axes of all scatterplots were designed to include all data points. Analysis of flow cytometry data was performed using FlowJo (BD) software version 10.8.0 for MAC OS X <https://www.flowjo.com/>. Uniform manifold projection (UMAP) analyses³⁵ were performed using the FlowJo (BD) UMAP plugin version 3.1. Data are represented as mean with SD unless specified. Sample size and number of experiments denoted in figure legends.

Reporting summary

Further information on research design is available in the Nature Research Reporting Summary linked to this article.

Data availability

All data generated or analyzed during this study are available as Supplementary Data. Source data are provided with this paper.

References

1. Diefenbach, A. Innate lymphoid cells in the defense against infections. *Eur. J. Microbiol. Immunol. (Bp)*. **3**, 143 (2013).
2. Ducimetière, L., Vermeer, M. & Tugues, S. The interplay between innate lymphoid cells and the tumor microenvironment. *Front. Immunol.* **10**, 2895 (2019).
3. Jarade, A., Di Santo, J. P. & Serafini, N. Group 3 innate lymphoid cells mediate host defense against attaching and effacing pathogens. *Curr. Opin. Microbiol.* **63**, 83–91 (2021).
4. Vivier, E. et al. Innate lymphoid. *Cells.: 10 Years . Cell* **174**, 1054–1066 (2018).
5. Spits, H. et al. Innate lymphoid cells—a proposal for uniform nomenclature. *Nat. Rev. Immunol.* **13**, 145–149 (2013).
6. Freud, A. G., Mundy-Bosse, B. L., Yu, J. & Caligiuri, M. A. The Broad Spectrum of Human Natural Killer Cell Diversity. *Immunity* **47**, 820–833 (2017).
7. Bernink, J. et al. Human type 1 innate lymphoid cells accumulate in inflamed mucosal tissues. *Nat. Immunol.* **14**, 221–229 (2013).
8. Fuchs, A. et al. Intraepithelial type 1 innate lymphoid cells are a unique subset of il-12- and il-15-responsive ifn-γ-producing cells. *Immunity* **38**, 769–781 (2013).
9. Mjösberg, J. M. et al. Human IL-25- and IL-33-responsive type 2 innate lymphoid cells are defined by expression of CRTH2 and CD161. *Nat. Immunol.* **12**, 1055–1062 (2011).
10. Moro, K. et al. Innate production of TH2 cytokines by adipose tissue-associated c-Kit+Sca-1+ lymphoid cells. *Nature* **463**, 540–544 (2010).
11. Price, A. E. et al. Systemically dispersed innate IL-13-expressing cells in type 2 immunity. *Proc. Natl Acad. Sci. U. S. A.* **107**, 11489–11494 (2010).
12. Neill, D. R. et al. Nuocytes represent a new innate effector leukocyte that mediates type-2 immunity. *Nature* **464**, 1367–1370 (2010).
13. Satoh-Takayama, N. et al. Microbial Flora Drives Interleukin 22 Production in Intestinal NKp46+ Cells that Provide Innate Mucosal Immune Defense. *Immunity* **29**, 958–970 (2008).
14. Hoorweg, K. et al. Functional Differences between Human NKp44- and NKp44+ RORC+ Innate Lymphoid Cells. *Front. Immunol.* **0**, 72 (2012).
15. Eberl, G. et al. An essential function for the nuclear receptor RORγt in the generation of fetal lymphoid tissue inducer cells. *Nat. Immunol.* **5**, 64–73 (2004).
16. Mebius, R. E., Rennert, P. & Weissman, I. L. Developing Lymph Nodes Collect CD4+CD3- LTβ+ Cells That Can Differentiate to APC, NK Cells, and Follicular Cells but Not T or B Cells. *Immunity* **7**, 493–504 (1997).
17. Cherrier, D. E., Serafini, N. & Di Santo, J. P. Innate Lymphoid Cell Development: A T Cell Perspective. *Immunity* **48**, 1091–1103 (2018).
18. Juelke, K. & Romagnani, C. Differentiation of human innate lymphoid cells (ILCs). *Curr. Opin. Immunol.* **38**, 75–85 (2016).
19. Scoville, S. D. et al. A progenitor cell expressing transcription factor RORγt generates all human innate lymphoid cell subsets. *Immunity* **44**, 1140 (2016).
20. Montaldo, E. et al. Human RORγt+CD34+ cells are lineage-specified progenitors of group 3 RORγt+ innate lymphoid cells. *Immunity* **41**, 988–1000 (2014).
21. Chen, L. et al. CD56 expression marks human group 2 innate lymphoid cell divergence from a shared NK cell and group 3 innate lymphoid cell developmental pathway. *Immunity* **49**, 464 (2018).
22. Lim, A. I. et al. Systemic Human ILC Precursors Provide a Substrate for Tissue ILC Differentiation. *Cell* **168**, 1086–1100.e10 (2017).

23. Lim, A. I. & Di Santo, J. P. ILC-poiesis: Ensuring tissue ILC differentiation at the right place and time. *Eur. J. Immunol.* **49**, 11–18 (2019).
24. Mazzurana, L. et al. Tissue-specific transcriptional imprinting and heterogeneity in human innate lymphoid cells revealed by full-length single-cell RNA-sequencing. *Cell Res.* **31**, 554–568 (2021).
25. Tuzlak, S. et al. Repositioning TH cell polarization from single cytokines to complex help. *Nat. Immunol.* **22**, 1210–1217 (2021).
26. Ma, C. S. et al. Unique and shared signaling pathways cooperate to regulate the differentiation of human CD4⁺ T cells into distinct effector subsets. *J. Exp. Med.* **213**, 1589–1608 (2016).
27. Okada, S. et al. Impairment of immunity to *Candida* and *Mycobacterium* in humans with bi-allelic RORC mutations. *Sci. (80-.)* **349**, 606–613 (2015).
28. Martínez-Barricarte, R. et al. Human IFN-γ immunity to mycobacteria is governed by both IL-12 and IL-23. *Sci. Immunol.* **3**, eaau6759 (2018).
29. Kerner, G. et al. Inherited human IFN-γ deficiency underlies mycobacterial disease. *J. Clin. Invest.* **130**, 3158–3171 (2020).
30. Bustamante, J., Boisson-Dupuis, S., Abel, L. & Casanova, J.-L. Mendelian susceptibility to mycobacterial disease: genetic, immunological, and clinical features of inborn errors of IFN-γ immunity. *Semin. Immunol.* **26**, 454–470 (2014).
31. Lim, A. I. et al. IL-12 drives functional plasticity of human group 2 innate lymphoid cells. *J. Exp. Med.* **213**, 569–583 (2016).
32. Nagasawa, M. et al. KLRG1 and NKp46 discriminate subpopulations of human CD117⁺CRTH2⁺ ILCs biased toward ILC2 or ILC3. *J. Exp. Med.* **216**, 1762–1776 (2019).
33. Campana, S. et al. Circulating ILC precursors expressing CD62L exhibit a type 2 signature distinctly decreased in psoriatic patients. *Eur. J. Immunol.* **51**, 1792–1798 (2021).
34. Oppmann, B. et al. Novel p19 protein engages IL-12p40 to form a cytokine, IL-23, with biological activities similar as well as distinct from IL-12. *Immunity* **13**, 715–725 (2000).
35. McInnes, L., Healy, J. & Melville, J. UMAP: Uniform Manifold Approximation and Projection for Dimension Reduction. (2020).
36. Kumar, N. et al. Identification of SR2211: A potent synthetic RORγ-selective modulator. *ACS Chem. Biol.* **7**, 672–677 (2012).
37. Capone, A. & Volpe, E. Transcriptional Regulators of T Helper 17 Cell Differentiation in Health and Autoimmune Diseases. *Front. Immunol.* **11**, 348 (2020).
38. Ruan, Q. et al. The Th17 immune response is controlled by the Rel-RORγ-RORγT transcriptional axis. *J. Exp. Med.* **208**, 2321–2333 (2011).
39. Rosain, J. et al. Mendelian susceptibility to mycobacterial disease: 2014–2018 update. *Immunol. Cell Biol.* **97**, 360–367 (2019).
40. De Beaucoudrey, L. et al. Mutations in STAT3 and IL12RB1 impair the development of human IL-17-producing T cells. *J. Exp. Med.* **205**, 1543–1550 (2008).
41. Ivanov, I. I. et al. The Orphan Nuclear Receptor RORγt Directs the Differentiation Program of Proinflammatory IL-17⁺ T Helper. *Cells Cell* **126**, 1121–1133 (2006).
42. Ciofani, M. et al. A validated regulatory network for Th17 cell specification. *Cell* **151**, 289 (2012).
43. Withers, D. R. et al. Transient inhibition of ROR-γt therapeutically limits intestinal inflammation by reducing TH17 cells and preserving ILC3. *Nat. Med.* **22**, 319 (2016).
44. Li, S. et al. Aryl Hydrocarbon Receptor Signaling Cell Intrinsically Inhibits Intestinal Group 2 Innate Lymphoid Cell Function. *Immunity* **49**, 915–928.e5 (2018).
45. Li, J., Doty, A. & Glover, S. Aryl hydrocarbon receptor signaling involves in the human intestinal ILC3/ILC1 conversion in the inflamed terminal ileum of Crohn's disease patients. *Inflamm. Cell Signal.* **3**, e1404 (2016).
46. Parks, O. B., Pociask, D. A., Hodzic, Z., Kolls, J. K. & Good, M. Interleukin-22 Signaling in the Regulation of Intestinal Health and Disease. *Front. Cell Dev. Biol.* **0**, 85 (2016).
47. Cupedo, T. et al. Human fetal lymphoid tissue-inducer cells are interleukin 17-producing precursors to RORC⁺ CD127⁺ natural killer-like cells. *Nat. Immunol.* **10**, 66–74 (2009).
48. Tindemans, I., Peeters, M. J. W. & Hendriks, R. W. Notch signaling in T helper cell subsets: Instructor or unbiased amplifier? *Front. Immunol.* **8**, 419 (2017).
49. Eixarch, H. et al. Inhibition of delta-like ligand 4 decreases Th1/Th17 response in a mouse model of multiple sclerosis. *Neurosci. Lett.* **541**, 161–166 (2013).
50. Schaller, M. A. et al. Notch ligand Delta-like 4 regulates disease pathogenesis during respiratory viral infections by modulating Th2 cytokines. *J. Exp. Med.* **204**, 2925–2934 (2007).
51. Meyer zu Horste, G. et al. RBPJ Controls Development of Pathogenic Th17 Cells by Regulating IL-23 Receptor Expression. *Cell Rep.* **16**, 392–404 (2016).
52. Mukherjee, S., Schaller, M. A., Neupane, R., Kunkel, S. L. & Lukacs, N. W. Notch ligand Dll4 enhances T cell differentiation by promoting IL-17 production and RORγT expression. *J. Immunol.* **182**, 7381 (2009).
53. Meng, L. et al. The Notch Ligand DLL4 Defines a Capability of Human Dendritic Cells in Regulating Th1 and Th17 Differentiation. *J. Immunol.* **196**, 1070–1080 (2016).
54. Bailis, W. et al. Notch simultaneously orchestrates multiple helper T cell programs independently of cytokine signals. *Immunity* **39**, 148 (2013).
55. Nalin, A. P. et al. Notch Regulates Innate Lymphoid Cell Plasticity during Human NK Cell Development. *J. Immunol.* **205**, 2679–2693 (2020).
56. Golub, R. The Notch signaling pathway involvement in innate lymphoid cell biology. *Biomed. J.* **44**, 133–143 (2021).
57. Kyoizumi, S. et al. Fate Decision Between Group 3 Innate Lymphoid and Conventional NK Cell Lineages by Notch Signaling in Human Circulating Hematopoietic Progenitors. *J. Immunol.* **199**, 2777–2793 (2017).
58. Chea, S. et al. Notch signaling in group 3 innate lymphoid cells modulates their plasticity. *Sci. Signal.* **9**, ra45 (2016).
59. Wong, S. H. et al. Rora is essential for nuocyte development. *Nat. Immunol.* **13**, 229 (2012).
60. Simoni, Y. et al. Human Innate Lymphoid Cell Subsets Possess Tissue-Type Based Heterogeneity in Phenotype and Frequency. *Immunity* **46**, 148–161 (2017).
61. Sander, G. R. & Powell, B. C. Expression of Notch Receptors and Ligands in the Adult Gut. *J. Histochem. Cytochem.* **52**, 509–516 (2004).
62. Verrier, T. et al. Phenotypic and Functional Plasticity of Murine Intestinal NKp46⁺ Group 3 Innate Lymphoid Cells. *J. Immunol.* **196**, 4731–4738 (2016).
63. Neurath, M. F. IL-23 in inflammatory bowel diseases and colon cancer. *Cytokine Growth Factor Rev.* **45**, 1–8 (2019).
64. van de Vosse, E. et al. IL-12Rβ1 deficiency: Mutation update and description of the IL12RB1 variation database. *Hum. Mutat.* **34**, 1329–1339 (2013).
65. Gladiator, A., Wangler, N., Trautwein-Weidner, K. & LeibundGut-Landmann, S. Cutting Edge: IL-17-Secreting Innate Lymphoid Cells Are Essential for Host Defense against Fungal Infection. *J. Immunol.* **190**, 521–525 (2013).
66. De Beaucoudrey, L. et al. Revisiting human IL-12Rβ1 deficiency: A survey of 141 patients from 30 countries. *Medicine* **89**, 381–402 (2010).
67. Altare, F. et al. Impairment of mycobacterial immunity in human interleukin-12 receptor deficiency. *Science* **280**, 1432–1435 (1998).

Annex 2

CD116+ fetal precursors migrate to the perinatal lung and give rise to human alveolar macrophages

Elza Evren, Emma Ringqvist, Jean-Marc Doisne, Anna Thaller, Natalie Sleiers, Richard A. Flavell, James P. Di Santo, and Tim Willinger

Published in 2021

Journal of Experimental Medicine

ARTICLE

CD116⁺ fetal precursors migrate to the perinatal lung and give rise to human alveolar macrophages

Elza Evren¹, Emma Ringqvist¹, Jean-Marc Doisne^{2,3}, Anna Thaller^{2,3,4}, Natalie Sleiers¹, Richard A. Flavell^{5,6*}, James P. Di Santo^{2,3*}, and Tim Willinger¹

Despite their importance in lung health and disease, it remains unknown how human alveolar macrophages develop early in life. Here we define the ontogeny of human alveolar macrophages from embryonic progenitors *in vivo*, using a humanized mouse model expressing human cytokines (MISTRG mice). We identified alveolar macrophage progenitors in human fetal liver that expressed the GM-CSF receptor CD116 and the transcription factor MYB. Transplantation experiments in MISTRG mice established a precursor-product relationship between CD34⁻CD116⁺ fetal liver cells and human alveolar macrophages *in vivo*. Moreover, we discovered circulating CD116⁺CD64⁻CD115⁺ macrophage precursors that migrated from the liver to the lung. Similar precursors were present in human fetal lung and expressed the chemokine receptor CX3CR1. Fetal CD116⁺CD64⁻ macrophage precursors had a proliferative gene signature, outcompeted adult precursors in occupying the perinatal alveolar niche, and developed into functional alveolar macrophages. The discovery of the fetal alveolar macrophage progenitor advances our understanding of human macrophage origin and ontogeny.

Introduction

The lung is a vital organ that mediates the uptake of oxygen and is continuously exposed to inhaled microbes, particles, and allergens. Alveolar macrophages are the most abundant cell type in the airways and are essential for healthy lung function and barrier immunity (Evren et al., 2020; Garbi and Lambrecht, 2017; Hussell and Bell, 2014; Joshi et al., 2018; Kopf et al., 2015; Kulikauskaite and Wack, 2020; Puttur et al., 2019). They remove airborne microbes and cell debris from the airways through phagocytosis, which is essential to prevent harmful inflammation and to maintain the essential gas exchange. Another important function of alveolar macrophages is the catabolism of lung surfactant. Alveolar macrophages are critically dependent on the cytokine GM-CSF that is produced by alveolar epithelial cells (Dranoff et al., 1994; Gschwend et al., 2021; Guillems et al., 2013; Schneider et al., 2014). Lack of GM-CSF and therefore alveolar macrophages results in pulmonary alveolar proteinosis (PAP) in both mice and humans due to the defective clearance of surfactant (Trapnell et al., 2019).

The cellular origin of macrophages varies depending on developmental age, organ of residence, and tissue state (Blériot et al., 2020; Guillems and Svedberg, 2021; Guillems et al., 2020; Jenkins and Allen, 2021). Studies in mice have demonstrated that macrophages arise either from embryonic progenitors or from blood monocytes that are derived from adult

hematopoiesis (Epelman et al., 2014; Ginhoux and Guillems, 2016; Perdiguero and Geissmann, 2016; Varol et al., 2015). Mouse alveolar macrophages are mostly of fetal origin in steady-state (Gomez Perdiguero et al., 2015; Guillems et al., 2013; Hashimoto et al., 2013; Schneider et al., 2014; Yona et al., 2013; Yu et al., 2017) with increased contribution from blood monocytes during aging (Gomez Perdiguero et al., 2015; Liu et al., 2019), infection (Aegerter et al., 2020; Machiels et al., 2017; McCubbrey et al., 2018; Misharin et al., 2017; Mould et al., 2017; Mould et al., 2019), fibrosis (Aran et al., 2019; Joshi et al., 2020; McQuattie-Pimentel et al., 2021; Misharin et al., 2017), and lung regeneration (Lechner et al., 2017). Alveolar macrophages develop in humans after birth when the lungs are inflated by air uptake (Alenghat and Esterly, 1984; Bharat et al., 2016). Humans undergoing lung transplantation have an alveolar macrophage compartment that is of mixed origin, composed of both resident host macrophages and donor-derived macrophages originating from circulating monocytes (Bittmann et al., 2001; Byrne et al., 2020; Eguíluz-Gracia et al., 2016; Kjellström et al., 2000; Nayak et al., 2016). However, the ontogeny of human macrophages is poorly understood because invasive *in vivo* experiments are impossible in humans.

To overcome this limitation, we previously developed a humanized mouse model, named MISTRG, which expresses critical

¹Center for Infectious Medicine, Department of Medicine Huddinge, Karolinska Institutet, Karolinska University Hospital, Stockholm, Sweden; ²Innate Immunity Unit, Institut Pasteur, Paris, France; ³Institut national de la santé et de la recherche médicale U1223, Paris, France; ⁴Université de Paris, Sorbonne Paris Cité, Paris, France; ⁵Department of Immunobiology, Yale University School of Medicine, New Haven, CT; ⁶Howard Hughes Medical Institute, Chevy Chase, MD.

*R.A. Flavell and J.P. Di Santo contributed equally to this paper; Correspondence to Tim Willinger: tim.willinger@ki.se.

© 2021 Evren et al. This article is available under a Creative Commons License (Attribution 4.0 International, as described at <https://creativecommons.org/licenses/by/4.0/>).

human factors for macrophages, such as GM-CSF and macrophage-CSF (M-CSF), through gene knock-in (Rongvaux et al., 2013; Rongvaux et al., 2014; Willinger et al., 2011a; Willinger et al., 2011b). MISTRG mice support human macrophage reconstitution after transplantation with human CD34⁺ hematopoietic stem and progenitor cells (HSPCs; Evren et al., 2021; Rongvaux et al., 2014; Saito et al., 2016; Sippel et al., 2019). This model therefore provides the opportunity to study the ontogeny of human macrophages in vivo (Alisjahbana et al., 2020; Evren et al., 2020).

We recently used MISTRG mice to dissect the development of human lung macrophages that are derived from blood monocytes (Evren et al., 2021). Specifically, we discovered that classical CD14⁺ blood monocytes derived from CD34⁺ HSPCs are the adult precursors of human alveolar macrophages. Blood monocyte-derived macrophages are most relevant in context of lung injury and inflammation. In early life and under physiological conditions, human alveolar macrophages are likely mostly of embryonic origin, i.e., independent of blood monocytes. We therefore now aimed to identify the fetal progenitor of human alveolar macrophages. We also examined the importance of cell origin on human lung macrophage specification by comparing the transcriptional signatures of human lung macrophages of fetal versus adult origin, as well as their ability to populate the perinatal niche, to self-renew, and to catabolize lung surfactant. We discovered that cell origin has an impact on alveolar niche occupation by macrophage precursors and on the functional identity of human lung macrophages. Specifically, we found that fetal macrophage precursors had a greater capacity to occupy the perinatal alveolar niche, whereas adult precursors generated IFN-responsive macrophages that are expanded in inflammatory lung diseases in humans, such as in severe coronavirus disease 2019 (COVID-19).

Results

Candidate progenitors of human lung macrophages are present in fetal liver

Due to the critical role of GM-CSF, we predicted that expression of GM-CSF receptor marks alveolar macrophage progenitors in human fetal tissue. Among fetal tissues, the liver is a hematopoietic organ (Cao et al., 2020; Park et al., 2020; Popescu et al., 2019) around the time of birth, when alveolar macrophages develop in mice (Guilliams et al., 2013; Yu et al., 2017). We therefore examined the presence of candidate precursors of alveolar macrophages in human fetal liver at the second trimester of gestation, the time of lung macrophage development in the human fetus (Dame et al., 1999). Consistent with our prediction, we identified CD45⁺CD34⁻ myeloid cells in fetal liver tissue that expressed the α -chain of the GM-CSF receptor (CD116) but did not express lineage (Lin) markers for T cells (CD3, TCR $\alpha\beta$, TCR $\gamma\delta$), B cells (CD19, CD20), natural killer cells (CD56, CD94, NKp46), and granulocytes (CD66abce; Fig. 1 A and Fig. S1). CD116⁺ myeloid cells consisted of CD64⁺ cells, containing fetal dendritic cells (CD88⁻CD1c/CD141^{hi}CD11c⁺HLA-DR^{hi}), monocytes (CD88⁺CD1c/CD141^{lo/mid}CD11b⁺HLA-DR⁺CD206⁻CD169⁻CD14⁺), and

macrophages (CD88⁺CD1c/CD141^{lo/mid}CD11b⁺HLA-DR⁺CD206⁺CD169⁺; Fig. 1 B), as well as of CD64⁻ cells comprising dendritic cells and putative precursor-like cells (CD88⁻CD1c/CD141⁻CD11c⁻HLA-DR^{mid}; Fig. 1, C and D). In summary, these data identify GM-CSF receptor-expressing candidate precursors of human lung macrophages in the fetal liver.

CD116⁺CD64⁻ fetal precursor-like cells express MYB and have a proliferative gene signature

To gain further insights into their distinctive features, we determined the gene expression profiles of fetal candidate progenitors of human alveolar macrophages by microarray (Fig. 2, A and B). For this purpose, potential fetal precursors of human alveolar macrophages among CD45⁺CD34⁻Lin⁻CD116⁺ cells were isolated from fetal liver. Specifically, we purified CD64⁺CD88⁺CD1c/CD141^{lo-mid}CD206⁻CD169⁻ fetal monocytes, described as precursors of mouse alveolar macrophages (Guilliams et al., 2013; Schneider et al., 2014; Yu et al., 2017), and precursor-like fetal cells that lacked expression of monocyte (CD14, CD64) and dendritic cell markers (CD1c, CD141). We then compared their gene expression profiles to that of CD14⁺CD16⁻ blood monocytes, adult precursors of human alveolar macrophages (Evren et al., 2021). Consistent with their cellular identity, CD14⁺CD16⁻ blood monocytes highly expressed monocytic genes, such as *CD14*, *FCGR1A* (encoding CD64), *ITGAM* (encoding CD11b), *C5AR1* (encoding CD88), *VCAN*, *CSF3R*, and *LYZ*, but these genes were also detected in fetal CD116⁺CD64⁻ precursor-like cells (Fig. 2 C and Table S1). In contrast, fetal CD116⁺CD64⁻ precursor-like cells had higher mRNA expression of the transcription factor *MYB* (Fig. 2 C and Table S1) that is expressed in HSPCs and myeloid progenitors (Bian et al., 2020). In addition, fetal CD116⁺CD64⁻ precursor-like cells expressed less *MAFB* (Fig. 2 C and Table S1), a transcription factor that antagonizes *MYB* and represses macrophage self-renewal (Aziz et al., 2009; Li et al., 2020; Soucie et al., 2016). Furthermore, fetal CD116⁺CD64⁻ precursor-like cells expressed genes and transcription factors (*GATA1*, *KLF1*, *TAL1*) associated with erythrocyte differentiation (Popescu et al., 2019), consistent with preferential erythroid-myeloid hematopoiesis in human fetal liver (Jardine et al., 2021). Therefore, fetal CD116⁺CD64⁻ precursor-like cells resembled *Myb*-expressing erythro-myeloid progenitors (EMPs) and EMP-derived CD64⁻ myeloid progenitors that further differentiate into CD64⁺ fetal monocytes and alveolar macrophages in mice (Gomez Perdiguero et al., 2015; Hoeffel et al., 2015; Li et al., 2020; Mass et al., 2016). Moreover, fetal CD116⁺CD64⁻ precursor-like cells preferentially expressed *MYC* and other genes promoting cell division and proliferation, such as *MKI67*, *TOP2A*, *PCNA*, cyclins, and cyclin-dependent kinases (Fig. 2 C and Table S1), similar to what has been reported for human fetal liver progenitors (Popescu et al., 2019). Global analysis confirmed that genes related to cell cycle and cell division were overrepresented in fetal CD116⁺CD64⁻ cells when compared with both adult and fetal monocytes (Fig. 2 D). These findings indicate that fetal CD116⁺CD64⁻ precursor-like cells have high proliferative capacity and resemble fetal progenitors of mouse alveolar macrophages.

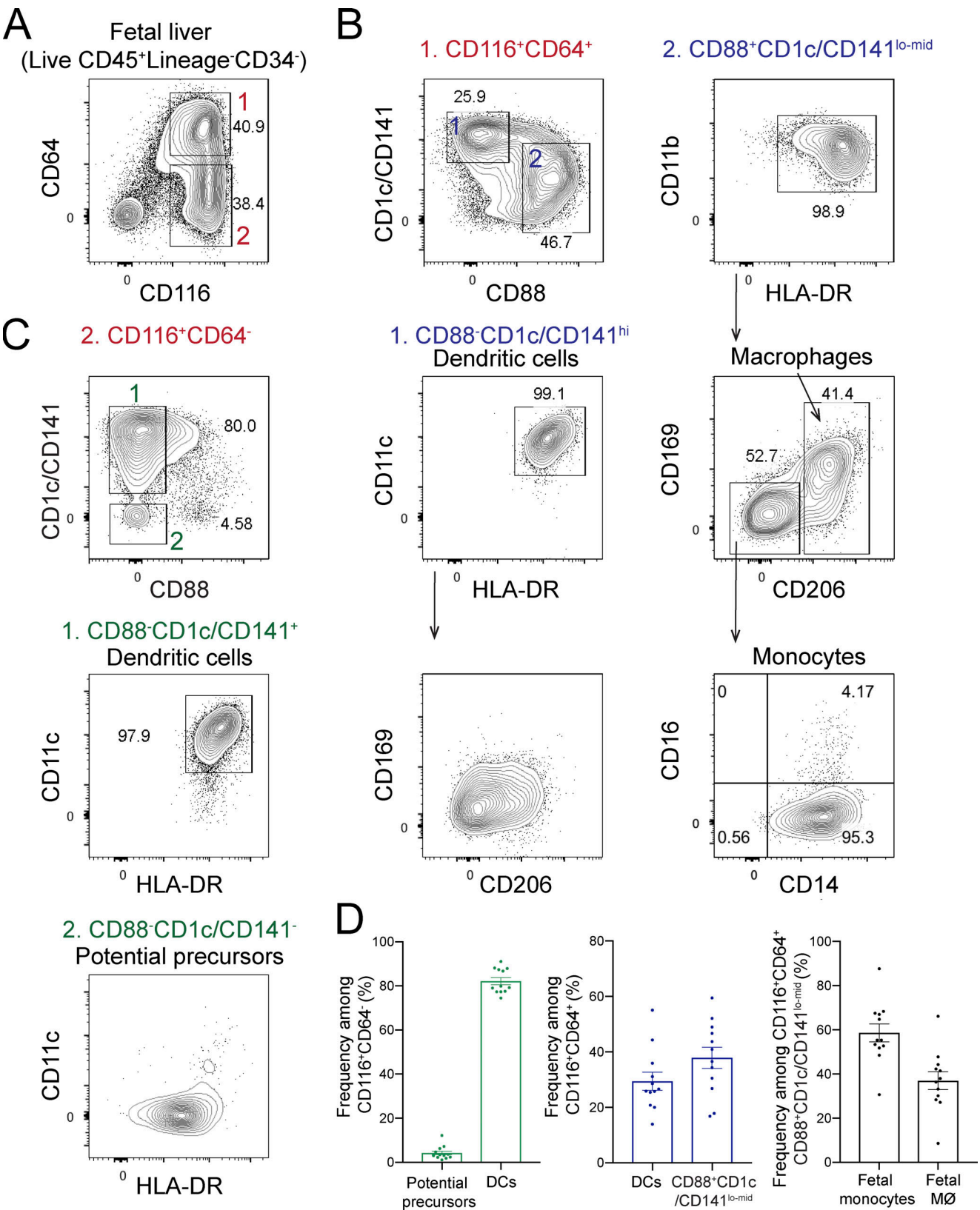


Figure 1. **Candidate alveolar macrophage progenitors are present in human fetal liver.** (A) Flow cytometry analysis of CD116-expressing cells within the CD34⁻ fraction of human fetal liver (17 wk of gestation). See Fig. S1 for gating strategy. After excluding cells expressing Lin markers (CD3, TCRαβ, TCRγδ, CD19, CD20, CD56, CD94, Nkp46, and CD66abce), CD45⁺CD116⁺ cells were divided into CD64⁺ (population 1) and CD64⁻ (population 2) subsets. (B) Flow cytometry of CD116⁺CD64⁺ cells as gated in A. CD116⁺CD64⁺ cells were separated into CD88⁻CD1c/CD141^{hi} (population 1) and CD88⁺CD1c/CD141^{lo-mid} (population 2) subsets, corresponding to dendritic cells (CD11c⁺HLA-DR^{hi}) and monocytes (CD11b⁺HLA-DR⁺CD206⁻CD169⁻) as well as macrophages (CD11b⁺HLA-

DR⁺CD206⁺CD169^{mid-hi}), respectively. **(C)** Flow cytometry of CD116⁺CD64⁻ cells as gated in A. Population 1 (CD88⁻CD1c/CD141⁺) contained CD11c⁺HLA-DR^{hi} dendritic cells. Population 2 (CD88⁻CD1c/CD141⁻) consisted of CD11c⁻HLA-DR^{mid} potential precursors. **(D)** Frequencies of the indicated populations in human fetal liver. DCs, dendritic cells; hi, high; lo-mid, low-mid; MØ, macrophages. Data are represented as mean ± SEM. Data (A–C) show one fetal liver sample (17 wk of gestation) representative of 12 samples from two independent experiments. Data (D) are pooled from two independent experiments with 12 fetal liver samples at 15–23 wk of gestation.

CD116-expressing fetal liver cells have human alveolar macrophage potential in vivo

Having identified candidate progenitor populations, we tested their ability to differentiate into lung macrophages in vivo. For this purpose, we performed transplantation experiments to establish precursor-product relationships. MISTRG mice are well-suited for this approach since (1) the empty alveolar niche (lack of mouse GM-CSF and therefore mouse alveolar macrophages) allows transplanted progenitors to colonize the niche; and (2) the expression of human GM-CSF in the alveolar space supports the differentiation into mature human alveolar macrophages (Evren et al., 2021; Rongvaux et al., 2014; Willinger et al., 2011b). We transplanted fetal liver populations into the airways of newborn MISTRG recipient mice, as the first week of life is the physiological time when the alveolar niche becomes colonized in mice (Guilliams et al., 2013). We first assessed the ability of fetal CD34⁻Lin⁻CD116⁺ candidate progenitors compared with that of CD34⁻Lin⁻CD116⁻ and CD34⁻Lin⁺CD116⁺ cells to reconstitute the alveolar niche after intranasal transplantation (Fig. 3 A). Transplanted CD34⁻Lin⁻CD116⁺ fetal liver cells colonized the lung and differentiated into human macrophages with an alveolar macrophage phenotype (CD11b⁺HLA-DR⁺CD206⁺CD169⁺; Bharat et al., 2016; Desch et al., 2016; Yu et al., 2016) within 10 wk of transfer and were retained at 24 wk, whereas neither CD34⁻Lin⁻CD116⁻ nor CD34⁻Lin⁺CD116⁻ cells were able to do so (Fig. 3, B–D; and Fig. S2 A). Human CD68⁺ macrophages derived from CD34⁻Lin⁻CD116⁺ cells could be visualized in the alveoli by immunohistochemistry, confirming their correct physiological localization (Fig. 3 E and Fig. S3 A).

We also examined whether human interstitial lung macrophages were present in MISTRG mice transplanted with fetal CD34⁻Lin⁻CD116⁺ cells, using a recently described gating strategy for human interstitial macrophages (Chakarov et al., 2019). Flow cytometry showed that the lungs of MISTRG mice transplanted with fetal CD34⁻Lin⁻CD116⁺ cells did not harbor any cells with a surface phenotype (CD11b⁺CD64⁺CD14⁺CD16⁻CD206⁺CD169⁺HLA-DR^{hi}) that is characteristic of human interstitial macrophages (Fig. S4 A). In contrast, human interstitial lung macrophages developed in MISTRG mice transplanted with human CD34⁺ HSPCs (Fig. S4 B) as we reported previously (Evren et al., 2021). These data suggest that the developmental potential of CD116⁺ fetal precursors in the lung may be restricted to becoming alveolar macrophages.

To test the function of fetal progenitor-derived macrophages, we determined their capacity to prevent PAP. We previously showed that nontransplanted MISTRG mice lack mouse alveolar macrophages and develop PAP at ~4 wk of age, which can be prevented by the transplantation with human CD34⁺ HSPCs (Evren et al., 2021; Willinger et al., 2011b). MISTRG mice transplanted with fetal CD34⁻Lin⁻CD116⁺ cells had lower amounts of protein in bronchoalveolar lavage (BAL) fluid than

nontransplanted MISTRG mice and mice transplanted with CD34⁻Lin⁻CD116⁻ or CD34⁻Lin⁺CD116⁻ cells, indicating PAP rescue (Fig. 3 F). Therefore, human alveolar macrophages arising from fetal CD34⁻Lin⁻CD116⁺ cells were functional since they were able to catabolize lung surfactant. Combined, these results establish a precursor-product relationship between fetal CD34⁻Lin⁻CD116⁺ cells and human alveolar macrophages.

Fetal CD116⁺ alveolar macrophage progenitors are able to migrate from the liver to the lung

We next predicted that fetal CD34⁻Lin⁻CD116⁺ lung macrophage progenitors traffic from the liver to the lung. Therefore, instead of transplanting fetal liver progenitors into the airways, we injected them into newborn MISTRG mice via the intrahepatic route to track their migration from the liver to the lung (Fig. 4 A). Consistent with our prediction, flow cytometry showed that alveolar macrophages (CD11b⁺HLA-DR⁺CD206⁺CD169⁺CD163⁺) populated the lungs of MISTRG mice 7 wk after intrahepatic injection of fetal CD34⁻Lin⁻CD116⁺ cells and had abundant M-CSF receptor (CD115) surface expression (Fig. 4 B and Fig. S2 A). This observation suggested that fetal macrophage precursors are highly responsive to M-CSF, the major factor driving macrophage proliferation. Fetal progenitor-derived human alveolar macrophages had expanded in MISTRG mice when analyzed at 24 wk after transplantation (Fig. 4, C and D). Immunohistochemistry confirmed the presence of human CD68⁺ macrophages in the lungs of MISTRG mice (Fig. 4 E and Fig. S3 B). Finally, intrahepatic transplantation with fetal CD34⁻Lin⁻CD116⁺ cells alleviated PAP, as shown by lower amounts of BAL protein, similar to mice transplanted with CD34⁺ HSPCs (Fig. 4 F). To further characterize circulating lung macrophage progenitors, we examined the blood of MISTRG mice after transplantation with CD116⁺ fetal liver cells (Fig. 4 G and Fig. S2 B). The blood of MISTRG mice transplanted with fetal CD34⁻Lin⁻CD116⁺ cells contained CD116⁺CD64⁻ cells expressing CD115, but not CD14 (Fig. 4 G), identifying them as potential circulating alveolar macrophage precursors derived from the transplanted fetal CD34⁻Lin⁻CD116⁺ cells. Furthermore, this finding revealed that these potential CD116⁺CD64⁻ fetal alveolar macrophage precursors in the circulation were distinct from HSPC-derived CD14⁺CD116⁺ blood monocytes, which are adult precursors of human alveolar macrophages, as we showed recently (Evren et al., 2021). Taken together, we demonstrate that macrophage progenitors in the fetal liver enter the circulation and migrate from the blood into the lung, where they develop into human alveolar macrophages.

CD116⁺CD64⁻ fetal liver cells generate mature human alveolar macrophages in vivo

Having shown that alveolar macrophage progenitor activity is present within CD34⁻Lin⁻CD116⁺ fetal liver cells and that they

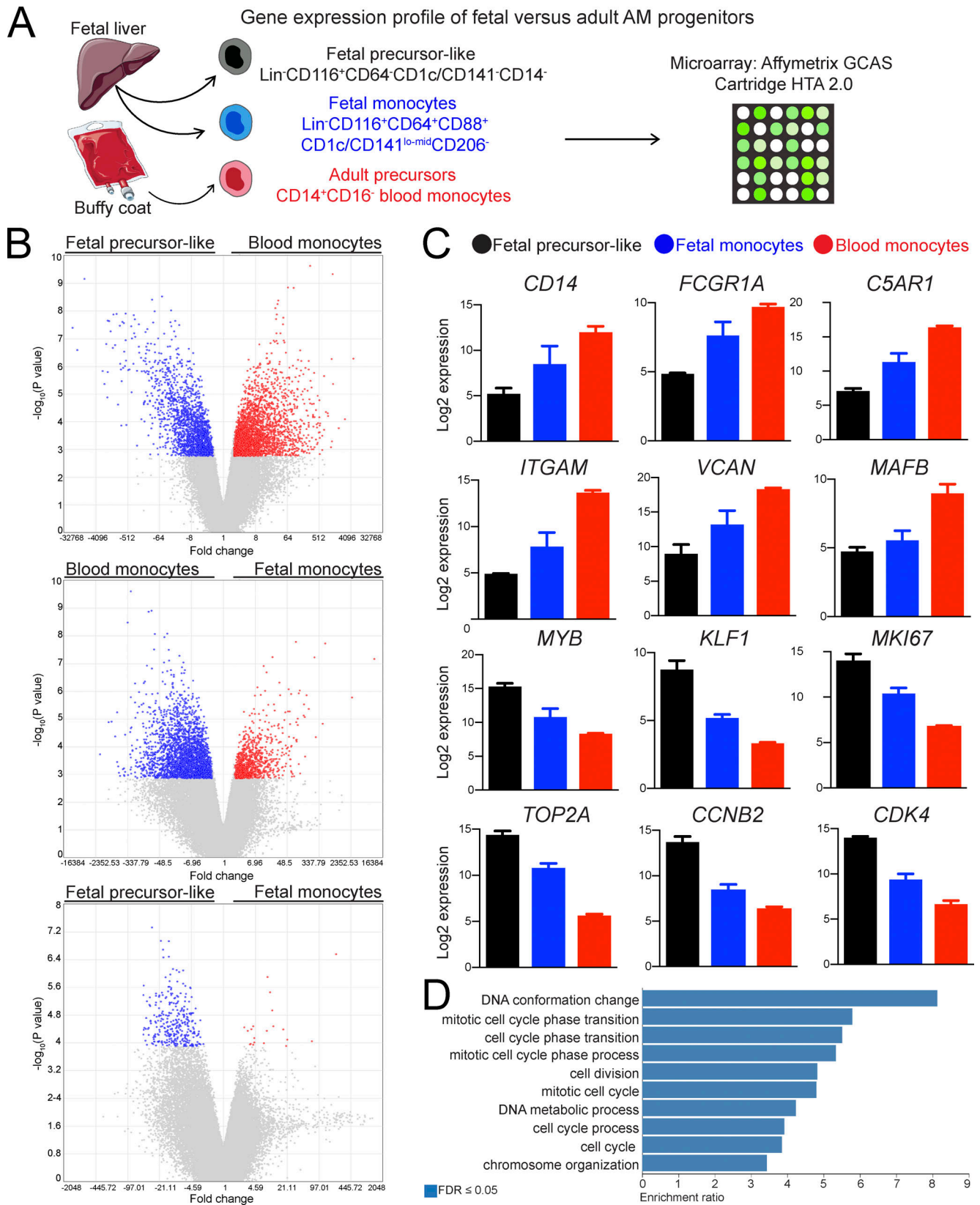


Figure 2. **Gene signatures of CD116⁺CD64⁻ fetal precursor-like cells, CD116⁺CD64⁺ fetal monocytes, and adult CD14⁺CD16⁻ blood monocytes.** (A) Experimental outline to define the gene expression profiles of the indicated human cell populations. Cartoon was adapted from Servier Medical Art. (B) Volcano plots of differentially expressed genes (DEGs) between the indicated cell populations. Fold change is plotted versus $-\log_{10}$ P value (not corrected for multiple testing). DEGs with a fold change ≥ 2 and an FDR-corrected P value ≤ 0.05 are highlighted in blue and red. (C) Bar graphs showing expression of selected genes in CD116⁺CD64⁻ fetal precursor-like cells, CD116⁺CD64⁺ fetal monocytes, and adult CD14⁺CD16⁻ blood monocytes. Data are represented as mean \pm SEM.

(D) Gene ontology over-representation analysis of DEGs up-regulated in CD116⁺CD64⁻ fetal precursor-like cells compared with adult CD14⁺CD16⁻ blood monocytes and CD116⁺CD64⁺ fetal monocytes. AM, alveolar macrophages; GCAS, GeneChip Array Station; HTA, Human Transcriptome Array; lo-mid, low-mid. Data (B–D) are from a single microarray experiment with three replicates per cell population (isolated from individual fetal liver or blood samples) obtained from four independent cell sorting experiments.

generate putative circulating CD116⁺CD64⁻ precursors (Fig. 4 G), we further fractionated the progenitor activity of CD34⁻Lin⁻CD116⁺ fetal liver cells. Specifically, we compared the macrophage potential of CD116⁺CD64⁻ to that of CD116⁺CD64⁺ fetal liver cells after intrahepatic injection into newborn MISTRG mice (Fig. 5 A). Both populations gave rise to human CD68⁺ lung macrophages (Fig. 5 B) with an alveolar macrophage phenotype (CD11b⁺HLA-DR⁺CD206⁺CD169⁺CD64⁺) with similar efficiency (Fig. 5, C and D). Further analysis revealed that CD116⁺CD64⁻ fetal progenitors more efficiently generated CD11b^{hi}CD163^{hi} macrophages, representing mature alveolar macrophages (Bharat et al., 2016) than CD116⁺CD64⁺ fetal progenitors (Fig. 5 C). Consistent with this observation, human macrophages derived from CD116⁺CD64⁻ fetal liver cells had the capacity to catabolize lung surfactant, a key function of alveolar macrophages, and to rescue PAP syndrome in MISTRG mice (Fig. 5 E). In contrast, macrophages arising from CD116⁺CD64⁺ fetal liver cells were unable to prevent PAP (Fig. 5 E).

Analysis of blood demonstrated the presence of circulating CD116⁺CD64⁻CD14⁻CD115⁺HLA-DR^{mid} human cells in MISTRG mice after transplantation with CD116⁺CD64⁺ or CD116⁺CD64⁻ fetal liver cells (Fig. 6 A). CD116⁺CD64⁻CD14⁻ cells found in the blood of MISTRG mice had the same surface phenotype as CD116⁺CD64⁻ fetal liver cells that give rise to human alveolar macrophages after transplantation into MISTRG mice. Therefore, their phenotypic similarity indicated that CD116⁺CD64⁻CD14⁻CD115⁺HLA-DR^{mid} cells in the blood likely corresponded to circulating alveolar macrophage precursors in transit from the liver to the lung. To further corroborate this notion, we performed bead-based fate-mapping of circulating human hematopoietic cells in MISTRG mice transplanted with CD116⁺ fetal liver cells (Fig. 6 B) as in our recent study (Evren et al., 2021). 1 wk after the i.v. injection of fluorescent beads, we could detect CD11b⁺HLA-DR⁺ cells in the lung of MISTRG mice, derived from circulating CD116⁺CD64⁻CD14⁻ cells that had captured the beads and migrated into the lung tissue, as bead⁺ cells were not present in the blood anymore after 1 wk (Fig. 6 C). The bead⁺ cells in the lung therefore likely represented developing alveolar macrophages (Evren et al., 2021). Taken together, we conclude that CD64⁻ fetal liver cells expressing CD116 are likely the main progenitor of mature human alveolar macrophages.

Finally, having identified potential circulating CD116⁺CD64⁻CD14⁻CD115⁺HLA-DR^{mid} alveolar macrophage precursors in MISTRG mice, we hypothesized that corresponding precursors are present in human fetal liver and lung. Consistent with our hypothesis, we found a population of CD116⁺CD64⁻CD14⁻HLA-DR^{mid} cells expressing CD115 as well as the chemokine receptor CX3CR1 in both fetal liver and fetal lung at 15–23 wk of gestation (Fig. 7, A and B; and Fig. S5). These data support the notion that human fetal liver progenitors populate the lung with CD116⁺CD64⁻CD115⁺CX3CR1⁺ alveolar macrophage precursors during the second gestational trimester.

Human alveolar macrophages derived from fetal and adult precursors have a similar turnover

Identifying both the fetal and adult progenitor in this study and in our previous work (Evren et al., 2021) gave us the opportunity to determine the impact of cellular origin on human alveolar macrophage function. Our results above demonstrated that lung macrophages derived from CD34⁻CD116⁺ fetal precursors and from adult precursors (CD34⁺ HSPCs developing into blood monocytes) had a similar capacity to prevent PAP development in MISTRG mice (Fig. 4 F and Fig. 5 E). Next, we compared the turnover of fetal progenitor-derived alveolar macrophages to that of alveolar macrophages of adult origin. For this purpose, we performed pulse-chase experiments with BrdU in MISTRG mice transplanted with either fetal CD34⁻Lin⁻CD116⁺ alveolar macrophage precursors or CD34⁺ HSPCs (Fig. 8 A). BrdU was administered continuously in the drinking water for 10 d to pulse-label alveolar macrophages and BrdU incorporation determined by flow cytometry. We observed a similar labeling frequency (~20%) of fetal- and adult-derived human alveolar macrophages at the end of the pulse period (Fig. 8, B and C). This showed that a fraction of human alveolar macrophages in MISTRG mice is actively proliferating in situ, similar to what has been reported for mouse alveolar macrophages (Guilliams et al., 2013). After the chase period of 4 wk, the BrdU label was diluted in both fetal- and adult-derived human alveolar macrophages (Fig. 8, B and C), likely through ongoing cell division. These data suggest that, irrespective of their fetal or adult origin, human macrophages reconstituting the alveolar niche in MISTRG mice are maintained by homeostatic proliferation.

Fetal macrophage precursors outcompete adult monocytes in occupying the perinatal alveolar niche in MISTRG mice

To assess the contribution of precursor origin to the human alveolar macrophage compartment, we performed competitive adoptive transfer experiments with alveolar macrophage precursors (Fig. 9 A). For this purpose, we administered human macrophage precursors into the airways of newborn MISTRG mice, i.e., adult precursors (CD14⁺CD16⁻ monocytes isolated from blood) mixed 1:1 with fetal precursors (CD34⁻Lin⁻CD116⁺CD64⁻CD14⁻ cells purified from fetal liver). We chose the first week of life for these experiments because it is the physiological time when niche colonization by alveolar macrophages occurs in both mice (Guilliams et al., 2013) and humans (Alenghat and Esterly, 1984; Bharat et al., 2016). We then used genetic differences in HLA alleles to distinguish fetal- from adult-derived alveolar macrophages (Fig. 9, B and C). Flow cytometry with HLA allele-specific antibodies demonstrated that fetal precursors outcompeted adult precursors of human alveolar macrophages in terms of their capacity to occupy the alveolar niche in MISTRG mice (Fig. 9, C and D). The preferential expansion of fetal CD116⁺CD64⁻ precursors is consistent with

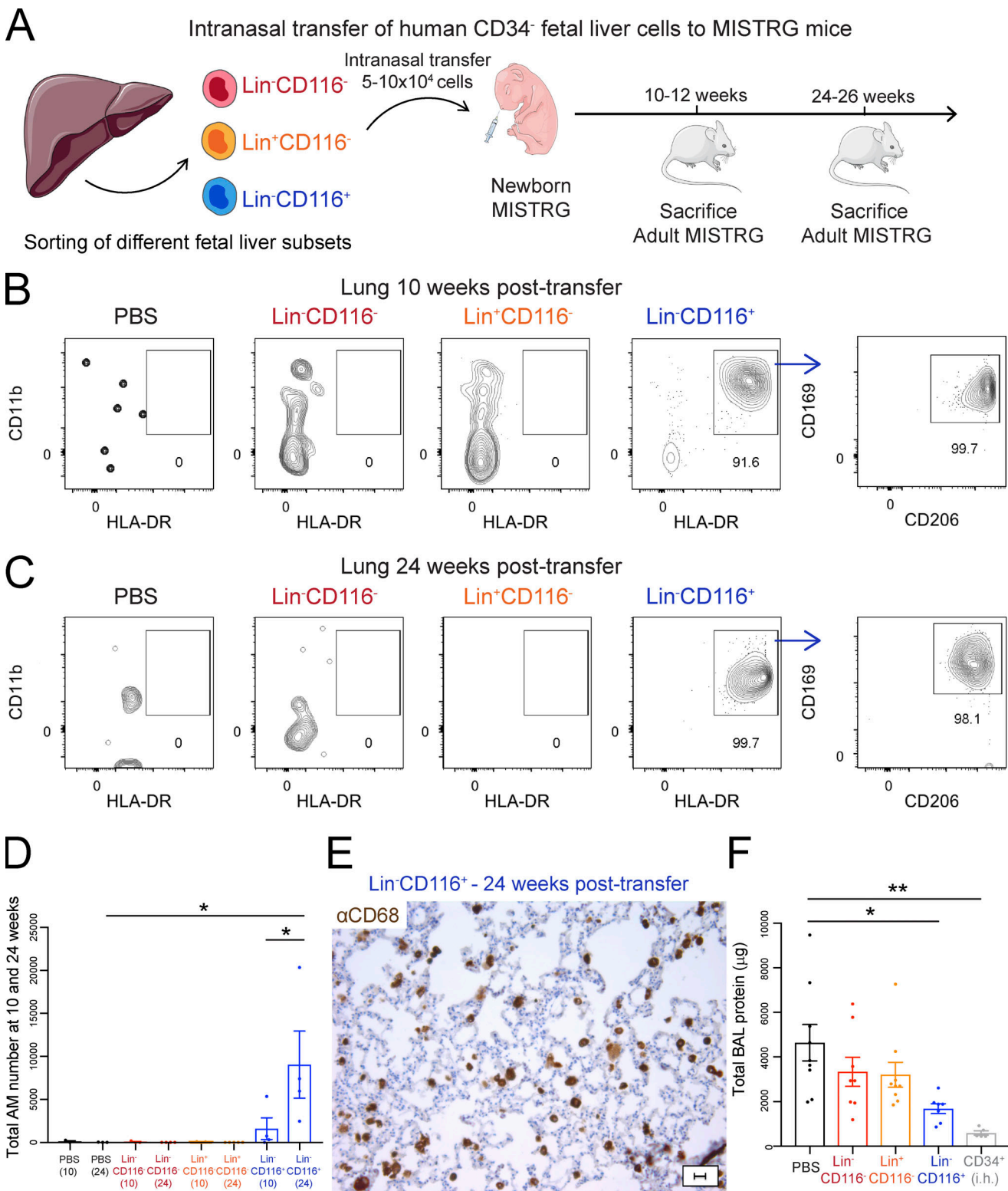


Figure 3. CD116-expressing fetal liver cells generate human alveolar macrophages in vivo. (A) Intranasal transfer of purified human Lin⁻CD116⁻, Lin⁺CD116⁻, and Lin⁻CD116⁺ populations from CD34⁺ fetal liver cells into newborn MISTRG mice. Lin markers were CD3, CD19, CD56, NKp46, and CD66abce. Control mice received PBS only. Cartoon was adapted from Servier Medical Art. (B and C) Flow cytometry of human CD45⁺CD11b⁺HLA-DR⁺CD206⁺CD169⁺ macrophages in lung tissue of MISTRG mice at 10 wk (B) and 24 wk (C) after transfer of the different fetal liver cell subsets. See Fig. S2 A for gating strategy. (D) Number of human alveolar macrophages (AM) in MISTRG mice at 10 and 24 wk after transplantation. (E) Immunohistochemistry of lung sections from MISTRG mice 24 wk after transplantation with human Lin⁻CD116⁺ fetal liver cells. Lung sections were stained with anti-human CD68 antibody (brown). Scale bar is 20 µm. (F) Amounts of total protein in the BAL fluid of MISTRG mice 24 wk after transplantation with human fetal liver cells. Control mice received PBS only or were transplanted with human CD34⁺ HSPCs from cord blood by intrahepatic injection (i.h.). αCD68, anti-CD68. Data are represented as mean ± SEM.

*, $P < 0.05$; **, $P < 0.01$ (one-way ANOVA with Tukey's multiple comparison post hoc test). Data (B and C) show one lung sample representative of three to five samples (individual mice) per group and time point from three independent experiments. Data (E) show one lung sample representative of four samples (individual mice) from three independent experiments. Data (D and F) are pooled from three independent experiments with $n = 3-5$ per group and time point (D) or $n = 5-9$ per group (F).

their greater expression of cell cycle genes (Fig. 2, C and D; and Table S1). These results are in line with mouse studies showing that fetal precursors of mouse alveolar macrophages have a greater expansion capacity than adult precursors due to their high intrinsic proliferative potential and metabolic activity (Li et al., 2020; van de Laar et al., 2016). We conclude that human alveolar macrophages of both fetal and adult origin can occupy the alveolar niche in MISTRG mice, have a similar turnover, and are able to clear lung surfactant. However, fetal-derived macrophages have a superior capacity to reconstitute the alveolar compartment in early life.

Gene signatures of human alveolar macrophages derived from fetal versus adult precursors

We compared the transcriptomes of fetal- versus adult-derived human lung macrophages to gain insights into potential functional differences. For this purpose, newborn MISTRG mice were transplanted by intrahepatic injection with CD34⁺ HSPCs or with CD34⁺ Lin⁻CD116⁺ fetal liver cells that were either CD64⁻ or CD64⁺. 3 mo after transplantation, human alveolar macrophages (CD45⁺CD11b⁺HLA-DR⁺CD206⁺CD169⁺) of different origin were isolated from the lung of MISTRG mice and their gene signatures determined by gene expression profiling (Fig. 10A). The human macrophage populations in MISTRG mice resembled resident macrophages found in the airways of healthy humans (Leach et al., 2020; Morse et al., 2019; Mould et al., 2021; Vieira Braga et al., 2019) as shown by the expression of typical signature genes, such as *MRC1* (encoding CD206), *MARCO*, *FABP4*, *PPARG*, *INHBA*, and *GPNMB* (Table S2). Overall, relatively few genes were differentially expressed between alveolar macrophages of adult origin (HSPC-derived) and alveolar macrophages of fetal origin (derived from either CD64⁻ or CD64⁺CD116⁺ fetal cells; Fig. 10 B and Table S2). This suggests that their gene signatures were largely shaped by cues from the lung environment, consistent with what has been reported for mouse alveolar macrophages (Gibbins et al., 2015; Lavin et al., 2014; van de Laar et al., 2016).

Lung macrophages derived from CD116⁺CD64⁻ and CD116⁺CD64⁺ fetal precursors had very similar transcriptomes with no statistically significant differences in gene expression (Fig. 10 B and Table S2). We therefore focused on comparing human lung macrophages derived from adult precursors with macrophages derived from fetal precursors. Among genes significantly up-regulated in lung macrophages of fetal origin were the chemokines *CXCL5* and *PPBP* (encoding *CXCL7*; Fig. 10 B and Table S2). Genes with higher expression in lung macrophages of adult origin included the T cell-attracting chemokines *CXCL9* and *CXCL10* as well as IFN-induced genes (*APOBEC3s*, *ISG20*, *IFI44L*, *GBP5*) and the transcription factor *STAT1* (Fig. 10, B and C; and Table S2). This gene signature resembled that of IFN-responsive *CXCL10*-macrophages that we identified previously

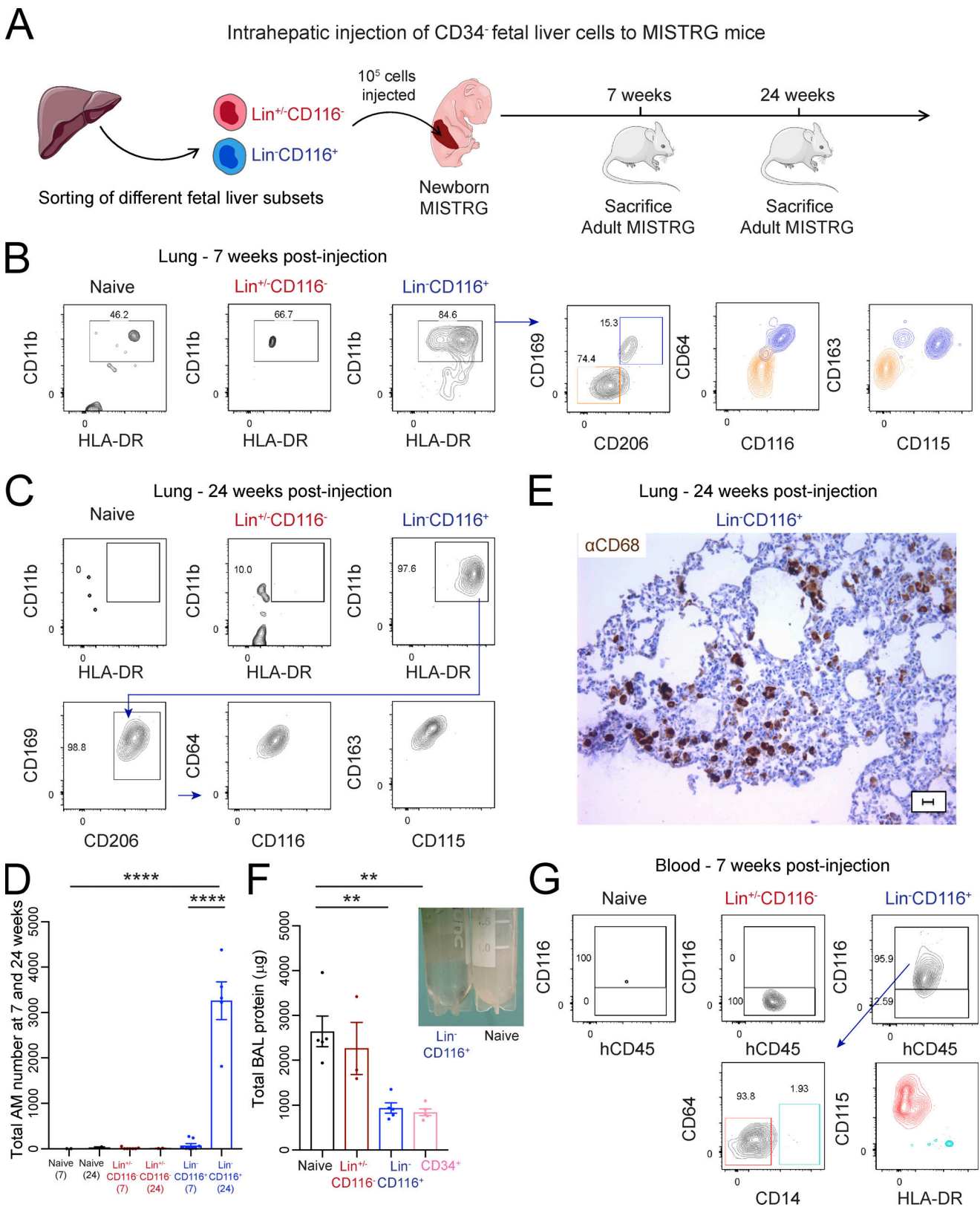
by single-cell RNA-sequencing in the lung of HSPC-engrafted MISTRG mice (Evren et al., 2021). A similar population of macrophages is associated with lung inflammation and expanded in the airways of humans with severe COVID-19 (Grant et al., 2021; Liao et al., 2020; Mulder et al., 2021; Wauters et al., 2021). Consistent with their host defense function, biological processes such as “defense response to virus” and “response to other organism” were over-represented within the gene signature of adult-derived lung macrophages (Fig. 10 D). We conclude that the local microenvironment has a strong effect on the gene signature of human lung macrophages, while adult precursors preferentially generate pro-inflammatory lung macrophages that have an IFN-induced gene signature.

Discussion

Alveolar macrophages are essential for lung health, but their ontogeny has been difficult to investigate in humans in view of the inability to perform invasive experiments. We recently demonstrated that CD14⁺ blood monocytes generate human alveolar macrophages in adult life (Evren et al., 2021). In the present study, we defined the development of human lung macrophages from embryonic progenitors and identified CD116⁺ fetal liver cells as precursors of human alveolar macrophages in early life.

Our findings support a model where CD34⁺ Lin⁻CD116⁺CD64⁻CD115⁺ macrophage progenitors originating from the fetal liver migrate into the lung, possibly in a CX3CR1-dependent manner, and develop into mature human alveolar macrophages after exposure to tissue-derived GM-CSF and M-CSF. After migration into the lung, CD116⁺CD64⁻ macrophage precursors up-regulated CD64 and other characteristic surface proteins, such as CD206 and CD169, consistent with their differentiation into mature macrophages that clear lung surfactant from the alveoli. We found that human alveolar macrophage precursors in fetal liver already expressed receptors for the key macrophage-instructing cytokines GM-CSF and M-CSF. Moreover, our data indicate that human GM-CSF and M-CSF, produced by the mouse epithelium in MISTRG mice are sufficient to instruct human alveolar macrophage development. TGFβ is another cytokine that promotes the differentiation of mouse alveolar macrophages (Yu et al., 2017), but in contrast with GM-CSF, it does not exclusively derive from a nonhematopoietic source. In MISTRG mice, human TGFβ is likely provided by human alveolar macrophages themselves (Branchett et al., 2021).

Apart from being responsive to instructive cytokines from the local environment, alveolar macrophage precursors need to be able to egress from the fetal liver into the circulation and migrate into the lung. In mice, fetal liver monocytes migrate into tissues in a CCR2-independent manner (Hoeffel et al., 2015; Rantakari et al., 2016), in contrast with adult monocytes (Ly6C^{hi}



Downloaded from http://rupress.org/jem/article-pdf/121/9/2021/0987142/76/jem_20210987.pdf by Institut Pasteur - Ceris user on 09 February 2023

Figure 4. CD116⁺ fetal liver cells are able to migrate to the lung and differentiate into human alveolar macrophages. (A) Intrahepatic injection of purified human Lin^{+/-}CD116⁻ and Lin⁻CD116⁺ populations from CD34⁻ fetal liver cells into newborn MISTRG mice. Lin markers were CD3, CD19, CD56, NKp46, and CD66abce. Cartoon was adapted from Servier Medical Art. (B and C) Flow cytometry of MISTRG lungs 7 wk (B) and 24 wk (C) after injection of human cells. Control mice were not injected with cells (naive). See Fig. S2 A for gating strategy. (D) Number of human alveolar macrophages (AM) in MISTRG mice at 10 and 24 wk after transplantation. (E) Immunohistochemistry of lung sections from MISTRG mice 24 wk after transplantation with human Lin⁻CD116⁺ fetal liver cells. Lung sections were stained with anti-human CD68 antibody (brown). Scale bar is 20 μm. (F) Amounts of total protein in the BAL fluid of MISTRG mice 24 wk

after transplantation with human Lin⁻CD116⁻ or Lin⁻CD116⁺ fetal liver cells. Control mice were transplanted with human CD34⁺ HSPCs from cord blood or were not injected with cells (naive). Data are represented as mean \pm SEM. Picture on the right shows BAL fluid obtained from MISTRG mice transplanted with Lin⁻CD116⁺ fetal liver cells or not transplanted with any human cells (naive). **(G)** Flow cytometry of MISTRG blood 7 wk after transplantation with the indicated human cells. Control mice were not injected with cells (naive). See Fig. S2 B for gating strategy. aCD68, anti-CD68; hCD45, human CD45. Data are represented as mean \pm SEM. **, $P < 0.01$; ****, $P < 0.0001$ (one-way ANOVA with Tukey's multiple comparison post hoc test). Data (B and C) show one lung sample representative of two to eight samples (individual mice) per group and time point from three independent experiments. Data (E) show one lung sample representative of five samples (individual mice) from three independent experiments. Data (D and F) are pooled from three independent experiments with $n = 2$ –8 per group and time point (D) or $n = 3$ –5 per group (F). Data (G) show one blood sample representative of seven to nine samples (individual mice) from two independent experiments.

in mice, CD14⁺ in humans; [Guilliams et al., 2018](#)). This underscores that fetal and adult precursors of alveolar macrophages are distinct, in line with our observation that HSPC-derived macrophage precursors, i.e., CD14⁺ blood monocytes ([Evren et al., 2021](#)), and CD64⁻CD14⁻ fetal macrophage precursors have different surface phenotypes and gene signatures. Colonization of tissues in the mouse embryo by macrophage precursors requires CX3CR1 and additional, as yet unknown, receptors ([Mass et al., 2016](#)). We found CX3CR1 expression on fetal alveolar macrophage precursors, and the CX3CR1 ligand CX3CL1 is expressed in the human fetal and adult lung ([Cao et al., 2020](#); [Travaglini et al., 2020](#)). Therefore, CX3CR1 is a potential candidate receptor mediating the trafficking of CD116⁺CD64⁻ macrophage precursors from the fetal liver to the lung.

The surface phenotype of the fetal progenitor of human alveolar macrophages is distinct from known progenitors that give rise to human monocytes during adult hematopoiesis in the bone marrow, such as CD34⁺CD64^{mid} granulocyte-monocyte progenitors ([Kawamura et al., 2017](#)), CD34⁺CD115⁺CD116⁻ monocyte-dendritic cell progenitors ([Lee et al., 2015](#)), CD34⁺CD64⁺CD115⁺CD116⁺ common monocyte progenitors ([Kawamura et al., 2017](#)), and CD34⁺CD64⁻CD115⁺CD116⁺ premonocytes ([Breton et al., 2015](#); [Kawamura et al., 2017](#)). Furthermore, CD116⁺CD64⁻CD14⁻ fetal progenitors of human alveolar macrophages are different from CD116⁺CD64⁺ fetal monocytes that express CD14. Instead, the gene signature of fetal CD34⁺Lin⁻CD116⁺CD64⁻ alveolar macrophage precursors suggests that they are the human equivalent of EMPs or downstream MYB⁺CD64⁻ myeloid progenitors, which up-regulate CD64 in response to M-CSF in vitro and give rise to CD64⁺ fetal monocytes and alveolar macrophages in mice ([Gomez Perdiguero et al., 2015](#); [Hoeffel et al., 2015](#); [Li et al., 2020](#); [Mass et al., 2016](#)).

We found that both CD116⁺CD64⁻ and CD116⁺CD64⁺ fetal liver cells gave rise to human macrophages with an alveolar macrophage surface phenotype and gene signature. However, only macrophages derived from CD116⁺CD64⁻ fetal precursors efficiently catabolized lung surfactant. Compared with their CD64⁺ counterparts, CD116⁺CD64⁻ fetal liver cells are likely the main progenitor of mature human alveolar macrophages based on their presence in the circulation and ability to migrate from the liver to the lung, their proliferative gene signature associated with efficient occupation of the alveolar niche, and their ability to turn over lung surfactant. It is possible that EMP-like CD116⁺CD64⁻ fetal precursors develop directly into alveolar macrophages. Alternatively, CD116⁺CD64⁻ fetal precursors could

further differentiate into CD116⁺CD64⁺ fetal monocytes and then into human alveolar macrophages.

Lung transplantation data suggest that alveolar macrophages in humans are derived from both embryonic precursors and circulating monocytes ([Bittmann et al., 2001](#); [Byrne et al., 2020](#); [Eguíluz-Gracia et al., 2016](#); [Kjellström et al., 2000](#); [Nayak et al., 2016](#)). The current work, combined with our previous study ([Evren et al., 2021](#)), demonstrates that, in a noncompetitive situation, CD116⁺ fetal liver cells and HSPC-derived CD14⁺ blood monocytes are precursors of human alveolar macrophages in early and adult life, respectively. In mice, fetal monocytes originating from CD115⁺ progenitors in the fetal liver ([Hoeffel et al., 2015](#)) seed the lung during the perinatal period and give rise to alveolar macrophages ([Guilliams et al., 2013](#); [Schneider et al., 2014](#); [Yu et al., 2017](#)). Similarly, under physiological conditions, CD116⁺CD64⁻ fetal precursors are likely the main progenitor of human alveolar macrophages in early life. Consistent with this idea, we found that fetal macrophage precursors had a greater ability to occupy the alveolar compartment in early life than adult blood monocytes. The observation that human CD116⁺ fetal precursors outcompeted CD14⁺ blood monocytes in populating the perinatal alveolar niche in MISTRG mice is in line with mouse studies ([van de Laar et al., 2016](#)) and with the need for fetal macrophage precursors to physiologically occupy the niche shortly after birth in mice ([Guilliams et al., 2013](#)) and humans ([Alenghat and Esterly, 1984](#); [Bharat et al., 2016](#)) in order to be ready for environmental exposure after birth. Overall, our findings are consistent with the concept that diverse, distinct fetal and adult hematopoietic precursors contribute to tissue-resident macrophages according to timed developmental waves ([Ginhoux and Guilliams, 2016](#)).

We not only identified the progenitor of human alveolar macrophages in early life but also addressed the fundamental question of whether cellular origin or cues from the local tissue environment determine the function of lung macrophages, taking advantage of our unique model system to answer this issue in the human context. We found that the local microenvironment shapes the transcriptome of human lung macrophages, irrespective of fetal or adult origin. Similar results have been reported for mouse alveolar macrophages ([Gibbins et al., 2015](#); [Lavin et al., 2014](#); [van de Laar et al., 2016](#)), indicating that this is conserved between species. Moreover, our data demonstrate that human macrophages originating from fetal or adult progenitors were both able to reconstitute an empty alveolar niche and to catabolize pulmonary surfactant, similar to what has been reported for mouse alveolar macrophages ([van de Laar et al., 2016](#)). Furthermore, mouse studies reported that fetal

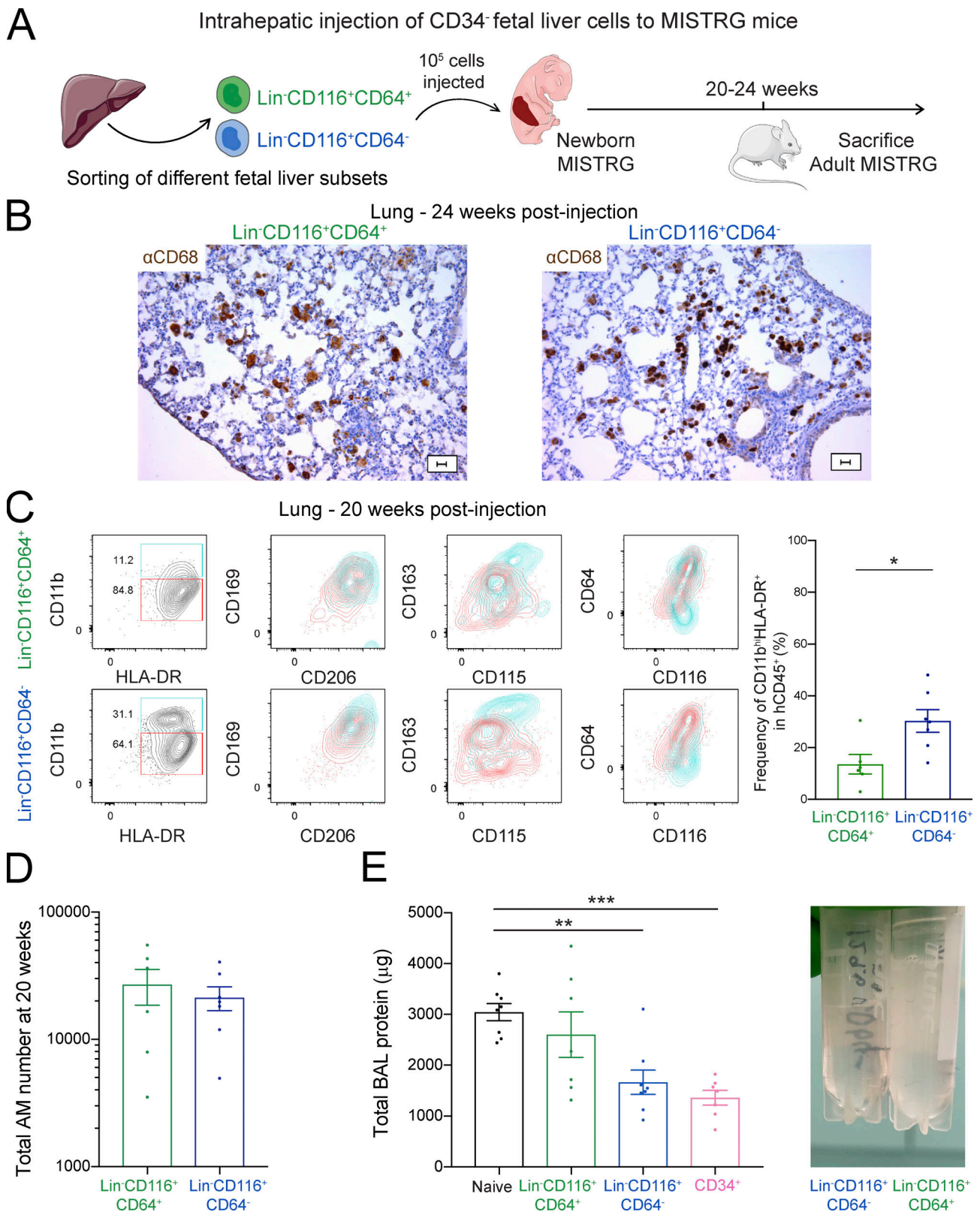


Figure 5. CD116⁺CD64⁻ fetal liver cells give rise to human alveolar macrophages in vivo. (A) Intrahepatic injection of purified human Lin⁻CD116⁺CD64⁻ and Lin⁻CD116⁺CD64⁺ populations from CD34⁺ fetal liver cells into newborn MISTRG mice. Lin markers were CD3, CD19, CD56, NKp46, and CD66abce. Cartoon was adapted from Servier Medical Art. (B) Immunohistochemistry of lung sections from MISTRG mice 24 wk after transplantation with either human Lin⁻CD116⁺CD64⁻ or Lin⁻CD116⁺CD64⁺ fetal liver cells. Lung sections were stained with anti-human CD68 antibody (brown). Scale bars are 20 μm. (C) Flow cytometry of human CD45⁺CD11b⁺HLA-DR⁺CD206⁺CD169⁺ lung macrophages in MISTRG mice 20 wk after transplantation. See Fig. S2 A for gating strategy. (D) Number of human alveolar macrophages (AM) derived from Lin⁻CD116⁺CD64⁻ and Lin⁻CD116⁺CD64⁺ fetal liver cells in MISTRG mice at 20 wk after

transplantation. (E) Amounts of total protein in the BAL fluid of MISTRG 20–24 wk after transplantation with human Lin[−]CD116⁺CD64[−] or Lin[−]CD116⁺CD64⁺ fetal liver cells. Newborn control MISTRG mice were either not transplanted or transplanted with human CD34⁺ HSPCs from cord blood. Picture on the right shows BAL fluid obtained from MISTRG mice transplanted with either Lin[−]CD116⁺CD64[−] or Lin[−]CD116⁺CD64⁺ fetal liver cells. aCD68, anti-CD68; hCD45, human CD45; hi, high. Data are represented as mean ± SEM. *, P < 0.05 (unpaired Student's t test), **, P < 0.01; ***, P < 0.001 (one-way ANOVA with Tukey's multiple comparison post hoc test). Data (B) show one lung sample representative of six to seven samples (individual mice) per group from two independent experiments. Data (C) show one lung sample representative of six to seven samples (individual mice) per group from two independent experiments. Data (C–E) are pooled from two independent experiments with n = 6 or 7 (C and D) or n = 7 or 8 (E) per group.

macrophage progenitors have a greater proliferative capacity than their adult counterparts (Li et al., 2020; van de Laar et al., 2016). Consistent with this concept, we found that fetal CD116⁺CD64[−] precursors of human alveolar macrophages had higher expression of genes associated with proliferation and outcompeted adult macrophage precursors (CD14⁺ blood monocytes) when reconstituting the alveolar niche. This indicates that fetal-derived human alveolar macrophages may occupy the niche faster than their adult-derived macrophages, but after niche colonization, both populations have a similar turnover and persist long-term.

In the healthy lung, resident macrophages of embryonic origin play an essential anti-inflammatory role by clearing inhaled microbes, dead cells, and surfactant. During severe lung injury, resident macrophages with a tissue-protective function are replaced by macrophages derived from recruited blood monocytes. We found that, compared with their counterparts originating from fetal precursors, lung macrophages derived from adult precursors had a gene signature characteristic of IFN-induced macrophages (Evren et al., 2021) that likely arise from the interaction with T lymphocytes (Mulder et al., 2021). These blood monocyte-derived macrophages are more pro-inflammatory and cause lung damage in important diseases, such as COVID-19 (Bost et al., 2020; Liao et al., 2020; Wauters et al., 2021). The human fetal progenitor that we identified is therefore a potential target to regenerate tissue-protective macrophages in order to limit organ damage and promote tissue repair in the injured lung.

The discovery of human lung macrophage progenitors and their developmental paths is an important step forward. Our in vivo study reveals not only the embryonic origin of human alveolar macrophages but also the impact of cell origin on human lung macrophage specification and function. Therefore, this study provides new insights into the ontogeny of human lung macrophages, which could be used in the long term to develop macrophage-based therapies for important lung diseases in humans.

Limitations of the study

A limitation of our experimental approach is that cell transplantation into an empty alveolar niche in MISTRG mice mainly assigns progenitor potential. However, the alveolar niche is also physiologically empty during development when macrophage precursors develop into alveolar macrophages early in life. Another limitation is that prenatal events of human lung macrophage development (Miah et al., 2021) cannot be studied and that human macrophage precursors develop in a mouse lung environment with potentially altered species-specific cell–cell interactions. The latter is relevant as environmental cues drive macrophage phenotype and function in different tissues (Amit

et al., 2016; Lavin et al., 2014). However, production of human GM-CSF and M-CSF by the mouse lung epithelium is sufficient to support the development of human alveolar macrophages in MISTRG mice. Moreover, certain types of human cells that may regulate alveolar macrophage function, such as basophils (Cohen et al., 2018), might not develop optimally in MISTRG mice. Despite its limitations, our study provides important information about the origin and development of human alveolar macrophages that is difficult to obtain with other approaches.

Materials and methods

Mice

MISTRG mice homozygous for the human genes encoding M-CSF, IL-3/GM-CSF, signal regulatory protein α (SIRP α), and thrombopoietin in the *Rag2^{−/−}Il2rg^{−/−}* 129 × BALB/c (N2) genetic background were previously described (Rongvaux et al., 2014). MISTRG mice were used under Material Transfer Agreements with Regeneron Pharmaceuticals and Yale University. For this study, we used an improved version of MISTRG mice with the SIRPA knock-in allele (Deng et al., 2015) instead of the SIRPA transgene as in the original MISTRG mice. As recipients for transplantation with human cells (see below), MISTRG mice were used that were either homozygous or heterozygous for SIRPA knock-in. Heterozygous mice were derived from breeding MISTRG mice (homozygous for SIRPA) with MITRG mice (lacking the SIRPA knock-in allele; Rongvaux et al., 2014). MISTRG mice were rederived by embryo transfer at Karolinska Institutet and maintained in individually ventilated cages under specific pathogen-free conditions without any prophylactic antibiotics. Mice (both males and females) were generally used at 7–26 wk after transplantation with human cells. Mice did not receive any irradiation as preconditioning before transplantation. Whenever possible, littermates were used as controls. All mouse experiments were performed in accordance with protocols approved by the Linköping Animal Experimentation Ethics Committee (#29-15, 03127-2020).

Human tissues

For transplantation of MISTRG mice, frozen fetal liver cells from second trimester were obtained from Yale University collected as part of a previous study (Rongvaux et al., 2014). Umbilical cord blood and buffy coats were obtained from caesarean sections and the Blood Bank at Karolinska University Hospital Huddinge, respectively. The collection of all human tissues was approved by local Ethical Review Boards at Karolinska Institutet (#2006/229-31/3, 2015/1368-31/4, 2015/2122-32, 2016/1415-32, 2018/2162-32) and Yale University (#0804003766). Flow cytometry of fetal liver and fetal lung was performed at Institut

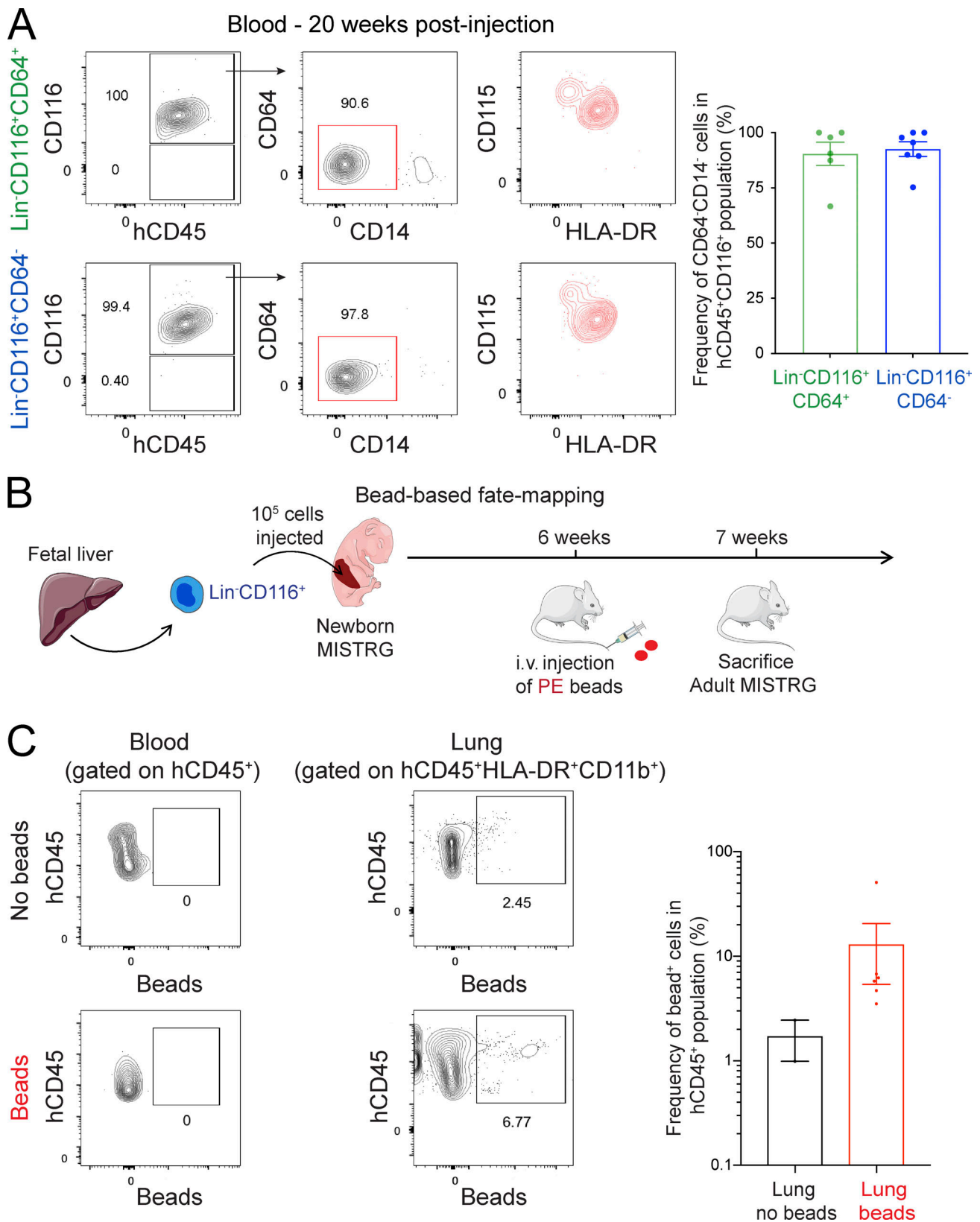


Figure 6. **Circulating CD116⁺CD64⁻CD14⁻CD115⁺ macrophage precursors migrate to the lung.** (A) Flow cytometry of MISTRG blood 20 wk after transplantation with human Lin⁻CD116⁺CD64⁻ or Lin⁻CD116⁺CD64⁺ fetal liver cells. See Fig. S2 B for gating strategy. Frequencies of circulating CD45⁺CD116⁺CD64⁻CD14⁻ cells after transplantation are shown on the right. (B) Fate-mapping of circulating cells in MISTRG mice transplanted with human Lin⁻CD116⁺ fetal liver cells. Blood cells were labeled by the i.v. injection of PE-conjugated fluorescent beads. Cartoon was adapted from Servier Medical Art. (C) Flow-cytometric analysis and frequency of bead⁺ cells in the lung and blood of MISTRG mice at day 7 after bead injection. hCD45, human CD45. Data are

represented as mean \pm SEM. Data (A) show one blood sample representative of six or seven samples (individual mice) per group from two independent experiments. Data (C) show one blood and lung sample representative of two to six samples per group from two independent experiments. Bar graphs (A and C) show data pooled from two independent experiments with $n = 6-7$ (A) or $n = 2-6$ (C) per group.

Pasteur with fetal tissues (15–23 wk of gestation) that were obtained from Advanced Bioscience Resources Inc. following approval by an institutional medical ethical committee at Institut Pasteur and by the French Ministry of Education and Research (#2018-1003(10)M1). Informed consent was obtained from all tissue donors following verbal and written information, and the investigations were conducted according to the Declaration of Helsinki.

Transplantation of MISTRG mice with human cells

For transplantation with human HSPCs, CD34⁺ cells were isolated from pooled cord blood by density gradient centrifugation and positive immunomagnetic selection using a CD34⁺ microbead kit (Miltenyi Biotec). Newborn MISTRG mice (3–5 d old) were transplanted with 10⁵ human CD34⁺ cells (usually >90% purity) by intrahepatic injection as previously described (Evren et al., 2021). HSPCs were pooled from several donors for transplantation.

For transplantation with human CD34⁻ fetal liver cells, the CD34⁻ fraction of fetal liver was obtained after isolation of CD34⁺ cells by density gradient centrifugation and positive immunomagnetic selection using a CD34⁺ microbead kit (Miltenyi Biotec) as described (Rongvaux et al., 2014). Frozen CD34⁻ depleted fetal liver cells were then further purified by cell sorting into the indicated cell populations (purity \geq 95%). Newborn MISTRG mice (3–5 d old) received purified cells either via the intranasal route (0.5–1 \times 10⁵ cells in 7 μ l PBS) or by intrahepatic injection (10⁵ cells in 20 μ l PBS). Control mice received PBS only or no cell injection as indicated. SIRPA homozygous and heterozygous MISTRG mice were used for intranasal and intrahepatic cell transfer, respectively. Recipient mice were analyzed at the indicated times after cell transfer.

For competitive precursor transfer experiments, CD14⁺CD16⁻ blood monocytes were purified from buffy coats as described (Evren et al., 2021). Blood monocytes were first enriched by negative immunomagnetic selection using EasySep Human Monocyte Enrichment kit (StemCell Technologies, Inc.), and then CD14⁺CD16⁻ monocytes were further purified by cell sorting (purity \geq 95%). CD45⁺CD34⁻Lin⁻CD116⁺CD64⁻CD14⁻ cells were purified by cell sorting from the CD34⁻ fraction of fetal liver (purity \geq 95%). Purified macrophage precursors (CD14⁺CD16⁻ blood monocytes and CD116⁺CD64⁻ fetal liver cells) were mixed 1:1 for adoptive transfer and administered intranasally into newborn MISTRG mice (3–4 \times 10⁵ cells in total). The input ratio was confirmed by flow cytometry based on CD14 surface expression. Surface expression of HLA-A and HLA-B alleles was determined for each cell origin (buffy coat or fetal liver) by flow cytometry with a panel of allele-specific antibodies. Cell origin of human lung macrophages obtained from MISTRG mice was determined with allele-specific HLA-A and HLA-B antibodies 13 wk after transfer.

Isolation of immune cells from transplanted MISTRG mice

Lungs were perfused with 10 ml ice-cold PBS and digested in RPMI 1640/5% FCS with 0.2 mg/ml of collagenase IV (Sigma-Aldrich) and 0.02 mg/ml of DNase I (Sigma-Aldrich) for 60 min at 37°C. Digested cells were then passed sequentially through 18- and 20-G needles before density gradient centrifugation using Lymphoprep (StemCell Technologies, Inc.). BAL fluid was collected by inflating the lungs three times with 0.8 ml PBS via a catheter inserted into the trachea. BAL fluid was then centrifuged, the pellet resuspended in RPMI 1640/5% FCS, and BAL cells purified for flow cytometry by density gradient centrifugation. The supernatants were frozen at -80°C and the total protein concentration in BAL supernatants determined using the Bicinchoninic acid assay kit (Thermo Fisher Scientific) according to the manufacturer's instructions. Blood was taken by cardiac puncture and diluted in 200 U/ml heparin (Sigma-Aldrich). Erythrocytes were removed using red blood cell lysis buffer (obtained from Karolinska University Hospital) and the remaining immune cells stained for flow cytometry analysis.

Cell isolation from fetal liver and fetal lung for flow cytometry

Fetal lungs were cut into small pieces and digested in RPMI 1640 (Life Technologies) with 25 μ g/ml Liberase TL (Roche), 100 μ g/ml DNase I (Roche), 100 U/ml penicillin, and 100 μ g/ml streptomycin (Thermo Fisher Scientific) for 60 min at 37°C and filtered through a 100- μ m cell strainer (Corning). Fetal livers were cleaned from vascular tissue, paddle-blended in a sterile bag, filtered through a 100- μ m cell strainer (Corning), and centrifuged on a Ficoll (GE Healthcare) density gradient. Mononuclear cells were recovered and CD34⁺ cells depleted using the CD34⁺ microbead kit (Miltenyi Biotec). Cell preparation steps were performed using RPMI 1640 supplemented with 100 U/ml penicillin, 100 μ g/ml streptomycin, and 2% FCS unless indicated otherwise. Cells were frozen in FCS with 10% DMSO (Sigma-Aldrich) at -80° until used for flow cytometry.

Flow cytometry and cell sorting

Single-cell suspensions from human fetal liver and lung as well as from lung and blood of MISTRG mice were stained with fluorochrome- or biotin-labeled anti-human antibodies in FACS buffer (PBS/2% FCS) for 30 min on ice, followed by secondary staining with streptavidin–Brilliant Violet 711 (BD Biosciences) for 30 min on ice. To exclude T cells, B cells, natural killer cells, and granulocytes, a Lin cocktail was used, which consisted of CD3, TCR $\alpha\beta$, TCR $\gamma\delta$, CD19, CD20, CD56, CD94, NKp46, and CD66abce (for flow cytometry of fetal liver and lung) or CD3, CD19, CD56, NKp46, and CD66abce (for cell sorting and flow cytometry of MISTRG mice). For staining of fetal liver and fetal lung, Fc receptors were blocked using IgG from human serum (Millipore Sigma) and nonspecific dye binding inhibited by using True-Stain Monocyte Blocker solution (BioLegend). After surface staining, cells were stained with fixable viability dye

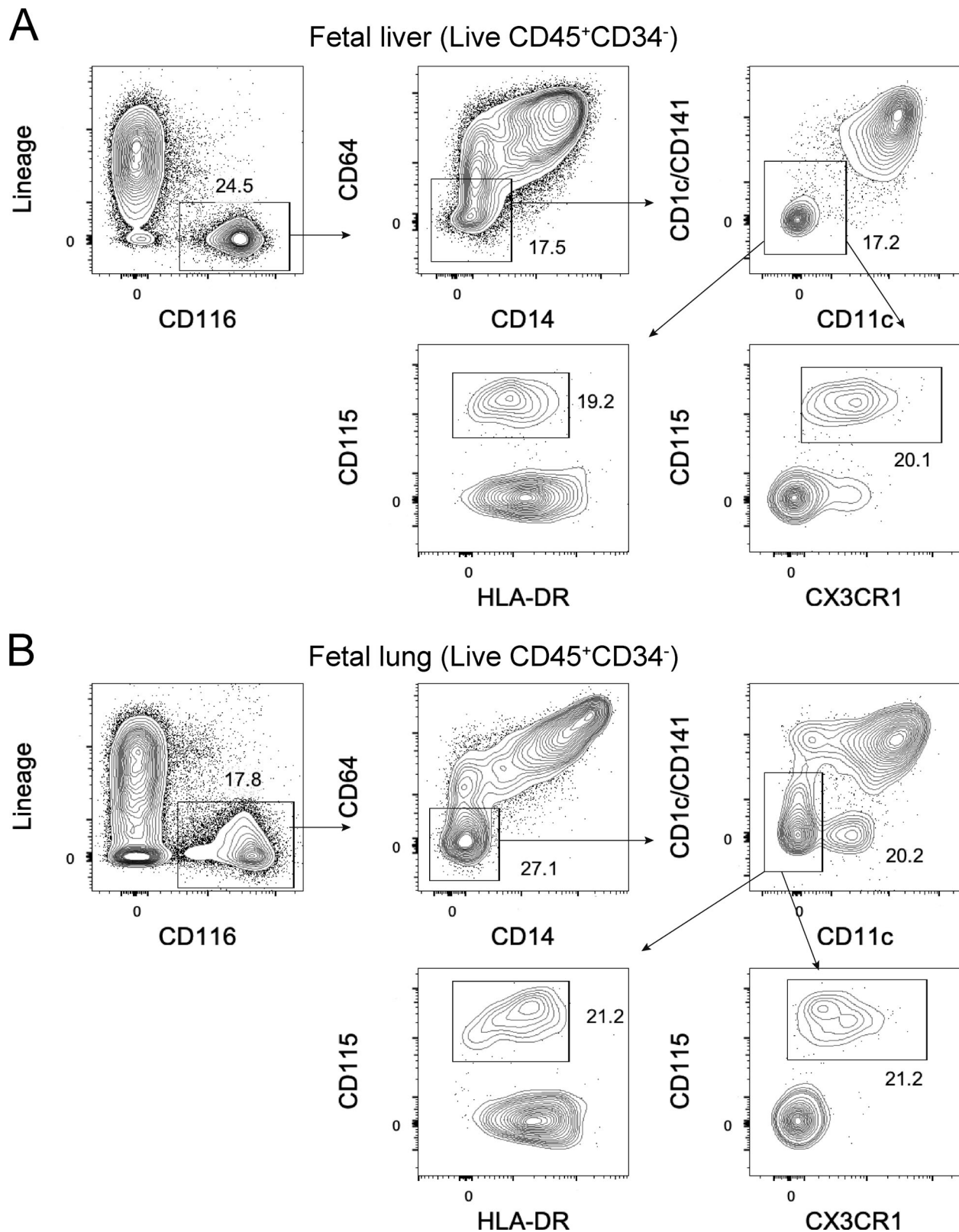


Figure 7. **Human fetal liver and lung contain CD116⁺CD64⁻CD115⁺CX3CR1⁺ lung macrophage precursors. (A and B)** Flow cytometry analysis of CD116-expressing macrophage precursors in human fetal liver (A) and fetal lung (B) at wk 21 and 22 of gestation, respectively. After pre-gating on CD45⁺CD34⁻ cells (see Fig. S5 for gating strategy), macrophage precursors were gated as shown. Lin markers were CD3, TCRαβ, TCRγδ, CD19, CD20, CD56, CD94, NKp46, and CD66abce. Data (A and B) are representative of fetal liver and fetal lung samples at 15–23 wk of gestation from two independent experiments (*n* = 12).

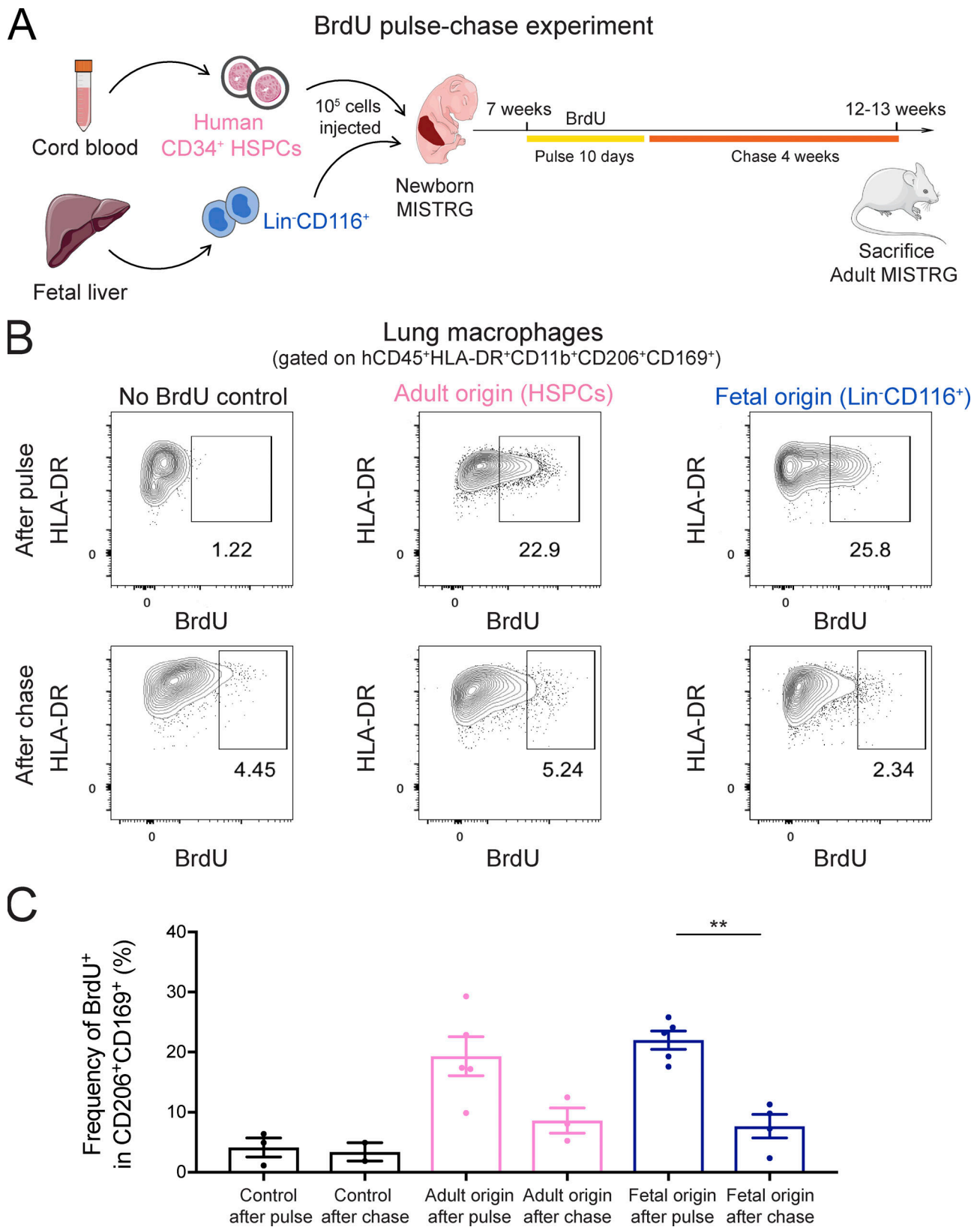


Figure 8. **Human alveolar macrophages derived from fetal and adult precursors have a similar turnover.** (A) Overview of BrdU pulse-chase experiment. MISTRG transplanted with either Lin⁻CD116⁺ fetal liver cells or CD34⁺ HSPCs by intrahepatic injection were pulsed with BrdU for 10 d, followed by a chase period without BrdU for 4 wk. Cartoon was adapted from Servier Medical Art. (B) Flow cytometry of BrdU incorporation in human alveolar macrophages of fetal versus adult origin. Numbers indicate the frequency of BrdU⁺ lung macrophages after the pulse and at the end of the chase period. Human lung macrophages were gated as CD45⁺CD11b⁺HLA-DR⁺CD206⁺CD169⁺ cells. Human lung macrophages from mice without BrdU administration were used as a

staining control (No BrdU control). (C) Frequencies of BrdU⁺ lung macrophages of fetal or adult origin after the pulse and at the end of the chase period. hCD45, human CD45. Data are represented as mean ± SEM. **, P < 0.01 (one-way ANOVA with Tukey's multiple comparison post hoc test). Data (B) show one lung sample representative of two to five samples (individual mice) per group from two independent experiments. Data (C) are pooled from two independent experiments with n = 2–5 per group.

eFluor506 or eFluor455UV (Thermo Fisher Scientific) according to the manufacturer's instructions. Cells were fixed in PBS/2% paraformaldehyde and acquired on a LSR II Fortessa or Symphony A5 flow cytometer (BD Biosciences), and data were analyzed with FlowJoV10 software. The indicated cell populations were sorted into RPMI 1640/30% FCS medium using a BD FACSAria III (BD Biosciences) or a MA900 (Sony Biotechnology) cell sorter.

The following antibodies were used for flow cytometry and cell sorting: biotinylated anti-human CD3 (OKT3; Thermo Fisher Scientific or UCHT1; BioLegend), CD19 (HIB19; Thermo Fisher Scientific or BioLegend), CD20 (2H7; BioLegend), CD56 (HCD56; BioLegend), CD66abce (REA1230 or TET2; Miltenyi Biotec), CD94 (REA113; Miltenyi Biotec), Nkp46 (9E2; BioLegend), TCRαβ (IP26; BioLegend), TCRγδ (B1; BD Biosciences), HLA-B12 (REA138; Miltenyi Biotec); conjugated anti-human CD1c BV785 (L161; BioLegend), CD1c BV650 (L161; BioLegend), CD11b PerCP-Cy5.5 (ICRF44; BioLegend), CD11b BUV737 (M1/70; BD Biosciences), CD11b BB515 (ICRF44; BD Biosciences), CD11c R718 (B-ly6; BD Biosciences), CD14 BV421 (M5E2; BioLegend), CD14 BV480 (MφP9; BD Biosciences), CD16 PE-Cy7 (3G8; BioLegend), CD33 BUV805 (WM53; BD Biosciences), CD34 PE-Dazzle594 (581; BioLegend), CD34 BV650 (563; BD Biosciences), CD34 FITC (581; BD Biosciences), CD45 APC-Cy7 (HI30; BioLegend), CD45 BUV395 (HI30; BD Biosciences), CD45 BV785 (HI30; BioLegend), CD64 BUV737 (10.1; BD Biosciences), CD64 PE-Dazzle594 (10.1; BioLegend), CD88 APC (S5/1; BioLegend), CD88 PE-Cy7 (S5/1; BioLegend), CD115 PE-Cy7 (9-4D2-1E4; BioLegend), CD116 PE (4H1; Thermo Fisher Scientific or BioLegend), CD141 BV785 (M80; BioLegend), CD141 BV650 (1A4; BD Biosciences), CD163 BV650 (GHI/61; BD Biosciences), CD169 APC (7-239; BioLegend), CD169 BV421 (7-239; BioLegend), CD206 BV605 (19.2; BD Biosciences), CX3CR1 BB515 (2A9-1; BD Biosciences), HLA-A2 AF700 (BB7.2; BioLegend), HLA-A9 APC (REA127; Miltenyi Biotec), HLA-B8 APC-Cy7 (REA145; Miltenyi Biotec), HLA-DR BUV395 (G46-6; BD Biosciences), HLA-DR APC-Fire750 (L243; BioLegend), HLA-DR BV650 (L243; BioLegend), and conjugated anti-mouse CD45 AF700 (30-F11; BioLegend).

Immunohistochemistry

PBS-perfused lungs were collected, fixed in 4% paraformaldehyde for 24–48 h, and then stored in 70% ethanol. Dehydrated lungs were embedded in paraffin and cut into 5-μm sections. Lung sections were rehydrated by successive washes in xylene (Sigma-Aldrich), 100% ethanol, 95% ethanol, 70% ethanol, and 50% ethanol. Heat-induced epitope retrieval was performed in citrate buffer (10 mM citrate, pH 6.0), and excess aldehyde was quenched with 0.2 M glycine. After blocking with 10% normal goat serum (Dako), sections were stained with mouse anti-human CD68 antibody (clone PG-M1; Dako), diluted 1:100 in

2% normal goat serum/PBS overnight at 4°C, followed by a biotinylated goat anti-mouse IgG secondary antibody (Dako), diluted 1:200 in 2% normal goat serum/PBS for 1 h at room temperature. Endogenous peroxidase activity was removed by an additional blocking step in 1% hydrogen peroxide/methanol (Sigma-Aldrich). Staining was revealed with the DAB Peroxidase (HRP) Substrate Kit and Vectastain Elite Kit (both from Vector Labs). Finally, slides were counterstained in hematoxylin (Sigma-Aldrich), dehydrated, and mounted using Permount.

Macrophage turnover

Newborn MISTRG pups were transplanted intrahepatically with either 10⁵ CD34⁺ HSPCs or Lin⁻CD116⁺ fetal liver cells and then used for BrdU pulse-chase experiments 7 wk after transplantation. For the BrdU pulse, transplanted MISTRG mice received an initial intraperitoneal injection of 1.5 mg BrdU (BD Biosciences) per mouse, followed by continuous BrdU treatment (0.8 mg/ml in drinking water supplemented with 10% sucrose) for 10 d (with fresh BrdU water prepared every 1–2 d). Mice were then either sacrificed following the pulse period or kept on drinking water without BrdU for a chase period of 4 wk. BrdU incorporation was determined in human CD11b⁺HLA-DR⁺CD206⁺CD169⁺ lung macrophages after pulse and after chase by flow cytometry using the BrdU APC Flow Kit (BD Biosciences). Human lung macrophages from HSPC-engrafted MISTRG mice that were not treated with BrdU were used as staining control to set up the BrdU⁺ gate.

Gene signatures of human lung macrophages and their precursors

To define the gene signature of adult precursors of human alveolar macrophages, CD14⁺CD16⁻ blood monocytes were purified from buffy coats by immunomagnetic selection and by cell sorting as described above. To define the gene signatures of fetal precursors of human alveolar macrophages, fetal monocytes (CD45⁺CD34⁻Lin⁻CD116⁺CD64⁺CD88⁺CD1c/CD141^{lo}CD206⁻CD169⁻) and fetal precursor-like cells (CD45⁺CD34⁻Lin⁻CD116⁺CD64⁻CD1c/CD141⁻CD14⁻) were purified from the CD34⁻ fraction of fetal liver by cell sorting. Both adult and fetal precursors (purity ≥95%) were directly sorted into RLT buffer or RLT plus buffer (Qiagen). Adult blood monocytes and fetal alveolar macrophage precursors had each three replicates, while there were four replicates for fetal monocytes, of which two replicates were pooled together after RNA extraction for a total of three replicates.

To define the gene signatures of human macrophages of different precursor origin, human cells with an alveolar macrophage surface phenotype (CD45⁺CD11b⁺HLA-DR⁺CD206⁺CD169⁺) were purified from MISTRG mice 13 wk after intrahepatic transplantation of newborn mice with either adult (2 × 10⁵ CD34⁺ HSPCs; three replicates) or fetal precursors (2 × 10⁵ CD34⁻Lin⁻CD116⁺CD64⁻ or CD34⁻Lin⁻CD116⁺CD64⁺ fetal liver cells; three and two replicates,

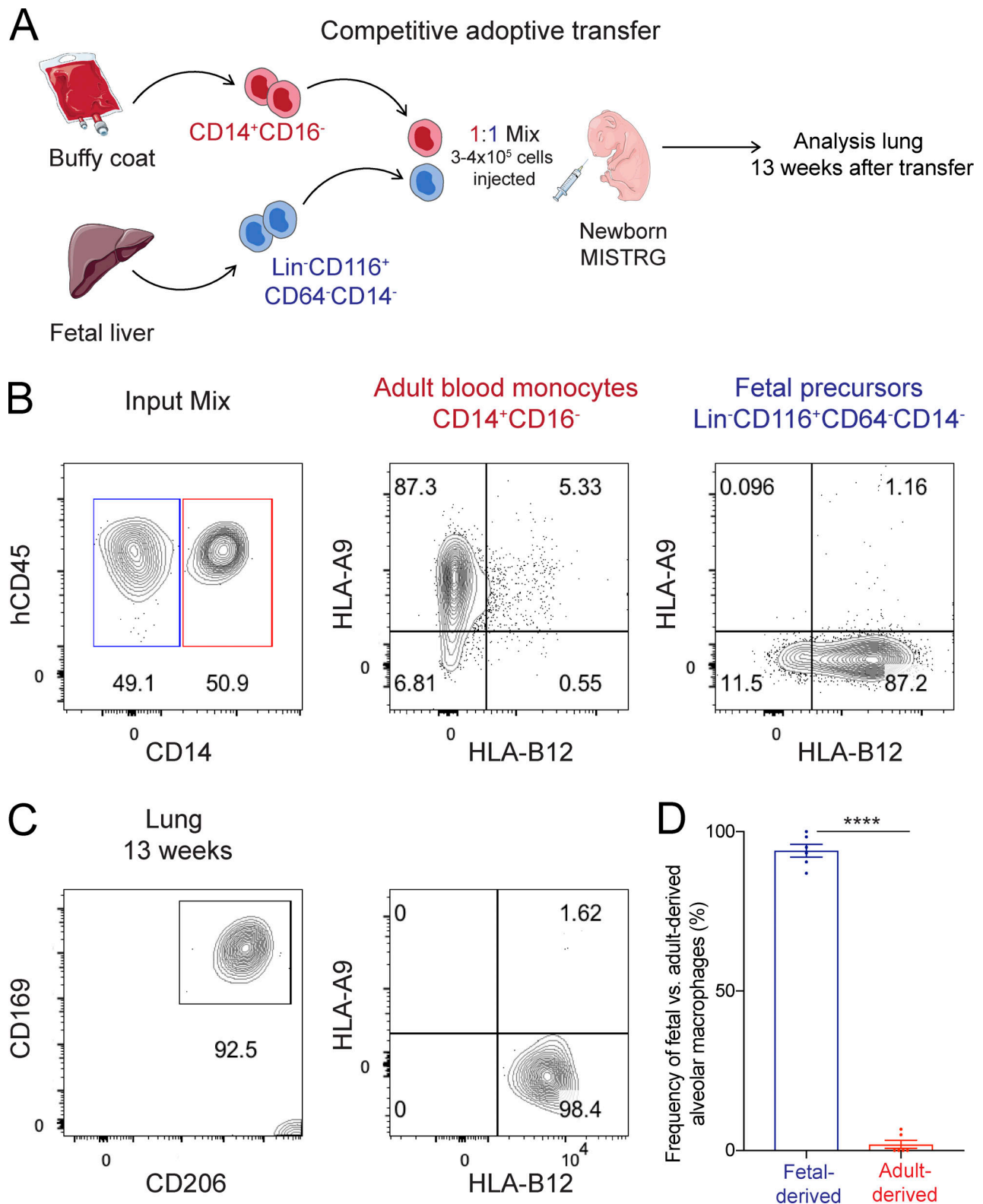


Figure 9. **Fetal macrophage precursors outcompete adult monocytes in occupying the perinatal alveolar niche in MISTRG mice.** (A) Experimental setup of competitive adoptive transfer experiment. Purified fetal and adult macrophage precursors (Lin⁻CD116⁺CD64⁻CD14⁻ fetal liver cells and CD14⁺CD16⁻ blood monocytes) were mixed 1:1 and administered intranasally into newborn MISTRG mice. Cartoon was adapted from Servier Medical Art. (B) Flow cytometry of cell mixture before transfer into MISTRG mice to verify the input ratio (left) and to determine surface expression of distinguishing HLA alleles (HLA-A9 versus HLA-B12). (C) Flow cytometry of human alveolar macrophages after competitive transfer of fetal and adult macrophage precursors into MISTRG mice. Human lung macrophages were gated as CD45⁺CD11b⁺HLA-DR⁺CD206⁺CD169⁺ cells. Fetal- versus adult-derived lung macrophages were distinguished by surface expression of HLA-A9 and HLA-B12 as in B. (D) Frequency of fetal- versus adult-derived human alveolar macrophages in MISTRG mice. hCD45,

human CD45. Data are represented as mean \pm SEM. ****, $P < 0.0001$ (unpaired Student's *t* test). Data (B) show one representative sample from two independent experiments. Data (C) show one lung sample representative of six samples (individual mice) from two independent experiments. Data (D) are pooled from two independent experiments with $n = 6$.

respectively). HSPC-engrafted MISTRG mice were injected i.v. with 2 μ g of PE-conjugated anti-human CD45 antibody (HI30; BioLegend) before lung harvest to exclude i.v. CD45-PE⁺ pulmonary intravascular macrophages from the sorted CD45⁺CD11b⁺HLA-DR⁺CD206⁺CD169⁺ subset as described (Evren et al., 2021).

Samples were sent to the Bioinformatics and Expression Analysis Core Facility at Karolinska Institutet for RNA extraction, amplification, and hybridization to human Clariom D cartridge microarrays (Applied Biosystems). Transcriptome Analysis Console software (Thermo Fisher Scientific) was used for the analysis of the microarray data. Signal values were log₂-transformed and normalized using the Signal Space Transformation–Robust Multiple-array Average method. Gene expression between different cell populations was compared using ANOVA with eBayes analysis. Multiple testing correction was performed based on Benjamini–Hochberg to calculate false discovery rate (FDR)-corrected *P* values. Genes with a fold change ≥ 2 and an FDR-corrected *P* value < 0.05 were considered differentially expressed between paired cell populations. Gene Ontology over-representation analysis (Biological Process) was performed with WebGestalt (<http://webgestalt.org/>) using default parameters.

The gene expression data are available in GEO under accession nos. GSE190256 (fetal and adult precursors of human alveolar macrophages) and GSE190257 (human alveolar macrophages of fetal versus adult origin).

Bead-based fate-mapping of circulating lung macrophage precursors

To fate-map circulating macrophage precursors, MISTRG mice were injected i.v. as described (Evren et al., 2021) with 100 μ l of 0.5- μ m-microsphere Fluoresbrite PC red/PE beads (Polysciences; diluted 1:10) 5–7 wk after intrahepatic transplantation with Lin[−]CD116⁺ fetal liver cells. With this protocol, injected beads were captured by CD116⁺CD64[−] circulating precursors, the cell subset present predominantly in the blood at this time point. Mice were sacrificed 7 d after bead injection, i.e., 6–8 wk after initial cell transplantation, and lungs harvested to determine the frequency of fluorescent bead⁺ lung macrophages by flow cytometry. Human lung macrophages from HSPC-engrafted MISTRG mice that were not injected with beads were used as staining control for the bead⁺ gate.

Quantification and statistical analysis

Statistical parameters including number of biological replicates and repeat experiments, data dispersion and precision measures (mean and SEM), and *P* values for statistical significance ($\alpha = 0.05$) are reported in the figures and figure legends. Student's *t* test was used to determine statistical significance between two groups. For multigroup comparisons, we applied one-way ANOVA with post hoc testing using Tukey's multiple comparison test. Statistical analysis was performed using GraphPad Prism 7.

Online supplemental material

Fig. S1 shows the gating strategy for flow cytometry of fetal liver cells in Fig. 1. Fig. S2 shows the flow cytometry gating strategy for human hematopoietic cells in the lung and blood of MISTRG mice in Figs. 3, 4, 5, and 6. Fig. S3 shows the immunohistochemistry controls for Figs. 3 and 4. Fig. S4 shows flow cytometry for human lung macrophages with an interstitial surface phenotype in MISTRG mice transplanted with either CD116⁺ fetal liver cells or HSPCs. Fig. S5 shows the flow cytometry gating strategy for fetal lung and fetal liver cells in Fig. 7. Table S1 (related to Fig. 2) contains the gene expression profiles of CD116⁺CD64[−] fetal precursors and CD116⁺CD64⁺ fetal monocytes from human fetal liver as well as the gene expression profile of CD14⁺CD16[−] adult monocytes from human blood. Table S2 (related to Fig. 10) contains the gene expression profiles of human lung macrophages derived from fetal precursors (CD116⁺CD64[−] or CD116⁺CD64⁺ fetal liver cells) or from adult precursors (CD34⁺ HSPCs) in MISTRG mice.

Acknowledgments

We acknowledge Regeneron Pharmaceuticals and Yale University, where MISTRG mice were generated with financial support from the Bill and Melinda Gates Foundation. We thank the Bioinformatics and Expression Analysis Core Facility, which is supported by the board of research at the Karolinska Institutet and the research committee at the Karolinska Hospital.

This work was supported by a faculty-funded career position at Karolinska Institutet (2-1060/2018), a Karolinska Institutet Research Foundation Grant (2020-01438), a Junior Investigator and Junior Project Research Grant from the Center for Innovative Medicine financed by Region Stockholm (2-538/2014; 20190152), as well as project grants from the Swedish Research Council (2015-02413; 2019-01099), the Swedish Heart-Lung Foundation (20190198), Petrus och Augusta Hedlunds Stiftelse (M-2021-1568), and the SciLifeLab National COVID-19 Research Program, financed by the Knut and Alice Wallenberg Foundation (C19PI:G:012) to T. Willinger. E. Evren was supported by a scholarship from the Royal Swedish Academy of Sciences (BS2021-0030). A. Thaller was supported by the European Union's Horizon 2020 research and innovation program (H2020 Marie Skłodowska-Curie Actions grant 765104). R.A. Flavell is an investigator of the Howard Hughes Medical Institute.

Author contributions: E. Evren designed, performed, and analyzed most experiments and wrote the paper. E. Ringqvist designed, performed, and analyzed experiments. J.-M. Doisne performed flow cytometry of fetal lung and fetal liver samples. A. Thaller prepared fetal tissues. N. Sleiers helped with mouse experiments. R.A. Flavell provided frozen fetal liver cells. J.P. Di Santo supervised flow cytometry of fetal lung and fetal liver samples. T.

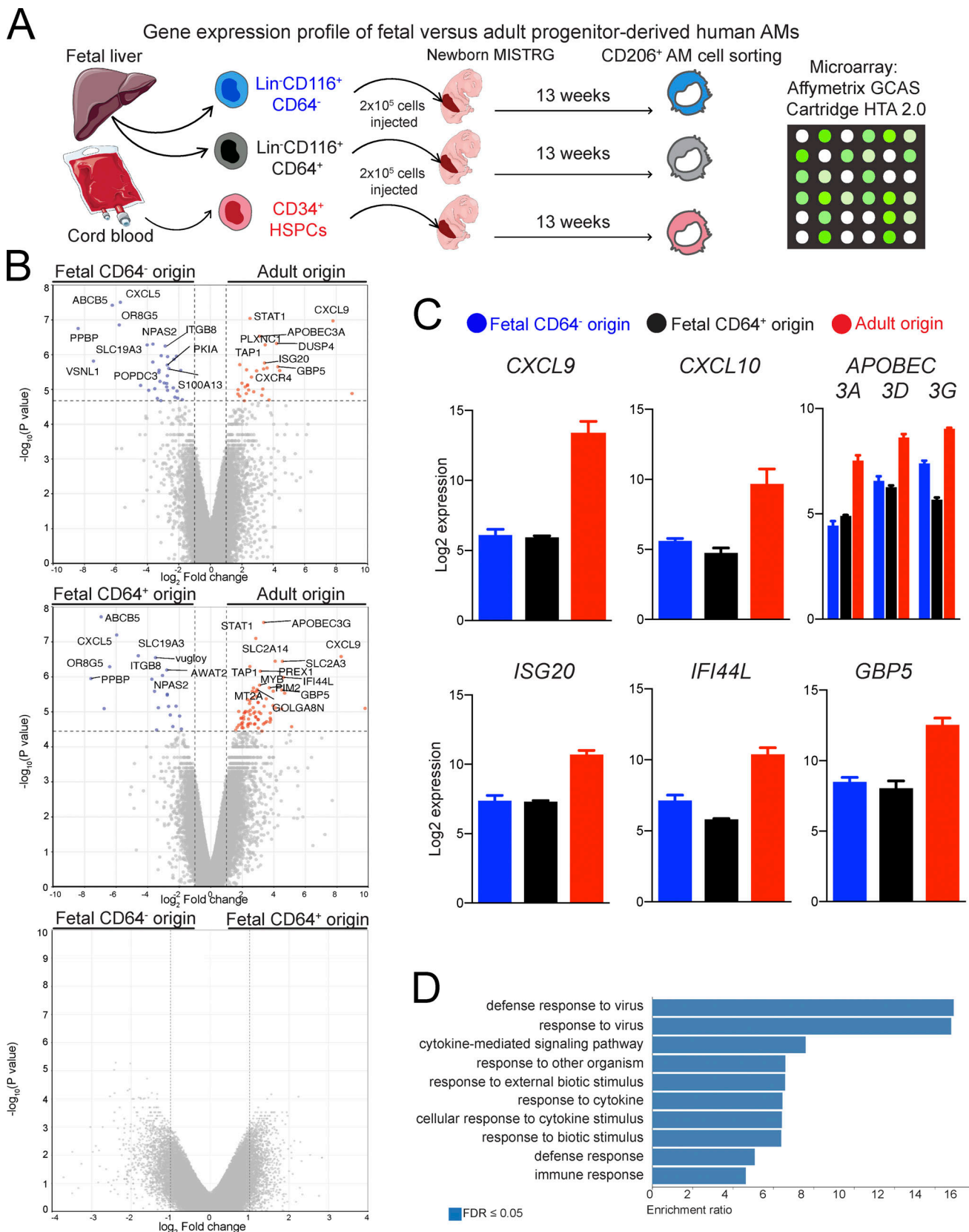


Figure 10. **Gene signatures of human alveolar macrophages of fetal versus origin.** (A) Experimental outline to define the gene expression profiles of human alveolar macrophages (AMs) derived from the indicated fetal and adult precursor populations. Cartoon was adapted from Servier Medical Art. (B) Volcano plots of differentially expressed genes (DEGs) between the indicated cell populations. Log₂ fold change is plotted versus -log₁₀ P value (not corrected for multiple testing). DEGs with a log₂ fold change ≥1 and an FDR-corrected P value ≤0.05 are highlighted in blue and red. (C) Bar graphs showing

expression of selected genes in human lung macrophages derived from fetal precursors (CD116⁺CD64⁻ and CD116⁺CD64⁺ fetal cells) and adult precursors (CD34⁺ HSPCs). Data are represented as mean \pm SEM. **(D)** Gene ontology analysis of DEGs up-regulated in human lung macrophages derived from adult precursors compared with fetal precursors. GCAS, GeneChip Array Station; HTA, Human Transcriptome Array. Data (B–D) are from a single microarray experiment with two to three replicates (individual mice) per cell population obtained from three independent cell sorting experiments.

Willinger conceived and supervised the study, acquired funding, designed and analyzed experiments, and wrote the paper.

Disclosures: R.A. Flavell reported personal fees from Glaxo Smith Kline and Zai Lab Ltd. during the conduct of the study; and personal fees from Symbiotix Biotherapies, Inc., GSK, Hatteras Venture Partners, Troy Therapeutics, Rheos Medicines Inc., Artizan Biosciences, Zai Lab Ltd., Ventus Therapeutics, EvolveImmune Therapeutics Inc., BiomX Ltd., L2 Diagnostics, LLC, and Genenta outside the submitted work. No other disclosures were reported.

Submitted: 7 May 2021

Revised: 5 November 2021

Accepted: 13 December 2021

References

- Aegerter, H., J. Kulikauskaite, S. Crotta, H. Patel, G. Kelly, E.M. Hessel, M. Mack, S. Beinke, and A. Wack. 2020. Influenza-induced monocyte-derived alveolar macrophages confer prolonged antibacterial protection. *Nat. Immunol.* 21:145–157. <https://doi.org/10.1038/s41590-019-0568-x>
- Alenghat, E., and J.R. Esterly. 1984. Alveolar macrophages in perinatal infants. *Pediatrics*. 74:221–223. <https://doi.org/10.1542/peds.74.2.221>
- Alisjahbana, A., I. Mohammad, Y. Gao, E. Evren, E. Ringqvist, and T. Willinger. 2020. Human macrophages and innate lymphoid cells: Tissue-resident innate immunity in humanized mice. *Biochem. Pharmacol.* 174:113672. <https://doi.org/10.1016/j.bcp.2019.113672>
- Amit, I., D.R. Winter, and S. Jung. 2016. The role of the local environment and epigenetics in shaping macrophage identity and their effect on tissue homeostasis. *Nat. Immunol.* 17:18–25. <https://doi.org/10.1038/ni.3325>
- Aran, D., A.P. Looney, L. Liu, E. Wu, V. Fong, A. Hsu, S. Chak, R.P. Naikawadi, P.J. Wolters, A.R. Abate, et al. 2019. Reference-based analysis of lung single-cell sequencing reveals a transitional profibrotic macrophage. *Nat. Immunol.* 20:163–172. <https://doi.org/10.1038/s41590-018-0276-y>
- Aziz, A., E. Soucie, S. Sarrazin, and M.H. Sieweke. 2009. MafB/c-Maf deficiency enables self-renewal of differentiated functional macrophages. *Science*. 326:867–871. <https://doi.org/10.1126/science.1176056>
- Bharat, A., S.M. Bhorade, L. Morales-Nebreda, A.C. McQuattie-Pimentel, S. Soberanes, K. Ridge, M.M. DeCamp, K.K. Mestan, H. Perlman, G.R. Budinger, and A.V. Misharin. 2016. Flow Cytometry Reveals Similarities Between Lung Macrophages in Humans and Mice. *Am. J. Respir. Cell Mol. Biol.* 54:147–149. <https://doi.org/10.1165/rcmb.2015-0147LE>
- Bian, Z., Y. Gong, T. Huang, C.Z.W. Lee, L. Bian, Z. Bai, H. Shi, Y. Zeng, C. Liu, J. He, et al. 2020. Deciphering human macrophage development at single-cell resolution. *Nature*. 582:571–576. <https://doi.org/10.1038/s41586-020-2316-7>
- Bittmann, I., T. Dose, G.B. Baretton, C. Müller, M. Schwaiblmair, F. Kur, and U. Löhrs. 2001. Cellular chimerism of the lung after transplantation. An interphase cytogenetic study. *Am. J. Clin. Pathol.* 115:525–533. <https://doi.org/10.1309/GAFN-5MPA-LY8E-DTPQ>
- Blériot, C., S. Chakarov, and F. Ginhoux. 2020. Determinants of Resident Tissue Macrophage Identity and Function. *Immunity*. 52:957–970. <https://doi.org/10.1016/j.immuni.2020.05.014>
- Post, P., A. Giladi, Y. Liu, Y. Bendjelal, G. Xu, E. David, R. Blecher-Gonen, M. Cohen, C. Medaglia, H. Li, et al. 2020. Host-Viral Infection Maps Reveal Signatures of Severe COVID-19 Patients. *Cell*. 181:1475–1488.e12. <https://doi.org/10.1016/j.cell.2020.05.006>
- Branchett, W.J., J. Cook, R.A. Oliver, N. Bruno, S.A. Walker, H. Stölting, M. Mack, A. O'Garra, S. Saglani, and C.M. Lloyd. 2021. Airway macrophage-intrinsic TGF- β 1 regulates pulmonary immunity during early-life allergen exposure. *J. Allergy Clin. Immunol.* 147:1892–1906. <https://doi.org/10.1016/j.jaci.2021.01.026>
- Breton, G., J. Lee, Y.J. Zhou, J.J. Schreiber, T. Keler, S. Pühr, N. Anandabapathy, S. Schlesinger, M. Caskey, K. Liu, and M.C. Nussenzweig. 2015. Circulating precursors of human CD1c⁺ and CD141⁺ dendritic cells. *J. Exp. Med.* 212:401–413. <https://doi.org/10.1084/jem.20141441>
- Byrne, A.J., J.E. Powell, B.J. O'Sullivan, P.P. Ogger, A. Hoffland, J. Cook, K.L. Bonner, R.J. Hewitt, S. Wolf, P. Ghai, et al. 2020. Dynamics of human monocytes and airway macrophages during healthy aging and after transplant. *J. Exp. Med.* 217:e20191236. <https://doi.org/10.1084/jem.20191236>
- Cao, J., D.R. O'Day, H.A. Pliner, P.D. Kingsley, M. Deng, R.M. Daza, M.A. Zager, K.A. Aldinger, R. Blecher-Gonen, F. Zhang, et al. 2020. A human cell atlas of fetal gene expression. *Science*. 370:eaba7721. <https://doi.org/10.1126/science.aba7721>
- Chakarov, S., H.Y. Lim, L. Tan, S.Y. Lim, P. See, J. Lum, X.M. Zhang, S. Foo, S. Nakamizo, K. Duan, et al. 2019. Two distinct interstitial macrophage populations coexist across tissues in specific subtissular niches. *Science*. 363:eaau0964. <https://doi.org/10.1126/science.aau0964>
- Cohen, M., A. Giladi, A.D. Gorki, D.G. Solodkin, M. Zada, A. Hladik, A. Miklosi, T.M. Salame, K.B. Halpern, E. David, et al. 2018. Lung Single-Cell Signaling Interaction Map Reveals Basophil Role in Macrophage Imprinting. *Cell*. 175:1031–1044.e18. <https://doi.org/10.1016/j.cell.2018.09.009>
- Dame, J.B., R.D. Christensen, and S.E. Juul. 1999. The distribution of granulocyte-macrophage colony-stimulating factor and its receptor in the developing human fetus. *Pediatr. Res.* 46:358–366. <https://doi.org/10.1203/00006450-199910000-00002>
- Deng, K., M. Pertea, A. Rongvaux, L. Wang, C.M. Durand, G. Ghiaur, J. Lai, H.L. McHugh, H. Hao, H. Zhang, et al. 2015. Broad CTL response is required to clear latent HIV-1 due to dominance of escape mutations. *Nature*. 517:381–385. <https://doi.org/10.1038/nature14053>
- Desch, A.N., S.L. Gibbings, R. Goyal, R. Kolde, J. Bednarek, T. Bruno, J.E. Slansky, J. Jacobelli, R. Mason, Y. Ito, et al. 2016. Flow Cytometric Analysis of Mononuclear Phagocytes in Nondiseased Human Lung and Lung-Draining Lymph Nodes. *Am. J. Respir. Crit. Care Med.* 193:614–626. <https://doi.org/10.1164/rccm.201507-1376OC>
- Dranoff, G., A.D. Crawford, M. Sadelain, B. Ream, A. Rashid, R.T. Bronson, G.R. Dickersin, C.J. Bachurski, E.L. Mark, J.A. Whitsett, et al. 1994. Involvement of granulocyte-macrophage colony-stimulating factor in pulmonary homeostasis. *Science*. 264:713–716. <https://doi.org/10.1126/science.8171324>
- Eguíluz-Gracia, I., H.H. Schultz, L.I. Sikkeland, E. Danilova, A.M. Holm, C.J. Pronk, W.W. Agace, M. Iversen, C. Andersen, F.L. Jahnsen, and E.S. Baekkevold. 2016. Long-term persistence of human donor alveolar macrophages in lung transplant recipients. *Thorax*. 71:1006–1011. <https://doi.org/10.1136/thoraxjnl-2016-208292>
- Epelman, S., K.J. Lavine, and G.J. Randolph. 2014. Origin and functions of tissue macrophages. *Immunity*. 41:21–35. <https://doi.org/10.1016/j.immuni.2014.06.013>
- Evren, E., E. Ringqvist, and T. Willinger. 2020. Origin and ontogeny of lung macrophages: from mice to humans. *Immunology*. 160:126–138. <https://doi.org/10.1111/imm.13154>
- Evren, E., E. Ringqvist, K.P. Tripathi, N. Sleiers, I.C. Rives, A. Alisjahbana, Y. Gao, D. Sarhan, T. Halle, C. Sorini, et al. 2021. Distinct developmental pathways from blood monocytes generate human lung macrophage diversity. *Immunity*. 54:259–275.e7. <https://doi.org/10.1016/j.immuni.2020.12.003>
- Garbi, N., and B.N. Lambrecht. 2017. Location, function, and ontogeny of pulmonary macrophages during the steady state. *Pflugers Arch.* 469:561–572. <https://doi.org/10.1007/s00424-017-1965-3>
- Gibbings, S.L., R. Goyal, A.N. Desch, S.M. Leach, M. Prabagar, S.M. Atif, D.L. Bratton, W. Janssen, and C.V. Jakubzick. 2015. Transcriptome analysis highlights the conserved difference between embryonic and postnatal-derived alveolar macrophages. *Blood*. 126:1357–1366. <https://doi.org/10.1182/blood-2015-01-624809>
- Ginhoux, F., and M. Guillemin. 2016. Tissue-Resident Macrophage Ontogeny and Homeostasis. *Immunity*. 44:439–449. <https://doi.org/10.1016/j.immuni.2016.02.024>

- Gomez Perdiguerro, E., K. Klapproth, C. Schulz, K. Busch, E. Azzoni, L. Crozet, H. Garner, C. Trouillet, M.F. de Bruijn, F. Geissmann, and H.R. Rodewald. 2015. Tissue-resident macrophages originate from yolk-sac-derived erythro-myeloid progenitors. *Nature*. 518:547–551. <https://doi.org/10.1038/nature13989>
- Grant, R.A., L. Morales-Nebreda, N.S. Markov, S. Swaminathan, M. Querrey, E.R. Guzman, D.A. Abbott, H.K. Donnelly, A. Donayre, I.A. Goldberg, et al. NU SCRIPT Study Investigators. 2021. Circuits between infected macrophages and T cells in SARS-CoV-2 pneumonia. *Nature*. 590: 635–641. <https://doi.org/10.1038/s41586-020-03148-w>
- Gschwend, J., S.P.M. Sherman, F. Ridder, X. Feng, H.E. Liang, R.M. Locksley, B. Becher, and C. Schneider. 2021. Alveolar macrophages rely on GM-CSF from alveolar epithelial type 2 cells before and after birth. *J. Exp. Med.* 218:e20210745. <https://doi.org/10.1084/jem.20210745>
- Guilliams, M., and F.R. Svedberg. 2021. Does tissue imprinting restrict macrophage plasticity? *Nat. Immunol.* 22:118–127. <https://doi.org/10.1038/s41590-020-00849-2>
- Guilliams, M., I. De Kleer, S. Henri, S. Post, L. Vanhoutte, S. De Prijck, K. Deswarte, B. Malissen, H. Hammad, and B.N. Lambrecht. 2013. Alveolar macrophages develop from fetal monocytes that differentiate into long-lived cells in the first week of life via GM-CSF. *J. Exp. Med.* 210: 1977–1992. <https://doi.org/10.1084/jem.20131199>
- Guilliams, M., A. Mildner, and S. Yona. 2018. Developmental and Functional Heterogeneity of Monocytes. *Immunity*. 49:595–613. <https://doi.org/10.1016/j.immuni.2018.10.005>
- Guilliams, M., G.R. Thierry, J. Bonnardel, and M. Bajenoff. 2020. Establishment and Maintenance of the Macrophage Niche. *Immunity*. 52:434–451. <https://doi.org/10.1016/j.immuni.2020.02.015>
- Hashimoto, D., A. Chow, C. Noizat, P. Teo, M.B. Beasley, M. Leboeuf, C.D. Becker, P. See, J. Price, D. Lucas, et al. 2013. Tissue-resident macrophages self-maintain locally throughout adult life with minimal contribution from circulating monocytes. *Immunity*. 38:792–804. <https://doi.org/10.1016/j.immuni.2013.04.004>
- Hoeffel, G., J. Chen, Y. Lavin, D. Low, F.F. Almeida, P. See, A.E. Beaudin, J. Lum, I. Low, E.C. Forsberg, et al. 2015. C-Myb(+) erythro-myeloid progenitor-derived fetal monocytes give rise to adult tissue-resident macrophages. *Immunity*. 42:665–678. <https://doi.org/10.1016/j.immuni.2015.03.011>
- Hussell, T., and T.J. Bell. 2014. Alveolar macrophages: plasticity in a tissue-specific context. *Nat. Rev. Immunol.* 14:81–93. <https://doi.org/10.1038/nri3600>
- Jardine, L., S. Webb, I. Goh, M. Quiroga Londoño, G. Reynolds, M. Mather, B. Olabi, E. Stephenson, R.A. Botting, D. Horsfall, et al. 2021. Blood and immune development in human fetal bone marrow and Down syndrome. *Nature*. 598:327–331. <https://doi.org/10.1038/s41586-021-03929-x>
- Jenkins, S.J., and J.E. Allen. 2021. The expanding world of tissue-resident macrophages. *Eur. J. Immunol.* 51:1882–1896. <https://doi.org/10.1002/eji.202048881>
- Joshi, N., J.M. Walter, and A.V. Misharin. 2018. Alveolar Macrophages. *Cell. Immunol.* 330:86–90. <https://doi.org/10.1016/j.cellimm.2018.01.005>
- Joshi, N., S. Watanabe, R. Verma, R.P. Jablonski, C.I. Chen, P. Cheresch, N.S. Markov, P.A. Reyfman, A.C. McQuattie-Pimentel, L. Sichizya, et al. 2020. A spatially restricted fibrotic niche in pulmonary fibrosis is sustained by M-CSF/M-CSFR signalling in monocyte-derived alveolar macrophages. *Eur. Respir. J.* 55:1900646. <https://doi.org/10.1183/13993003.00646-2019>
- Kawamura, S., N. Onai, F. Miya, T. Sato, T. Tsunoda, K. Kurabayashi, S. Yotsumoto, S. Kuroda, K. Takenaka, K. Akashi, and T. Ohteki. 2017. Identification of a Human Clonogenic Progenitor with Strict Monocyte Differentiation Potential: A Counterpart of Mouse cMoPs. *Immunity*. 46: 835–848.e4. <https://doi.org/10.1016/j.immuni.2017.04.019>
- Kjellström, C., K. Ichimura, X.J. Chen, G.C. Riise, and V.P. Collins. 2000. The origin of alveolar macrophages in the transplanted lung: a longitudinal microsatellite-based study of donor and recipient DNA. *Transplantation*. 69:1984–1986. <https://doi.org/10.1097/00007890-200005150-00046>
- Kopf, M., C. Schneider, and S.P. Nobs. 2015. The development and function of lung-resident macrophages and dendritic cells. *Nat. Immunol.* 16:36–44. <https://doi.org/10.1038/ni.3052>
- Kulikauskaitė, J., and A. Wack. 2020. Teaching Old Dogs New Tricks? The Plasticity of Lung Alveolar Macrophage Subsets. *Trends Immunol.* 41: 864–877. <https://doi.org/10.1016/j.it.2020.08.008>
- Lavin, Y., D. Winter, R. Blecher-Gonen, E. David, H. Keren-Shaul, M. Merad, S. Jung, and I. Amit. 2014. Tissue-resident macrophage enhancer landscapes are shaped by the local microenvironment. *Cell*. 159: 1312–1326. <https://doi.org/10.1016/j.cell.2014.11.018>
- Leach, S.M., S.L. Gibbings, A.D. Tewari, S.M. Atif, B. Vestal, T. Danhorn, W.J. Janssen, T.D. Wager, and C.V. Jakubzick. 2020. Human and Mouse Transcriptome Profiling Identifies Cross-Species Homology in Pulmonary and Lymph Node Mononuclear Phagocytes. *Cell Rep.* 33:108337. <https://doi.org/10.1016/j.celrep.2020.108337>
- Lechner, A.J., I.H. Driver, J. Lee, C.M. Conroy, A. Nagle, R.M. Locksley, and J.R. Rock. 2017. Recruited Monocytes and Type 2 Immunity Promote Lung Regeneration following Pneumonectomy. *Cell Stem Cell*. 21: 120–134.e7. <https://doi.org/10.1016/j.stem.2017.03.024>
- Lee, J., G. Breton, T.Y. Oliveira, Y.J. Zhou, A. Aljoufi, S. Pühr, M.J. Cameron, R.P. Sékaly, M.C. Nussenzweig, and K. Liu. 2015. Restricted dendritic cell and monocyte progenitors in human cord blood and bone marrow. *J. Exp. Med.* 212:385–399. <https://doi.org/10.1084/jem.20141442>
- Li, F., K.M. Okreglicka, L.M. Pohlmeier, C. Schneider, and M. Kopf. 2020. Fetal monocytes possess increased metabolic capacity and replace primitive macrophages in tissue macrophage development. *EMBO J.* 39: e103205. <https://doi.org/10.15252/emj.2019103205>
- Liao, M., Y. Liu, J. Yuan, Y. Wen, G. Xu, J. Zhao, L. Cheng, J. Li, X. Wang, F. Wang, et al. 2020. Single-cell landscape of bronchoalveolar immune cells in patients with COVID-19. *Nat. Med.* 26:842–844. <https://doi.org/10.1038/s41591-020-0901-9>
- Liu, Z., Y. Gu, S. Chakarov, C. Bleriot, I. Kwok, X. Chen, A. Shin, W. Huang, R.J. Dress, C.A. Dutertre, et al. 2019. Fate Mapping via Ms4a3-Expression History Traces Monocyte-Derived Cells. *Cell*. 178: 1509–1525.e19. <https://doi.org/10.1016/j.cell.2019.08.009>
- Machiels, B., M. Dourcy, X. Xiao, J. Javaux, C. Mesnil, C. Sabatel, D. Desmecht, F. Lallemand, P. Martinive, H. Hammad, et al. 2017. A gamma-herpesvirus provides protection against allergic asthma by inducing the replacement of resident alveolar macrophages with regulatory monocytes. *Nat. Immunol.* 18:1310–1320. <https://doi.org/10.1038/ni.3857>
- Mass, E., I. Ballesteros, M. Farlik, F. Halbritter, P. Günther, L. Crozet, C.E. Jacome-Galarza, K. Händler, J. Klughammer, Y. Kobayashi, et al. 2016. Specification of tissue-resident macrophages during organogenesis. *Science*. 353:aaf4238. <https://doi.org/10.1126/science.aaf4238>
- McCubbrey, A.L., L. Barthel, M.P. Mohning, E.F. Redente, K.J. Mould, S.M. Thomas, S.M. Leach, T. Danhorn, S.L. Gibbings, C.V. Jakubzick, et al. 2018. Deletion of c-FLIP from CD11b^{hi} Macrophages Prevents Development of Bleomycin-induced Lung Fibrosis. *Am. J. Respir. Cell Mol. Biol.* 58:66–78. <https://doi.org/10.1165/rcmb.2017-0154OC>
- McQuattie-Pimentel, A.C., Z. Ren, N. Joshi, S. Watanabe, T. Stoeger, M. Chi, Z. Lu, L. Sichizya, R.P. Aillon, C.I. Chen, et al. 2021. The lung microenvironment shapes a dysfunctional response of alveolar macrophages in aging. *J. Clin. Invest.* 131:e140299. <https://doi.org/10.1172/JCI140299>
- Miah, M., I. Goh, and M. Haniffa. 2021. Prenatal Development and Function of Human Mononuclear Phagocytes. *Front. Cell Dev. Biol.* 9:649937. <https://doi.org/10.3389/fcell.2021.649937>
- Misharin, A.V., L. Morales-Nebreda, P.A. Reyfman, C.M. Cuda, J.M. Walter, A.C. McQuattie-Pimentel, C.I. Chen, K.R. Anekalla, N. Joshi, K.J.N. Williams, et al. 2017. Monocyte-derived alveolar macrophages drive lung fibrosis and persist in the lung over the life span. *J. Exp. Med.* 214: 2387–2404. <https://doi.org/10.1084/jem.20162152>
- Morse, C., T. Tabib, J. Sembrat, K.L. Buschur, H.T. Bittar, E. Valenzi, Y. Jiang, D.J. Kass, K. Gibson, W. Chen, et al. 2019. Proliferating SPP1/MERTK-expressing macrophages in idiopathic pulmonary fibrosis. *Eur. Respir. J.* 54:1802441. <https://doi.org/10.1183/13993003.02441-2018>
- Mould, K.J., L. Barthel, M.P. Mohning, S.M. Thomas, A.L. McCubbrey, T. Danhorn, S.M. Leach, T.E. Fingerlin, B.P. O'Connor, J.A. Reisz, et al. 2017. Cell Origin Dictates Programming of Resident versus Recruited Macrophages during Acute Lung Injury. *Am. J. Respir. Cell Mol. Biol.* 57: 294–306. <https://doi.org/10.1165/rcmb.2017-0061OC>
- Mould, K.J., N.D. Jackson, P.M. Henson, M. Seibold, and W.J. Janssen. 2019. Single cell RNA sequencing identifies unique inflammatory airspace macrophage subsets. *JCI Insight*. 4:e126556. <https://doi.org/10.1172/jci.insight.126556>
- Mould, K.J., C.M. Moore, S.A. McManus, A.L. McCubbrey, J.D. McClendon, C.L. Griesmer, P.M. Henson, and W.J. Janssen. 2021. Airspace Macrophages and Monocytes Exist in Transcriptionally Distinct Subsets in Healthy Adults. *Am. J. Respir. Crit. Care Med.* 203:946–956. <https://doi.org/10.1164/rccm.202005-1989OC>
- Mulder, K., A.A. Patel, W.T. Kong, C. Piot, E. Halitzki, G. Dunsmore, S. Khalilnezhad, S.E. Irac, A. Dubuisson, M. Chevrier, et al. 2021. Cross-tissue single-cell landscape of human monocytes and macrophages in health and disease. *Immunity*. 54:1883–1900.e5. <https://doi.org/10.1016/j.immuni.2021.07.007>

- Nayak, D.K., F. Zhou, M. Xu, J. Huang, M. Tsuji, R. Hachem, and T. Mohanakumar. 2016. Long-Term Persistence of Donor Alveolar Macrophages in Human Lung Transplant Recipients That Influences Donor-Specific Immune Responses. *Am. J. Transplant.* 16:2300–2311. <https://doi.org/10.1111/ajt.13819>
- Park, J.E., L. Jardine, B. Gottgens, S.A. Teichmann, and M. Haniffa. 2020. Prenatal development of human immunity. *Science.* 368:600–603. <https://doi.org/10.1126/science.aaz9330>
- Perdiguerro, E.G., and F. Geissmann. 2016. The development and maintenance of resident macrophages. *Nat. Immunol.* 17:2–8. <https://doi.org/10.1038/ni.3341>
- Popescu, D.M., R.A. Botting, E. Stephenson, K. Green, S. Webb, L. Jardine, E.F. Calderbank, K. Polanski, I. Goh, M. Efremova, et al. 2019. Decoding human fetal liver haematopoiesis. *Nature.* 574:365–371. <https://doi.org/10.1038/s41586-019-1652-y>
- Puttur, F., L.G. Gregory, and C.M. Lloyd. 2019. Airway macrophages as the guardians of tissue repair in the lung. *Immunol. Cell Biol.* 97:246–257. <https://doi.org/10.1111/imcb.12235>
- Rantakari, P., N. Jäppinen, E. Lokka, E. Mokkala, H. Gerke, E. Peuhu, J. Ivaska, K. Elima, K. Auvinen, and M. Salmi. 2016. Fetal liver endothelium regulates the seeding of tissue-resident macrophages. *Nature.* 538:392–396. <https://doi.org/10.1038/nature19814>
- Rongvaux, A., H. Takizawa, T. Strowig, T. Willinger, E.E. Eynon, R.A. Flavell, and M.G. Manz. 2013. Human hemato-lymphoid system mice: current use and future potential for medicine. *Annu. Rev. Immunol.* 31:635–674. <https://doi.org/10.1146/annurev-immunol-032712-095921>
- Rongvaux, A., T. Willinger, J. Martinek, T. Strowig, S.V. Gearty, L.L. Teichmann, Y. Saito, F. Marches, S. Halene, A.K. Palucka, et al. 2014. Development and function of human innate immune cells in a humanized mouse model. *Nat. Biotechnol.* 32:364–372. <https://doi.org/10.1038/nbt.2858>
- Saito, Y., J.M. Ellegast, A. Rafiei, Y. Song, D. Kull, M. Heikenwalder, A. Rongvaux, S. Halene, R.A. Flavell, and M.G. Manz. 2016. Peripheral blood CD34⁺ cells efficiently engraft human cytokine knock-in mice. *Blood.* 128:1829–1833. <https://doi.org/10.1182/blood-2015-10-676452>
- Schneider, C., S.P. Nobs, M. Kurrer, H. Rehrauer, C. Thiele, and M. Kopf. 2014. Induction of the nuclear receptor PPAR- γ by the cytokine GM-CSF is critical for the differentiation of fetal monocytes into alveolar macrophages. *Nat. Immunol.* 15:1026–1037. <https://doi.org/10.1038/ni.3005>
- Sippel, T.R., S. Radtke, T.M. Olsen, H.P. Kiem, and A. Rongvaux. 2019. Human hematopoietic stem cell maintenance and myeloid cell development in next-generation humanized mouse models. *Blood Adv.* 3:268–274. <https://doi.org/10.1182/bloodadvances.2018023887>
- Soucie, E.L., Z. Weng, L. Geirsdóttir, K. Molawi, J. Maurizio, R. Fenouil, N. Mossadegh-Keller, G. Gimenez, L. VanHille, M. Beniazza, et al. 2016. Lineage-specific enhancers activate self-renewal genes in macrophages and embryonic stem cells. *Science.* 351:aad5510. <https://doi.org/10.1126/science.aad5510>
- Trapnell, B.C., K. Nakata, F. Bonella, I. Campo, M. Griese, J. Hamilton, T. Wang, C. Morgan, V. Cottin, and C. McCarthy. 2019. Pulmonary alveolar proteinosis. *Nat. Rev. Dis. Primers.* 5:16. <https://doi.org/10.1038/s41572-019-0066-3>
- Travaglini, K.J., A.N. Nabhan, L. Penland, R. Sinha, A. Gillich, R.V. Sit, S. Chang, S.D. Conley, Y. Mori, J. Seita, et al. 2020. A molecular cell atlas of the human lung from single-cell RNA sequencing. *Nature.* 587:619–625. <https://doi.org/10.1038/s41586-020-2922-4>
- van de Laar, L., W. Saelens, S. De Prijck, L. Martens, C.L. Scott, G. Van Isterdael, E. Hoffmann, R. Beyaert, Y. Saeys, B.N. Lambrecht, and M. Guillems. 2016. Yolk Sac Macrophages, Fetal Liver, and Adult Monocytes Can Colonize an Empty Niche and Develop into Functional Tissue-Resident Macrophages. *Immunity.* 44:755–768. <https://doi.org/10.1016/j.immuni.2016.02.017>
- Varol, C., A. Mildner, and S. Jung. 2015. Macrophages: development and tissue specialization. *Annu. Rev. Immunol.* 33:643–675. <https://doi.org/10.1146/annurev-immunol-032414-112220>
- Vieira Braga, F.A., G. Kar, M. Berg, O.A. Carpaij, K. Polanski, L.M. Simon, S. Brouwer, T. Gomes, L. Hesse, J. Jiang, et al. 2019. A cellular census of human lungs identifies novel cell states in health and in asthma. *Nat. Med.* 25:1153–1163. <https://doi.org/10.1038/s41591-019-0468-5>
- Wauters, E., P. Van Mol, A.D. Garg, S. Jansen, Y. Van Herck, L. Vanderbeke, A. Bassez, B. Boeckx, B. Malengier-Devlies, A. Timmerman, et al. CON-TAGIOUS collaborators. 2021. Discriminating mild from critical COVID-19 by innate and adaptive immune single-cell profiling of bronchoalveolar lavages. *Cell Res.* 31:272–290. <https://doi.org/10.1038/s41422-020-00455-9>
- Willinger, T., A. Rongvaux, T. Strowig, M.G. Manz, and R.A. Flavell. 2011a. Improving human hemato-lymphoid-system mice by cytokine knock-in gene replacement. *Trends Immunol.* 32:321–327. <https://doi.org/10.1016/j.it.2011.04.005>
- Willinger, T., A. Rongvaux, H. Takizawa, G.D. Yancopoulos, D.M. Valenzuela, A.J. Murphy, W. Auerbach, E.E. Eynon, S. Stevens, M.G. Manz, and R.A. Flavell. 2011b. Human IL-3/GM-CSF knock-in mice support human alveolar macrophage development and human immune responses in the lung. *Proc. Natl. Acad. Sci. USA.* 108:2390–2395. <https://doi.org/10.1073/pnas.1019682108>
- Yona, S., K.W. Kim, Y. Wolf, A. Mildner, D. Varol, M. Breker, D. Strauss-Ayali, S. Viukov, M. Guillems, A. Misharin, et al. 2013. Fate mapping reveals origins and dynamics of monocytes and tissue macrophages under homeostasis. *Immunity.* 38:79–91. <https://doi.org/10.1016/j.immuni.2012.12.001>
- Yu, Y.R., D.F. Hotten, Y. Malakhau, E. Volker, A.J. Ghio, P.W. Noble, M. Kraft, J.W. Hollingsworth, M.D. Gunn, and R.M. Tighe. 2016. Flow Cytometric Analysis of Myeloid Cells in Human Blood, Bronchoalveolar Lavage, and Lung Tissues. *Am. J. Respir. Cell Mol. Biol.* 54:13–24. <https://doi.org/10.1165/rcmb.2015-0146OC>
- Yu, X., A. Buttgerit, I. Lelios, S.G. Utz, D. Cansever, B. Becher, and M. Greter. 2017. The Cytokine TGF- β Promotes the Development and Homeostasis of Alveolar Macrophages. *Immunity.* 47:903–912.e4. <https://doi.org/10.1016/j.immuni.2017.10.007>

Supplemental material

Fetal liver

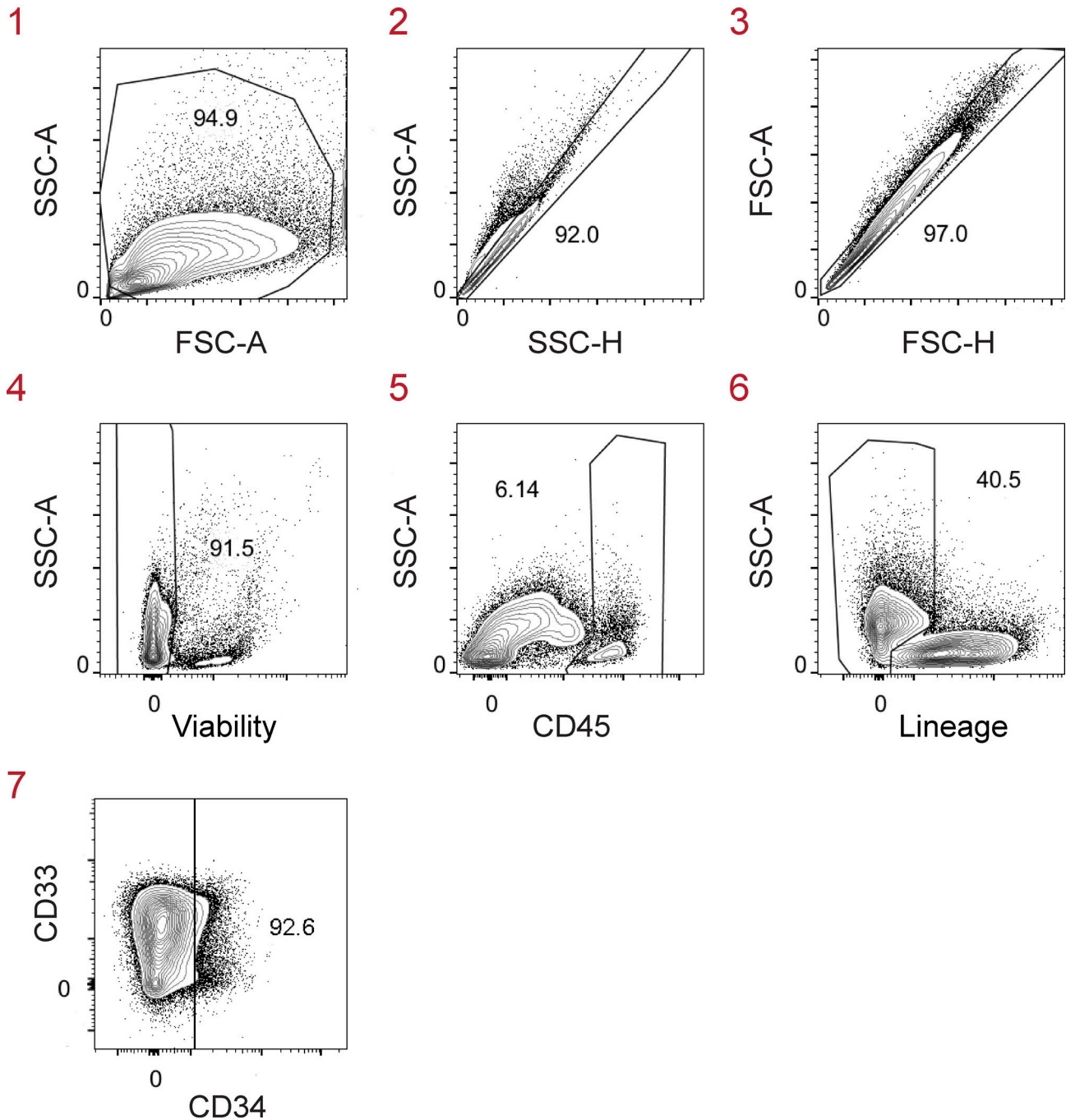


Figure S1. **Gating strategy to identify candidate macrophage precursors in human fetal liver.** Single-cell suspensions from fetal liver (17 wk gestation) were first gated on live CD45⁺Lin⁻CD34⁻ single cells before gating on CD116⁺ cells as shown in Fig. 1 A. Lin markers were CD3, TCRαβ, TCRγδ, CD19, CD20, CD56, CD94, NKp46, and CD66abce. FSC-A, forward scatter area; FSC-H, forward scatter height; SSC-A, side scatter area; SSC-H, side scatter height. Data are representative of two independent experiments with 12 fetal liver samples at 15–23 wk of gestation. The red numbers indicate the order of the flow cytometry plots (sequential gating of cells).

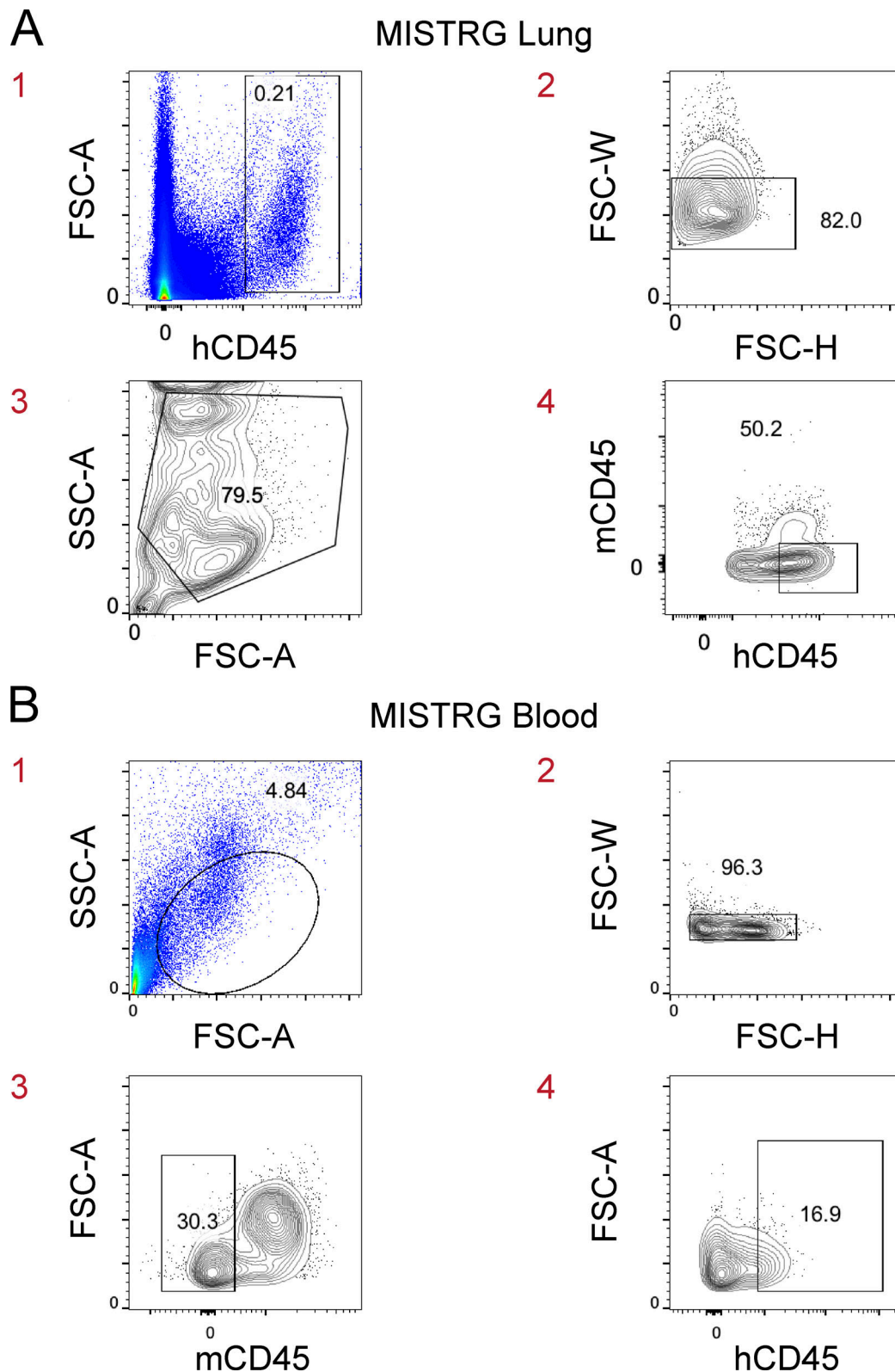


Figure S2. **Gating strategy to identify human hematopoietic cells in MISTRG mice.** (A) Single-cell suspensions from the lung of MISTRG mice were gated on human CD45⁺ single cells before gating on human lung macrophages in Fig. 3, B and C, Fig. 4, B and C, and Fig. 5 C. hCD45, human CD45; mCD45, mouse CD45. (B) Blood cells from MISTRG mice were gated on human CD45⁺ single cells before gating on circulating human macrophage precursors in Fig. 4 G and Fig. 6 A. FSC-A, forward scatter area; FSC-H, forward scatter height; FSC-W, forward scatter width; hCD45, human CD45; mCD45, mouse CD45; SSC-A, side scatter area. Data (A) show one lung sample representative of three to five samples (individual mice) from three independent experiments. Data (B) show one blood sample representative of seven to nine samples (individual mice) from two independent experiments. The red numbers indicate the order of the flow cytometry plots (sequential gating of cells).

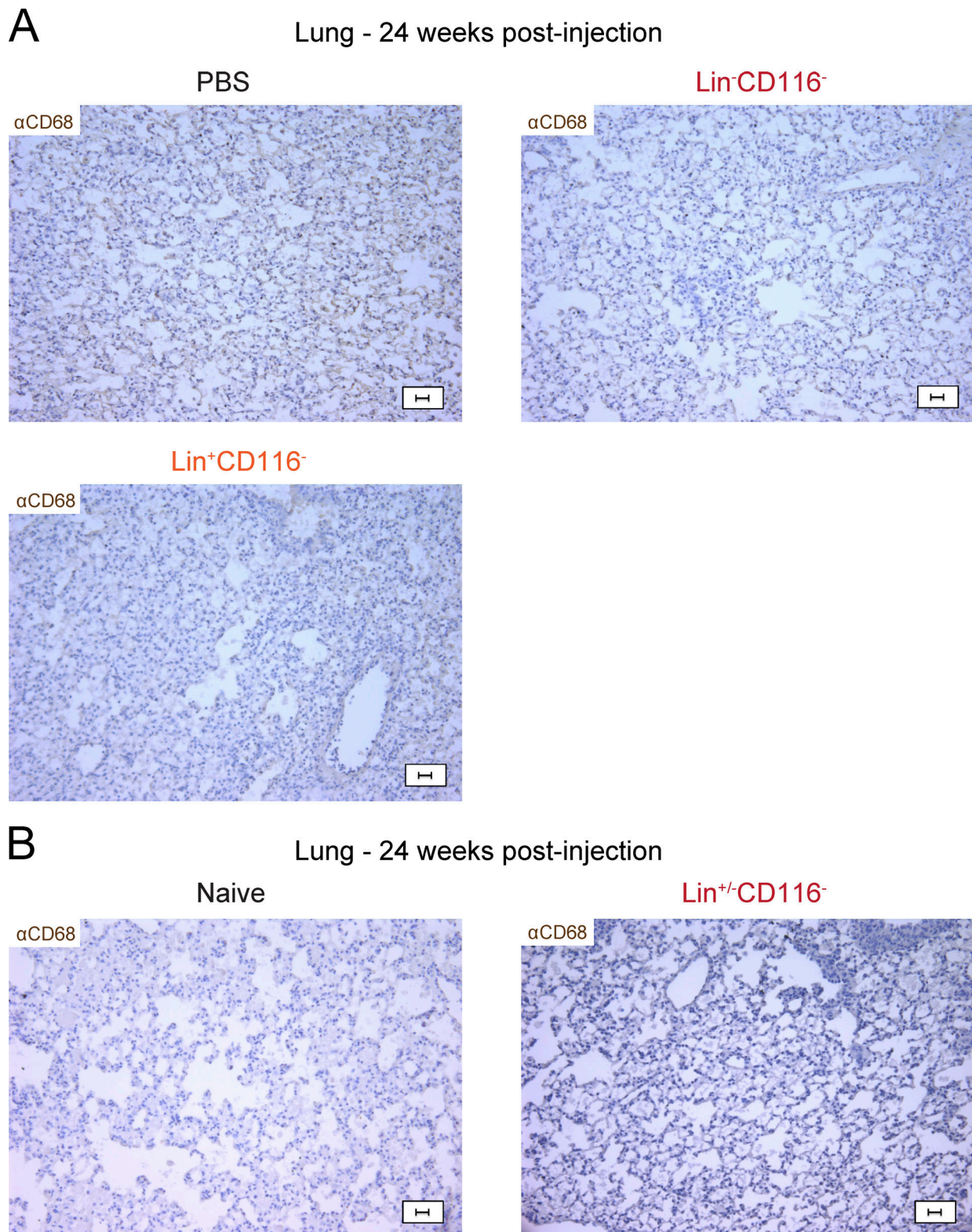


Figure S3. **Controls for immunohistochemistry of lung sections. (A and B)** Immunohistochemistry of lung sections from MISTRG mice 24 wk after intranasal (A) or intrahepatic (B) transplantation with the indicated cell populations (as in Fig. 3 E and Fig. 4 E). Control mice received PBS or no cells (naive). Lung sections were stained with anti-human CD68 antibody (brown). Scale bars are 20 μm . αCD68 , anti-CD68. Data (A and B) show one lung sample representative of three to four samples (individual mice) from three independent experiments (A) or representative of two samples (individual mice) from two independent experiments (B).

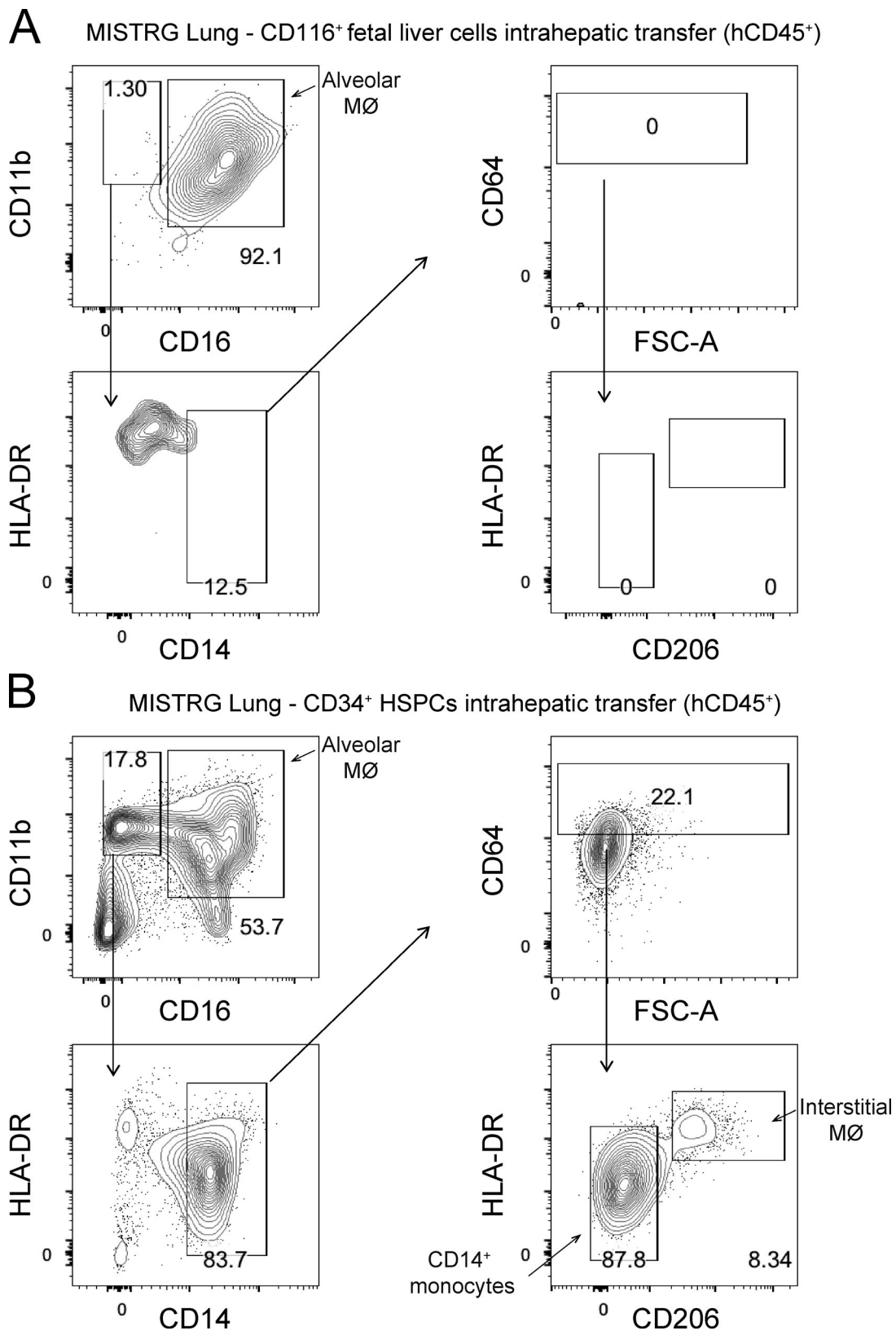


Figure S4. **Human interstitial lung macrophages do not develop in MISTRG mice transplanted with CD116⁺ fetal liver cells. (A and B)** Flow cytometry of human interstitial macrophages in lung tissue from MISTRG mice 24 wk after transplantation with human CD116⁺ fetal liver cells (A) or CD34⁺ HSPCs (B). Interstitial lung macrophages were gated as CD45⁺CD11b⁺CD14⁺CD16⁻CD64⁺CD206⁺HLA-DR⁺ cells. FSC-A, forward scatter area; hCD45, human CD45; MØ, macrophages. Data (A and B) show one lung sample representative of three to five samples (individual mice) per group from three independent experiments.

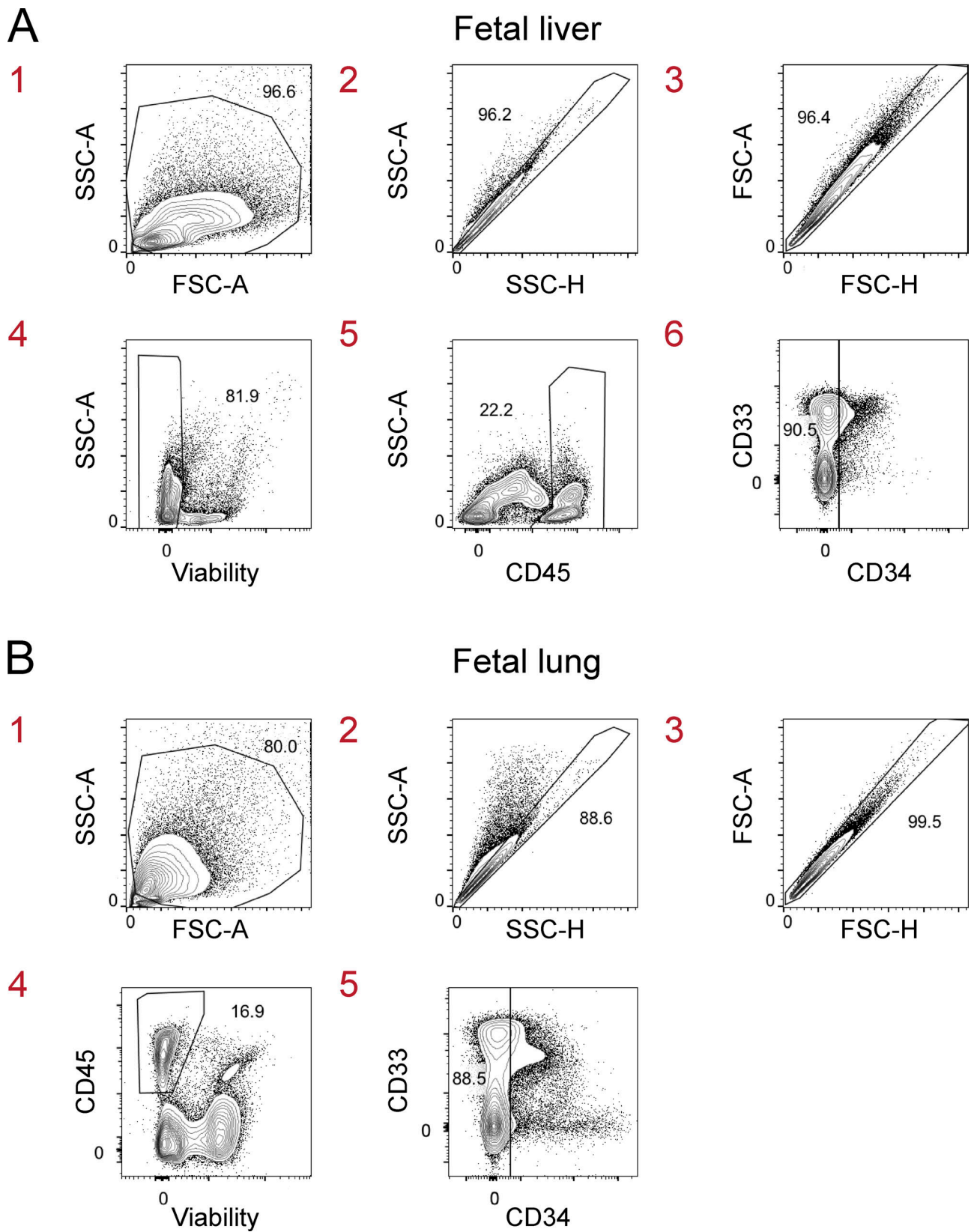


Figure S5. **Gating strategy to identify macrophage precursors in human fetal liver and lung. (A and B)** Single-cell suspensions from human fetal liver (A) and lung (B) at wk 21 and 22 of gestation, respectively, were first gated on live CD45⁺CD34⁻ single cells before gating on macrophage precursors in Fig. 7, A and B. FSC-A, forward scatter area; FSC-H, forward scatter height; SSC-A, side scatter area; SSC-H, side scatter height. Data are representative of two independent experiments. Data (A and B) are representative of two independent experiments with 12 fetal liver and lung samples at 15–23 wk of gestation. The red numbers indicate the order of the flow cytometry plots (sequential gating of cells).

Table S1 and Table S2 are provided online as separate Excel files. Table S1 shows gene expression profiles of human CD14⁺ blood monocytes, CD116⁺CD64⁺ fetal liver monocytes, and CD116⁺CD64⁻ fetal alveolar macrophage (AM) precursors. Table S2 shows gene expression profiles of human lung macrophages derived from CD116⁺CD64⁺ fetal monocytes, CD116⁺CD64⁻ fetal precursors, and CD34⁺ HSPCs in MISTRG mice.

Annex 3

Dichotomous metabolic networks govern human ILC2 proliferation and function

Laura Surace, Jean-Marc Doisne, Carys A. Croft, Anna Thaller, Pedro Escoll, Solenne Marie, Natalia Petrosevoli, Vincent Guillemot, Valerie Dardalhon, Davide Topazio, Antonia Cama, Carmen Buchrieser, Naomi Taylor, Ido Amit, Olimpia Musumeci and James P. Di Santo

Published on the 22nd of October 2021

Journal: Nature Immunology



OPEN

Dichotomous metabolic networks govern human ILC2 proliferation and function

Laura Surace¹, Jean-Marc Doisne¹, Carys A. Croft^{1,2}, Anna Thaller^{1,2}, Pedro Escoll³, Solenne Marie¹, Natalia Petrosevoli⁴, Vincent Guillemot⁴, Valerie Dardalhon⁵, Davide Topazio⁶, Antonia Cama⁷, Carmen Buchrieser³, Naomi Taylor⁵, Ido Amit⁸, Olimpia Musumeci⁹ and James P. Di Santo¹✉

Group 2 innate lymphoid cells (ILC2s) represent innate homologs of type 2 helper T cells (T_H2) that participate in immune defense and tissue homeostasis through production of type 2 cytokines. While T lymphocytes metabolically adapt to micro-environmental changes, knowledge of human ILC2 metabolism is limited, and its key regulators are unknown. Here, we show that circulating 'naive' ILC2s have an unexpected metabolic profile with a higher level of oxidative phosphorylation (OXPHOS) than natural killer (NK) cells. Accordingly, ILC2s are severely reduced in individuals with mitochondrial disease (MD) and impaired OXPHOS. Metabolomic and nutrient receptor analysis revealed ILC2 uptake of amino acids to sustain OXPHOS at steady state. Following activation with interleukin-33 (IL-33), ILC2s became highly proliferative, relying on glycolysis and mammalian target of rapamycin (mTOR) to produce IL-13 while continuing to fuel OXPHOS with amino acids to maintain cellular fitness and proliferation. Our results suggest that proliferation and function are metabolically uncoupled in human ILC2s, offering new strategies to target ILC2s in disease settings.

ILCs have important roles in systemic as well as local tissue immunity and are involved in early immune responsiveness and regenerative processes that restore homeostasis^{1–3}. Five ILC subsets (ILC1, ILC2, ILC3, lymphoid tissue inducer cells (LTI) and NK cells) have been described both in mice and humans based on their transcription factor dependency and signature cytokine production^{4–10}. ILC2s rely on the transcription factor GATA-3 for development and for regulation of the expression of type 2 cytokines, including IL-5, IL-9 and IL-13, and amphiregulin in response to alarmins, such as IL-33 (refs. ^{11–15}). ILC2s reside mostly in barrier tissues; however, they can also enter the circulation and traffic between tissues^{16–20}. In mice, two subsets have been identified: the tissue-resident natural ILC2s (nILC2s) and the inflammatory ILC2s (iILC2s), which are generated following the induction of type 2 inflammation in response to IL-25 and have the capacity to migrate^{21–23}. Whether this dichotomy exists in humans is still a matter of debate. Human circulating ILC2s are described as CD45RA⁺ naive cells, which reside in a resting state and are then recruited into tissues to become activated^{17,24}. Circulating and tissue-resident human ILC2s have

heterogeneous phenotypes and functions^{1,7,25}, but their key regulators remain poorly defined.

Mitochondria play a central role in cellular metabolism and are integral to a functional immune response²⁶. Immunometabolism studies on T cells have defined specific metabolic programs (glycolysis and OXPHOS) following activation and differentiation^{27–31}. Metabolite tracing revealed that activated T cells are preferentially glycolytic and take up glutamine to replenish tricarboxylic acid (TCA) cycle intermediates during cell proliferation and cytokine production³². By contrast, memory T cells exhibit a metabolic switch to fatty acid (FA) metabolism, mitochondria fusion and increased respiration^{33–35}. However, single-cell metabolic flux analysis revisited this concept of a direct naive-to-activated T cell metabolic switch, showing that naive T cells are metabolically heterogeneous and explore 'metabolic checkpoints' before engaging into a specific program, which would then dictate downstream function³⁰. While ILC2s have been reported to rely on nutrients other than glucose, including FA^{36,37} and arginine³⁸, it is not known how different metabolic identities in ILC2s are generated following activation and linked to their biological roles. Here, we show that circulating naive human ILC2s reside in a highly active metabolic state relying on branched chain amino acids (BCAAs) and arginine to support mitochondrial OXPHOS. Following activation, ILC2s leverage their enhanced amino acid metabolism for rapid proliferation but engage glycolysis for effector cytokine production. The independent regulation of proliferation and effector function by dichotomous metabolic pathways opens avenues for manipulating ILC2s in disease settings.

We used MitoTracker Green FM and tetramethylrhodamine (TMRM) staining as described in ref. ³⁹ to assess mitochondrial mass and membrane polarization ($\Delta\psi_m$) in human blood ILC2s isolated from healthy donors. CD56⁺CD16⁺ NK^{dim} cells (Extended Data Fig. 1a,b) were used as an ILC reference for comparison. Previous studies suggested that blood ILC2s were naive^{17,24}; however, fluorescence-activated cell sorting (FACS) analysis revealed that they have two times the mitochondrial mass of NK^{dim} cells (Fig. 1a). Despite heterogeneity across donors (Extended Data Fig. 1c), TMRM intensity and TMRM/MitoTracker ratios were consistently higher in ILC2s at steady state (Fig. 1a). As mitochondria fission and

¹Innate Immunity Unit, Institut Pasteur, Inserm U1223, Paris, France. ²Université de Paris, Sorbonne Paris Cité, Paris, France. ³Biology of Intracellular Bacteria Unit, Institut Pasteur, CNRS UMR 3525, Paris, France. ⁴Bioinformatics and Biostatistics Hub, Center of Bioinformatics, Biostatistics, and Integrative Biology, Institut Pasteur, Paris, France. ⁵Institut de Génétique Moléculaire de Montpellier, University of Montpellier, CNRS, Montpellier, France. ⁶Department of Otolaryngology, Hospital 'Mazzini', Teramo, Italy. ⁷Department of Maxillofacial and Otolaryngology, Hospital 'F. Renzetti', Lanciano, Italy. ⁸Department of Immunology, Weizmann Institute of Science, Rehovot, Israel. ⁹Unit of Neurology and Neuromuscular Disorders, Department of Clinical and Experimental Medicine, University of Messina, Messina, Italy. ✉e-mail: james.di-santo@pasteur.fr

fusion are associated with glycolysis and OXPHOS, respectively⁴⁰, we studied mitochondrial morphology and confirmed that ILC2s have higher mitochondrial mass and polarization than that observed in NK cells and they present fused mitochondria (Extended Data Fig. 1d,e). Because of their relative scarcity in blood, we could not monitor real-time ILC2 oxygen consumption or glycolytic rates. Instead, we measured ATP and ADP by mass spectrometry. We found that circulating ILC2s have high cytosolic ATP/ADP ratios compared to that observed in NK^{dim} cells (Extended Data Fig. 1f and Supplementary Data 1), consistent with enhanced mitochondrial function and inhibition of glycolysis. Memory T cells have highly polarized mitochondria and enhanced OXPHOS compared to naive T cells^{27–41}. When comparing TMRM and MitoTracker patterns in ILC2s versus in naive and central/effector memory CD4⁺ T cell subsets (Extended Data Fig. 2a), ILC2s showed a distinct mitochondrial signature, suggesting exposure to environmental signals.

We next assessed the bioenergetic profile of tissue ILC2s. Despite their scarcity (Extended Data Fig. 2b), tonsil ILC2s appeared to have similar phenotypic and functional profiles as their blood counterparts²⁷. Tonsil ILC2s (detected as Lin⁻CD127⁺CD161⁺GATA-3⁺ST2⁺ cells; Extended Data Fig. 2c–e) showed similar mitochondria polarization and mass as blood ILC2s (Extended Data Fig. 2f), suggesting a close metabolic relationship. One explanation is that some tonsil ILC2s may be blood derived and not (yet) affected metabolically by local environmental signals, which could include IL-2, IL-7, IL-33 and/or other cytokines.

Individuals with MDs (impaired OXPHOS) have a twofold reduction in frequencies of blood NK^{dim} cells and a preferential loss of long-lived ‘memory-like’ NK^{dim} cells³⁹. Reductions in blood ILC2s in individuals with MDs were even more profound (about 80%) (Fig. 1b and Extended Data Fig. 3a), while other lymphoid subsets (CD4⁺ and CD8⁺ T cells) were less affected (Extended Data Fig. 3b). Interestingly, residual ILC2s in individuals with MDs showed decreased GATA-3 expression (Fig. 1c), decreased mitochondrial mass and polarization (Fig. 1d) and more Annexin-V⁺ cells (Extended Data Fig. 3c), suggesting a requirement for mitochondrial function in ILC2 homeostasis.

As defects in components of the mitochondrial ETC underlie MDs in affected individuals (Supplementary Table 1), we corroborated these findings by exposing blood ILC2s to ETC inhibitors (Extended Data Fig. 3d,e). Inhibition of complexes I (rotenone) and III (antimycin A) significantly decreased the percentage of MitoTracker⁺TMRM⁺ cells (Fig. 1e,f) and impaired membrane potential, but not mitochondrial mass, in both ILC2s and NK^{dim} cells (Fig. 1g and Extended Data Fig. 3e). We observed that rotenone and antimycin A, but not complex II inhibition (TTFA), strongly impaired ILC2 survival, whereas NK^{dim} cells were largely unaffected (Fig. 1h). These results further support the essential role for active ETC complex I and complex III for survival of blood ILC2s.

We next purified ILC2s and analyzed the cellular metabolome using high-resolution mass spectrometry (Supplementary Data 1). Pathway analysis revealed an enrichment in metabolites from

arginine, BCAAs (valine, leucine/isoleucine) and glutamine metabolism (Extended Data Fig. 4a). Valine and isoleucine were the most abundant amino acids in circulating ILC2s, followed by arginine and glutamate (Fig. 2a). Arginine and glutamine/glutamate have been described to play a role in lymphocyte proliferation^{38,41,42}, while BCAAs are essential amino acids required for mTOR activation⁴³. We detected enhanced expression of *SLC3A2* (light subunit of the LAT1 receptor) and *SLC43A2* (LAT4) in ILC2s (Fig. 2b). LAT1 and LAT4 preferentially transport BCAAs. Steady-state blood ILC2s showed high surface expression of CD98 (LAT1) but not GLUT1 (glucose transporter) or CD36 (FA transporter). ASCT2 (glutamine transporter) was also highly expressed (Fig. 2c), providing an explanation for the high glutamate levels observed in circulating ILC2s (Fig. 2c). We found a similar pattern of nutrient transporter expression on tonsil ILC2s (Extended Data Fig. 4b).

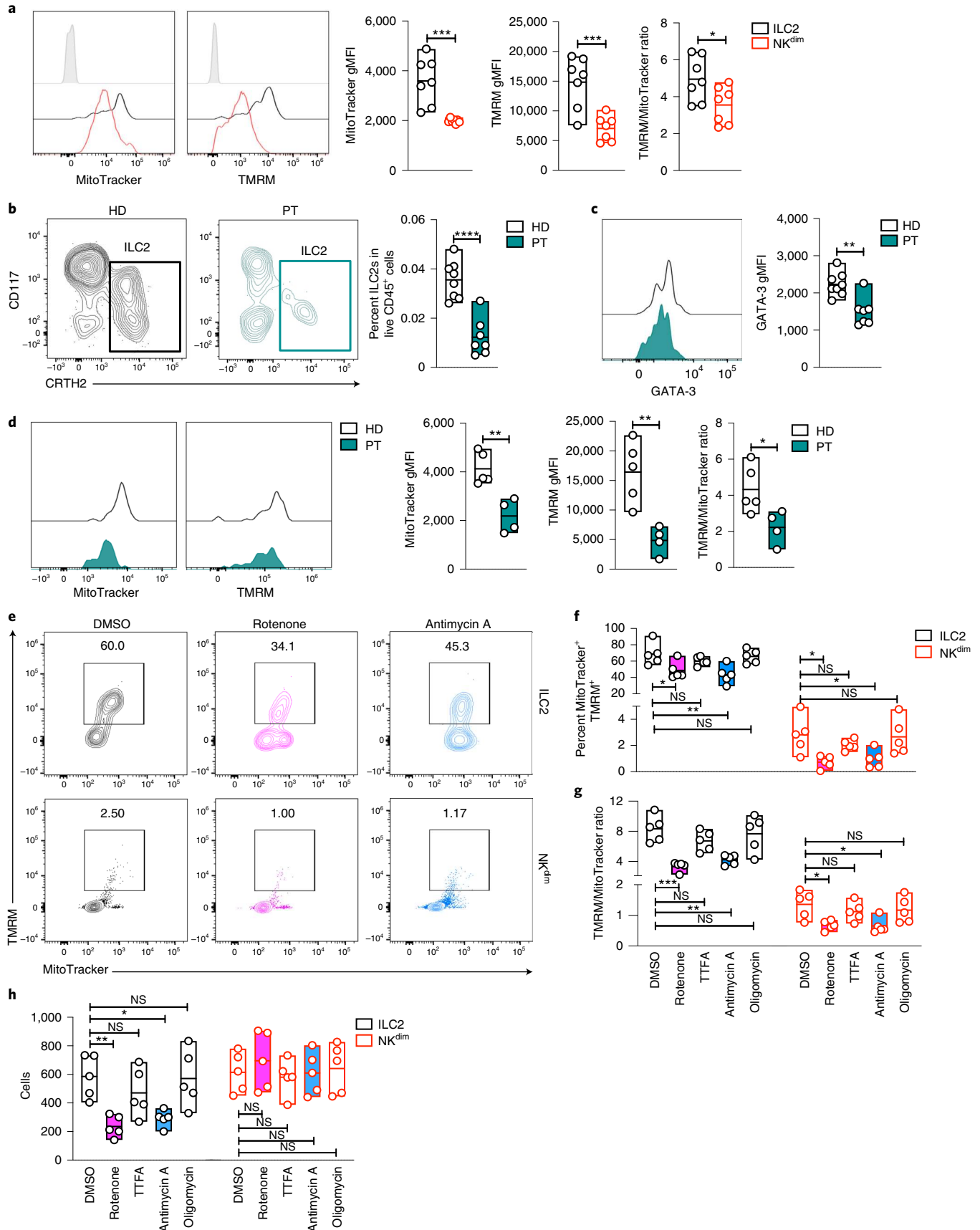
Pharmacological inhibition of glycolysis (2DG), arginase-1 (nor-NOHA), glutamine conversion to glutamate (BPTES) and BCAA transaminase that converts BCAA into glutamate (BCATi) (Fig. 2d) did not impact ILC2 cell number at the concentration used (Extended Data Fig. 4c). However, inhibition of arginase-1 and BCAT resulted in a reduced percentage of MitoTracker⁺TMRM⁺ ILC2s (Fig. 2e,f), with a significant reduction in mitochondrial $\Delta\psi_m$ (Extended Data Fig. 4d). The TMRM-to-MitoTracker ratio was also decreased (Fig. 2g), suggesting an impact on OXPHOS more than mitochondria remodeling or biogenesis. Given the observed heterogeneity in freshly sorted ILC2s (Extended Data Fig. 1c), we analyzed individual ILC2 TMRM profiles after treatment with OXPHOS inhibitors. Responses were uniform (Extended Data Fig. 4e), suggesting that the dependence of circulating ILC2s on OXPHOS/oxygen consumption and amino acids represents a fundamental property required to sustain mitochondrial activity. Corroborating these findings, we found upregulation of enzymes involved in the TCA cycle but low expression of enzymes involved in glycolysis and FA oxidation (Extended Data Fig. 5 and Supplementary Data 2). We also observed upregulation of enzymes involved in the conversion of BCAAs into glutamate and acetyl-CoA as well as upregulation of arginase-1 and ornithine aminotransferase, consistent with the role of BCAAs and arginine in fueling the TCA cycle (Extended Data Fig. 5) also described in differentiated T cells⁴⁴. Together, our data show that circulating ILC2s are not in a resting metabolic state but already show elevated profiles characterized by increased BCAA and arginine levels that sustain OXPHOS required for cell fitness and survival.

To gain insight into the metabolic changes that circulating ILC2s undergo following exposure to tissue-derived cytokines, we cultured sorted blood ILC2s with IL-2 and IL-7, which support basal proliferation without activation^{11,45}, or with IL-2, IL-7 and IL-33 that can fully activate ILC2s with robust proliferation and secretion of type 2 cytokines^{11,45,46}. Circulating ILC2s are CRTH2⁺ST2⁻ (Extended Data Fig. 6a), and a combination of IL-2 and IL-7 upregulated the IL-33 receptor (ST2) (Extended Data Fig. 6b,c), allowing IL-33 to exert its effects. Accordingly, IL-33 alone (or the combinations

Fig. 1 | Complex I and III of the electron transport chain (ETC) support ILC2 survival. **a**, TMRM and MitoTracker measurement in freshly sorted ILC2s and NK^{dim} cells. Representative plots show MitoTracker and TMRM geometric mean fluorescence intensity (gMFI) and the ratio between the gMFI of TMRM and MitoTracker ($n = 7$). **b–d**, Comparison of healthy donors (HD; black) and individuals with MD (PT; green). Representative plots show the percentage of ILC2s in live CD45⁺ cells (**b**), GATA-3 gMFI in circulating ILC2s (**c**) (HD = 7; PT = 7) and MitoTracker and TMRM gMFI and the ratio between the geometric mean of TMRM and MitoTracker (**d**) (HD = 5; PT = 4). **e–h**, Freshly sorted ILC2s and NK^{dim} cells were cultured without additional cytokines for 18 h in DMSO, rotenone (1 μ M), antimycin A (1 μ M), 2-thenoyltrifluoroacetone (TTFA; 1 μ M) or oligomycin (1 μ M). Representative TMRM and MitoTracker FACS plots (**e**), percentage of MitoTracker⁺TMRM⁺ cells in live CD45⁺ cells (**f**), the ratio between the geometric mean of TMRM and MitoTracker (**g**) and cell counts calculated by FACS (**h**) are shown ($n = 5$). The data in **a** are representative of five independent experiments with two to five donors each. Each dot in **b** represents one donor. The data in **c** and **d** are representative of two independent experiments with two to five healthy donors and two to four individuals with MD. The data in **e–h** are representative of three independent experiments with at least three donors each. Floating bars in **a–h** indicate the mean, minimum and maximum values within the dataset. Statistics were assessed by one-way analysis of variance (ANOVA) with a Dunnett correction; NS, not significant ($P > 0.05$); * $P < 0.05$; ** $P < 0.01$; *** $P < 0.001$; **** $P < 0.0001$.

of IL-2 and IL-33 or IL-7 and IL-33) did not promote ILC2 proliferation or mitochondria polarization (Extended Data Fig. 6d,e). As expected, basal proliferation in cells treated with IL-2 and IL-7

was enhanced by IL-33 (Fig. 3a), and production of type 2 cytokines was clearly induced (Extended Data Fig. 6f). ILC2s stimulated with IL-2, IL-7 and IL-33 showed an increase in mitochondrial $\Delta\psi_m$



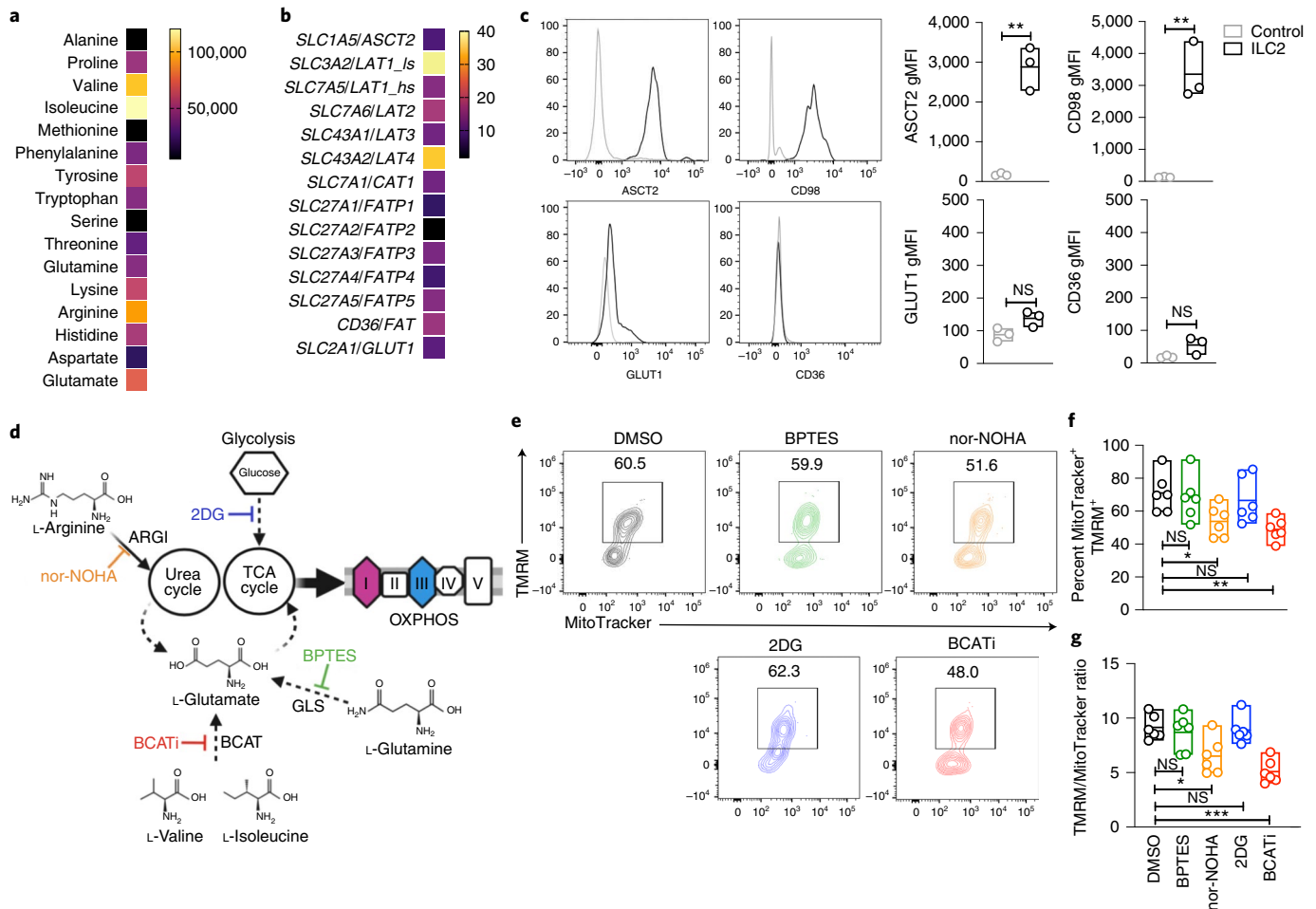


Fig. 2 | BCAA and arginine metabolism fuel OXPPOS in steady-state ILC2s. a, Heat map of amino acid intensities quantified by label-free mass spectrometry in freshly sorted ILC2s. **b**, Nutrient receptor analysis in fresh ILC2s by RNA sequencing (RNA-seq) (median value among three donors; relative expression). **c**, Representative plots of ASCT2 (glutamine transporter), CD98 (LAT1; large amino acid transporter), GLUT1 (glucose transporter) and CD36 (FA receptor) and MFI quantification of each receptor versus isotype control ($n=3$). **d-g**, Freshly sorted ILC2s were cultured without additional cytokines for 18 h in DMSO, *N*^o-hydroxy-nor-arginine (nor-NOHA; 1 μ M), BCAA transferase inhibitor (BCATi; 1 μ M), bis-2-(5-phenylactamido-1,3,4-thiadiazol-2-yl)ethyl sulfide (BPTES; 1 μ M) or 2-deoxy-D-glucose (2DG; 1 μ M) to selectively inhibit the pathways depicted in the schematic in **d**; ARG1, arginase-1; GSL, glutaminase. A representative TMRM and MitoTracker FACS plot in ILC2s (**e**), the percentage of MitoTracker⁺TMRM⁺ cells (**f**) and the ratio between TMRM and MitoTracker MFI (**g**) ($n=6$) are shown. The data in **a** are summarized from four donors, and a minimum of two technical replicates were analyzed per run. Data in **b** were extracted from an RNA-seq dataset, and the median was calculated from the values of three healthy donors. Data in **c** are representative of three independent experiments with at least three donors each. Data in **d-g** are summarized from two independent experiments with at least two donors, and plots are representative of a total of four independent experiments. The floating bars in **c**, **f** and **g** indicate the mean, minimum and maximum values within the dataset. Statistics were assessed by two-tailed t-test (**c**) and one-way ANOVA with Dunnett correction (**f** and **g**); NS, not significant ($P>0.05$); * $P<0.05$; ** $P<0.01$; *** $P<0.001$.

and a slight decrease in mitochondrial mass (Fig. 3b and Extended Data Fig. 6g). Analysis of oxygen consumption rate (OCR) showed that IL-33 increased ILC2 basal and maximal respiration (Fig. 3c and Extended Data Fig. 6h) as well as the spare respiratory capacity (SRC) compared to cells stimulated in IL-2 and IL-7 (Fig. 3d). Together, these results indicate that IL-33-activated ILC2s show enhanced OXPPOS and maintain high cellular fitness despite stresses associated with elevated metabolic activity.

We next cultured ILC2s with or without IL-33 under hypoxic conditions (3% oxygen). We observed that hypoxia led to a decrease in ILC2 survival as well as a loss of GATA-3 and ST2 protein (both gMFI and percentage of positive cells; Fig. 3e-g and Extended Data Fig. 7a). We did not find significant changes in the expression of other ILC2-related proteins or more general lymphoid markers (Extended Data Fig. 7a), suggesting that hypoxia regulates a specific program centered around GATA-3 and ST2. As previously reported,

the HIF-1 α -PKM axis modulates murine ILC2 bioenergetic balance and IL-33 responsiveness⁴⁷. We found enhanced expression of HIF-1 α (Extended Data Fig. 7b) and PKM concomitant with a reduction in GATA-3 and ST2 transcription (Extended Data Fig. 7c) in IL-33-stimulated ILC2s under hypoxic conditions, confirming this HIF-1 α -PKM-ST2 axis in human ILC2s. We further observed that inhibition of ETC complexes I and III impaired survival and accentuated apoptosis of cytokine-activated ILC2s (Fig. 3h and Extended Data Fig. 7d), resulting in a loss of mitochondrial membrane potential and mass (Fig. 3i and Extended Data Fig. 7e). Together, these results confirm the crucial role of ETC function and oxygen in the homeostasis of cytokine-activated ILC2s.

IL-33 stimulated ILC2s to increase their glycolytic capacity (Fig. 3j) while maintaining elevated OXPPOS and SRC (Fig. 3c,d). We hypothesized that ILC2s should rely on different nutrient sources to support their bioenergetic settings. Comparison

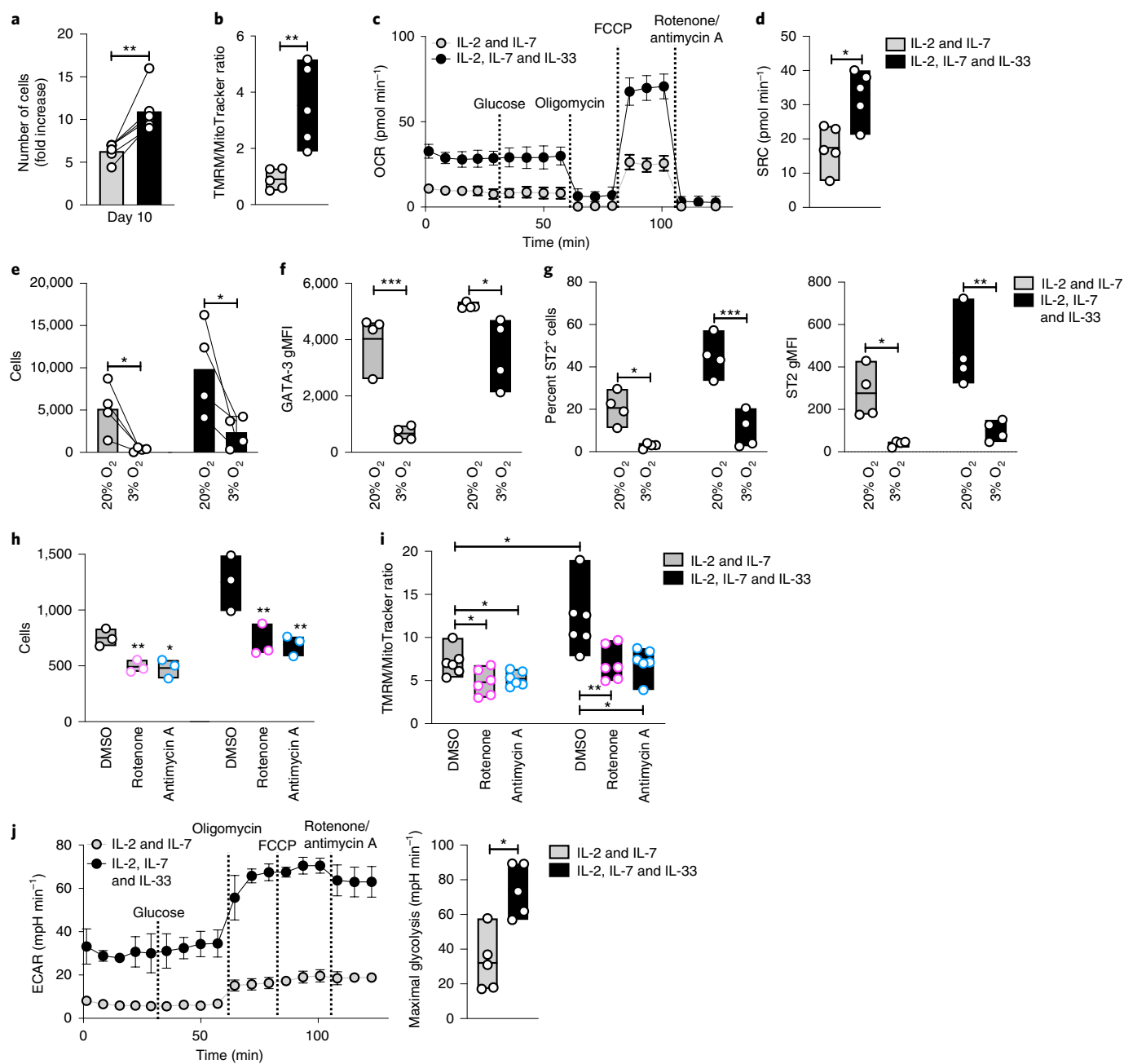


Fig. 3 | Activated ILC2s increase oxygen consumption and glycolytic capacity. **a–d** and **h–j**, ILC2s were expanded for 7 d in the presence of IL-2 and IL-7, and then IL-33 was added or not for 72 h. **a**, Number of cells at day 10 ($n=6$). **b**, Ratio between TMRM and MitoTracker MFI ($n=5$). **c, d**, Seahorse measurements following the addition of glucose, oligomycin, fluoro-carbonyl cyanide phenylhydrazone (FCCP) and a combination of rotenone and antimycin A, including OCR (**c**) and SRC (maximal respiratory capacity after FCCP – basal respiratory capacity) (**d**) ($n=5$). **e–g**, Cells were cultured at 20% or 3% oxygen in IL-2 and IL-7 or IL-2, IL-7 and IL-33 for 5 d. Cell count (**e**), GATA-3 expression (**f**), percent ST2⁺ cells and ST2 expression (**g**) were analyzed by FACS. **h, i**, Cells were treated for the last 18 h with 1 μ M rotenone, 1 μ M antimycin A or DMSO ($n=5$). The total cell counts (**h**) ($n=3$) and the ratio between TMRM and MitoTracker MFI (**i**) ($n=6$) were calculated by FACS. **j**, Extracellular acidification rate (ECAR) and maximal glycolysis were analyzed by Seahorse, performed as in **c** and **d** ($n=5$). Data in **a–d** and **j** are representative of five independent experiments with three to five donors each. Data in **e–i** are representative of three independent experiments with at least three donors each. The bars in **a, c, e** and **j** (left plot) represent mean \pm s.e.m., and the floating bars in **b, d, f–i** and **j** (right plot) indicate the mean, minimum and maximum values within the dataset. Statistics were assessed by two-tailed *t*-test (**a–d** and **j**) and one-way ANOVA with Tukey correction (**e–i**); NS, not significant ($P > 0.05$); * $P < 0.05$; ** $P < 0.01$; *** $P < 0.001$.

of ILC2 metabolomes after cytokine stimulation showed elevated BCAAs and glutamine and a loss of arginine compared to naive ILC2s (Fig. 4a and Supplementary Data 1). Specific changes that accompanied IL-33 exposure included an increase in pyruvate and lactate, consistent with augmented glycolysis (Fig. 3j). IL-33-activated ILC2s showed an increase in the expression of GLUT1, ASCT1 and

ASCT2 compared to naive levels (Fig. 4b), whereas CD98 levels were unchanged, suggesting that amino acid accumulation might not depend on increased uptake from the environment.

We next studied how these different nutrients are required for maintenance of mitochondrial activity in cytokine-activated ILC2s. We found that BCAAs are the main nutrient source maintaining

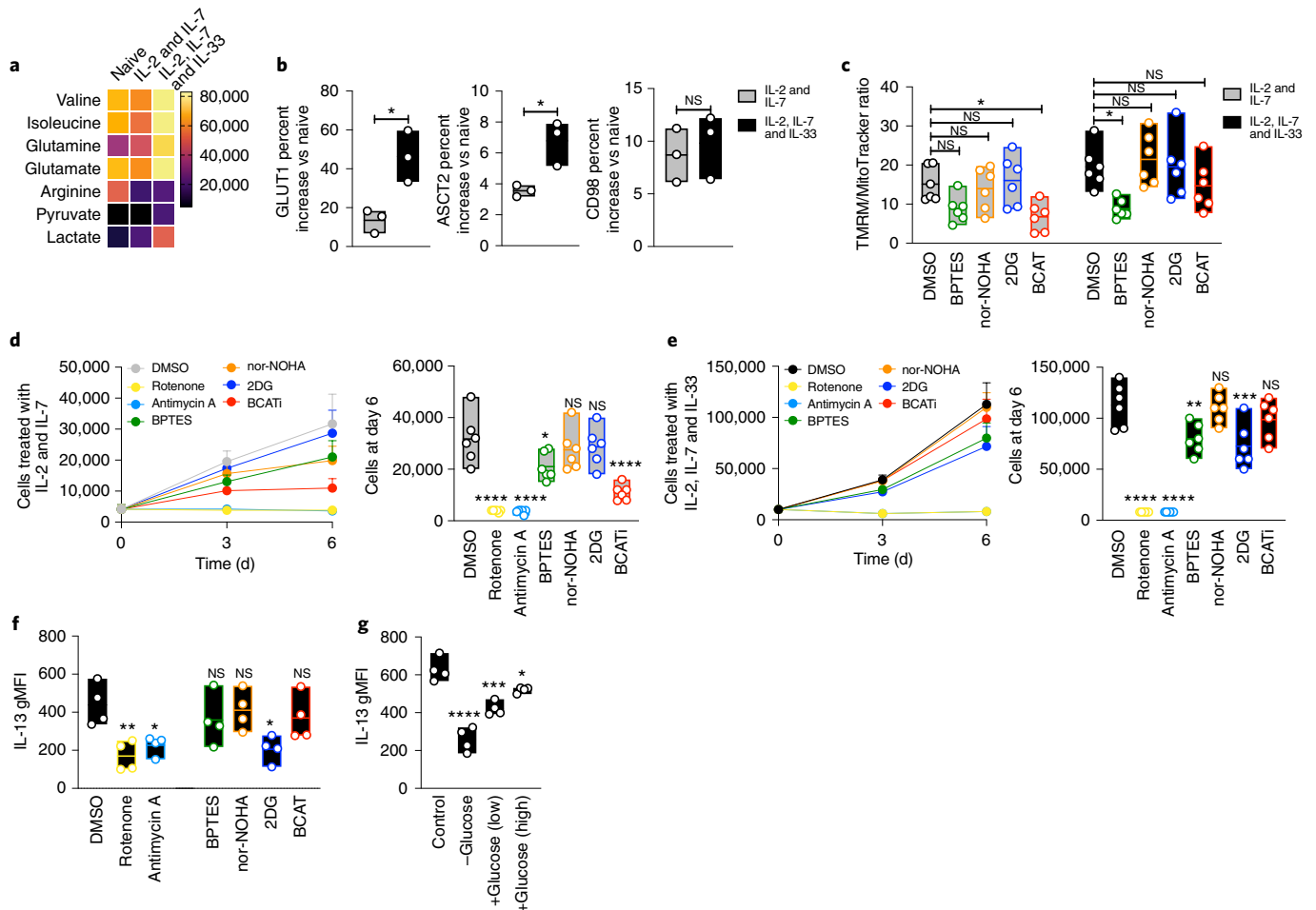


Fig. 4 | IL-33-stimulated ILC2s use amino acid metabolism to sustain cellular fitness and glucose for cytokine production. a–c, ILC2s were expanded for 7 d in IL-2 and IL-7, and IL-33 was added or not for 72 h. **a**, A heat map of amino acid intensities quantified by label-free mass spectrometry in naive cells and in ILC2s treated with either IL-2 and IL-7 or IL-2, IL-7 and IL-33 is shown. **b**, Percentage increase of nutrient receptors in primed (IL-2 and IL-7) or activated (IL-2, IL-7 and IL-33) cells versus naive ILC2s ($n = 3$). **c**, ILC2s were cultured for 18 h with 1 μ M BPTES, 1 μ M 2DG, 1 μ M nor-NOHA, 1 μ M BCATi or DMSO in the indicated cytokine combinations. TMRM and MitoTracker were measured by FACS ($n = 6$). **d, e**, Cells were cultured for 6 d with IL-2 and IL-7 (**d**) or with IL-2, IL-7 and IL-33 (**e**) and 1 μ M rotenone, 1 μ M antimycin A, 1 μ M BPTES, 1 μ M 2DG, 1 μ M nor-NOHA, 1 μ M BCATi or DMSO. The cell counts at day 6 are shown ($n = 6$). **f**, Expression of IL-13. ILC2s were expanded in IL-2 and IL-7 for 7 d with or without inhibitors as described in **d** and **e**, and IL-33 was added for the last 6 h. **g**, ILC2s were expanded in IL-2 and IL-7 for 7 d, and IL-33 was added for the last 6 h to cells starved for 1 h and under a glucose add-back condition. IL-13 expression was monitored by FACS (**f, g**) ($n = 4$). Data in **a** are summarized from four donors, and a minimum of two technical replicates were analyzed per run. Data in **b** are representative of three independent experiments with three donors each. Data in **c** are summarized from two experiments with three donors each and are representative of a total of four independent experiments. Data in **d** and **e** are summarized from two experiments with three donors each and are representative of a total of three independent experiments. Data in **f** and **g** are representative of a total of three independent experiments with at least three donors. Floating bars in **b–g** indicate the mean, minimum and maximum values within the dataset. Bars in **d** and **e** (left plots) represent mean \pm s.e.m. Statistics were assessed by two-tailed *t*-test (**b**) and one-way ANOVA (**c–g**) with Dunnett correction; NS, not significant ($P > 0.05$); * $P < 0.05$; ** $P < 0.01$; *** $P < 0.001$.

OXPPOS in IL-2- and IL-7-stimulated ILC2s, while glutamine was also crucial in the context of IL-33 (Fig. 4c and Extended Data Fig. 8a). By contrast, BCATi did not have any obvious effect (in line with previous findings⁴⁸), and no changes in ILC2 mitochondrial mass or viability were detected under any conditions (Extended Data Fig. 8b,c). We found an increase in the uptake of fluorescently labeled long-chain FA BODIPY only following IL-33 treatment (Extended Data Fig. 8d), consistent with a recent study showing the formation of FA lipid droplets following IL-33 chronic stimulation³⁵. Still, inhibiting FA β -oxidation did not affect ILC2 mitochondrial mass or $\Delta\psi_m$ (Extended Data Fig. 8e), suggesting that FAs might not play a crucial role in sustaining ILC2 bioenergetic needs. Additional studies are needed to fully clarify the role of FAs in human ILC2s. Curiously, inhibition of glycolysis (using 2DG) did not impact mito-

chondrial polarization in cytokine-activated ILC2s, suggesting that these cells might couple glucose consumption to other functions.

To assess the effects of long-term inhibition of nutrient pathways, we extended the ILC2 cultures for 7 d (Fig. 4d,e and Extended Data Fig. 8f). As expected, cells did not survive in the presence of rotenone and antimycin A irrespective of cytokine combination. Long-term BPTES treatment impacted the survival of ILC2s when exposed to IL-2 and IL-7 or to IL-2, IL-7 and IL-33, while treatment with BCATi only had an effect in the absence of IL-33, consistent with our results on mitochondrial activity. In agreement with previous reports^{49–52} and our data on glycolytic capacity (Fig. 3j), long-term inhibition of glycolysis affected highly proliferative IL-33-stimulated ILC2s but not basal proliferation induced by IL-2 and IL-7 alone. These results indicate that amino acid

metabolism remains a central orchestrator of cellular fitness during cytokine-induced ILC2 proliferation.

We next studied the effect of metabolic inhibitors on ILC2 cytokine production. Blocking glycolysis or ETC complexes I or III decreased IL-13 and IL-5 production (Fig. 4f and Extended Data Fig. 9a,b). Amphiregulin production was less affected (Extended Data Fig. 9c), suggesting that pro- and anti-inflammatory ILC2 pathways might rely on different metabolic programs. Moreover, glucose starvation ablated IL-13 production, while glucose 'add-back' (at low or high concentration) partially restored IL-13 production (Fig. 4g and Extended Data Fig. 9d). It has been shown that glucose impacts lymphocyte function and proliferation through mTOR, an essential nutrient sensor³⁵. Moreover, reactive oxygen species (ROS) have been reported to play a crucial role in mouse ILC activation⁵³. We found that IL-33 induced ROS production in human ILC2s (Extended Data Fig. 9e). Treatment of ILC2s with a ROS scavenger or rapamycin (an mTOR inhibitor) reduced IL-13 production (Extended Data Fig. 9f). Taken together, these results demonstrate the unique role for glycolysis and ROS in coupling IL-33 activation to ILC2 cytokine production.

Here, we provide an in-depth characterization of human ILC2 metabolism at steady state and after cytokine activation. Our analysis identified the enhanced metabolic state of ILC2s compared to other innate lymphoid cell subsets and further deciphered the dichotomous nutrient pathways that sustain ILC2 survival, proliferation and function. Human ILC2 metabolism is poorly understood, with circulating ILC2s being described as resting naive cells with a migratory phenotype^{17,24}. We show that they are instead highly energetic with a defined metabolic profile characterized by high expression of CD98 and elevated rates of amino acid uptake to sustain OXPHOS. These metabolic profiles provide cells with the capacity to respond to increased metabolic demands following activation^{28,31} and represent environment-specific metabolic adaptation^{54,55}, suggesting that human circulating ILC2s might have metabolic 'experience'. The heightened metabolic profile of circulating ILC2s was strongly OXPHOS/oxygen-dependent, as shown by the analysis of individuals with MDs and hypoxic experiments. Following activation, ILC2s do not undergo a metabolic switch from OXPHOS to glycolysis but rather maintain a dichotomous cellular metabolism with persistent OXPHOS and enhanced glycolysis. The former assures ILC2 survival (with glutamine as an anaplerotic substrate to maintain cell fitness), while glucose uptake and glycolysis sustain IL-13 production.

Our findings provide a working model for understanding how ILC2 metabolism conditions ILC function. Moreover, the peculiar metabolic features of steady-state and cytokine-activated ILC2s might represent potential targets for modulating these cells in diverse disease contexts.

Online content

Any methods, additional references, Nature Research reporting summaries, source data, extended data, supplementary information, acknowledgements, peer review information; details of author contributions and competing interests; and statements of data and code availability are available at <https://doi.org/10.1038/s41590-021-01043-8>.

Received: 19 February 2021; Accepted: 9 September 2021;

Published online: 22 October 2021

References

- Eberl, G., Colonna, M., Di Santo, J. P. & McKenzie, A. N. J. Innate lymphoid cells: a new paradigm in immunology. *Science* **348**, aaa6566 (2015).
- Spits, H. et al. Innate lymphoid cells—a proposal for uniform nomenclature. *Nat. Rev. Immunol.* **13**, 145–149 (2013).
- Vivier, E. et al. Innate lymphoid cells: 10 years on. *Cell* **174**, 1054–1066 (2018).
- Serafini, N. et al. Gata3 drives development of RORγt⁺ group 3 innate lymphoid cells. *J. Exp. Med.* **211**, 199–208 (2014).
- Cupedo, T. et al. Human fetal lymphoid tissue-inducer cells are interleukin 17-producing precursors to RORC⁺ CD127⁺ natural killer-like cells. *Nat. Immunol.* **10**, 66–74 (2009).
- Eberl, G. et al. An essential function for the nuclear receptor RORγt in the generation of fetal lymphoid tissue inducer cells. *Nat. Immunol.* **5**, 64–73 (2004).
- Artis, D. & Spits, H. The biology of innate lymphoid cells. *Nature* **517**, 293–301 (2015).
- Bernink, J. H. et al. Human type 1 innate lymphoid cells accumulate in inflamed mucosal tissues. *Nat. Immunol.* **14**, 221–229 (2013).
- Lim, A. I. et al. Systemic human ILC precursors provide a substrate for tissue ILC differentiation. *Cell* **168**, 1086–1100 (2017).
- Robinette, M. L. et al. Transcriptional programs define molecular characteristics of innate lymphoid cell classes and subsets. *Nat. Immunol.* **16**, 306–317 (2015).
- Mjösberg, J. M. et al. Human IL-25- and IL-33-responsive type 2 innate lymphoid cells are defined by expression of CRTH2 and CD161. *Nat. Immunol.* **12**, 1055–1062 (2011).
- Neill, D. R. et al. Nuocytes represent a new innate effector leukocyte that mediates type-2 immunity. *Nature* **464**, 1367–1370 (2010).
- Hoyler, T. et al. The transcription factor GATA3 controls cell fate and maintenance of type 2 innate lymphoid cells. *Immunity* **37**, 634–648 (2012).
- Wilhelm, C. et al. An IL-9 fate reporter demonstrates the induction of an innate IL-9 response in lung inflammation. *Nat. Immunol.* **12**, 1071–1077 (2011).
- Mohapatra, A. et al. Group 2 innate lymphoid cells utilize the IRF4–IL-9 module to coordinate epithelial cell maintenance of lung homeostasis. *Mucosal. Immunol.* **9**, 275–286 (2016).
- Björklund, Å. K. et al. The heterogeneity of human CD127⁺ innate lymphoid cells revealed by single-cell RNA sequencing. *Nat. Immunol.* **17**, 451–460 (2016).
- Mazzurana, L. et al. Tissue-specific transcriptional imprinting and heterogeneity in human innate lymphoid cells revealed by full-length single-cell RNA-sequencing. *Cell Res.* **31**, 554–568 (2021).
- Moro, K. et al. Innate production of T_H2 cytokines by adipose tissue-associated c-Kit⁺Sca-1⁺ lymphoid cells. *Nature* **463**, 540–544 (2010).
- Stier, M. T. et al. IL-33 promotes the egress of group 2 innate lymphoid cells from the bone marrow. *J. Exp. Med.* **215**, 263–281 (2018).
- Huang, Y. et al. SIP-dependent interorgan trafficking of group 2 innate lymphoid cells supports host defense. *Science* **359**, 114–119 (2018).
- Miller, M. M. et al. BATF acts as an essential regulator of IL-25-responsive migratory ILC2 cell fate and function. *Sci. Immunol.* **5**, eaay3994 (2020).
- Ricardo-Gonzalez, R. R. et al. Tissue-specific pathways extrude activated ILC2s to disseminate type 2 immunity. *J. Exp. Med.* **217**, e20191172 (2020).
- Huang, Y. et al. IL-25-responsive, lineage-negative KLRG1^{hi} cells are multipotential 'inflammatory' type 2 innate lymphoid cells. *Nat. Immunol.* **16**, 161–169 (2015).
- van der Ploeg, E. K. Steroid-resistant human inflammatory ILC2s are marked by CD45RO and elevated in type 2 respiratory diseases. *Sci. Immunol.* **6**, eabd3489 (2021).
- Klose, C. S. N. & Artis, D. Innate lymphoid cells control signalling circuits to regulate tissue-specific immunity. *Cell Res.* **30**, 475–491 (2020).
- Weinberg, S. E., Sena, L. A. & Chandel, N. S. Mitochondria in the regulation of innate and adaptive immunity. *Immunity* **42**, 406–417 (2015).
- Buck, M. D. et al. Mitochondrial dynamics controls T cell fate through metabolic programming. *Cell* **166**, 63–76 (2016).
- Buck, M. D., O'Sullivan, D. & Pearce, E. L. T cell metabolism drives immunity. *J. Exp. Med.* **212**, 1345–1360 (2015).
- van der Windt, G. J. W., Chang, C.-H. & Pearce, E. L. Measuring bioenergetics in T cells using a Seahorse extracellular flux analyzer. *Curr. Protoc. Immunol.* **113**, 3.16B.1–3.16B.14 (2016).
- Hartmann, F. J. et al. Single-cell metabolic profiling of human cytotoxic T cells. *Nat. Biotechnol.* **39**, 186–197 (2021).
- Puleston, D. J., Villa, M. & Pearce, E. L. Ancillary activity: beyond core metabolism in immune cells. *Cell Metab.* **26**, 131–141 (2017).
- Ma, E. H. et al. Metabolic profiling using stable isotope tracing reveals distinct patterns of glucose utilization by physiologically activated CD8⁺ T cells. *Immunity* **51**, 856–870 (2019).
- Nicoli, F. et al. Naive CD8⁺ T-cells engage a versatile metabolic program upon activation in humans and differ energetically from memory CD8⁺ T-cells. *Front. Immunol.* **9**, 2736 (2018).
- O'Sullivan, D. et al. Memory CD8⁺ T cells use cell intrinsic lipolysis to support the metabolic programming necessary for development. *Immunity* **41**, 75–88 (2014).

35. Pearce, E. L. et al. Enhancing CD8 T cell memory by modulating fatty acid metabolism. *Nature* **460**, 103–107 (2009).
36. Wilhelm, C. et al. Critical role of fatty acid metabolism in ILC2-mediated barrier protection during malnutrition and helminth infection. *J. Exp. Med.* **213**, 1409–1418 (2016).
37. Karagiannis, F. et al. Lipid-droplet formation drives pathogenic group 2 innate lymphoid cells in airway inflammation. *Immunity* **52**, 620–634 (2020).
38. Monticelli, L. A. et al. Arginase 1 is an innate lymphoid cell-intrinsic metabolic checkpoint controlling type 2 inflammation. *Nat. Immunol.* **17**, 656–665 (2016).
39. Surace, L. et al. Polarized mitochondria as guardians of NK cell fitness. *Blood Adv.* **5**, 26–38 (2020).
40. Rambold, A. S. & Pearce, E. L. Mitochondrial dynamics at the interface of immune cell metabolism and function. *Trends Immunol.* **39**, 6–18 (2018).
41. Geiger, R. et al. L-Arginine modulates T cell metabolism and enhances survival and anti-tumor activity. *Cell* **167**, 829–842 (2016).
42. Carr, E. L. et al. Glutamine uptake and metabolism are co-ordinately regulated by ERK/MAPK during T lymphocyte activation. *J. Immunol.* **185**, 1037–1044 (2010).
43. Wolfson, R. L. & Sabatini, D. M. The dawn of the age of amino acid sensors for the mTORC1 Pathway. *Cell Metab.* **26**, 301–309 (2017).
44. Kelly, B. & Pearce, E. L. Amino assets: how amino acids support immunity. *Cell Metab.* **32**, 154–175 (2020).
45. Lim, A. I. et al. IL-12 drives functional plasticity of human group 2 innate lymphoid cells. *J. Exp. Med.* **213**, 569–583 (2016).
46. Bartemes, K. R., Kephart, G. M., Fox, S. J. & Kita, H. Enhanced innate type 2 immune response in peripheral blood from patients with asthma. *J. Allergy Clin. Immunol.* **134**, 671–678 (2014).
47. Li, Q. et al. E3 ligase VHL promotes group 2 innate lymphoid cell maturation and function via glycolysis inhibition and induction of interleukin-33 receptor. *Immunity* **48**, 258–270 (2018).
48. Shao, D. et al. Glucose promotes cell growth by suppressing branched-chain amino acid degradation. *Nat. Commun.* **9**, 2935 (2018).
49. Jacobs, S. R. et al. Glucose uptake is limiting in T cell activation and requires CD28-mediated Akt-dependent and independent pathways. *J. Immunol.* **180**, 4476–4486 (2008).
50. Sukumar, M. et al. Inhibiting glycolytic metabolism enhances CD8⁺ T cell memory and antitumor function. *J. Clin. Invest.* **123**, 4479–4488 (2013).
51. Tanimine, N. et al. Differential effects of 2-deoxy-D-glucose on in vitro expanded human regulatory T cell subsets. *PLoS ONE* **14**, e0217761 (2019).
52. Menk, A. V. et al. Early TCR signaling induces rapid aerobic glycolysis enabling distinct acute T cell effector functions. *Cell Rep.* **22**, 1509–1521 (2018).
53. Di Luccia, B. et al. ILC3s integrate glycolysis and mitochondrial production of reactive oxygen species to fulfill activation demands. *J. Exp. Med.* **216**, 2231–2241 (2019).
54. Pearce, E. L. & Pearce, E. J. Metabolic pathways in immune cell activation and quiescence. *Immunity* **38**, 633–643 (2013).
55. Pearce, E. L., Poffenberger, M. C., Chang, C.-H. & Jones, R. G. Fueling immunity: insights into metabolism and lymphocyte function. *Science* **342**, 1242454 (2013).

Publisher's note Springer Nature remains neutral with regard to jurisdictional claims in published maps and institutional affiliations.



Open Access This article is licensed under a Creative Commons Attribution 4.0 International License, which permits use, sharing, adaptation, distribution and reproduction in any medium or format, as long as you give appropriate credit to the original author(s) and the source, provide a link to the Creative Commons license, and indicate if changes were made. The images or other third party material in this article are included in the article's Creative Commons license, unless indicated otherwise in a credit line to the material. If material is not included in the article's Creative Commons license and your intended use is not permitted by statutory regulation or exceeds the permitted use, you will need to obtain permission directly from the copyright holder. To view a copy of this license, visit <http://creativecommons.org/licenses/by/4.0/>.

© The Author(s) 2021

Methods

Cell isolation from blood and tissue samples. Blood samples from healthy donors were randomly selected (age and sex) and obtained from *Establissement Francais du Sang* (EFS) under protocol HS 2105-24405. Peripheral blood mononuclear cells (PBMCs) from individuals with MD were obtained from the Unit of Neurology and Neuromuscular Disorders at 'University of Messina' with informed consent through an Institutional Review Board protocol (protocol 88/17 del 31 set 2017) in compliance with ethical regulations. No statistical methods were used to predetermine sample sizes, but our sample sizes are similar to those reported in previous publications^{9,11,17}. The number of participants for each experiment was dependent on donors' availability. No direct compensation was given by the authors to the healthy donors or individuals with MD. Isolation of human PBMCs and single-cell suspensions was achieved by Ficoll-Paque (GE Healthcare) density gradient centrifugation. Data collection and analysis were not blinded to the conditions of the experiments.

Cell culture and reagents. All in vitro culture experiments were performed in Yssel's medium prepared in house by using IMDM (Invitrogen) and 0.25% (wt/vol) bovine serum albumin (Sigma), 1.8 mg liter⁻¹ 2-amino ethanol, 40 mg liter⁻¹ apo-transferrin, 5 mg liter⁻¹ insulin and penicillin/streptomycin and supplemented with 2% human AB serum (EFS). FACS-sorted cells were plated in the presence of the human cytokines IL-2 (50 ng ml⁻¹; Miltenyi), IL-7 (50 ng ml⁻¹; Miltenyi) and IL-33 (50 ng ml⁻¹; R&D), which were provided in various combinations and at specific times as indicated. For the hypoxia experiments, cells were cultured at 3% oxygen in the XVivo System (BioSperix) at constant pressure, humidity and 5% CO₂. Chemical inhibitors used to study metabolic pathways (2DG, BPTES, etomoxir, TTFa, antimycin A, rotenone, oligomycin A, MitoTempo and rapamycin) were purchased from Sigma. BCAT1 and nor-NOHA were purchased from Cayman Chemicals. Cell viability was assessed by Annexin-V and live-dead staining by FACS. Cells were counted at the microscope after trypan blue staining or, when in limited number, by FACS.

Flow cytometry and cell sorting. Cells were stained with surface antibodies and Fixable Viability Dye eFluor 506 (eBioscience) in PBS supplemented with 2% fetal calf serum for 30 min on ice. For experiments involving intracellular staining of cytokines, cells were stimulated for 6 h with cytokines, and, during the last 3 h, Golgi Plug and Golgi Stop (BD) were added to the cultures. Cells were washed with PBS and fixed and permeabilized for 45 min at room temperature using a Cytotfix/Cytoperm kit (BD). Intracellular staining was performed at room temperature for 30 min in the dark. Annexin-V staining was performed using Annexin-V-binding buffer (BD). Samples were acquired with an LSRFortessa (BD) and analyzed by FlowJo10.7.1 (TreeStar). For cell sorting, PBMCs were depleted of T cells, B cells, plasmacytoid dendritic cells, monocytes and erythrocytes by labeling with biotin-conjugated antibodies followed by anti-biotin microbeads and AutoMACS separation (Miltenyi) according to manufacturer's instruction. Cells were sorted in bulk to a purity of ≥99% (FACSARIA II; BD).

Antibodies. Surface GLUT1 expression was monitored as a function of binding to its ligand, the envelope glycoprotein of the human T lymphotropic virus (HTLV). A recombinant HTLV envelope receptor-binding domain (H_{REB}) fused to an enhanced green fluorescent protein (eGFP)-coding sequence was used as previously described³⁶. Surface ASCT2 was similarly evaluated; expression was monitored as a function of binding to its ligand, the RD114 envelope glycoprotein of the feline endogenous retrovirus, fused with a murine Fc tag and revealed with an Alexa Fluor-647-conjugated anti-mouse IgG (Invitrogen).

Antibodies for ILC2 enrichment, including anti-hCD3 biotin (clone OKT3, 13-0037-82), anti-hCD4 biotin (RPA-T4, 13-0049-82), anti-hCD19 biotin (HIB19, 13-0199-82), anti-hCD14 biotin (61D3, 13-0149-82), anti-hCD123 biotin (6H6, 13-1239-82) and anti-hCD235a biotin (HIR2 GA-R2, 13-9987-82), were purchased from eBioscience. Antibodies used for ILC2 sorting, including anti-hCD3 FITC (UCHT1, 11-0038), anti-hCD4 FITC (OKT4, 11-0048), anti-hCD5 FITC (UCHT2, 11-0059), anti- $\alpha\beta$ TCR FITC (IP26, 564451), anti-h $\gamma\delta$ TCR FITC (B1.1, 11-9986) and anti-hCD127 (IL-7 α) PE-Cy7 (eBioRDR5, 25-1278-42) were purchased from eBioscience. Anti-hCD14 FITC (TUK4, 130-080-701), anti-hCD19 FITC (LT19, 130-104-650) and anti-hCD159a (NKG2A) PE (REA110, 130-113-566) were purchased from Miltenyi. Anti-hCD294 (CRTH2) Alexa Fluor 647 (BM16, 558042) and anti-hCD7 BV711 (M-T701, 564018) were purchased from BD. Anti-hCD45 AF700 (HI30, 560566), anti-hCD94 APC-Fire750 (DX22, 305518), anti-hCD117 BV605 (104D2, 313218), anti-hCD16 BV650 (3G8, 302042) and anti-hCD56 BV756 (5.1H11, 362550) were purchased from BioLegend. Antibodies for FACS analysis (extracellular and intracellular staining), including anti-hAnnexinV BV395 (564871), anti-hCD3 BUV737 (UCHT1, 612750), anti-hCD5 BUV737 (UCHT2, 612842), anti-hCD14 BUV737 (M5E2, 612763), anti-hCD19 BUV737 (SJ25C1, 612756), anti-hCD45 BV805 (HI30, 612891) and anti-hIL-13 BV421 (JES10-5A2, 624124), were purchased from BD. Anti-hST2 APC (hIL33Rcap, 17-9338-42) and anti-hAmphiregulin (AREG559, 17-5370-42) were purchased from eBioscience, and anti-hIL-5 (TRFK5, 504311) and anti-hHIF1 α (546-16, 359704) were purchased from BioLegend.

Mitochondrial mass, membrane potential by FACS and confocal microscopy and FA uptake. Mitochondrial mass, membrane potential and FA uptake of freshly sorted or cytokine-activated ILC2s were assessed by staining cells with 50 nM MitoTracker Green FM (Thermo Fisher), 25 nM TMRM (Sigma-Aldrich) and BODIPY FL-C₁₆ (Thermo Fisher), respectively, for 30 min at 37°C and 5% CO₂. Cells were washed twice in cold 1× PBS, stained with surface antibodies and analyzed by FACS. For confocal microscopy, cells were stained at 37°C for 30 min with 300 ng ml⁻¹ of Hoechst H33342 (Life Technologies) to stain nuclei, 100 nM MitoTracker Green FM to stain mitochondria and 25 nM TMRM to assess mitochondrial membrane potential (non-quenching mode, TMRM maintained in the cell medium). Cells were plated in a 384-well plate (40,000 cells per well), and image acquisitions of multiple fields per well were performed on an automated confocal microscope (OPERA QEHS, Perkin Elmer) using ×60 objectives, excitation lasers at 405, 488 and 561 nm and emission filters at 450, 540 and 600 nm, respectively. Confocal images were transferred to the Columbus Image Data Storage and Analysis System (Perkin Elmer) for high content analyses as previously reported⁵⁷ and used the standard deviation/mean approach⁵⁸.

Metabolite extraction, mass spectrometry and data analysis. Methods for metabolite extraction, data acquisition and data analysis were developed and performed by General Metabolics. FACS-sorted ILC2s (100,000 cells) were pelleted and washed in prewarmed (37°C) ammonium carbonate (75 mM) washing buffer. Preheated (70°C) 70% ethanol (99.9% purity) extraction solvent was added, and samples were incubated for 3 min. After centrifugation (8,000g for 10 min at 0°C), the supernatants were collected and stored at -80°C until analysis. The analysis was performed on a platform consisting of an Agilent Series 1100 LC pump coupled to a Gerstel MPS2 autosampler and an Agilent 6520 Series Quadrupole time-of-flight mass spectrometer equipped with an electrospray source operated in negative and positive mode as previously reported⁵⁹. All steps of data processing and analysis were performed with Matlab R2010b (MathWorks) using functions embedded in the bioinformatics, statistics, database and parallel computing toolboxes. For each run, a matrix list was produced with the intensity of each mass peak in each analyzed sample. An accurate *m/z* was recalculated with a weighted average of the values, and a list of putative metabolites was compiled from the KEGG database. Raw intensities for each metabolite are included in Supplementary Data 1. For each ion, the best metabolite match was chosen among all candidates based on the deviation from the theoretical *m/z* and a heuristic probability associated with the theoretical ion fragment, which was set lower for, for example, rare adducts, fragments or molecules containing several heteroatoms. Significant changes in metabolite levels compared to the entire dataset were determined by calculating *z* scores for each sample and ion individually, as previously reported⁵⁶. Results were run in iPath3 (<https://pathways.embl.de>), an online tool for data mapping. A Principal-component analysis was applied to the samples coming from two different screenings using the stats R package. The screenings were simultaneously analyzed considering only metabolites present in both screenings (total = 122 metabolites). The first principal component indicated that most of the variance of the data corresponded to the screening effect, as expected from the batch effect that each screening represented. The second most variable effect corresponded to the donors. Pathway analysis was done with Qlucone Omic Explorer v3.

RNA isolation, library construction, sequencing and analysis. ILC2s (10³ cells) were sorted by FACS directly into 50 ml of lysis/binding buffer (Life Technologies). mRNA was captured with 15 ml of Dynabeads oligo(dT) (Life Technologies), washed according to manufacturer's instructions and eluted at 85°C with 6 ml of 10 mM Tris-HCl (pH 7.5). We used a derivation of MARS-seq as described in ref. ⁶⁰, developed for single-cell RNA-seq, to produce expression libraries of two replicates per population. Libraries were sequenced at an average depth of 5 million reads per library on an Illumina NextSeq and aligned to the human reference genome (hg19). Reads were mapped using hisat (version 0.1.6); duplicate reads were filtered if they had identical unique molecular identifiers. Expression levels were calculated and normalized to the total number of reads using HOMER software. RNA-seq datasets have been deposited in the Gene Expression Omnibus (GEO) public repository (accession number GSE183669).

Transcriptional profiling by BioMark. ILC2s were sorted as small bulks (25 cells) directly in 96-well qPCR plates with RT mix 1 (5× VILO Reaction Mix, 200 U μ l⁻¹ SUPERase-In, 10% NP-40 and nuclease free water). Reverse transcription was performed according to manufacturer's protocols (Fluidigm). The dynamic Array IFC chip was prepared according to manufacturer's protocols and analyzed in the Biomark System (Fluidigm). Cycle threshold (C_t) values were collected from the machine and processed using Prism 8.

Cellular metabolism by Seahorse extracellular flux analyzer. OCRs and ECARs were measured for freshly sorted, IL-2-, IL-7- and/or IL-33-stimulated ILC2s (100,000 cells). XF medium (non-buffered RPMI 1640 containing 10 mM glucose, 2 mM L-glutamine and 1 mM sodium pyruvate) was used under basal conditions. Addition of 1 μ M oligomycin, 1.5 μ M FCCP and 100 nM rotenone + 1 μ M

antimycin A was performed using portal injection in a 96-well XF or XFe Extracellular Flux Analyzer (Seahorse Bioscience).

Statistical analysis. Flow cytometry data were analyzed using FlowJo v.10 (TreeStar). Statistical analyses were done using a two-tailed *t*-test or one-way ANOVA test with Dunnett correction when comparing multiple groups to specific conditions or a Tukey correction for multiple comparisons when comparing more than two conditions of interest (GraphPad Prism v.8 and v.9). The statistical tests, replicate experiments and *P* values are all cited in the figures and/or figure captions. Statistical tests were justified as appropriate for every figure, and the data meet the assumptions of the tests. The ranges of *x* and *y* axes for scatter plots were determined to include all of the data points. The sample size for each experiment and the replicate number of experiments are included in the figure legends as well as the specific test used for the analysis.

Reporting Summary. Further information on research design is available in the Nature Research Reporting Summary linked to this article.

Data availability

All the data generated and/or analyzed during this study are included in this manuscript as Supplementary Information. RNA-seq datasets have been deposited in the GEO public repository (accession number [GSE183669](https://www.ncbi.nlm.nih.gov/geo/query/acc.cgi?acc=GSE183669)). Source data are provided with this paper.

References

- Manel, N. et al. The ubiquitous glucose transporter GLUT-1 is a receptor for HTLV. *Cell* **115**, 449–459 (2003).
- Escoll, P. et al. *Legionella pneumophila* modulates mitochondrial dynamics to trigger metabolic repurposing of infected macrophages. *Cell Host Microbe* **22**, 302–316 (2017).
- Duchen, M. R., Surin, A. & Jacobson, J. Imaging mitochondrial function in intact cells. *Methods Enzymol.* **361**, 353–389 (2003).
- Fuhrer, T. et al. High-throughput, accurate mass metabolome profiling of cellular extracts by flow injection-time-of-flight mass spectrometry. *Anal. Chem.* **83**, 7074–7080 (2011).
- Jaitin, D. A. et al. Massively parallel single-cell RNA-seq for marker-free decomposition of tissues into cell types. *Science* **343**, 776–779 (2014).

Acknowledgements

We thank all the members of the Innate Immunity Unit for helpful discussions, the Centre de Recherche Translationnelle and the logistic department of Institut Pasteur. We thank the CB-UTechS platform for cytometry support and the Imagopole-CiTech (part of France-BioImaging supported by ANR grant no. ANR-10-INSB-04-01, Conseil de la Région Ile-de-France, FRM) for technical support. The Innate Immunity Unit is supported by grants from the Institut National de la Santé et de la Recherche Médicale (INSERM), Institut Pasteur, the Agence National pour le Recherche (ANR) and the European Research Council (ERC) under the European Union's Horizon 2020 research and innovation program (695467, ILC_REACTIVITY). A.T. is supported by European Union's Horizon 2020 research and innovation program under the Marie Skłodowska-Curie grant agreement no. 765104. C.B.'s group was supported by the Fondation pour la Recherche Médicale (FRM) grant no. EQU201903007847 and the grant no. ANR-10-LABX-62-IBEID. L.S. was supported by an SNSF-Early PostDoc. Mobility fellowship and a Marie Curie grant (H2020- MSCA-IF-2017).

Author contributions

The study was conceptualized by L.S. and J.P.D. Experiments were coordinated by L.S. FACS and subsequent analyses were performed by L.S., C.A.C., A.T., J.-M.D. and S.M. Confocal microscopy analysis was performed by P.E., C.B. and L.S. Bioinformatic analyses were performed by N.P. and V.G. RNA-seq experiments were conducted by I.A. O.M., V.D., N.T., D.T. and A.C. provided resources. L.S. and J.P.D. wrote the paper. Funding was acquired by L.S. and J.P.D., and the study was supervised by J.P.D.

Competing interests

The authors declare no competing interests.

Additional information

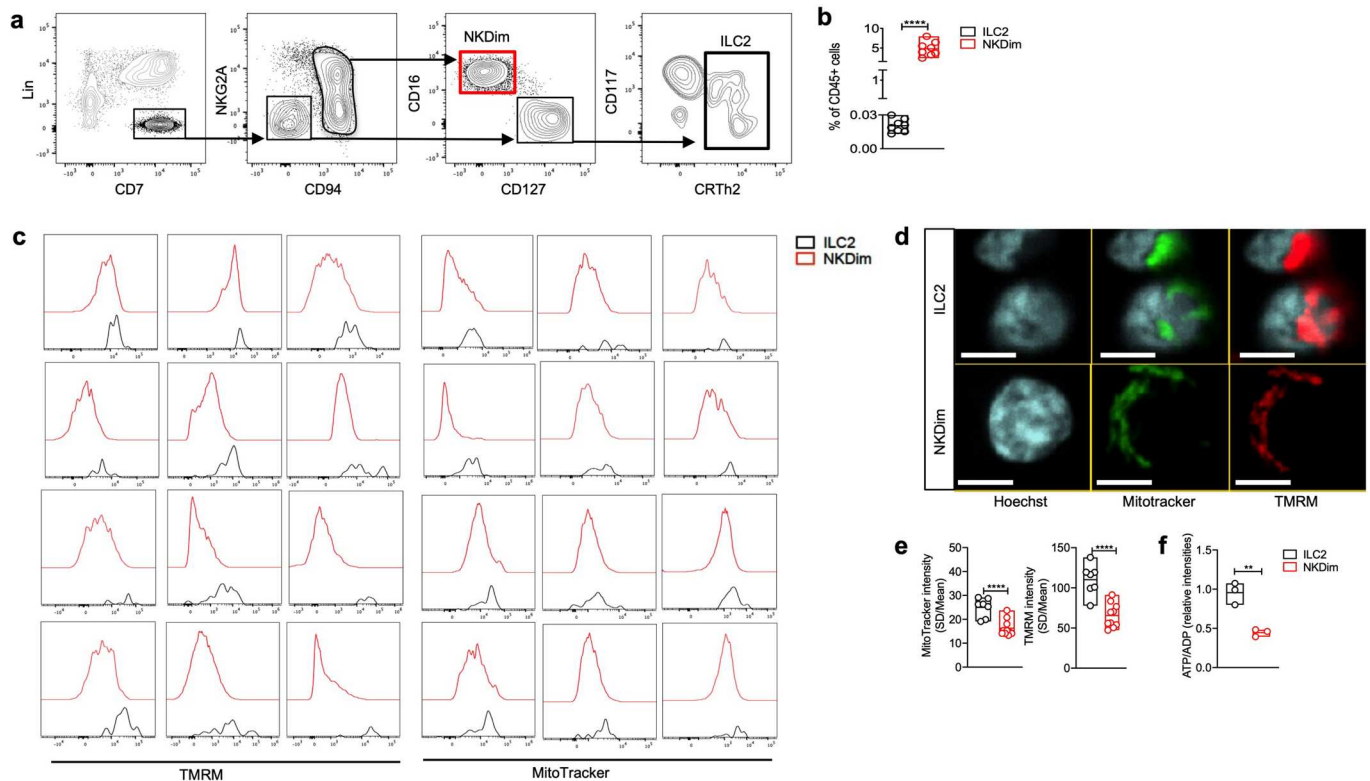
Extended data is available for this paper at <https://doi.org/10.1038/s41590-021-01043-8>.

Supplementary information The online version contains supplementary material available at <https://doi.org/10.1038/s41590-021-01043-8>.

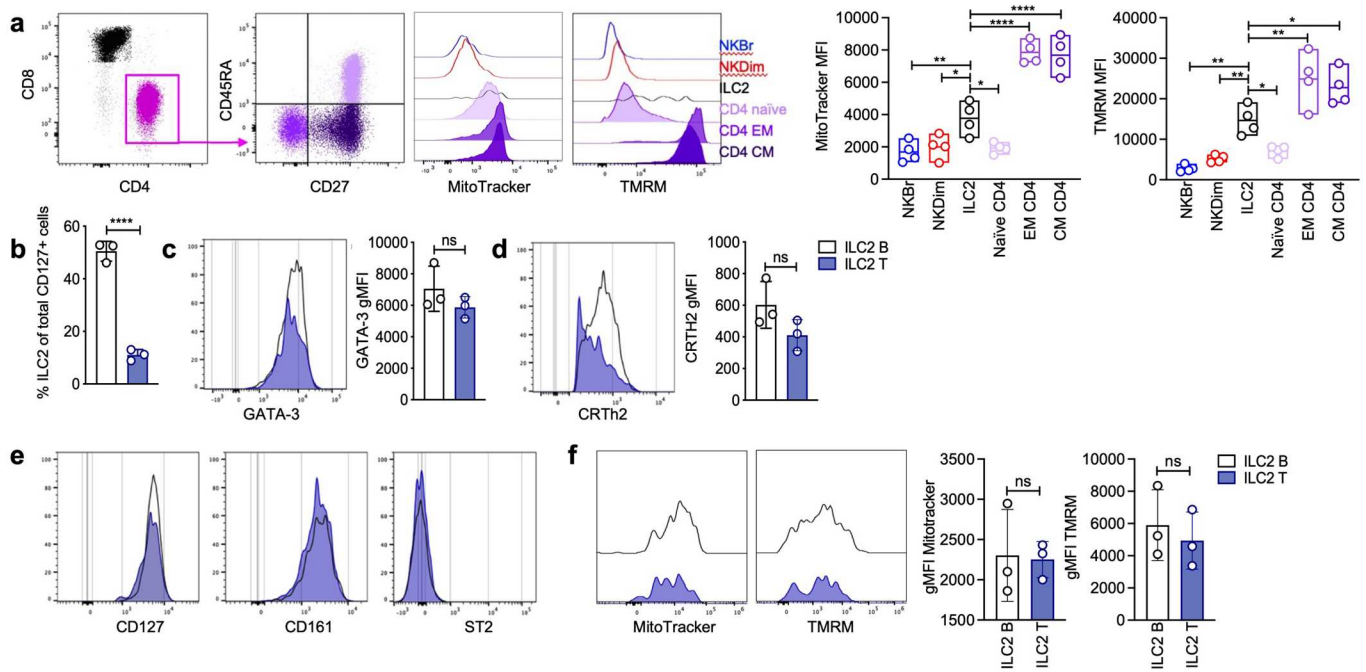
Correspondence and requests for materials should be addressed to James P. Di Santo.

Peer review information *Nature Immunology* thanks Jörg Fritz and the other, anonymous, reviewer(s) for their contribution to the peer review of this work. L. A. Dempsey was the primary editor on this article and managed its editorial process and peer review in collaboration with the rest of the editorial team.

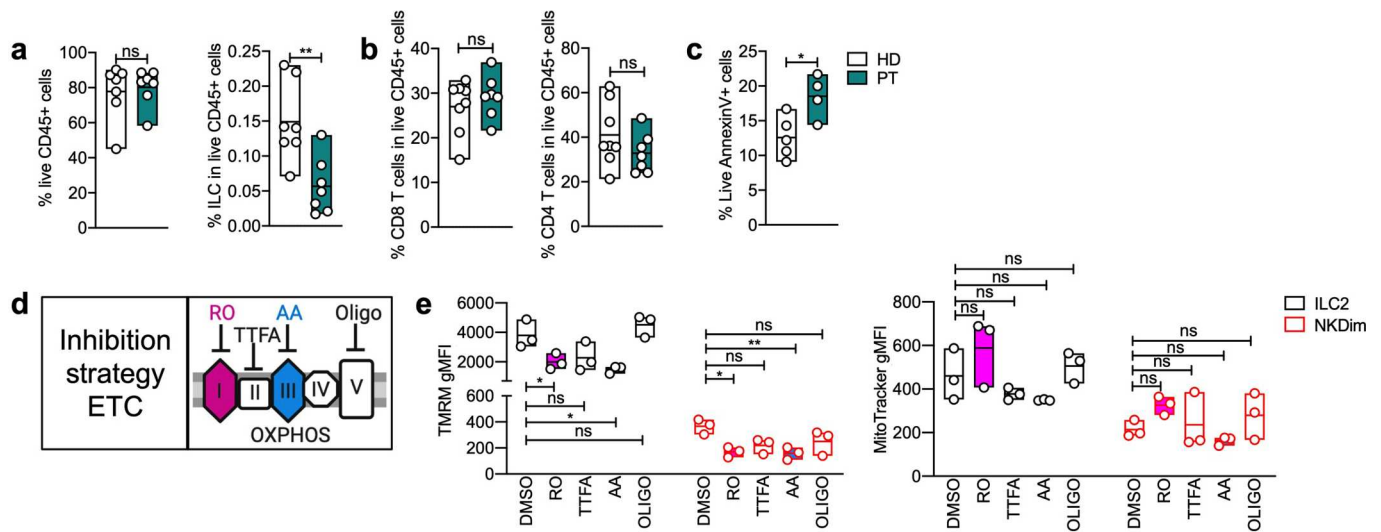
Reprints and permissions information is available at www.nature.com/reprints.



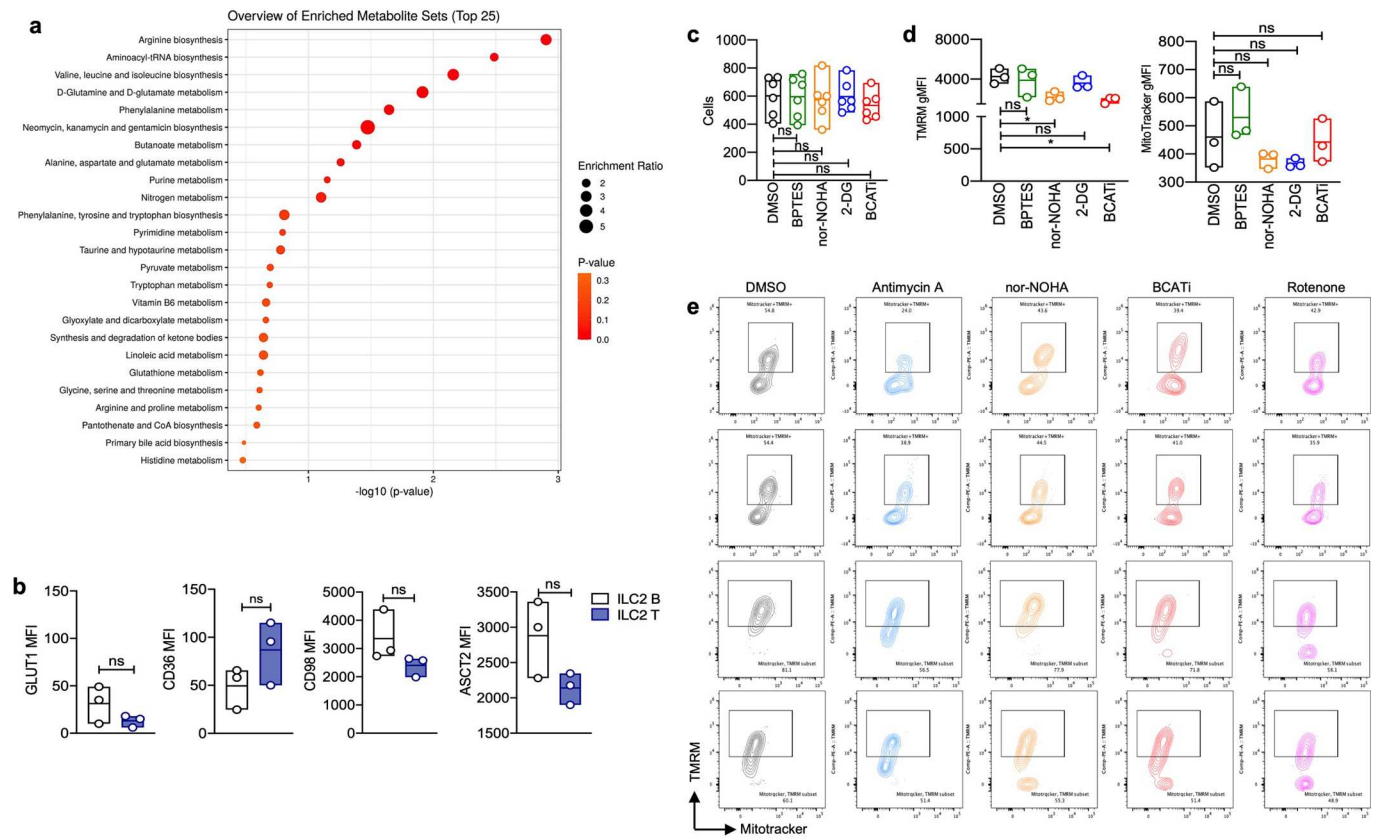
Extended Data Fig. 1 | Human ILC2 have fused and polarized mitochondria. **a**, ILC2 Gating strategy Live CD45⁺ CD7⁺ Lin⁻ CD94⁻ NKG2A⁻ CD56⁻ CD16⁻ CD127⁺ CRTh2⁺ (ILC2) and Live CD45⁺ CD7⁺ Lin⁻ CD94⁺ CD16⁺ (NKDim). **b**, Percentage of ILC2 and NKDim in live CD45⁺ cells. **c**, FACS measurement of TMRM and MitoTracker in healthy donors of fresh ILC2 and NKDim (n = 12). **d**, Confocal microscopy in fresh ILC2 and NKDim (n = 7). **e**, MitoTracker and TMRM intensity (SD/Mean). **f**, ATP and ADP intensities quantified by label-free mass spectrometry in freshly sorted ILC2 and NKDim cells (n = 3). **a-b**, Data representative of 10 independent experiments with 2 to 4 donors each. **c**, Data from 12 healthy donors from at least 5 independent experiments. **d-e**, Data representative of 2 independent experiments with at least 3 donors. Dots are single cells in the analyzed field. Scale bar 5 μm. **f**, Each dot represents a donor. A minimum of 2 technical replicates were analyzed per run. **b, e, f**, Floating bars indicate the mean, minimum and maximum values within the dataset. Statistics were assessed by two tailed t-test (**b, e, f**), not significant (ns), p > 0.05; **p < 0.01; ****p < 0.0001.



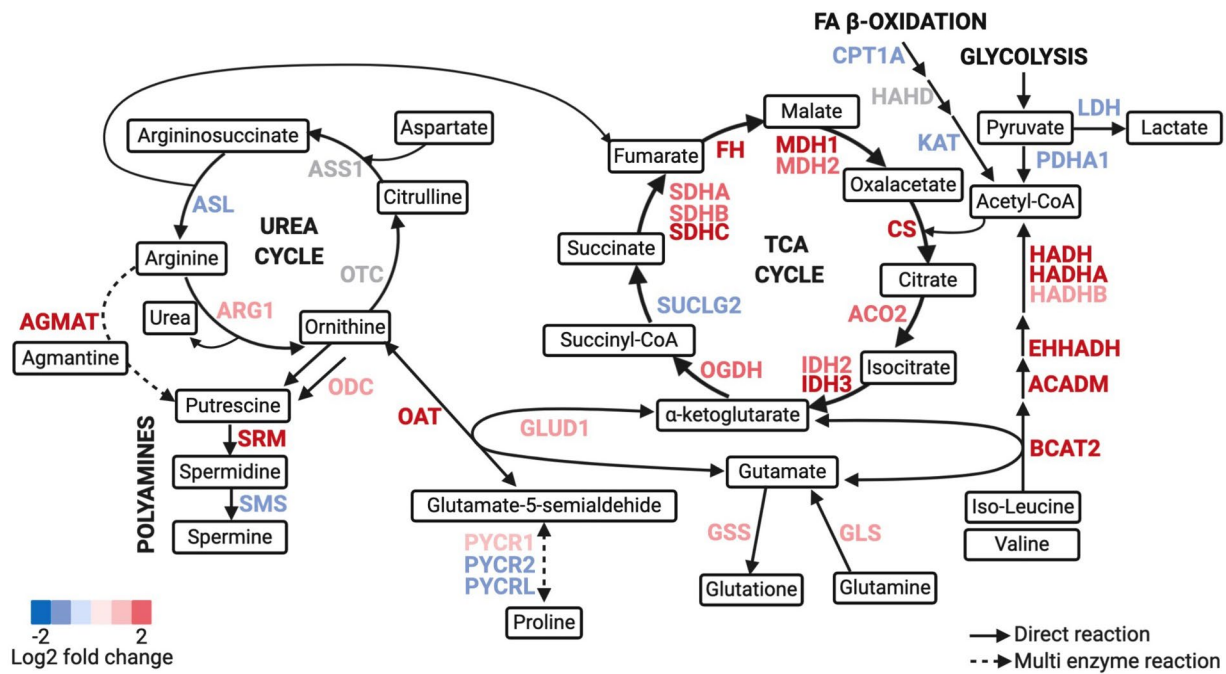
Extended Data Fig. 2 | ILC2 have enhanced mitochondrial activity compared to naïve T cells. **a**, Gating strategy for CD4⁺ T cells subsets in the blood of healthy donors. FACS measurement of TMRM and MitoTracker gMFI in the indicated subsets (n=4). **b-f**, Paired blood and tonsil samples were collected from pediatric donors. The percentage of ILC2 (**b**), GATA-3 gMFI (**c**), CRTh2 gMFI (**d**), representative plots of CD127, CD161, ST2 (**e**), TMRM and Mitotracker gMFI (**f**) were monitored by FACS (n=3). **a**, Data representative of 2 experiments with at least 3 donors each. **b-f**, Data are representative of 2 independent experiments with 3 donors each. **a**, Floating bars indicate the mean, minimum and maximum values within the dataset. **b-f**, Bars are \pm s.e.m. Statistics were assessed by one-way ANOVA with Dunnett correction (**a**) and two tailed t-test (**b-f**), not significant (ns), $p > 0.05$; * $p < 0.05$; ** $p < 0.01$; **** $p < 0.0001$.



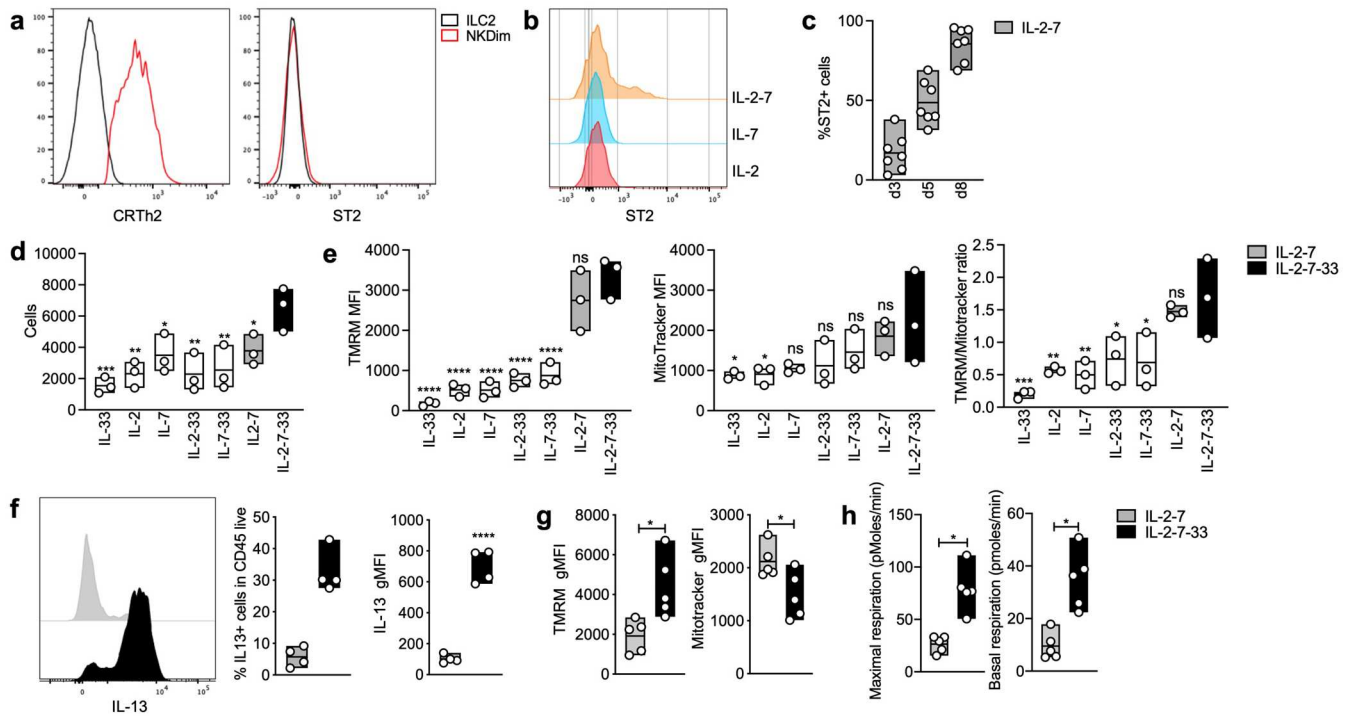
Extended Data Fig. 3 | ILC2 are reduced in patients with mitochondrial diseases. **a-c**, Comparison of healthy donors (HD, black) and patients with mitochondrial diseases (PT, green). The percentage of live CD45⁺ cells, total ILC **(a)** CD8⁺ and CD4⁺ T cells **(b)** and live Annexin-V⁺ cells **(c)** was measured by FACS (HD = 7, PT = 7). **d-e**, Freshly sorted ILC2 and NKDim were cultured with no additional cytokines for 18h in DMSO, Rotenone (1uM), Antimycin A (1uM), TTFa (1uM) or Oligomycin (1uM), as indicated in the inhibition strategy **(d)**. TMRM and MitoTracker gMFI were measured by FACS **(e)** (n = 3). **a-c**, Each dot represents a donor. **d-e**, Data representative of 3 independent experiments with at least 3 donors each. **a-c, e**, Floating bars indicate the mean, minimum and maximum values within the dataset. Statistics were assessed by two tailed t-test **(a-c)**, and one-way ANOVA with Dunnett correction **(e)**, not significant (ns), p > 0.05; *p < 0.05; **p < 0.01; ***p < 0.001; ****p < 0.0001.



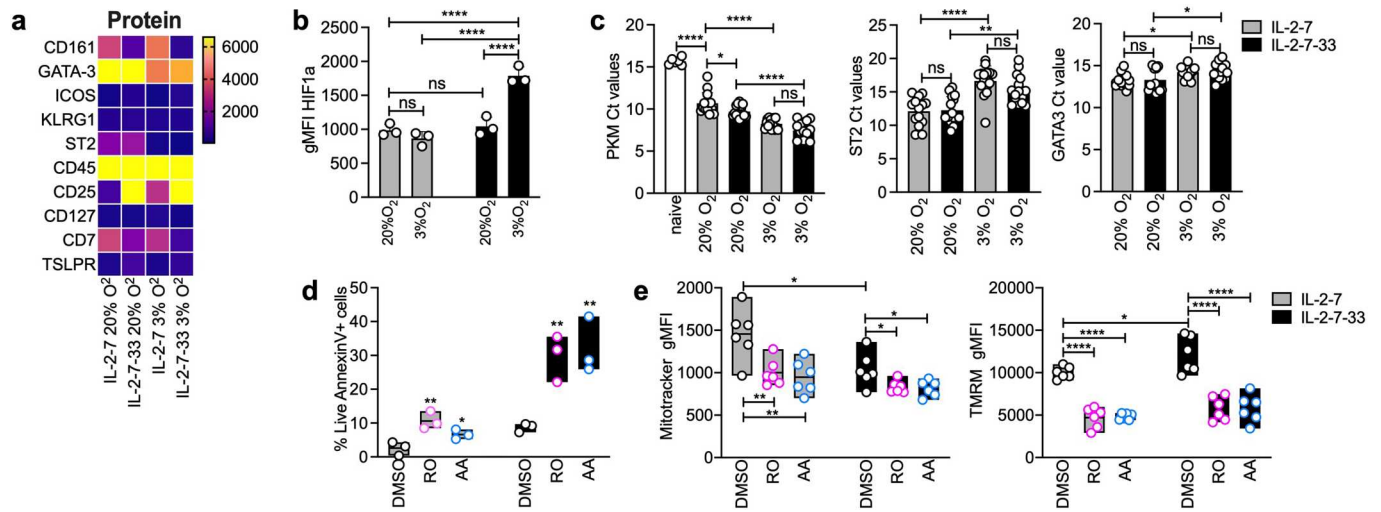
Extended Data Fig. 4 | Branched amino acid and Arginine metabolism support OXPHOS in circulating ILC2. **a**, Enrichment analysis done by Metaboanalyst. Metabolite intensities were used as input and human metabolome was used as reference. **b**, Paired blood and tonsil samples were collected from pediatric donors. GLUT1, CD36, CD98 and ASCT2 were measured by FACS ($n = 3$). **c-d**, Freshly sorted ILC2 were cultured w/o additional cytokines for 18h in DMSO, nor-NOHA (1 μ M), BCATi (1 μ M), BPTES (1 μ M) or 2DG (1 μ M). Cell counts (**c**) ($n = 6$) and TMRM and MitoTracker MFI (**d**) ($n = 3$) were measured by FACS. **e**, FACS analysis of TMRM and Mitotracker staining in ILC2 cultured w/o additional cytokines for 18h in DMSO, Rotenone (1 μ M), Antimycin A (1 μ M), nor-NOHA (1 μ M) and BCATi (1 μ M). **a**, Data summarized from 4 donors. A minimum of 2 technical replicates were analyzed per run. **b**, Data are representative of 2 independent experiments with 3 donors each. **c-d**, Data are representative of 4 independent experiments with at least 2 donors each. **e**, Data are shown for 4 donors from 2 independent experiments. **b-d**, Floating bars indicate the mean, minimum and maximum values within the dataset. Statistics were assessed by two tailed t-test (**b**) and one-way ANOVA with Dunnett correction (**c-d**), not significant (ns), $p > 0.05$; * $p < 0.05$.



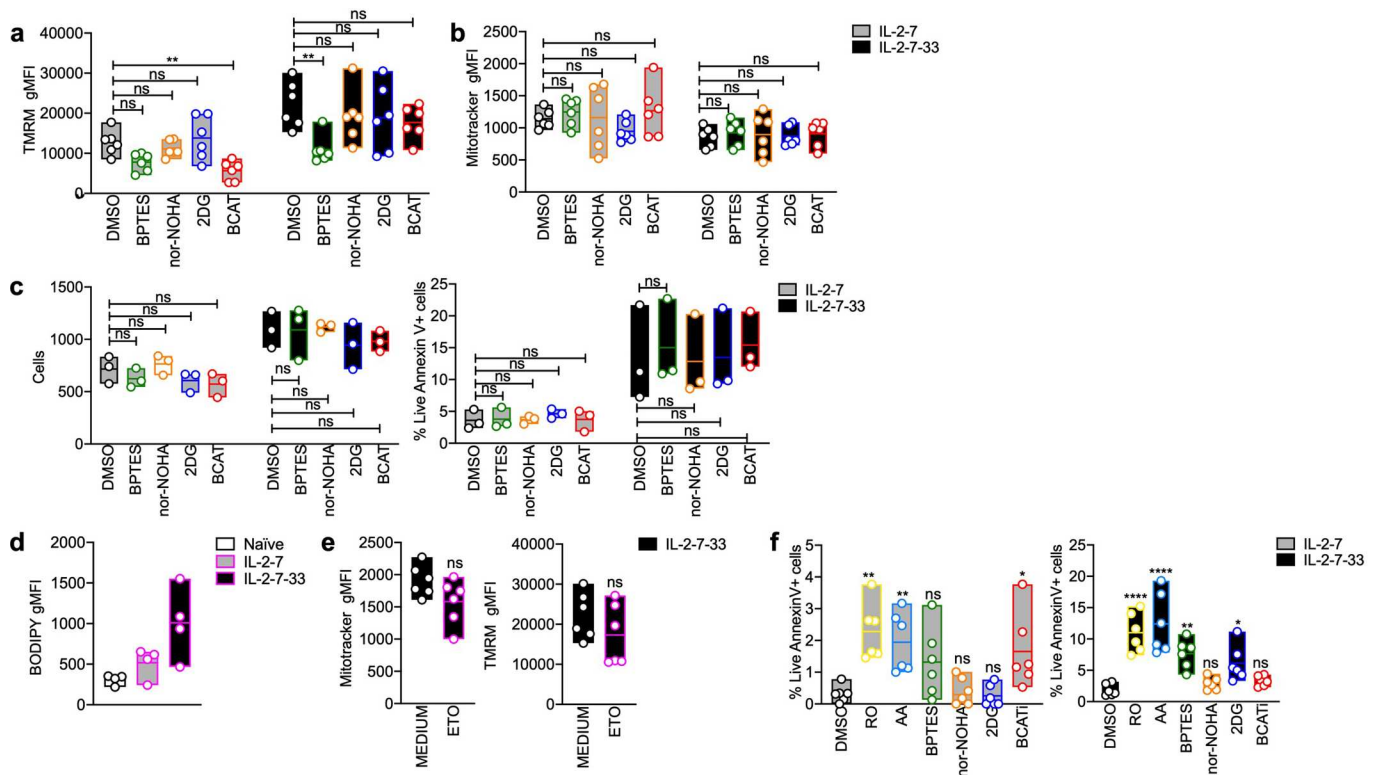
Extended Data Fig. 5 | Branched amino acid and Arginine are used as building blocks to sustain TCA cycle and OXPHOS. Enzyme analysis comparing RNA-seq data to published NK cell dataset for the calculation of the fold change. Data extracted from RNA-seq dataset. Median calculated from values of 3 healthy donors.



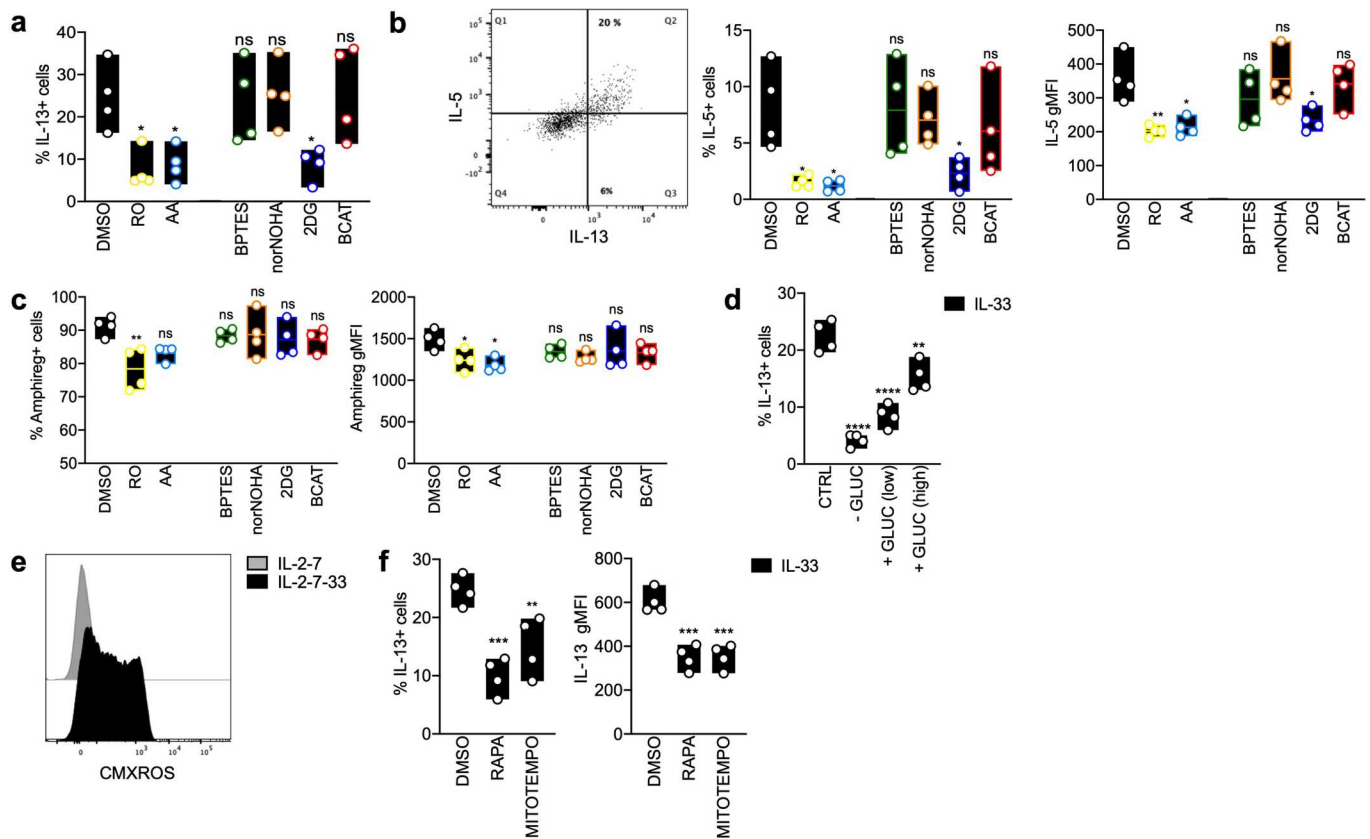
Extended Data Fig. 6 | Activated ILC2 upregulate ST2 and enhance OXPHOS. **a**, Representative FACS plots of CRTh2 and ST2 in blood ILC2. **b**, ILC2 were cultured for 18h with IL-2, IL-7 or IL-2-7 and levels of ST2 were monitored by FACS. **c**, ILC2 were expanded for 3, 5 or 7 days in IL-2-7 and ST2 was measured by FACS (n=7). **d,e**, ILC2 were expanded for 7 days in the indicated cytokine combinations. Cell number was assessed by trypan blue (**d**), TMRM and MitoTracker gMFI were measured by FACS (**e**) (n=3). **f-h**, ILC2 were expanded for 7 days in IL-2-7 and then IL-33 was added or not for 72h. Levels of IL-13 (**f**) (n=4), TMRM and MitoTracker (**g**) were measured at d10 by FACS (n=5). **h**, Maximal and basal respiration were measured by seahorse upon addition of Glucose, Oligomycin, FCCP and a combination of Rotenone + Antimycin A (n=5). **a,b** Plot representative of 3 different donors. **c-e**, Data are representative of two experiments with 3 to 4 donors each. **f**, Data are representative of 3 experiments with at least 3 donors each. **g-h**, Data are representative of 5 independent experiments with 3 to 5 donors each. **c-h**, Floating bars indicate the mean, minimum and maximum values within the dataset. Statistics were assessed by one-way ANOVA with Tukey correction (**d,e**) and two tailed t-test (**f-h**), not significant (ns), $p > 0.05$; * $p < 0.05$; ** $p < 0.01$; *** $p < 0.001$; **** $p < 0.0001$.



Extended Data Fig. 7 | Oxygen consumption is crucial upon ILC2 activation. a-c. Cells were cultured at 20% or 3% oxygen in IL-2-7 or IL-2-7-33 for 5 days. The gMFI of the indicated makers in the heatmap (**a**) and HIF1a gMFI (**b**) were analyzed by FACS (n=3). The level of expression of PKM, ST2 and GATA-3 transcripts was measured by Biomark (**c**) (n=15). **d-e**, 1uM RO, or 1uM AA or with DMSO were added for 18h to the culture. Annexin V and L/D (**d**) (n=3), Mitotracker and TMRM MFI (**e**) (n=6) were analyzed by FACS. **a**, Data pooled from 3 independent experiments with 3 donors each. **b**, Data representative of 3 independent experiments. **c**, Data pooled from 2 independent experiments. **d-e**, Data are representative of a total of 4 independent experiments with 3 donors each. **b-c**, Bars are \pm s.e.m.; **d-e**, Floating bars indicate the mean, minimum and maximum values within the dataset. Statistics were assessed by one-way ANOVA with Tukey correction (**b-e**), not significant (ns), $p > 0.05$; * $p < 0.05$; ** $p < 0.01$; *** $p < 0.001$; **** $p < 0.0001$.



Extended Data Fig. 8 | Activated ILC2 use different nutrients to sustain proliferation. a-e, ILC2 were expanded for 7 days in IL-2-7 and then IL-33 was added or not for 72h. Inhibitors or DMSO were added at the concentrations indicated in Fig. 4 for 18h. MitoTracker and TMRM (**a-b**) ($n=6$), cell counts and Annexin V (**c**) were monitored by FACS ($n=3$). **d-e**, Bodipy (**d**) ($n=4$), MitoTracker and TMRM (**e**) ($n=6$) were analyzed by FACS in naïve, IL-2-7 and IL-2-7-33 stimulated ILC2. **f**, Cells were cultured for 6 days in IL-2-7 and 1 μ M RO, 1 μ M AA, 1 μ M BPTES, or 1 μ M 2DG, or 1 μ M nor-NOHA, or 1 μ M BCATi or DMSO. Annexin V was measured by FACS ($n=6$). **a-b** Data are summarizing 2 experiments with 3 donors each. Representative of a total of 4 independent experiments. **c-e**, Data are representative of 3 independent experiments with at least 3 donors each. **f**, Data are summarizing 2 experiments with 3 donors each. Representative of a total of 3 independent experiments. Floating bars indicate the mean, minimum and maximum values within the dataset. Statistics were assessed by one-way ANOVA with Dunnett correction (**a-d, f**) and two tailed t-test in (**e**), not significant (ns), $p > 0.05$; * $p < 0.05$; ** $p < 0.01$; *** $p < 0.001$; **** $p < 0.0001$.



Extended Data Fig. 9 | Activated ILC2 use different pathways to sustain function and proliferation. **a-c**, ILC2 were expanded in IL-2-7 for 7 days ± inhibitors as described in (Fig. 4d-e). IL-33 was added for the last 6 hours. Percentage of IL-13+ cells (**a**) IL-5+ cells and gMFI (**b**) and amphiregulin+ cells and gMFI (**c**) were measured by FACS (n = 4). **d**, ILC2 were expanded in IL-2-7 for 7 days and then IL-33 was added for the last 6 hours on cells starved for 1 hour and on glucose add-back condition. Percentage of IL-13+ cells was measured by FACS (n = 4). **e**, ILC2 were expanded for 7 days in IL-2-7 and then IL-33 was added or not for 72h. Levels of ROS was measured by FACS (n = 4). **f**, ILC2 were expanded in IL-2-7 for 7 days in the presence or not of the inhibitors MitoTempo (1uM) and Rapamycin (25nM). IL-33 was added for 6 hours. Percentage of IL-13+ cells was measure by FACS (n = 4). **a-d**, Data are representative of 3 independent experiments with at least 3 donors each. **e-f**, Data are representative of 2 independent experiments with at least 3 donors each. Floating bars indicate the mean, minimum and maximum values within the dataset. Statistics were assessed by one-way ANOVA with Dunnett correction (**a-f**), not significant (ns), p > 0.05; *p < 0.05; **p < 0.01; ***p < 0.001; ****p < 0.0001.

Annex 4

Polarized mitochondria as guardians of NK cell fitness

Laura Surace, Jean-Marc Doisne, Pedro Escoll, Solenne Marie, Valerie Dardalhon, Carys Croft, Anna Thaller, Davide Topazio, Angelo Sparaneo, Antonia Cama, Olimpia Musumeci, Aurelio d'Ecclesia, Carmen Buchrieser, Naomi Taylor, and James P. Di Santo

Published on the 29th of December 2020

Journal: Blood Advances

Polarized mitochondria as guardians of NK cell fitness

Laura Surace,^{1,2} Jean-Marc Doisne,^{1,2} Pedro Escoll,^{3,4} Solenne Marie,^{1,2} Valerie Dardalhon,⁵ Carys Croft,^{1,2,6} Anna Thaller,^{1,2,6} Davide Topazio,⁷ Angelo Sparaneo,⁸ Antonia Cama,⁹ Olimpia Musumeci,¹⁰ Aurelio d'Ecclesia,⁷ Carmen Buchrieser,^{3,4} Naomi Taylor,⁵ and James P. Di Santo^{1,2}

¹INSERM U1223, Paris, France; ²Innate Immunity Unit and ³Biology of Intracellular Bacteria Unit, Institut Pasteur, Paris, France; ⁴UMR 3525, Centre National de la Recherche Scientifique (CNRS), Paris, France; ⁵Institut de Génétique Moléculaire de Montpellier, University of Montpellier, CNRS, Montpellier, France; ⁶BioSPC, Université de Paris, Paris, France; ⁷Head and Neck Department, "Casa Sollievo della Sofferenza," Scientific Institute for Research and Health Care (IRCCS), San Giovanni Rotondo, Italy; ⁸Laboratory of Oncology, "Casa Sollievo della Sofferenza," IRCCS, San Giovanni Rotondo, Italy; ⁹Maxillofacial Surgery Unit, Department of Neuroscience, University Federico II, Naples, Italy; and ¹⁰Unit of Neurology and Neuromuscular Disorders, Department of Clinical and Experimental Medicine, University of Messina, Messina, Italy

Key Points

- CD56^{Br} and CD56^{Dim} human NK cells have distinct bioenergetic requirements at steady state and upon activation.
- Mitochondrial dynamics and oxidative phosphorylation orchestrate NK cell function and fitness.

Distinct metabolic demands accompany lymphocyte differentiation into short-lived effector and long-lived memory cells. How bioenergetics processes are structured in innate natural killer (NK) cells remains unclear. We demonstrate that circulating human CD56^{Dim} (NKDim) cells have fused mitochondria and enhanced metabolism compared with CD56^{Br} (NKBr) cells. Upon activation, these 2 subsets showed a dichotomous response, with further mitochondrial potentiation in NKBr cells vs paradoxical mitochondrial fission and depolarization in NKDim cells. The latter effect impaired interferon- γ production, but rescue was possible by inhibiting mitochondrial fragmentation, implicating mitochondrial polarization as a central regulator of NK cell function. NKDim cells are heterogeneous, and mitochondrial polarization was associated with enhanced survival and function in mature NKDim cells, including memory-like *human cytomegalovirus*-dependent CD57⁺ NKG2C⁺ subsets. In contrast, patients with genetic defects in mitochondrial fusion had a deficiency in adaptive NK cells, which had poor survival in culture. These results support mitochondrial polarization as a central regulator of mature NK cell fitness.

Introduction

Dynamic changes in energetic pathways govern lymphocyte maturation, activation, and long-term persistence. Naïve T cells reside in a resting basal metabolic state, where oxidative phosphorylation (OXPHOS) is sufficient to actively maintain the cells in quiescent state.¹ Proliferating T cells use glycolysis to keep up with ATP production and tricarboxylic acid cycle intermediates to favor the biosynthesis of materials that support division, differentiation, and cytokine production.^{2,3} Long-lived memory cells increase fatty acid (FA) β -oxidation in a TRAF6-mediated prosurvival pathway.^{1,4,5} Whereas changes in metabolic processes in T cells have been well studied, our knowledge of natural killer (NK) cell metabolism remains incomplete.

Human NK cells can be divided into 2 subpopulations based on differential expression of CD56 (NCAM) and CD16 (Fc γ RIIIA; low-affinity Fc receptor). In the blood of healthy donors (HDs), these subpopulations are identified as CD56^{Dim}CD16⁺ NK (NKDim) cells, which are highly cytotoxic, and CD56^{Bright}CD16⁻ NK (NKBr) cells, which are less cytotoxic but strong cytokine producers (interferon- γ [IFN- γ], tumor necrosis factor- α [TNF- α]).^{6,7} NKBr and NKDim cells differentially express cytokine and homing receptors and show distinct tissue distributions.^{6,8,9} Previous studies have begun to explore the metabolic requirements of resting and activated NK cells.¹⁰⁻¹⁴ Peripheral blood NK cells increase

Submitted 21 September 2020; accepted 24 November 2020; published online 29 December 2020. DOI 10.1182/bloodadvances.2020003458.

Sent data sharing requests via email to the corresponding author, James P. Di Santo (james.di-santo@pasteur.fr).

The full-text version of this article contains a supplement.
© 2020 by The American Society of Hematology

glycolysis and OXPHOS upon cytokine stimulation.¹² Specifically, upon interleukin-2 (IL-2)/12 stimulation, NKBr cells were reported to be metabolically more responsive compared with NKDim cells.¹² FA and glutamine pathways are upregulated in naïve NK cells¹⁵; however, excess of lipids blocks glycolysis, blunting NK cell antitumoral activity.¹⁶ Overall, how environmental signals associated with NK cell survival and activation are integrated via reprogramming of intracellular energetic pathways remains unclear.

Mitochondria are highly dynamic organelles, shaped continuously by fusion and fission reactions.¹⁷ Mitochondrial fusion, mediated by mitofusins and dynamin-like GTPase (OPA1), drives network formation, sustaining OXPHOS and cell survival,¹⁸ whereas mitochondrial fragmentation is regulated by a cytosolic GTPase dynamin-related protein 1 and is associated with mitophagy.¹⁹ Mitochondrial diseases (MDs) are rare inheritable disorders that include genetic mutations affecting mitochondrial structure, leading to impaired OXPHOS and decreased mitochondrial DNA integrity.^{20,21} Although human adaptive NKG2C⁺ NK cells in *human cytomegalovirus* (HCMV)-exposed individuals have elevated mitochondrial OXPHOS,¹⁰ it is not known whether altered mitochondrial dynamics impair NK cell differentiation. Here we analyzed how mitochondria regulate human NK cell homeostasis and function.

Materials and methods

Cell isolation from blood and tissue samples

Blood samples from HDs were obtained from the *Establissement Francais du Sang* (Paris, France). Tonsils were obtained from pediatric patients undergoing routine tonsillectomy ("Casa Sollievo della Sofferenza," Scientific Institute for Research and Health Care). Peripheral blood mononuclear cells (PBMCs) from MD patients were obtained from the Unit of Neurology and Neuromuscular Disorders at the University of Messina. Informed consent was obtained from all patients and included protocols approved by institutional review boards. Ficoll-Paque (GE Healthcare) was used for PBMC isolation, and cells were studied fresh (unless otherwise indicated). Tonsils were mechanically disrupted, and cells were frozen before use.

Cell culture

All in vitro culture experiments were performed in Yssel's medium.²² Sorted cells were cultured in human IL-15 (50 ng/mL; Miltenyi), IL-12 (50 ng/mL; MBL), and IL-18 (50 ng/mL; R&D), provided in various combinations as indicated for 18 hours. To assess metabolic pathways, inhibitors were added during the 18 hours: 1 mM of [³H] 2-deoxy-d-glucose (2-DG), 4 μM of bis-2-(5-phenylacetamido-1,3,4-thiadiazol-2-yl)ethyl sulfide (BPTES), 20 μM of etomoxir (ETO), 25 μM of mitochondrial division inhibitor 1 (Mdivi-1), 10 μM of rotenone (RO), 10 μM of antimycin A (AA), and 2 nM of oligomycin A (all from Sigma). For 12-day cultures, 5 μM of Mdivi-1 was used.

Flow cytometry and cell sorting

Cells were stained with surface antibodies and Flexible Viability Dye eFluor 506 (eBioscience) in phosphate-buffered saline/2% fetal calf serum for 30 minutes on ice. Surface glucose receptor 1 (GLUT-1) expression and glutamine receptor (ASCT2) expression were monitored as a function of binding to ligands as previously

described.^{23,24} For intracellular staining, cells were stimulated for 18 hours, and Golgi Plug/Golgi Stop (BD) were added for the last 3 hours. Cells were fixed/permeabilized using Cytofix/Cytoperm (BD) and then stained. Samples were acquired using the LSRFortessa (BD) and analyzed by FlowJ10 software (Tree Star). For cell sorting, PBMCs were lineage depleted using biotin-conjugated anti-CD3, anti-CD4, anti-CD19, anti-CD14, anti-CD123, and anti-CD235a (eBioscience) followed by antibiotin microbeads and AutoMACS separation (Miltenyi) according to the manufacturer's instructions. Cells were bulk sorted to a purity of ≥99% or single-cell index sorted (FACS Aria II; BD) as previously reported.²²

RNA isolation, library construction, sequencing, and analysis

A total of 10³ NKDim (2 donors with 2 technical replicates) or NKBr cells (2 donors with no technical replicates) were sorted directly into 50 μL of lysis/binding buffer (Life Technologies). Messenger RNA was captured with 15 μL of Dynabeads oligo(dT) (Life Technologies) before washing and elution. Massively parallel single-cell RNA sequencing was performed as described.²² Libraries were sequenced (Illumina NextSeq) to an average depth of 5 million reads per library and aligned to the human reference genome (hg19). Reads were mapped using hisat (version 0.1.6); duplicate reads were filtered if they had identical unique molecular identifiers. Expression levels were calculated and normalized to the total number of reads using HOMER software (<http://homer.salk.edu>).

Cellular metabolism by seahorse extracellular flux analyzer

Oxygen consumption rates (OCRs) and extracellular acidification rates (ECARs) were measured for freshly sorted NK cells (200 000 cells) stimulated with IL-15 ± IL-12/18 (18 hours). XF media (containing 10 mM of glucose, 2 mM of L-glutamine, and 1 mM of sodium pyruvate) was used under basal conditions. Addition of 1 μM of oligomycin, 1.5 μM of carbonyl cyanide-4-(trifluoromethoxy)phenylhydrazone (FCCP), and 1 μM of RO + 1 μM of AA was performed using portal injection in an extracellular flux analyzer (Seahorse Bioscience).

Mitochondrial mass and membrane potential by fluorescence-activated cell sorting and confocal microscopy

Mitochondrial mass and membrane potential of freshly sorted or cytokine-activated NK cells were assessed by staining cells with 50 nM of MitoTracker Green FM (Thermo Fisher) and 25 nM of tetramethyl rhodamine methyl ester (TMRM; Sigma Aldrich), respectively, at 37°C for 30 minutes before surface staining. For confocal microscopy, nuclei of MitoTracker/TMRM-stained cells were counterstained with 300 ng/mL of Hoechst H33342 (Life Technologies). Cells were plated in 384-well plates (40 000 cells per well), and image acquisitions of multiple fields per well were performed on an automated confocal microscope (OPERA QEHS; Perkin Elmer) using 60× objectives, excitation lasers at 405, 488, and 561, and emission filters at 450, 540, and 600, respectively. Confocal images were transferred to the Columbus Image Data Storage and Analysis System (Perkin Elmer) for high-content analyses of mitochondrial morphology as previously reported,²⁵ and the standard deviation/mean approach was used for quantifying

mitochondrial membrane potential on confocal images using TMRM dye.²⁶

Statistical analysis

Data are represented as medians unless specified. The sample size for each experiment and the replicate number of experiments are included in the figure legends as well as the specific test used for the analysis (Prism software).

Results

Monitoring metabolic profiles of NKDim and NKBr cells at steady state and after activation

To assess metabolic pathways that condition human NK cell responses, we compared characteristics of purified circulating NKBr (Lin⁻CD7⁺CD56^{high}CD16⁻CD127⁺) and NKDim cells (Lin⁻CD7⁺CD56^{low}CD16⁺CD127⁻; supplemental Figure 1A). Specifically, we compared freshly isolated NKBr and NKDim cells (steady state) with cells that underwent either IL-15 priming²⁷ or IL-12/IL-15/IL-18 activation²⁸⁻³¹ (Figure 1A).

Glucose and glutamine are key substrates of the mitochondrial bioenergetic pathways and have been reported to be essential nutrients for NK cell activation.^{12,13,28} We therefore characterized GLUT-1 (*SLC2A1*) and ASCT2 (*SLC1A5*) expression in freshly sorted NKBr and NKDim cells. We found higher *SLC2A1* levels in NKDim cells, whereas *SLC1A5* expression was higher in NKBr cells (supplemental Figure 1B). These subset-specific differences were confirmed at the protein level, with a higher percentage of NKDim cells expressing GLUT-1 and NKBr cells expressing ASCT2 (Figure 1B; supplemental Figure 1C). IL-15-primed NKDim cells did not significantly upregulate either of these receptors, whereas the frequency of ASCT2⁺ NKBr cells increased after IL-15 exposure. NK cell activation (IL-12/18) enhanced the average expression levels of both receptors on both subsets. Although we did not detect any change in the already high percentage of ASCT2⁺ NKBr cells, we found increased frequencies of GLUT-1⁺ NKDim and NKBr cells as well as ASCT2⁺ NKDim cells after stimulation with IL-12 and IL-18 (Figure 1B).

We further studied nutrient receptors CD98 (a component of the L-amino acid transporter), CD71 (transferrin receptor), and CD36 (FA translocase). CD71 was expressed at higher levels in NKBr compared with NKDim cells at steady state; however, expression increased in response to cytokine stimulation for both subsets. CD98 and CD36 were upregulated in both subsets only upon activation (supplemental Figure 1C). Analysis of [³H]L-glutamine and 2-DG uptake showed increased uptake in both subsets upon priming and activation, with NKDim cells showing significantly greater glucose uptake than NKBr cells (supplemental Figure 1D). FAs are another important nutrient source that can fuel mitochondrial pathways. Because multiple FA transporters exist, we measured FA uptake using BODIPY-FLC16.³² We found that upon activation, NKBr cells took up more long-chain FAs than NKDim cells (Figure 1C).

To clarify which of these various nutrients are required for NKBr and NKDim cells to exert their function, we studied the effects of inhibitors targeting glycolysis (2-DG), FA β -oxidation (ETO), and glutamine conversion into glutamate (BPTES). We found that IFN- γ and TNF- α were produced by NK cells only upon activation, and

NKBr cells produced higher levels of both cytokines compared with NKDim cells^{15,27,29} (Figure 1D; supplemental Figure 1E). Treatment with 2-DG inhibited IFN- γ and TNF- α production by both NK cell subsets, consistent with a requirement for increased glucose uptake in this process. Although BPTES treatment did not alter the production of effector cytokines in either subset, both IFN- γ and TNF- α were significantly decreased in NKBr cells after treatment with ETO, suggesting that FA oxidation is important for NKBr cell activation and function (Figure 1D; supplemental Figure 1E). None of these inhibitors had an impact on NK cell viability (supplemental Figure 1F) or cytotoxic function (supplemental Figure 1G).

Distinct bioenergetics in NKBr and NKDim cells upon cytokine priming vs activation

We used the Seahorse bioanalyzer³³ to quantitate OCRs (indicator of OXPHOS) and ECARs (reflecting lactate production and glycolysis) in purified NK cell subsets. NKDim cells exhibited increased maximal ECARs after FCCP compared with NKBr cells (Figure 2A), indicating elevated maximal glycolysis capacity. NKDim cells also showed increased basal OCRs, higher maximal OCRs, and increased ATP-linked respiration when compared with NKBr cells (Figure 2B; supplemental Figure 2A), indicating that NKDim cells rely mainly on OXPHOS to produce ATP at steady state. SRC was higher in NKDim compared with NKBr cells (Figure 2C), consistent with latent mitochondrial capacity. RNA sequencing analysis confirmed that NKDim cells expressed higher levels of transcripts involved in OXPHOS compared with NKBr cells (Figure 2D; supplemental Figure 2B-D), providing a mechanistic explanation for the differential bioenergetics of these 2 NK cell subsets at baseline.

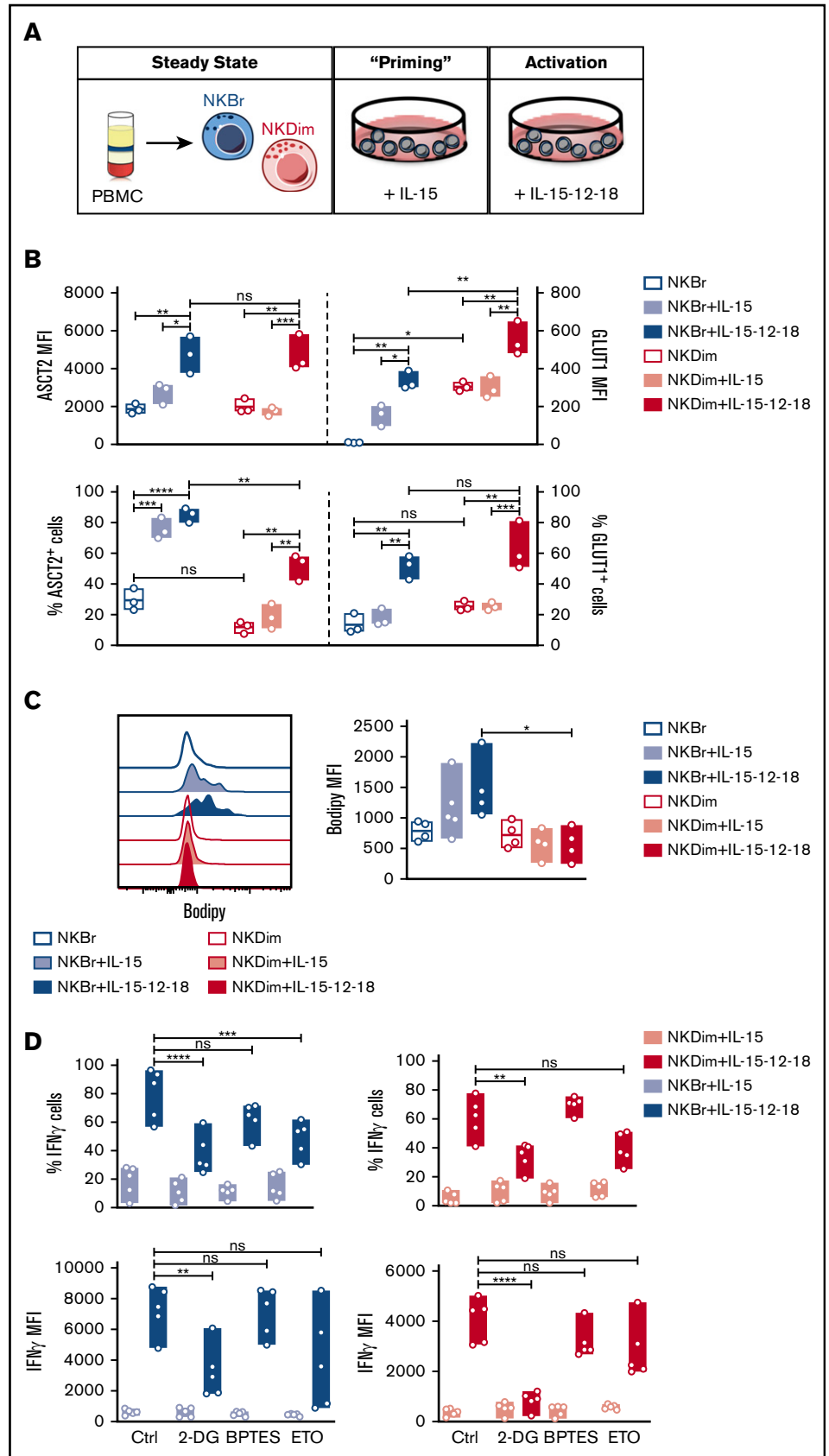
We next compared the impact of priming (IL-15) vs activation (IL-12/18) on the bioenergetics of these human NK cell subsets. NKDim cells maintained a high glycolytic rate after exposure to IL-15 (Figure 2E), whereas NKBr cells increased their aerobic capacity. After cytokine activation, both subsets showed higher maximal glycolysis (Figure 2E), consistent with the ability of these factors to promote NK cell proliferation and function. IL-15 induced a small increase in basal OCRs in NKDim cells, whereas maximal SRC remained stable (Figure 2F-G; supplemental Figure 2E), suggesting steady-state NKDim cells were already operating close to their bioenergetic limit. In contrast, IL-15-stimulated NKBr cells showed an increase in maximal OCRs and SCR, consistent with mitochondrial activation (Figure 2F-G). NKBr cells did not increase ATP-linked respiration, implying these cells might also rely on other pathways for ATP production (supplemental Figure 2E). In contrast, NK cell activation with IL-12/18 elicited a metabolic shift in NKDim cells, which showed decreased maximal OCRs, ATP-linked respiration, and SRC, whereas NKBr cells continued to have substantially large mitochondrial SRC (Figure 2F-G; supplemental Figure 2E). Cells with elevated SRC are more fit and have better survival capacity,^{5,19,34} suggesting a fundamental difference in the bioenergetic stability of these 2 NK cell subsets after activation.

Distinct mitochondrial polarization patterns explain metabolic dichotomy in stimulated NKBr and NKDim cells

To explore the basis for the differences in metabolic profiles in cytokine-stimulated NKBr and NKDim cells, we further characterized mitochondrial mass and membrane polarization ($\Delta\psi_m$) using

Figure 1. Energetic substrate use in NKBr vs NKDim cells at steady state and upon activation.

(A) In vitro model of NKBr and NKDim cell priming and activation. (B-D) Freshly fluorescence-activated cell-sorted NKDim and NKBr cells, IL-15 primed or activated with IL-15/12/18 (18 h) were monitored for cell-surface expression of the GLUT-1 and ASCT2 transporters and percentage of positive cells (B) (data from 3 independent experiments with 1 HD each) and FL-BODIPY-C16 uptake (C) (data from 3 independent experiments with 1 or 2 HDs each). (D) Expression of IFN- γ and percentage of IFN- γ -producing cells were monitored in NKBr and NKDim cells incubated with IL-15 or IL-15/12/18 for 18 hours in the presence of different inhibitors: 1 mM of 2-DG, 4 μ M of BPTES, or 20 μ M of ETO (data are mean \pm standard error of the mean [SEM]; data summarized from 3 independent experiments with at least 2 HDs each). $P > .05$ was considered not significant (ns). * $P < .05$, ** $P < .01$, *** $P < .001$, **** $P < .0001$ using 2-way analysis of variance with Tukey's correction. MFI, mean fluorescence intensity.



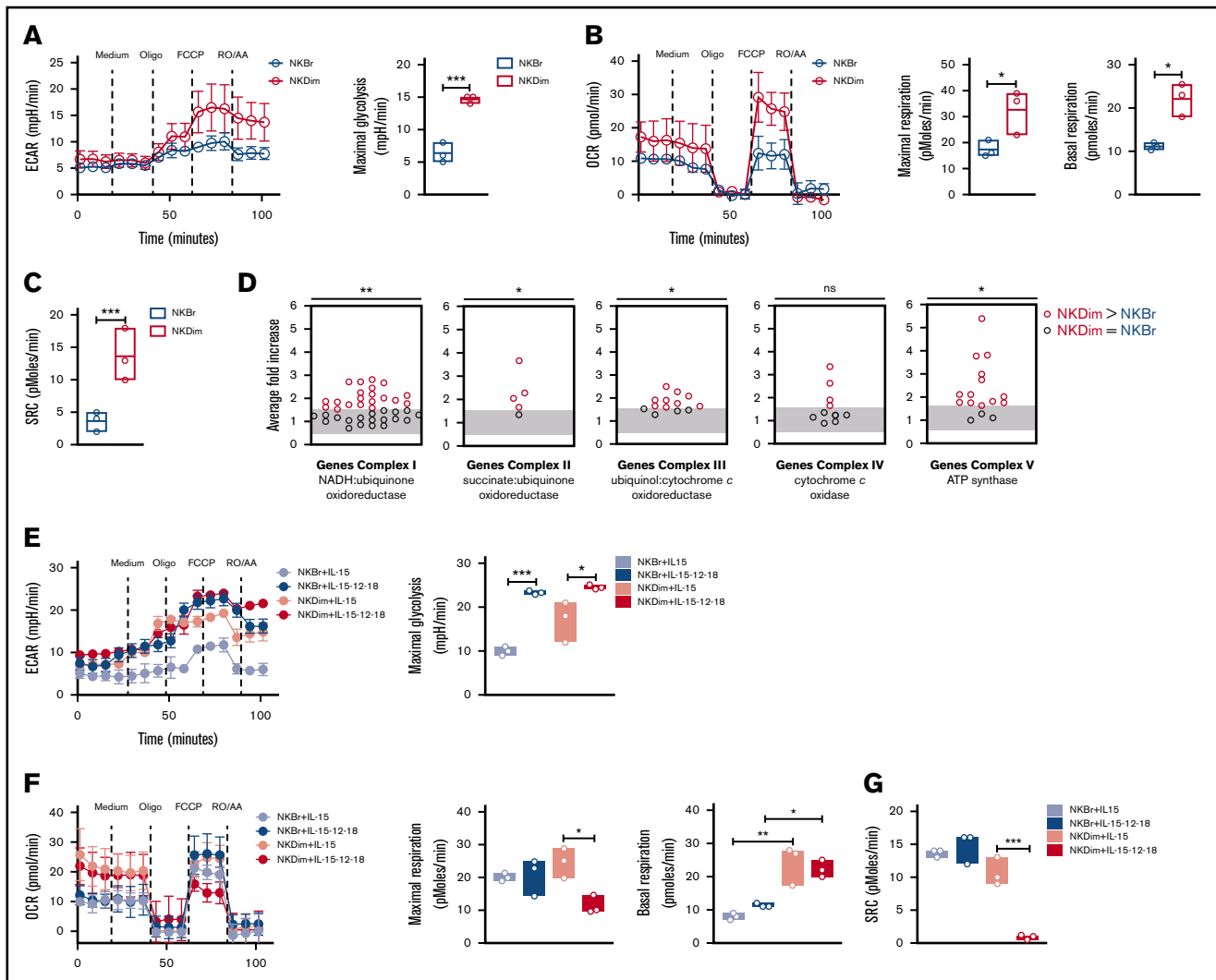


Figure 2. Steady-state CD56^{Dim} NK cells have latent mitochondrial activity and undergo a metabolic switch upon cytokine stimulation. (A-C) Metabolic function analyzed by extracellular flux analysis (EFA) in freshly fluorescence-activated cell-sorted (FACS) NKBr and NKDim cells. Cells were sequentially treated with glucose medium (medium), oligomycin A (Oligo), FCCP, and RO plus AA as indicated. (A) ECARs and maximal glycolysis (average values after glucose injection minus average basal ECAR values). (B) OCR plot. Calculation of the maximal respiration (average maximal OCR after FCCP) and basal respiration (average basal respiration after medium injection). (C) Mitochondrial spare respiratory capacity (SRC; average maximal OCR values after FCCP injection minus baseline OCR; data are representative of 3 independent experiments with 2 or 3 donors each). (D) Average fold increase comparing NKBr and NKDim cells is shown for all genes in OXPHOS complexes. Each dot represents the median relative expression level across donors. (E-G) EFA analysis in FACS NKBr and NKDim cells cultured for 18 hours in presence of IL-15 ± IL-12/18. Cells were sequentially treated as indicated above. ECAR and maximal glycolysis (E), OCR, maximal, and basal respiration (F), and SRC (G) (data are representative of 3 independent experiments; data are mean ± SEM). $P > .05$ was considered not significant (ns; or not indicated). $*P < .05$, $**P < .01$, $***P < .001$ using 1-way analysis of variance with Tukey's correction.

MitoTracker Green FM and TMRM staining^{19,25,35} (Figure 3; supplemental Figure 3A). We found that NKBr and NKDim cells had similar mitochondrial masses; however, NKDim cells showed higher TMRM levels and TMRM/MitoTracker ratios at steady state (Figure 3A-C). Single-cell and bulk gene expression analyses clearly demonstrated that TMRM⁺ NKDim cells had an active OXPHOS and bioenergetic metabolism compared with TMRM⁻ cells (supplemental Figure 3B-D), suggesting NKBr cells exhibit a low energy state compared with NKDim cells.

Although mitochondrial mass did not change after IL-15 stimulation, both subsets showed an augmented $\Delta\psi_m$ (Figure 3A-C), consistent with the heightened levels of OXPHOS (Figure 2F). Because IL-15

primes NK cells in lymphoid tissues,²⁷ tissue-resident NK cells would be expected to have enhanced metabolic profiles compared with those in circulation. Tonsillar NK cells are largely enriched in NKBr cells³⁶ (supplemental Figure 3E-F) that have higher mitochondrial mass compared with both circulating subsets, with $\Delta\psi_m$ values similar to those of circulating NKDim cells at steady state (supplemental Figure 3G-H). These results suggest that tonsillar NK cells are metabolically primed.

IL-12 and IL-18 stimulation of blood NK cells did not affect mitochondrial mass (Figure 3A-C). Still, we detected a significant decrease in $\Delta\psi_m$ in NKDim cells but not in NKBr cells after activation (Figure 3A-C), in agreement with the Seahorse data

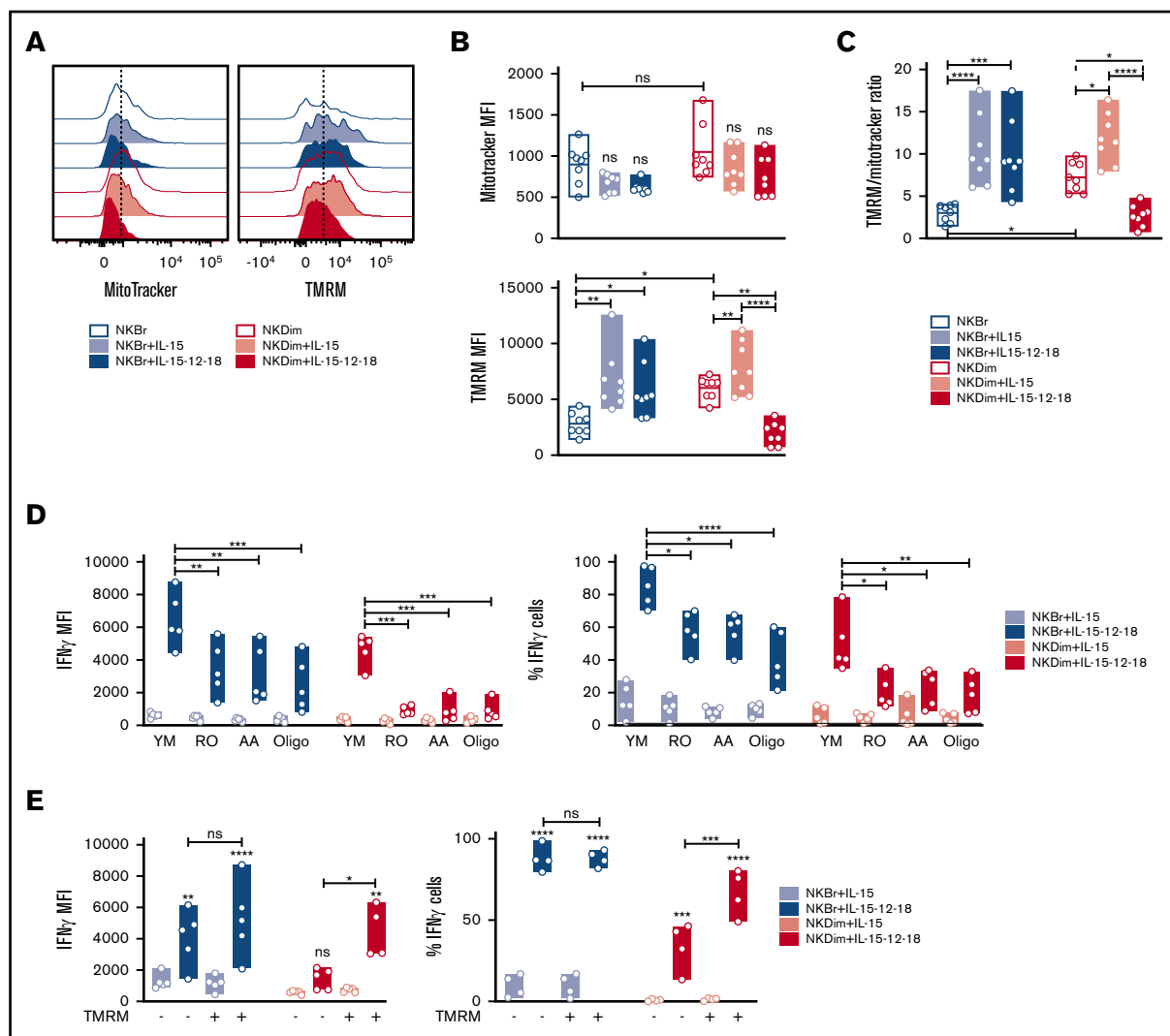


(Figure 2F-G). Addition of IL-12 or IL-18 alone to NK cells cultures did not affect mitochondria polarization, suggesting that a synergistic effect of the 2 cytokines is required to elicit the metabolic changes observed in NKDim cells (supplemental Figure 4A).

To assess the impact of OXPHOS on NK cells function, we used pharmacological inhibitors, including RO and AA, which inhibit complex I and complex III of the electron transport chain, respectively, and oligomycin A, which inhibits mitochondrial ATPase. At the concentrations used, these inhibitors showed no non-specific toxicity in culture (supplemental Figure 4B). We observed that RO, AA, and oligomycin A inhibited production of IFN- γ and TNF- α in NKBr cells (twofold) and to a larger extent in NKDim cells (eightfold; Figure 3D; supplemental Figure 4C). The same reduction was observed in the percentages of IFN- γ ⁺ and

TNF- α ⁺ NKDim and NKBr cells (Figures 3D and 4C), whereas no difference was reported in the cytotoxic markers tested in either subset (supplemental Figure 4D). Moreover, sorted and activated TMRM⁺ NKDim cells showed increased IFN- γ production and percentage of IFN- γ ⁺ cells compared with TMRM⁻ cells. No differences were observed comparing activated TMRM⁺ and TMRM⁻ NKBr cells (Figure 3E), demonstrating the importance of mitochondria polarization and OXPHOS in enhancing cytokine production, especially in NKDim cells.

Mitochondrial fragmentation and fusion govern NK cell function

Mitochondrial GTPases drive fission and fusion, which enhance glycolysis and OXPHOS, respectively.^{17,25} We next characterized

(Figure 4B-C; supplemental Figure 5B). In contrast, NKBr cells did not show any significant changes in mitochondrial fragmentation after cytokine priming or activation (Figure 4A,C; supplemental Figure 5C). Thus, the mitochondrial response in NKBr and NKDim cells during priming and activation was dichotomous: NKDim cells increased mitochondrial polarity upon IL-15 priming but fragmented their mitochondria after activation, whereas NKBr cells maintained fused and polarized mitochondria after priming and activation (Figure 4A-D; supplemental Figure 5B-C).

We next examined the effect of Mdivi-1, a selective inhibitor of mitochondrial fragmentation, on NK cell function. Mdivi-1 increased mitochondrial polarization in NK cells (supplemental Figure 6A) and had no apparent nonspecific toxicity (supplemental Figure 6B). Mdivi-1 significantly increased IFN- γ and TNF- α production by IL-15-primed NKDim cells and IL-12 + IL-18-activated NKDim but not NKBr cells (Figure 4E; supplemental Figure 6C), consistent with the previously observed dichotomous response. Mdivi-1 had no effect on cytotoxicity-related parameters in either subset (supplemental Figure 6D). These results show that mitochondrial dynamics differ in NKBr and NKDim cells and that mitochondrial fusion promotes OXPHOS and cytokine production by NKDim cells.

Mitochondrial polarization is associated with cellular fitness and effector function in NKDim cells

The dichotomous mitochondrial response to IL-12/18 stimulation observed in NKDim cells suggests that the effector capacity of these cells may be short lived. Nevertheless, a subset of long-lived memory NK cells has been described after exposure to HCMV³⁸⁻⁴⁰ and other chronic infections.⁴¹ Multiple studies, along with our data, have shown that mitochondrial fusion and OXPHOS improve overall cellular fitness and function.^{5,19,34}

Interestingly, frequencies of TMRM⁺ NK cells in the blood of healthy individuals were highly variable and largely confined to the NKDim compartment (Figure 5A). Within NKDim cells, TMRM expression was enriched in more mature CD57⁺ cells⁸ and also significantly increased within the NKG2C⁺NKG2A⁻ subset (Figure 5B-C; supplemental Figure 7A-B) that is expanded in HCMV⁺ individuals.³⁸⁻⁴⁰ When comparing HCMV⁻ and HCMV⁺ individuals, we found that TMRM expression was highly upregulated in CD57⁺NKG2C⁺NKG2A⁻ NK cells as previously reported¹⁰ (Figure 5B-C; supplemental Figure 7A-B). Still, we found elevated mitochondrial $\Delta\psi_m$ within CD57⁺NKG2C⁻NKG2A⁻ but not CD57⁺NKG2C⁻NKG2A⁺ NKDim cells (supplemental Figure 7A-B), suggesting that mitochondrial polarization and OXPHOS are not unique features of the NKG2C⁺ subset but may rather mark fully matured NK cells.

To determine whether the mitochondrial polarization associated with HCMV exposure imprints survival and functional advantages on NKDim cells, we isolated total NKDim cells from HCMV⁺ and HCMV⁻ donors and stimulated them under priming or activation conditions. We observed that HCMV⁻ NKDim cells proliferated extensively upon stimulation with activating cytokines before abruptly dying at ~day 6 (Figure 5D). In contrast, HCMV⁺ NKDim cells showed slower expansion, but cells persisted until the experimental end point (Figure 5D), consistent with the presence of fused mitochondria. To improve cellular fitness in HCMV⁻ NKDim cells, we added Mdivi-1 to the cultures and observed improved expansion levels, although still reduced compared with stimulated

HCMV⁺ NKDim cells (Figure 5D), suggesting Mdivi-1 could partially rescue mitochondrial fragmentation in cytokine-stimulated HCMV⁻ NKDim cells, thereby blocking cell death.

As expected, CD57⁺NKG2C⁺NKG2A⁻ cells were highly enriched in stimulated HCMV⁺ NKDim cultures (Figure 5E); however, NKG2C⁺ cells accounted for only 50% of total cells, indicating that other subsets (not expressing NKG2C) can expand upon long-term stimulation. Moreover, expanded HCMV⁻ NKDim cells treated with Mdivi-1 remained NKG2C⁻ (Figure 5E), demonstrating that Mdivi-1-induced survival did not convert CD57⁺NKG2C⁻NKG2A⁻ NKDim to NKG2C⁺ NKDim cells. An analysis of the function showed that surviving NKDim cells at day 12 could produce high levels of IFN- γ irrespective of HCMV status (Figure 5F). These results indicate that Mdivi-1 can partially restore not only survival but also function of HCMV⁻ NKDim cells (Figure 5F). CD107a and cytotoxic markers were at comparable levels in HCMV⁻ and HCMV⁺ NKDim cells (Figure 5G; supplemental Figure 7C).

NK cells from OPA1-deficient patients have less polarized mitochondria, reduced cellular fitness, and impaired memory-like NK cell homeostasis

We studied MD patients with an OPA1 missense mutation (A495V) to better understand the role of mitochondrial fusion in NK cell homeostasis. Compared with HDs, MD patients had similar percentages of NKBr but lower frequencies of NKDim cells (Figure 6A). Concerning the percentages of TMRM⁺ cells, we did not find any effect on NKBr cells, whereas TMRM⁺ NKDim cells were reduced in MD patients compared with HDs (Figure 6B). As expected, MD patients showed lower overall levels of TMRM uptake; however, NKDim homeostasis seemed more strongly dependent on OPA1 function.

We further analyzed the phenotype of NKDim cells in MD patients. In this cohort, all patients were HCMV⁺ by serological analysis; we therefore compared them with HCMV⁺ and HCMV⁻ HDs. As expected,⁴² the percentages of CD57⁺ NKDim cells were higher in HCMV⁺ donors and similar between MD patients and HDs (Figure 6C). However, MD patients had lower percentages of CD16⁺ cells and striking deficiency in CD57⁺NKG2C⁺NKG2A⁻ compared with HCMV⁺ HDs (Figure 6C). This result suggests that maintenance of mitochondrial polarization is a factor contributing to the formation of memory-like NK cells. We cultured NKDim cells from an MD patient and compared them with NKDim cells derived from a HCMV⁺ HD and HCMV⁻ HD. Consistent with Figure 5D, we found that NKDim cells from the HCMV⁺ HD could extensively expand during culture, whereas NKDim cells from the HCMV⁺ MD patient could not (Figure 6D). Together, these results suggest that maintenance of fused mitochondria imparts cellular fitness to HCMV-conditioned adaptive NKDim cells.

Discussion

It is well appreciated that mitochondria orchestrate cellular metabolism; however, the importance of these organelles in NK cell biology is poorly understood. In this report, we identify distinct patterns of mitochondrial polarization in NKBr and NKDim subsets that explain their differential metabolic performances at steady state and after cytokine stimulation. Our analysis of mature NK cells in HCMV⁺ and HCMV⁻ donors together with patients with MD allows

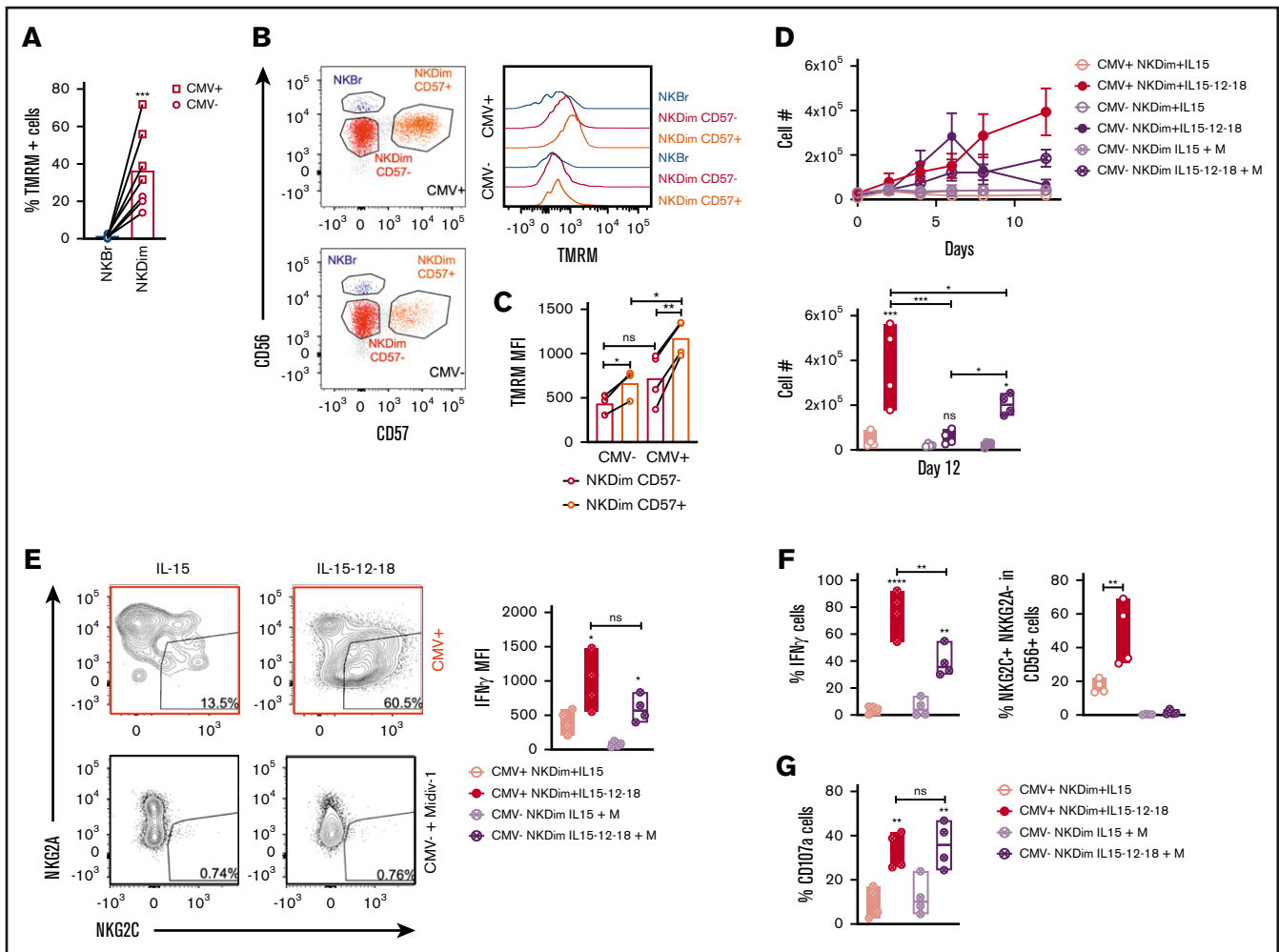


Figure 5. Mitochondrial fusion maintains NK cell survival and cellular fitness. (A) Percentage of TMRM⁺ cells in NKBr and NKDim cells (data from 7 HDs). (B-C) Quantification of TMRM in CD57⁺ NKDim and CD57⁻ NKDim cells in CMV⁺ and CMV⁻ donors: representative plots (B) and quantification (C) (geometric mean fluorescence intensity [MFI]). (D-G) NKDim cells were cultured with IL-15 or IL-15/12/18 for 12 days. Mdivi-1 was added or not to NKDim cells from CMV⁻ donors. (D) Growth curves of NKDim cells isolated from CMV⁺ and CMV⁻ HDs and cell numbers at end point. (E) Representative fluorescence-activated cell sorting (FACS) analysis of NKG2C and NKG2A and percentage of NKG2C⁺NKG2A⁻ cells in the indicated culture conditions at day 12. Quantification by FACS of IFN- γ and percentage of IFN- γ ⁺ cells (F) and CD107a⁺ cells (G) at day 12 (data are mean \pm SEM; data summarized from 3 independent experiments with at least 2 HDs each). $P > .05$ was considered not significant (ns). * $P < .05$, ** $P < .01$, *** $P < .001$, **** $P < .0001$ using 2-way analysis of variance with Tukey's correction.

us to propose mitochondrial remodeling that regulates OXPHOS as an essential gatekeeper of NK cell effector functions.

Several reports have shown that acquisition of T-cell effector functions is strictly dependent on glycolysis. Exploring the energy requirements of NK cells, we similarly found that NKDim cells principally rely on glucose upon activation with IL-12/18. Interestingly, we found that NKBr cells consume both glutamine and FA upon activation, as described for efficient cytokine producers maintaining elevated cellular fitness.³⁴ NKBr cells are preferentially enriched in secondary lymphoid organs at low oxygen concentrations and restricted nutrient availability; therefore, they maintain high SRC upon cytokine stimulation for both longevity and rapid cytokine production. NKDim cells undergo metabolic reprogramming to glycolysis because they are preferentially recruited to sites of inflammation, where they rapidly get activated⁴³ and proliferate. How OXPHOS is related to cytokine production in

lymphocytes is a matter of debate. Moreover, this dichotomous response of NKBr vs NKDim cells mirrors observations made with central and effector memory T cells, respectively.⁸ NKBr cells, which rely on FAs and maintain elevated SRC upon activation, resemble central memory T cells, whereas NKDim cells, metabolically reprogrammed to glycolysis, partially resemble effector memory T cells.^{1,5,8} Moreover, together with cytokine-mediated activation, other environmental factors can have an impact on NK cell activation, such as the presence of target cells.⁶ Unraveling the metabolic profiles of NK cell subsets upon different activation modes might help to better define the molecular basis of NK cell function.

At steady state, NKDim cells express OXPHOS genes, have elevated OCRs and ECARs, and have increased mitochondrial polarization compared with NKBr cells. We found that TMRM⁺ NKDim cells were enriched in CD57⁺ cells,⁸ suggesting that

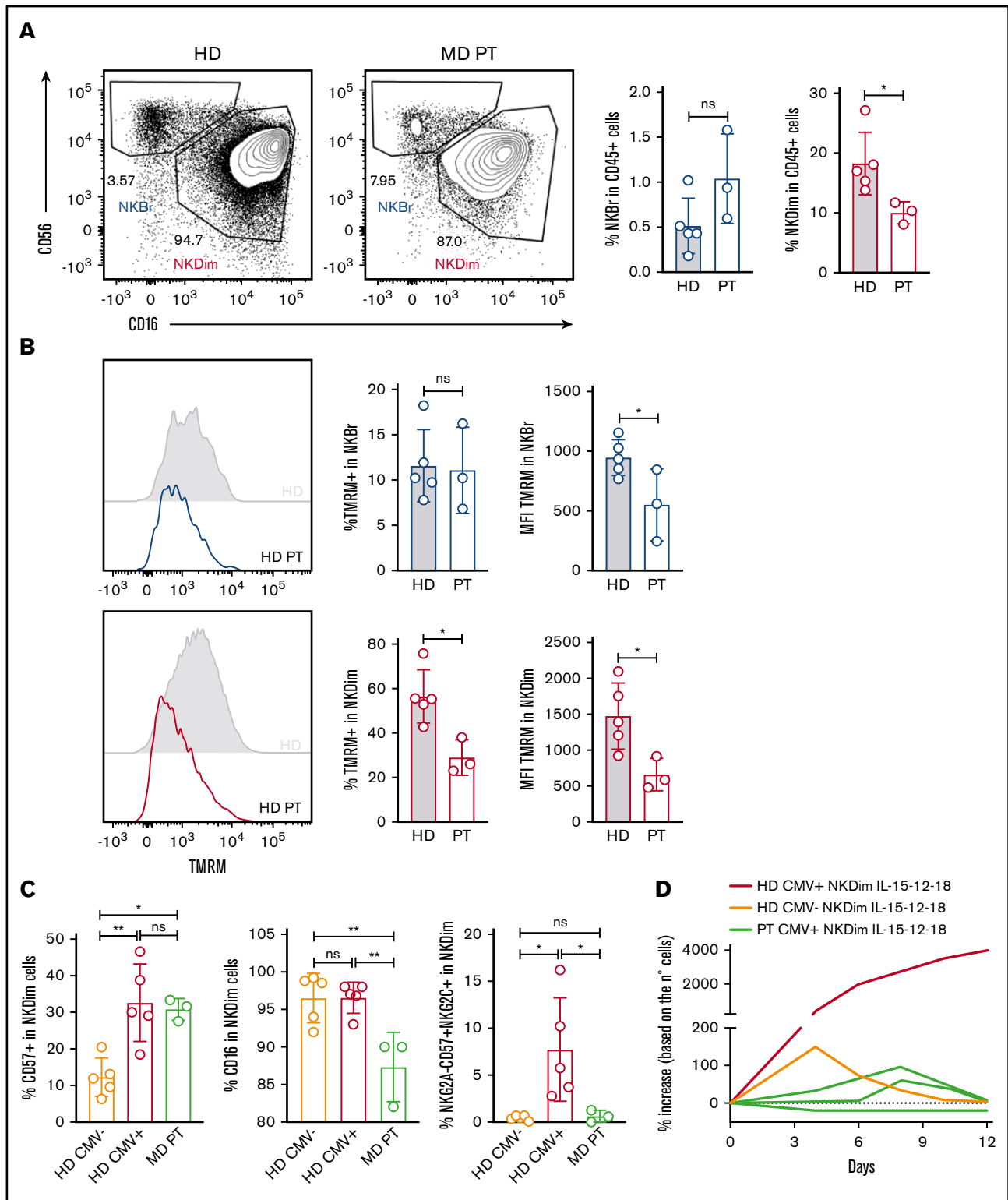


Figure 6. NK cells from MD patients have loss of memory-like NK cells and showed reduced cellular fitness. (A) Representative plots of NKBr and NKDim cells in HDs and MD patients with OPA1 mutation. Percentage of NKBr and NKDim cells in CD45⁺ cells. (B) Representative histograms of mitochondrial polarization in NKDim and NKBr cells comparing HDs and MD patients. Percentage of TMRM⁺ cells and TMRM intensity in NKBr and NKDim cells. (C) HDs and MD patients were compared with 5 CMV⁺ HDs by fluorescence-activated cell sorting (FACS). FACS analysis of the percentage of CD57⁺, CD16⁺, and CD57⁺NKG2A⁻NKG2C⁺ cells in NKDim cells. (D) Cells from 2 HDs and 3 MD patients were cultured in IL-15/12/18 for 12 days. Percentage of increase was calculated based on the number of cells (red, CMV⁺ HD; orange, CMV⁻ HD; green, MD patients; data summarized from 2 independent experiments with at least 2 HDs each and 3 MD patients). *P* > .05 was considered not significant (ns). **P* < .05, ***P* < .01 using 1-way analysis of variance with Tukey's correction.

mitochondrial polarization and OXPHOS are features of fully mature NK cells rather than markers of NKG2C⁺ cells in HCMV⁺ donors.¹⁰ NKDim cells isolated from HCMV⁺ donors were able to persist after long-term activation, whereas activated NKDim cells from HCMV⁻ donors survived only in the presence of Mdivi-1. HCMV broadly affects NK cell biology via epigenetic changes^{38,44} and favors mitochondrial biogenesis through the protein UL37.⁴⁵ This mitochondrial pathway provides a potential mechanistic explanation for the survival advantage observed in memory-like NK cells.

Still, additional metabolic reprogramming pathways independent of HCMV may operate to assure survival of mature NK cells. MD patients can manifest leukopenia and severe recurrent infections.⁴⁶ Deficiencies in the GTPase OPA1 are frequent in MDs,⁴⁷ and we found that OPA1-mutated patients had fewer NKDim cells and general loss of NK cell mitochondrial polarization. Similar to NK cells from HCMV⁺ HDs, NK cells from HCMV⁺ MD patients had higher levels of CD57 but very low frequencies of NKG2C⁺ NK cells. Moreover, NKDim cells from MD patients expanded poorly in response to cytokines. These results indicate that mitochondrial fusion is essential for maintenance of adaptive NK cells and overall cellular fitness.

Our comprehensive metabolic analysis identifies mitochondrial polarization as a gatekeeper of NKBr and NKDim cell priming, activation, and function. Because OXPHOS and mitochondrial fusion promote long-term persistence and improve cytokine production by NK cells, enhancing this pathway may extend the scope and efficacy of NK cell-based therapies.

Acknowledgments

The authors thank all members of the Innate Immunity Unit, the Centre de Recherche Translationnelle (Institut Pasteur), I. Amit (Weizmann Institute of Science), T. Wai (Institut Pasteur), and L. Muscarella ("Casa Sollievo della Sofferenza") for helpful discussions. The authors also thank the CB-UTechS and Imagopole-CiTech for cytometric and technical support.

References

1. Pearce EL, Pearce EJ. Metabolic pathways in immune cell activation and quiescence. *Immunity*. 2013;38(4):633-643.
2. Chang C-H, Curtis JD, Maggi LB Jr., et al. Posttranscriptional control of T cell effector function by aerobic glycolysis. *Cell*. 2013;153(6):1239-1251.
3. Peng M, Yin N, Chhangawala S, Xu K, Leslie CS, Li MO. Aerobic glycolysis promotes T helper 1 cell differentiation through an epigenetic mechanism. *Science*. 2016;354(6311):481-484.
4. Bantug GR, Galluzzi L, Kroemer G, Hess C. The spectrum of T cell metabolism in health and disease. *Nat Rev Immunol*. 2018;18(1):19-34.
5. Nicoli F, Papagno L, Frere JJ, et al. Naïve CD8⁺ T-cells engage a versatile metabolic program upon activation in humans and differ energetically from memory CD8⁺ T-cells. *Front Immunol*. 2018;9:2736.
6. Freud AG, Mundy-Bosse BL, Yu J, Caligiuri MA. The broad spectrum of human natural killer cell diversity. *Immunity*. 2017;47(5):820-833.
7. Lanier LL, Le AM, Warner NL, Babcock GF. Subpopulations of human natural killer cells defined by expression of the Leu-7 (HNK-1) and Leu-11 (NK-15) antigens. *J Immunol*. 1983;131(4):1789-1796.
8. Collins PL, Cella M, Porter SI, et al. Gene regulatory programs conferring phenotypic identities to human NK cells. *Cell*. 2019;176(1-2):348-360.e12.
9. Crinier A, Milpied P, Escalière B, et al. High-dimensional single-cell analysis identifies organ-specific signatures and conserved NK cell subsets in humans and mice. *Immunity*. 2018;49(5):971-986.e5.
10. Cichocki F, Wu C-Y, Zhang B, et al. ARID5B regulates metabolic programming in human adaptive NK cells. *J Exp Med*. 2018;215(9):2379-2395.
11. Donnelly RP, Loftus RM, Keating SE, et al. mTORC1-dependent metabolic reprogramming is a prerequisite for NK cell effector function. *J Immunol*. 2014;193(9):4477-4484.

The CB-UTechS and Imagopole-CiTech are supported by grant ANR-10-INSB-04-01 from the Agence Nationale de la Recherche. The Innate Immunity Unit receives support from the INSERM, Institut Pasteur, the Agence Nationale de la Recherche (ANR-10-LABX-73-REVIVE), and the European Research Council (advanced grant 695467-ILC_REACTIVITY). C.B.'s group receives support from the Fondation pour la Recherche Médicale (EQU201903007847) and grant ANR-10-LABX-62-IBEID from the Agence Nationale de la Recherche. L.S. was supported by a Swiss National Science Foundation Early Postdoctoral Mobility fellowship and Marie Curie grant H2020- MSCA-IF-2017. A.T. received funding from the EU Horizon 2020 research and innovation program under Marie Skłodowska-Curie grant agreement 765104. C.C. is part of the Pasteur-Paris University (PPU) International PhD Program that received funding from the European Union's Horizon 2020 research and innovation program under the Marie Skłodowska-Curie grant agreement 665807.

Authorship

Contribution: L.S. and J.P.D. conceptualized the study; L.S. was responsible for cell culture; L.S., C.C., A.T., and J.-M.D. performed fluorescence-activated cell sorting; S.M. and L.S. were responsible for Biomark analysis; P.E., C.B., and L.S. performed confocal microscopy; A.C., A.S., D.T., O.M., A.d.E., V.D., and N.T. provided resources; L.S. and J.P.D. wrote the paper; L.S. and J.P.D. provided funding; and J.P.D. supervised the study.

Conflict-of-interest disclosure: The authors declare no competing financial interests.

ORCID profiles: L.S., 0000-0001-8152-0611; J.-M.D., 0000-0001-6714-1308; P.E., 0000-0002-5933-094X; C.C., 0000-0002-4392-5498; A.T., 0000-0002-0698-8561; O.M., 0000-0002-9208-1527; C.B., 0000-0003-3477-9190; J.P.D.S., 0000-0002-7146-1862.

Correspondence: James P. Di Santo, Innate Immunity Unit, Inserm U1223, Institut Pasteur, 25 rue du Docteur Roux, 75724 Paris, France; e-mail: james.di-santo@pasteur.fr.

12. Keating SE, Zaiatz-Bittencourt V, Loftus RM, et al. Metabolic reprogramming supports IFN- γ production by CD56bright NK cells. *J Immunol*. 2016;196(6):2552-2560.
13. Loftus RM, Assmann N, Kedia-Mehta N, et al. Amino acid-dependent cMyc expression is essential for NK cell metabolic and functional responses in mice. *Nat Commun*. 2018;9(1):2341.
14. Zheng X, Qian Y, Fu B, et al. Mitochondrial fragmentation limits NK cell-based tumor immunosurveillance. *Nat Immunol*. 2019;20(12):1656-1667.
15. Marçais A, Cherfils-Vicini J, Viant C, et al. The metabolic checkpoint kinase mTOR is essential for IL-15 signaling during the development and activation of NK cells. *Nat Immunol*. 2014;15(8):749-757.
16. Michelet X, Dyck L, Hogan A, et al. Metabolic reprogramming of natural killer cells in obesity limits antitumor responses. *Nat Immunol*. 2018;19(12):1330-1340.
17. Rambold AS, Pearce EL. Mitochondrial dynamics at the interface of immune cell metabolism and function. *Trends Immunol*. 2018;39(1):6-18.
18. Cogliati S, Frezza C, Soriano ME, et al. Mitochondrial cristae shape determines respiratory chain supercomplexes assembly and respiratory efficiency. *Cell*. 2013;155(1):160-171.
19. Buck MD, O'Sullivan D, Pearce EL. T cell metabolism drives immunity. *J Exp Med*. 2015;212(9):1345-1360.
20. Kapnick SM, Pacheco SE, McGuire PJ. The emerging role of immune dysfunction in mitochondrial diseases as a paradigm for understanding immunometabolism. *Metabolism*. 2018;81:97-112.
21. Walker UA, Collins S, Byrne E. Respiratory chain encephalomyopathies: a diagnostic classification. *Eur Neurol*. 1996;36(5):260-267.
22. Lim AI, Li Y, Lopez-Lastra S, et al. Systemic human ILC precursors provide a substrate for tissue ILC differentiation. *Cell*. 2017;168(6):1086-1100.e10.
23. Manel N, Kinet S, Battini J-L, Kim FJ, Taylor N, Sitbon M. The HTLV receptor is an early T-cell activation marker whose expression requires de novo protein synthesis. *Blood*. 2003;101(5):1913-1918.
24. Laval J, Touhami J, Herzenberg LA, et al. Metabolic adaptation of neutrophils in cystic fibrosis airways involves distinct shifts in nutrient transporter expression. *J Immunol*. 2013;190(12):6043-6050.
25. Escoll P, Song O-R, Viana F, et al. Legionella pneumophila modulates mitochondrial dynamics to trigger metabolic repurposing of infected macrophages. *Cell Host Microbe*. 2017;22(3):302-316.e7.
26. Duchen MR, Surin A, Jacobson J. Imaging mitochondrial function in intact cells. *Methods Enzymol*. 2003;361:353-389.
27. Lucas M, Schachterle W, Oberle K, Aichele P, Diefenbach A. Dendritic cells prime natural killer cells by trans-presenting interleukin 15. *Immunity*. 2007;26(4):503-517.
28. Gardiner CM, Finlay DK. What fuels natural killers? Metabolism and NK cell responses. *Front Immunol*. 2017;8:367.
29. Mavropoulos A, Sully G, Cope AP, Clark AR. Stabilization of IFN-gamma mRNA by MAPK p38 in IL-12- and IL-18-stimulated human NK cells. *Blood*. 2005;105(1):282-288.
30. Cooper MA, Fehniger TA, Caligiuri MA. The biology of human natural killer-cell subsets. *Trends Immunol*. 2001;22(11):633-640.
31. Jacobs R, Hintzen G, Kemper A, et al. CD56bright cells differ in their KIR repertoire and cytotoxic features from CD56dim NK cells. *Eur J Immunol*. 2001;31(10):3121-3127.
32. O'Sullivan TE, Sun JC, Lanier LL. Natural killer cell memory. *Immunity*. 2015;43(4):634-645.
33. van der Windt GJW, Chang C-H, Pearce EL. Measuring bioenergetics in T cells using a Seahorse extracellular flux analyzer. *Curr Protoc Immunol*. 2016;113:3.16B.1-3.16B.14.
34. van der Windt GJW, O'Sullivan D, Everts B, et al. CD8 memory T cells have a bioenergetic advantage that underlies their rapid recall ability. *Proc Natl Acad Sci USA*. 2013;110(35):14336-14341.
35. Gautam N, Sankaran S, Yason JA, Tan KSW, Gascoigne NRJ. A high content imaging flow cytometry approach to study mitochondria in T cells: MitoTracker Green FM dye concentration optimization. *Methods*. 2018;134-135:11-19.
36. Ferlazzo G, Thomas D, Lin S-L, et al. The abundant NK cells in human secondary lymphoid tissues require activation to express killer cell Ig-like receptors and become cytolytic. *J Immunol*. 2004;172(3):1455-1462.
37. Buck MD, O'Sullivan D, Klein Geltink RI, et al. Mitochondrial dynamics controls T cell fate through metabolic programming. *Cell*. 2016;166(1):63-76.
38. Gumá M, Angulo A, Vilches C, Gómez-Lozano N, Malats N, López-Botet M. Imprint of human cytomegalovirus infection on the NK cell receptor repertoire. *Blood*. 2004;104(12):3664-3671.
39. Hammer Q, Rückert T, Borst EM, et al. Peptide-specific recognition of human cytomegalovirus strains controls adaptive natural killer cells. *Nat Immunol*. 2018;19(5):453-463.
40. Lopez-Vergés S, Milush JM, Schwartz BS, et al. Expansion of a unique CD57⁺NKG2Chi natural killer cell subset during acute human cytomegalovirus infection. *Proc Natl Acad Sci USA*. 2011;108(36):14725-14732.
41. Björkström NK, Lindgren T, Stoltz M, et al. Rapid expansion and long-term persistence of elevated NK cell numbers in humans infected with hantavirus. *J Exp Med*. 2011;208(1):13-21.
42. Holder KA, Lajoie J, Grant MD. Natural killer cells adapt to cytomegalovirus along a functionally static phenotypic spectrum in human immunodeficiency virus infection. *Front Immunol*. 2018;9:2494.
43. Melsen JE, Lugthart G, Lankester AC, Schilham MW. Human circulating and tissue-resident CD56(bright) natural killer cell populations. *Front Immunol*. 2016;7:262.

44. Schlums H, Cichocki F, Tesi B, et al. Cytomegalovirus infection drives adaptive epigenetic diversification of NK cells with altered signaling and effector function. *Immunity*. 2015;42(3):443-456.
45. Kaarbø M, Ager-Wick E, Osenbroch PØ, et al. Human cytomegalovirus infection increases mitochondrial biogenesis. *Mitochondrion*. 2011;11(6): 935-945.
46. Tarasenko TN, Pacheco SE, Koenig MK, et al. Cytochrome c oxidase activity is a metabolic checkpoint that regulates cell fate decisions during T cell activation and differentiation. *Cell Metab*. 2017;25(6):1254-1268.e7.
47. Carelli V, Musumeci O, Caporali L, et al. Syndromic parkinsonism and dementia associated with OPA1 missense mutations. *Ann Neurol*. 2015;78(1): 21-38.

LISTE DES ÉLÉMENTS SOUS DROITS

Liste de **tous les éléments retirés** de la version complète de la thèse
faute d'en détenir les droits

Figures

Légende de l'image	N° de l'image	Page(s) dans la thèse
NK cell CD56 ^{bright} and CD56 ^{dim} subsets (A) Flow cytometric analysis (B) schematic representation of phenotype and effector functions (adapted from Cooper <i>et al.</i> ¹²²)	Figure 3	32
Schematic representation of human FcγRs (adapted from Bruhns and Jönsson ²⁵⁰)	Figure 6	44